ESTABLISHING A FACILITY TO MEASURE PACKED COLUMN HYDRODYNAMICS

by

Sarel Marais Lamprecht

Thesis submitted in partial fulfillment
of the requirements for the Degree
of

MASTER OF SCIENCE IN ENGINEERING
(CHEMICAL ENGINEERING)

in the Department of Process Engineering
at the University of Stellenbosch

Supervised by

Prof. J.H. Knoetze and Prof. A.J. Burger

STELLENBOSCH

December 2010

Declaration

I, the undersigned, hereby declare that the work contained in this thesis is my own original work and that I have not previously in its entirety or in part submitted it at any university for a degree.

…….. ……

Signature Date

Abstract

Distillation continues to be the most widely used method of separation in the processing industry, in spite of its inherently low thermodynamic efficiency. Two of the critical distillation research needs that arose from the US-Initiative Vision 2020 were to develop a better understanding of the physical phenomena as well as developing better predictive models. Also, characterisation of modern packing materials is required to assist in the CO_2 capture optimisation.

This thesis deals with both these aspects by establishing a facility that can accurately measure the hydraulic capacity of packed columns. This setup eliminates mass transfer and specific attention can be given to the hydrodynamic behaviour of packed columns. Two phenomena that have a large impact on the mass transfer efficiency of packing materials are the loading and flooding point. The loading point is signified by the following: a.) where the packed column hold-up increases, b.) higher increase in pressure drop, and c.) a decrease in Height Equivalent to a Theoretical Plate (HETP). The onset of flooding is where the shear forces between the gas and liquid become so large (relative to the gravitational forces) that a net upwards movement of liquid occurs, resulting in liquid droplets being heavily entrained. This is normally accompanied by a sharp increase in HETP, pressure drop and liquid hold-up.

The prediction of these operating limits is of great value but, despite the many contributions that were made from 1960 to 2010, there is still room for improvement. The operating region of particular interest is between the loading and flooding point, especially for fluids with physical properties significantly different from that of water. In the past, this operating region was not of great importance, but industries are constantly striving to increase their production with minimal capital expenditure. Thus, packed columns are being pushed to their limits and a good understanding of the phenomena occurring near these operational limits is now required.

A 400 mm diameter glass packed bed setup (with a bed height of 3000 mm) was designed and constructed to test the effect of the following parameters on packed bed pressure drop and liquid hold-up:

- Gas and liquid physical properties
- Gas and liquid rates
- Type of packing (either random or structured)

The experimental setup has been designed so that in the future the influences of the above mentioned parameters on entrainment can also be measured. Initially, hydrodynamic tests on random packing materials (1.5” Pall® Rings, 1.5” IMTP®, 1.5” Intalox® Ultra™) were conducted over a liquid range of 6 - 122 $m^3/(m^2 \cdot h)$. Through a

thorough literature study it was found that the most likely semi-theoretical model, that would be able to predict the pressure drop and the liquid hold-up over most of the random packing test range, was the model developed by Billet [1991; 1993; 1995; 1999]. The other models found throughout the literature had at least one of the following deficiencies:

- Limited to only the pre-loading region.
- Tested (and thus applicable) only over a very select group of packing materials with no attempt to generalise.
- Lacked the proper validation of significantly variable fluid properties over multitudes of liquid and gas rates especially, at higher gas and liquid rates.

The experimental setup was successfully commissioned, noting the following maximum experimental errors: Vapour flow factor - 2.6 %; liquid rate - 0.75 %; packed bed pressure drop - 0.75 %; liquid hold-up - 1.25 % and entrainment - 1.05 %. Significant deviations were observed between the experimental hold-up and the hold-up from the predictive model of Billet (using Pall® Rings). Careful inspection revealed that this predictive model potentially uses two definitions for hold-up at flooding, one which has a theoretical basis and the other purely empirical. Upon substituting the theoretical value with the empirical value, a significant improvement was observed between the measured and predicted results. Deviations were still observed near the flooding point and were attributed to the difficulty of obtaining reliable flooding data. The range of liquid hold-up prediction by Billet was only verified up to a liquid rate of 82 $m^3/(m^2 \cdot h)$ and the pressure drop prediction only verified up to a liquid rate of 60 $m^3/(m^2 \cdot h)$. This reinforces the need for high liquid, high gas rate data. Due to the empirical nature of the liquid hold-up at flooding prediction, and since pressure drop prediction is directly linked to liquid hold-up, another model was used to compare the experimental pressure drop data.

The KG-TOWER® simulator was used to predict IMTP® data and compare it to the experimentally measured values. It was found that the experimental IMTP® data followed the same trends as those from KG-TOWER® within the operating limits of the program. Thus, since the experimental data follows similar trends as models found in the literature, as well as falling within their reliable limits, the experimental setup can correctly measure the parameters in question.

The experimental data from the different random packings were compared to one another by using a statistical method to determine the loading point and onset of flooding. This method uses prediction confidence intervals by fitting empirical curves to each operating region and was found to be useful in determining these critical points from experimental hydraulic data (in the absence of HETP data).

The only useful comparison was between IMTP® and Intalox® Ultra™ as they both have roughly the same density, size and void fraction. It was found that, on average, the pressure drop of Intalox® Ultra™ is 20 % lower than that of IMTP® over the entire operating range. The hydraulic operating range of Intalox® Ultra™ was found to be on average 16 % larger than that of IMTP®.

It is recommended that further testing should be done to investigate the influence of fluid properties (specifically liquid viscosity and to a lesser extent surface tension) on the hydraulic capacity of packed columns. Also, high gas and high liquid rate data should be generated to assist current modelling techniques. Lastly, a comparative characterisation between Intalox® Ultra™ and Raschig Super-Rings would serve as a benchmark for fourth generation random packings.

Samevatting

Distillasie is vandag nog die skeidingsproses wat die meeste gebruik word in the prosesnywerhede ten spyte van ‘n lae termodinamiese effektiwiteit. Twee van die kritieke distillasie navorsing behoeftes wat vanuit die US-Initiative Vision 2020 ontstaan het, was om die fisiese verskynsels beter te verstaan, asook om beter voorspellende modelle te ontwikkel. Die karakterisering van moderne pakking materiale is ook nodig vir die optimering van die verwydering van CO_2 uit uitlaatstrome.

Hierdie tesis spreek beide van hierdie faktore aan deur ‘n fasiliteit op te rig wat die hidrouliese kapasiteit van gepakte kolomme akkuraat kan meet. Hierdie opstelling elimineer massa-oordrag en dus kan spesifieke aandag gegee word aan die hidrodinamiese gedrag van gepakte kolomme. Twee verskynsels wat ‘n groot impak het op die massa-oordrag effektiwiteit van pakkingsmateriale is die ladingspunt en die vloedpunt. Die ladingspunt word deur die volgende gekenmerk: a.) waar die vloeistof inhoud in die gepakte bed toeneem, b.) ‘n toename in drukval en c.) ‘n afname in die hoogte ekwivalent aan ‘n teoretiese plaat (HETP). Die vloed gebied word gekenmerk waar die skuifkragte tussen die vloeistof en gas so groot raak (relatief tot die gravitasionele kragte), dat daar ‘n netto opwaartse beweging van vloeistof druppels in die kolom is. Hierdie gaan normaalweg gepaard met ‘n skerp toename in HETP, drukval en vloeistof inhoud.

Die voorspelling van hierdie bedryfslimiete is baie waardevol, maar ten spyte van die bydrae wat tussen 1960 en 2010 gemaak was, is daar nog steeds ruimte vir verbetering. Die spesifieke bedryfsgebied van belang is die gebied tussen die ladingspunt en die vloedpunt en spesifiek vir sisteme waar die fisiese eienskappe van die vloeistowwe drasties verskil van die van water. In die verlede was hierdie gebied van minder belang gewees, maar maatskappye probeer deesdae hul produksie opstoot met minimale kapitale uitleg. Dus is ‘n goeie kennis van massa-oordrag verskynsels naby aan die bedryfslimiete van kardinale belang.

‘n 400 mm Diameter gepakte kolom (met ‘n bed hoogte van 3000 mm en bestaande uit glas) opstelling is ontwerp en gebou om die effek van die volgende parameters te toets op gepakte bed drukval en vloeistof inhoud:

- Gas en vloeistof fisiese eienskappe
- Gas vloeistof vloeitempos
- Tipe pakking (beide ongeordend en gestruktureerd)

Die eksperimentele opstelling is ontwerp om die bogenoemde eienskappe op vloeistof-meesleuring te meet vir toekomstige navorsing. Hidrodinamiese toetse op ongeordende pakkingsmateriale (1.5” Pall® Ringe, 1.5” IMTP®, 1.5” Intalox® Ultra™) is uitgevoer vir vloeistof vloeitempos tussen 6 en 122 $m^3/(m^2 \cdot h)$. Vanuit ‘n deeglike literatuurstudie is daar gevind dat die mees toepaslike semi-teoretiese model, wat die drukval sowel as die

vloeistof inhoud kan voorspel oor al die bedryfsgebiede, is die model wat deur Billet [1991; 1993; 1995; 1999] ontwikkel is. Die ander modelle in die literatuur het ten minste een van die volgende tekortkominge gehad:

- Is slegs van toepassing in die voor-ladings gebied.
- Is slegs van toepassing vir ‘n paar pakkingsmateriale en geen poging is aangewend om dit te veralgemeen nie.
- Is nie geldig waar die vloeistof eienskappe drasties verskil van ‘n lug/water sisteem nie, sowel as by hoë gas en vloeistof vloeitempos.

Die eksperimentele opstelling is suksesvol in werking gestel met die volgende waargenome eksperimentele foute: Gas vloei faktor – 2.6 %; vloeistof vloeitempo – 0.75 %; gepakte bed drukval – 0.75 %; vloeistof inhoud – 1.25 %; vloeistof-meesleuring tempo – 1.05 %. Noemenswaardige verskille is waargeneem tussen die eksperimentele en teoretiese vloeistof inhoud (deur Pall® Ringe te gebruik). Na gelang van noukeurige inspeksie, is daar gevind dat die Billet-model twee moontlike definisies voorstel vir die voorspelling van vloeistofinhoud by die vloedpunt. Een van hierdie is teoreties van aard en die ander een suiwer empiries. ‘n Vervanging van die teoretiese waardes met die empiriese waardes het gelei tot ‘n merkwaardige verbetering tussen die eksperimentele en teoretiese voor-spellings.

Daar was nog steeds verskille naby aan die vloedpunt, maar dit kon toegeskryf word aan die feit dat min betroubare data naby aan die vloedpunt beskikbaar is. Die voorspelling van vloeistof inhoud deur Billet is slegs gekontroleer tot ‘n vloeistof vloeitempo van 82 $m^3/(m^2 \cdot h)$ en die drukval slegs tot ‘n vloeistof vloeitempo van 60 $m^3/(m^2 \cdot h)$. Die bogenoemde bewys dus die tekort aan hoë gas- en hoë vloeistofvloeitempo data. Die voorspellende model se drukval is gekoppel aan die vloeistof inhoud, en dus is ‘n ander model gebruik om die eksperimentele drukval data teen te vergelyk.

Die KG-TOWER® simulasie program is gebruik om die IMTP® drukval te voorspel en dit het goed vergelyk met die eksperimentele data. Dus, aangesien die eksperimentele data dieselfde tendens toon as dié van die modelle in die literatuur en aangesien dit binne die modelle se foutbande val, kan die eksperimentele opstelling die verlangde parameters akkuraat meet.

Die eksperimentele data van al drie pakkingsmateriale is teenoor mekaar vergelyk deur gebruik te maak van ‘n statistiese metode wat die ladings- en vloedpunt bepaal. Hierdie metode maak gebruik van voorspellings vertroue intervalle deur empiriese kurwes op die eksperimentele data in elke bedryfsgebied te pas. Hierdie metode is ontwikkel om toepaslike te wees in die afwesigheid van HETP data.

Die enigste nuttige vergelyking is tussen IMTP® en Intalox® Ultra™ omdat albei dieselfde pakkingsdigtheid, grootte en pakkings oop ruimte het. Daar is gevind dat die drukval van

Intalox® Ultra™ ‘n gemiddeld van 20 % laer is as dié van IMTP® oor die hele bedryfsgebied. Die hidrouliese bedryfsgebied van Intalox® Ultra™ is 16 % groter as dié van IMTP®.

Daar word voorgestel dat bykomende toetswerk gedoen moet word om die invloed van vloeistof eienskappe (spesifiek vloeistof viskositeit en vloeistof oppervlak spanning) op die hidrouliese kapasiteit van gepakte kolomme te ondersoek. Bykomende toestwerk by hoë gas- en hoë vloeistofvloeitempo word benodig om die bestaande modelle aan te vul. Laastens, sal ‘n vergelykende studie tussen Intalox® Ultra™ en Raschig Super-Rings die grondslag lewer vir die karakterisering van vierde generasie ongeordende pakkingsmateriale.

Acknowledgements

I would like to convey my sincere gratitude towards my supervisors Prof. J.H. Knoetze, Prof. A.J. Burger and Dr. C.E. Schwarz for their continuous encouragement, patience, support and critique.

Without the financial support from Sasol Pty (Ltd), the South African Department of Trade and Industry through THRIP and Koch-Glitsch this project would not have been made possible.

To my parents Johan and Carine Lamprecht for your continuous love and support throughout not only the good times, but also during the difficult periods.

To my close friend, Eben Uys, without your daily support, mechanical - and design reasoning when the going was tough, as well as all the memorable moments we had during the past few years, I want to extent my sincere gratitude. I will treasure our friendship for the rest of my life.

The Process Engineering workshop, Jannie Barnard, Anton Cordier and Howard Koopman, should take the glory for helping with the construction of a versatile and brilliant experimental setup. I would also like to thank the lab assistants: Alvin Peterson, Vincent Carolisson and Ollie Jooste for their help in the laboratory.

Dr. A.B. Erasmus for his help in designing the column internals.

Lastly, I want to thank my Lord and Saviour, Jesus Christ for blessing me with this opportunity and giving me the necessary strength, courage and guidance in situations when all seemed lost.

Table of Contents

List of Tables

List of Figures

Glossary

Absolute Average Relative Error (AARE)

Defined as the average deviation of all the predicted values in a model that are compared to their respective experimental values. This is only valid over the experimentally tested region and for a single predicted variable. The AARE is calculated with the following equation:

$$AARE_i(\%) = \frac{100}{N} \cdot \sum_{i=1}^{N} \left| \frac{x_i^{calculated} - x_i^{measured}}{x_i^{measured}} \right|$$

Where:

x_i is the evaluated parameter
N is the number of data points in the sample size

Dry Bed Pressure Drop

Defined as the pressure drop measured across a bed filled with either random or structured packing, in the absence of liquid.

Flooding

Defined when the shear forces between the gas and liquid increase relative to the gravitational forces up to a point (vapour flow factor at a specific liquid rate) where the liquid droplets have a net upward movement into the column. It is normally associated with a sharp increase in height equivalent to a theoretical plate as well as a sharp increase in pressure drop and liquid hold-up over the packed bed.

Hydraulic Capacity

Defined as the range of operability within a packed column before it starts to flood. It's often given in terms of pressure drop or liquid hold-up, as these are all linked to a vapour flow factor.

Irrigated Pressure Drop

See packed bed pressure drop.

Liquid Hold-up

Defined as the amount of liquid that is held-up in-between the packing segments/ elements at any given time during normal operation.

Loading point

Defined as the point (vapour flow factor at a specific liquid rate) at which the shear forces between the gas and liquid increases relative to the gravitational forces up to a point where the liquid droplets flowing down the column becomes suspended. It's normally associated with a decrease in HETP.

Mean Relative Deviation

See AARE.

Packed Bed Pressure Drop

Defined as the pressure drop measured across a bed filled with either random or structured packing. The packing material is wetted with the operating liquid mixture.

Packed Column

Defined as a distillation tower with either random or structured packing as contacting device.

Packing Factors

Defined as packing specific constant(s) in a theoretical model to account for the difference between the model assumptions and real world applications.

Quadratic Diameter

A square column with side length dimensions equal to the stated diameter [Ranke et al., 2000].

Random Packing

Defined as a gas-liquid contacting device that consists of discrete pieces of packing of a specific geometrical shape. These are randomly packed in a column shell.

Souders Diagram

A diagram with the abscissa consisting of the natural logarithm of gas phase capacity factor (C_G) and the ordinate consisting of the natural logarithm of the ratio between the liquid (C_L) - and gas phase capacity factors.

Structured Packing

Defined as a gas-liquid contacting device that consists of crimped layers of wire-mesh or corrugated sheets which form a distinctive pattern.

Vapour Flow Factor

Defined as the gas velocity flowing upwards in a packed column that is adjusted for the density of the gas (Measured in $[(m/s)\cdot(kg/m^3)^{0.5}]$).

Wallis Diagram

A diagram with abscissa consisting of gas phase capacity factor $(C_G)^{0.5}$ and the ordinate consisting of the liquid phase capacity factor $(C_L)^{0.5}$.

Nomenclature

Symbol	Description	Reference Equation(s)	Units
a, a_p, a_i	Packing geometrical surface area	2.14, 2.50, 2.51, 2.52, 2.55, 2.56, 2.58, 2.60, 2.61, 2.62, 2.63, 2.65, 2.93, 2.94, 2.95, 2.103, 2.117, 2.118, 2.120, 2.121	m^2/ m^3
a_e	Brunazzi & Paglianti effective wetted surface area	2.94, 2.103	m^2
a_h	Billet packing hydraulic surface area	2.61, 2.62, 2.63	m^2/ m^3
A	SRP packing specific constant	2.32	-
A	Cross-sectional area of measuring vessel	3.2	m^2
A_G	Cross-sectional area of channel open to vapour flow	2.85, 2.87, 2.92, 2.100	m^2
A_0	Contraction area	8.1, 8.2	m^2
B	Channel base dimension	2.39, 2.49	m
B	SRP packing specific constant	2.32	-
B_L	Non-dimensional liquid load	2.77, 2.78	-
B_1, B_2, B_3, B_4,	Brunazzi and Paglianti packing specific constants	2.90, 2.105	-
c	McNulty and Hsieh linear regression factor	2.3	-
C_D, K	Coefficient of discharge	8.1, 8.2	-
C_G, C_S	Gas capacity factor (gas velocity corrected for density)	2.1, 2.3, 2.5, 2.6, 2.8	m/s
C_{Fl}	Flooding constant	2.66, 2.69, 2.71	-
C_h	Billet hold-up constant	2.62, 2.63	-
C_L	Liquid capacity factor	2.2, 2.3, 2.8	m/s

$C_{p,0}$	Billet pressure drop constant	2.54, 2.57	-
C_0, C_1, C_3, C_4	Robbins pressure drop packing constants	2.19, 2.20, 2.25	-
C_1, C_2, C_3	Stichlmair packing specific constants	2.127, 2.129	-
d_c, d_s,	Column diameter	2.48, 2.53, 2.80, 2.117, 2.118	m
d_e	Brunazzi & Paglianti equivalent channel diameter	2.86, 2.87, 2.88, 2.92, 2.93, 2.94, 2.101, 2.103, 2.104, 2.105	m
d_G	Brunazzi & Paglianti equivalent diameter for gas flow	2.92	m
d_h	Column hydraulic diameter	2.71	m
d_{hG}	SRP & Delft vapour phase hydraulic diameter	2.37, 2.38, 2.39, 2.42, 2.43, 2.44	m
d_p	Packing element diameter	2.53, 2.55, 2.78, 2.79, 2.80	m
d_p	Stichlmair particle diameter	2.126	m
d_T	Diameter of liquid droplets	2.71, 2.72	m
$(dP/dz)_{total}$	Packed column total pressure drop	2.81, 2.112, 2.115, 2.119	Pa/m
$(dP/dz)_F$	Brunazzi & Paglianti pressure drop friction term	2.81, 2.82	Pa/m
$(dP/dz)_G$	Brunazzi & Paglianti pressure drop gravitational term	2.81, 2.84	Pa/m
$(dP/dz)_A$	Brunazzi & Paglianti pressure drop acceleration term	2.81, 2.83	Pa/m
$(dP/dz)_{F,d}$	Brunazzi & Paglianti friction directional changes term	2.82, 2.85, 2.100, 2.101, 2.107	Pa/m
$(dP/dz)_{F,c}$	Brunazzi & Paglianti friction concentrated term	2.82, 2.86	Pa/m
$(dP/dz)_f$	Woerlee pressure drop due to friction at vapour/liquid interface	2.108	Pa/m
$(dP/dz)_g$	Woerlee pressure drop due to geometry configuration	2.108	Pa/m

f	Fraction of flooding	2.3	-
f	Friction factor	2.31, 2.32, 2.109, 2.110	-
f_g	Woerlee geometrical friction factor	2.110	-
f_G	Brunazzi & Paglianti gas friction factor	2.86, 2.89, 2.90, 2.105	-
f_i	Brunazzi & Paglianti interfacial friction factor	2.102, 2.105	-
f_m	Brunazzi & Paglianti mean friction factor	2.101	-
f_p	Woerlee packing specific friction factor	2.110, 2.113, 2.115, 2.116, 2.117, 2.119	-
f_p^*	Woerlee adjusted packing specific friction factor	2.117	-
f_0	Stichlmair friction factor for flow over a single particle	2.126, 2.127, 2.129	-
f_1, f_2	Spiegel & Meier resistance factor	2.9, 2.10, 2.11	-
f_∞	Woerlee packing friction factor at infinite Reynolds number	2.113, 2.114	-
$F_{G,lp}$	SRP loading point vapour flow factor	2.37, 2.38	[(m/s)·(kg/m^3)]
F_{pd}	Robbins dry bed packing factor	2.21, 2.22, 2.23, 2.24, 2.25	-
F_p	Kister & Gill packing specific factor	2.5, 2.7	-
F_t	Correction factor for under-wetting	2.26, 2.28	-
F_V	Vapour flow factor	2.12, 2.16, 2.52, 2.56, 2.76, 2.79	[(m/s)·(kg/m^3)]
F_V	Vapour flow factor at 100 % capacity	2.16	[(m/s)·(kg/m^3)]
$F_{V,Fl}$	Vapour flow factor at the flooding point	2.76	[(m/s)·(kg/m^3)]
F_1	Woerlee laminar coefficient of packing friction	2.113	-

g	Gravitational constant	2.27, 2.37, 2.38, 2.51, 2.60, 2.61, 2.62, 2.63, 2.65, 2.66, 2.71, 2.72, 2.78, 2.84, 2.106, 2.107, 2.112, 2.125, 2.131, 2.132, 3.1, 3.2	m/s^2
g_{eff}	Effective gravity	2.26, 2.27	-
G	Gas mass flow rate	2.4	$lb/(ft^2 \cdot s)$
G	Gas loading	2.21, 2.22, 2.25	$lb/(ft^2 \cdot h)$
Δh	Difference in liquid level	3.1	m
h	Crimp height	2.39	m
$h_{L,Fl}$	Column hold-up at flooding	2.59, 2.60, 2.65, 2.70, 2.71, 2.73, 2.74, 2.76	m^3/m^3
h_L	Total column hold-up	2.56, 2.57, 2.59, 2.64, 2.76, 2.79, 2.122, 2.123, 2.124, 2.128, 2.131	m^3/m^3
h_L^*	Spiegel & Meier adjusted liquid hold-up	2.14	-
$h_{L,S}$	Pre-loading column hold-up	2.10, 2.13, 2.14, 2.57, 2.59, 2.61, 2.70, 2.76, 2.77, 2.130, 2.131, 2.132	m^3/m^3
h_{pb}	Height of packed bed	2.42, 2.44, 2.45	m
h_{pe}	Height of packing element	2.45, 2.48	m
h_t	SRP & Delft packed column hold-up	2.26, 2.33, 2.50	m^3/m^3
h_t	Brunazzi & Paglianti dynamic liquid hold-up	2.94, 2.95	m^3/m^3
$h_{t,s}$	SRP packed column pre-loading hold-up	2.34, 2.40	m^3/m^3
h_0	Woerlee free falling liquid film thickness	2.120, 2.121	m
H	Packing element height	2.91	m
K, f_w	Wall friction factor	2.52, 2.53, 2.56, 2.79, 2.80, 2.122, 2.123	-
l	Liquid load	2.13	$[m^3/(m^2 \cdot h)]$
L	Liquid mass flow rate	2.60, 2.66	kg/h
L	Liquid mass flow rate	2.4	$lb/(ft^2 \cdot s)$

L	Liquid loading	2.23, 2.24	lb/(ft^2·h)
L_{eq}	Brunazzi & Paglianti channel equivalent length to a single bend pressure drop	2.86, 2.101	m
L'	Lower limit of predicted interval	4.1	-
m	McNulty and Hsieh linear regression factor	2.3	-
m	Spiegel & Meier packing specific factor	2.8, 2.17	-
ΔM_L	Change in liquid mass	3.2	kg
n	Number of measured observations	4.1, 4.3	-
n	Number of generated observations	4.2	-
N_c	Number of flow direction changes in a packing element	2.86, 2.91, 2.101	-
P	Absolute pressure	8.1	Pa
ΔP	Measured pressure drop	3.1, 3.2, 8.2	Pa
ΔP_d	Robbins dry bed pressure drop	2.19, 2.25	in. H_2O/ft
ΔP_{dry}	Stichlmair dry bed pressure drop	2.126, 2.128	Pa
ΔP_{Fl}	Column pressure drop at flooding	2.7	Pa/m
$\Delta P_{irrigated}$	Stichlmair irrigated bed pressure drop	2.128, 2.131, 2.132	Pa
$\Delta P_{preload}$	Delft pre-loading pressure drop	2.41	Pa/m
$\Delta P/\Delta Z$	SRP total column pressure drop	2.36	Pa/m
$(\Delta P/H)_{dry}$	Billet dry bed pressure drop	2.52	Pa/m
$(\Delta P/H)_{irrigated}$	Billet irrigated pressure drop	2.56	Pa/m
$\Delta P_d/\Delta Z$	SRP dry bed pressure drop	2.31, 2.34	Pa/m
Q	Volumetric discharge rate	8.2	m^3/s
r_0	Woerlee hydraulic radius	2.110, 2.112, 2.115, 2.119, 2.120	m

s_E	Residual mean square	4.2, 4.3	-
$s_{\hat{Y}}$	Estimated variance of predicted $\hat{Y}$ for a given X	4.1, 4.2	-
S	Corrugation geometry	2.26, 2.31, 2.35, 2.39, 2.49	m
S_G	Brunazzi & Paglianti channel perimeter wetted by the gas	2.85, 2.88, 2.100, 2.104	m
S_i	Brunazzi & Paglianti interfacial chord	2.100	m
t	Confidence interval	4.1	-
T	Temperature	8.1	K
$u_{G,e}$	Effective vapour velocity	2.31, 2.33, 2.41, 2.83, 2.86, 2.89, 2.101, 2.102	m/s
$u_{G,s}$, u_{SG}, u_G	Superficial vapour velocity	2.1, 2.6, 2.19, 2.33, 2.38, 2.83, 2.110, 2.115, 2.119, 2.126	m/s
u_{int}	Woerlee interface velocity	2.110, 2.112, 2.119	m/s
$u_{L,Fl}$	Billet liquid velocity at flooding	2.67	m/s
u_L	Liquid velocity	2.61, 2.62, 2.63, 2.75, 2.78	$m^3/(m^2 \cdot s)$
$u_{L,e}$	Brunazzi & Paglianti effective liquid velocity	2.102, 2.106	m/s
$u_{L,s}$	Superficial Liquid velocity	2.2, 2.26, 2.37, 2.38, 2.47, 2.94, 2.95	m/s
u_V	Billet vapour velocity	2.59, 2.64	$m^3/(m^2 \cdot s)$
$u_{V,Fl}$	Vapour velocity at flooding	2.59, 2.60, 2.64, 2.65, 2.67, 2.71, 2.75	$m^3/(m^2 \cdot s)$
U'	Upper limit of predicted interval	4.1	-
V, G	Vapour mass flow rate	2.60, 2.66, 8.1	kg/h
w_G'	Effective gas velocity component	2.11, 2.12	m/s
w_L'	Effective liquid velocity component	2.11, 2.13	m/s
X	Flow parameter	2.4	-
X	Measured input variable	4.2	-

X_{ave}	Mean value of X	4.2	-
Y	Capacity parameter	2.5	-
Y	Measured output variable	4.3	-
$\hat{Y}$	Predicted value	4.1, 4.3	-
Z	Packed bed height	2.131, 2.132	m

Greek Symbols	***Description***	***Reference Equation(s)***	***Units***
α	Packing inclination angle	2.110, 2.111, 2.112, 2.114, 2.116, 2.117, 2.118, 2.119, 2.120	degrees
α_0	Effective inclination angle at infinite column diameter	2.118	degrees
σ, σ_L	Liquid surface tension	2.14, 2.30, 2.72	mN/m
δ, h	Liquid film thickness	2.39, 2.43, 2.50, 2.51, 2.105, 2.106, 2.120	m
δ_0	Brunazzi & Paglianti liquid film thickness in absence of gas flow	2.105	m
θ	Corrugation angle	2.26, 2.28, 2.33, 2.37, 2.38, 2.42, 2.44, 2.46, 2.47, 2.48, 2.51, 2.85, 2.94, 2.100, 2.106, 2.107, 2.122, 2.123, 2.124	degrees
μ , μ_L, η_L	Dynamic liquid viscosity	2.12, 2.14, 2.19, 2.26, 2.51, 2.60, 2.61, 2.62, 2.63, 2.66, 2.70, 2.78, 2.94, 2.95, 2.105, 2.106, 2.112, 2.120	Pa·s
μ	Maćkowiak packing specific factor	2.79	-
μ	Ratio of dynamic liquid viscosity to that of water	2.3	-
μ_L	Dynamic liquid viscosity	2.23, 2.24	mPa·s
η_V, μ_G	Dynamic vapour viscosity	2.66, 2.110, 2.120	Pa·s
η_W, μ_W, $\mu_{L,0}$	Dynamic viscosity of water	2.70, 2.95, 2.105	Pa·s

ε	Packing void fraction	2.26, 2.33, 2.37, 2.38, 2.52, 2.53, 2.55, 2.56, 2.57, 2.60, 2.65, 2.71, 2.73, 2.74, 2.78, 2.79, 2.80, 2.93, 2.94, 2.115, 2.117, 2.119, 2.120, 2.122, 2.123, 2.124, 2.126, 2.128, 2.132	-
ρ_L	Liquid density	2.1, 2.2, 2.4, 2.6, 2.26, 2.27, 2.38, 2.51, 2.60, 2.61, 2.62, 2.63, 2.65, 2.66, 2.67, 2.71, 2.72, 2.78, 2.94, 2.106, 2.120, 2.124, 2.125, 2.131, 2.132, 3.1, 8.2	kg/m^3
ρ_L	Liquid density	2.23, 2.24	lb/ft^3
ρ_G	Vapour density	2.1, 2.2, 2.4, 2.6, 2.12, 2.19, 2.27, 2.31, 2.38, 2.41, 2.83, 2.84, 2.86, 2.89, 2.101, 2.107, 2.110, 2.115, 2.119, 2.120, 2.124, 2.125, 2.126	kg/m^3
ρ_G	Vapour density	2.21, 2.22, 2.25	lb/ft^3
ρ_V	Vapour density	2.60, 2.65, 2.66, 2.67, 2.71, 2.72	kg/m^3
ρ_w	Density of water	2.70	kg/m^3
ν	Kinematic liquid viscosity	2.5	mm^2/s
ζ_{GL}	Delft vapour/liquid interaction factor	2.41, 2.42	-
ζ_{GG}	Delft vapour interaction factor between adjacent elements	2.41, 2.44	-
ζ_{DC}	Delft vapour/liquid phases directional change factor	2.41, 2.45	-
φ	Delft fraction of triangular passages occupied by liquid	2.42, 2.44, 2.49	-
ξ_{GL}	Delft vapour/liquid friction factor	2.42, 2.43	-

ξ_{bulk}	Delft bulk zone directional change factor	2.45, 2.46	-
ξ_{wall}	Delft wall zone directional change factor	2.45, 2.47	-
ψ	Delft fraction of vapour channels ending at the wall	2.45, 2.48	-
ψ_0	Billet dry bed resistance coefficient	2.52, 2.54	-
ψ_{Fl}	Billet resistance coefficient at flooding	2.65, 2.66	-
ψ_L	Billet irrigated bed resistance coefficient	2.56, 2.57	-
λ_0	Maćkowiak phase flow ratio at the flooding point	2.73, 2.74, 2.75	-
$\tau_{w,G}$	Brunazzi & Paglianti shear stress at channel wall	2.85, 2.89, 2.100	-
τ_i	Brunazzi & Paglianti interfacial shear stress	2.100	-
Θ	Woerlee relative interface position	2.110, 2.112, 2.119	-
$\psi_{G\text{-}L}$	Woerlee gas/liquid interaction parameter	2.119, 2.120	-
ψ_G	Illiuta & Larachi gas phase dimensionless body force	2.122, 2.123	-
η_e	Illiuta & Larachi packing fractional wetted area	2.122, 2.123, 2.124	-
ψ_L	Illiuta & Larachi liquid phase dimensionless body force	2.123, 2.125	-

Abbreviations	
AARE	Absolute average relative error
HETP	Height equivalent to a theoretical plate
AIChE	American institute for chemical engineers
MOC	Maximum operable capacity
GPDC	General pressure drop correlation charts
PTFE	Polytetrafluoroethylene
MSDS	Material safety data sheet
HAZOP	Hazard and operability procedure
P&ID	Piping and instrumentation diagram
LPG	Liquid petroleum gas
HMI	Human machine interface
PLC	Programmable logic controller
ANN-DA	Artificial neural network and dimensional analysis
ANOVA	Analysis of variance

1 Introduction

The unit operation known as distillation has been around for ages and continues to be the most widely used method of separation in the chemical engineering industry, in spite of its inherently low thermodynamic efficiency [Olujić et al., 2009]. Distillation is used commercially for numerous applications. An important example is where crude oil is cracked and then separated into its multitude of components which are used for either heating, power generation or packaging purposes etc.

Distillation is by no means a mature technology. Energy consumption and over-design of columns is a major concern in the industry due to the lack of accurate mass transfer and hydraulic models, which in turn predicts the column diameter (higher capital costs). It has been proposed that by improving the estimation of the height equivalent to a theoretical plate (HETP), energy - and capital savings of 5 % and 20 % respectively, may be possible [Erasmus, 2004]. Due to the sheer size of distillation related technologies throughout the industrial world the above mentioned savings accumulate to large sums of money. At the AIChE Spring Meeting in 2000 a special panel of experts concluded that there is no real alternative to distillation and that it would still be the key unit operation in 20 years' time. Some replacement unit operations are also expected (hybrid/combined processes) but won't exceed 20% [Spiegel & Meier, 2003].

The most critical research needs for distillation that resulted from the US-Initiative Vision 2020 were the following [Spiegel & Meier, 2003]:

- Improved understanding of physical phenomena
- Better *in situ* sampling
- Analytical and flow-visualisation methods
- Better predictive modelling

This thesis deals with the first and last point of that vision by establishing a facility that can accurately measure the hydraulic capacity of packed columns. Additional measurements will not only help to develop a better understanding of the physical phenomena, but will also assist with the development of better predictive modelling techniques. A brief background overview into the subject of distillation is given in the remainder of this chapter.

1.1 The Distillation Process

Distillation is a process of physically separating a mixture, comprising of components with different boiling points (relative volatilities), into two or more products. This is done by preferentially boiling the more volatile component from the mixture. When a liquid mixture of two volatile components is heated, the vapour leaving the mixture will have a higher concentration of the more volatile component than the liquid from which it was evolved [Kister, 1992].

The distillation process comprises of the following steps:

- A vapour-liquid system is created
- Mass transfer between the phases is facilitated
- The phases are separated

Distillation continues to be the primary method of separation in processing plants, in spite of its low thermodynamic efficiency of roughly 10 % [Kister, 1992; Olujić et al., 2009]. The principles governing the separation process are fundamental and are therefore unlikely to be replaced. In distillation both thermodynamic and hydrodynamic characteristics determine the separation efficiency that can be achieved. Thermodynamic laws govern the maximum possible separation split, while hydrodynamics is related to the study of fluids in motion. There are, however, certain conditions where distillation is not the best separation method. These include the following [Kister, 1992]:

- The difference in volatility between the components is small.
- A small quantity of a high boiling-point component is to be recovered from the feed.
- A compound is thermally unstable even under vacuum conditions.
- The mixture is extremely corrosive and highly fouling.
- Mixtures containing components with a very low volatility.

In an attempt to increase the energy efficiency of distillation columns, new advances have been made by combining column configurations. Some of these are: 1) reactive distillation columns, 2) dividing wall columns and 3) internally heat integrated distillation columns [Olujić et al., 2009].

Mass transfer is known as the net movement of a component from one location in a mixture to another where the component exists in a different concentration. The driving force behind mass transfer is the difference in concentration of the component between the two locations [Seader & Henley, 1998]. In traditional fractionating distillation the vapour rising through the column is enriched by the more volatile component, while the liquid flowing down the column is enriched by the less volatile component. This enrichment

by mass transfer is facilitated by the column internals, which is the subject of the next section.

1.2 Column Internals

Column internals may be classified as either trays or packing and are used in tray - and packed columns respectively. The function of these internals is to provide a large interfacial area for vapour/liquid contact and thus for mass transfer to occur. The difference between tray and packed columns can be described as follow:

- In distillation towers using trays, the contact between vapour and liquid is established by bubbling the vapour through the liquid. Thus, the liquid is the continuous phase and the vapour the dispersed phase.
- In packed columns the packing material provides a large surface area for the liquid to wet and the area between the vapour and liquid phases is provided by liquid films and drops. Thus, the vapour is the continuous phase and the liquid the dispersed phase. However, some authors state that at high enough liquid to vapour ratios phase inversion is possible in a packed column. This means that the liquid is then the continuous phase and the vapour is the dispersed phase [Kister, 1992; Billet, 1999].

A short description of trays will be given below followed by a more detailed description of packing material, which is the focus of this thesis.

1.2.1 Trays

Trays can be divided into three basic types, namely sieve trays, valve trays and bubble-cap trays. Sieve trays comprises of a flat perforated plate. Due to this simplistic design, sieve trays are inexpensive compared to other tray designs. At low vapour flow rates, they suffer from liquid flowing into the holes (weeping), giving them a poor turndown ratio [Kister, 1992]. The turndown ratio is defined as the ratio of the vapour flow rate at the onset of entrainment to the minimum vapour rate when the liquid weeps through the perforations.

Valve trays also consist of a flat perforated plate, but each perforation is equipped with a fixed or movable disk. These disks cover most of the open area and prevent the liquid from weeping at low vapour flow rates giving the valve tray a high turndown ratio. The disks move vertically up and expose more of the hole at higher vapour flow rates [Kister, 1992]. The upper limit of the opening is controlled by the length of the restrictive legs at

the bottom of the valve unit. Valve trays are often preferred above sieve trays because of a high turndown ratio although their cost is 20 % higher than sieve trays [Lockett, 1986].

The third type of tray is the bubble-cap tray. It has the oldest design and was the workhorse of distillation prior to 1960. The bubble-cap tray is a flat perforated plate with risers (pipes) around the holes and caps in the form of inverted cups over the risers. The bubble-cap trays have a unique ability to operate at low vapour and liquid flow rates giving it a high turndown ratio. It should be noted that the cost of bubble-cap trays are about 2-3 times higher than the cost of sieve trays [Lockett, 1986].

Many other high capacity trays are currently available, but since tray columns are not the focus of this thesis, the discussion regarding trays will be limited to the above.

1.2.2 Packing Material

Packing material may be divided into the following three classes:

- ***Random or dumped packing***: This packing consists of discrete pieces of packing of a specific geometrical shape which are randomly packed in a column shell.
- ***Structured packing***: This packing consists of crimped layers of wire-mesh or corrugated sheets which form a distinctive pattern. These sheets consist of triangular corrugated channels arranged in parallel planes. Each parallel plane is placed side-by-side with opposing 45^{o} inclination angles and the gas and liquid is forced into these "closed" flow channels. Additionally, the elements are stacked at alternating 90^{o} angles and inducing sharp directional changes in the two-phase flow [Schultes et. al., 2010].
- ***Grids***: This type of packing is similar to structured packing except, instead of wire-mesh or corrugated sheets an open-lattice structure is used.

Random packing was developed first, followed by structured packing and grids. The two most widely used types are random and structured packing. Grids are limited to primarily heat transfer and wash services [Kister, 1992]. A history of the development of the different packing types is discussed below, followed by selection criteria when to use random and structured packing.

Random Packing:

The development of random packing can be divided into four distinct phases. These distinct phases are also known as generations, where each successive generation improved on its predecessor in terms of hydraulic capacity and the efficiency of the packing (a definition of the hydraulic capacity is given in section 2.1). However, the big improvements in hardware have been made [Spiegel & Meier, 2003] which leads to smaller improvements from successive generations.

The first and second generations consisted mainly of ring and saddle shapes, while the third generation are hybrid ring/saddle shapes [Schultes et. al, 2010]. The ring feature promotes mass transfer and the saddle shape reduces pressure drop. The third generation packing materials have tongues which deliberately promotes droplet formation with the belief of an increased mass transfer rate [Schultes et. al, 2010]. However, this droplet formation leads to a higher pressure drop as well as liquid entrainment at lower gas velocities. This is due to the droplets filling the void spaces between the packing elements and providing additional drag resistance to the rising gas flow [Schultes et. al, 2010]. The fourth generation of packing materials moves away from the ring/saddle and hybrid configurations by using an open, uniform material distribution of sinusoidal waves, as well as multiple contact points. This encourages turbulent liquid film flow and minimised droplet formation [Schultes et. al, 2010].

Random packing is normally classified by its nominal diameter, the void fraction (% free space), specific area, specific weight and specific type of packing. Random packing is known to perform better than structured packing at higher liquid rates (> 45 $m^3/(m^2 \cdot h)$) and at higher pressures (> 14 bar) [Kister, 1992]. Cheap plastic random packing material is commonly used in scrubbers to remove CO_2 from process lines as part of CO_2 sequestration.

Table 1.1 presents some of the well-known designs of the different random packing generations [Kister, 1992; Schultes et. al., 2010]:

Table 1.1: Different random packing generation examples

First generation (1895-1950s)	*Second generation (1950s-1970s)*	*Third generation (1970s-late 1990s)*	*Fourth Generation (late 1990s-present)*
Raschig Ring	Intalox® Saddle	IMTP®	Raschig Super Ring
Lessing Ring	Super Intalox® packing	CMR®	Intalox® Ultra™
Berl Saddle	Pall® Ring	Levapak	
	Hy-Pak packing	Nutter Rings™	
		FLEXIMAC™	
		Hiflow® Ring	
		Intalox® Snowflake	

Structured Packing:

During the evolution of random packing, a need for high efficiency packing with an extremely low pressure drop per theoretical stage arose. This led to the development of structured packing [Billet, 1995]. As for random packing, structured packing also evolved through four generations of distinct different packing.

The first two generations of structured packing were manufactured from wire gauze and were expensive compared to random packing. The third generation of structured packing, which was manufactured from sheet metal, revolutionised the packing industry. With a high capacity, lower cost, and lower sensitivity to solids, while retaining a high efficiency, these corrugated sheet packing types became highly competitive with conventional internals [Kister, 1992].

The sharp directional changes in flow between the element interfaces lead to restrictive forces that affect both capacity and pressure drop. Thus, the third generation packing types were modified into high capacity types (HC™) to overcome premature flooding at the loading point and can be viewed as a fourth generation. These packings are characterised by bending one or both ends of the corrugated channels from 45^{o} to 0^{o} on the vertical axis at the packing interface [Schultes et. al, 2010]. Lastly, fluid dynamic investigations have led to new generation (still classified as 4^{th}) that incorporates a regular sequence of waves above and below the plain of the metal sheet at 45^{o} angle of orientation (Raschig Super-Pak). The adjacent sheets are assembled side-by-side with opposing inclination waves to form a layer [Schultes et. al, 2010].

Structured packing is normally classified by its void fraction, specific area and specific type of packing. Other characteristics are crimp - and element geometry as well as surface features. Structured packing is known to perform better than random packing at low liquid rates (< 45 $m^3/(m^2 \cdot h)$) and at vacuum and atmospheric pressures.

Table 1.2 presents some of the well-known designs of the different structured packing generations [Kister, 1992; Schultes et. al, 2010]:

Table 1.2: Examples of different structured packing generation

First generation (1940s-1950s)	*Second generation (1950s-1970s)*	*Third generation (1970s- late 1990s)*	*Fourth Generation (late 1990s-present)*
Panapak	Goodloe®	Sulzer Mellapak®	Mellapakplus®
	Hyperfil®	Koch Flexipac®	Sulzer Optiflow®
	Sulzer, Koch BX	Montzpak-B®	Flexiapk®HC™
		Gempak®	Montz-PakM®
			Raschig Super-Pak

There are certain scenarios where packed columns are favoured over tray columns. According to Kister [1992], these include:

- Vacuum systems
- Low-pressure-drop applications
- Vacuum column revamps
- Small-diameter columns
- Corrosive systems
- Foaming as well as emulsion systems
- Systems where low liquid hold-up is required
- Batch distillation

Structured packing is known to perform poorly in aqueous systems and can be attributed to poor wetting due to a high surface tension. Also, the poor performance in systems with high viscosity is not yet fully understood [Erasmus, 2004]. Whilst packing has its advantages, there are still scenarios where tray columns are preferred over packed columns. According to Kister [1992], these include:

- Solids present in feed
- High liquid rates
- Large diameter columns
- Complex columns
- Feed composition variation
- Chemical reaction/absorption

Most of the above scenarios are based on practical considerations. The most concerning fact is that trays are sometimes favoured above packing based purely on the uncertainty in predicting the performance of packing [Erasmus, 2004]. This problem is more severe in structured packing than in random packing, and even in 2010 it still tends to be a problem.

1.3 Modelling of distillation and absorption

In order to utilize the advantages that modern column internals offer, accurate mathematical models are required to predict their efficiency and capacity. There are two general types of models that are used in the modelling of distillation and absorption equipment [Seader & Henley, 1998]. These two models are the equilibrium model and the non-equilibrium model, the latter also known as the rate-based approach.

The equilibrium model has been used for almost a century and this model is based on the two-film theory that was suggested by Lewis & Whitman in the 1920s. This model divides a

column into a number of stages that are in thermodynamic equilibrium. This means that the liquid and vapour leaving such a stage is in equilibrium. HETP (Height Equivalent to a Theoretical Plate) is a convenient way of expressing equilibrium stage calculations for packed columns yet this method lacks a sound theoretical basis [Seader & Henley, 1998]. On the other hand tray efficiencies are used to link these theoretical stages to real trays or beds of packing in columns. While these concepts are adequate in describing binary mixtures, they are extremely confusing to use in multi-component mixtures [Kister, 1992].

The non-equilibrium model or rate-based approach was developed due to the limitations of the equilibrium model in multi-component and non-ideal systems [Krishnamurthy & Taylor, 1985]. This model assumes thermodynamic equilibrium only between the interface of the vapour and liquid phases. Rate equations govern the rate at which mass and heat is transferred from the interface to the bulk of the liquid and vapour phases leaving the non-equilibrium stage [Kister, 1992]. This model is by no means an exact model and still requires a considerable amount of further development.

Since no exact models are available at present, simplified mass transfer - and hydraulic models are used to predict the capacity and efficiency of column internals. A large database of correlations and semi-empirical models is available for random packing. Structured packing offers significant advantages over random packing in certain applications, but there seems to be a lack of accurate efficiency models for structured packing [Erasmus, 2004; Fair et al., 2000]. Erasmus [2004] concluded that not one of the models could accurately predict all of the parameters associated with the hydraulic capacity of the structured packing he investigated.

With the concept of hydraulic capacity in mind, a new concept of hydrodynamics is introduced, as described in the next section.

1.4 Hydrodynamics

For both equilibrium and rate-based simulations it is of utmost importance to know the hydraulic capacity of the packing, as it determines the diameter of the column [Schultes et. al, 2010]. The hydraulic capacity is defined as the region of operability in a column and is characterised by the pressure drop over the column, as well as the liquid hold-up within the column. Other characteristics include entrainment, maximum operable capacity, loading - and flooding point. A more detailed description will be given in section 2.1.

The column diameter is calculated after determining the flow rates and the compositions in the column for an equilibrium simulation. With a rate-based simulation, the diameter of the column is an input to the model [Kister, 1992]. Thus, the modelling of the hydraulic capacity is extremely important if an accurate and reliable rate-based simulation is desired.

In earlier years, the lack of computing power and the need for vast number of system specific variables has led to only a few rate-based models being implemented with limited success. Also, within the loading region (detailed description given in literature review) there is an in increase in the HETP of a column. This is why it is advised to design columns to operate at 80 % of their capacity at flooding [Billet, 1999]. This confirms the importance of being able to predict the hydraulic capacity of packed columns.

A large amount of research was done during 1960-2000 in the field of hydrodynamics, with significant contributions in the modelling of both structured - and randomly packed columns. From 2000 onwards little or no new models have surfaced in the field of structured and randomly packed column hydrodynamic modelling. An exception on the above statement is the general model by Maćkowiak [2009] which can predict pressure drop for random and structured packing under the influence of single phase flow (more on this in section 2.3.1).

Some of the more recent hydrodynamic models related to random - and structured packing have been developed by Bravo et al. [1985], Stichlmair et al. [1989], Maćkowiak [1990; 1991; 2009], Kister & Gill [1991], Robbins [1991], Spiegel & Meier [1992], Rocha et al. [1993], Olujic et al. [1997; 1999; 1999], Brunazzi & Paglianti [1997], Verschoof et al. [1999], Billet & Schultes [1999], Piché et al [2001; 2001], Woerlee et al. [2001], Ranke et al. [2001] and finally Illiuta et al. [2001]. The prediction parameters of the above mentioned models can be found in Table 2.11. Many of these hydraulic models were derived from either 1) a range of system-specific experiments, 2) a pooled database of industrial data or 3) a limited range of application. With a pooled database, experimental errors could have a significant effect on the reliability of the data used in the modelling approaches.

Erasmus [2004] concluded that the structured packing models investigated from the literature predicted a conservative dependency on liquid viscosity with regards to column pressure drop and liquid hold-up. This creates an opportunity for future research and sets the scene for this project.

1.5 Project Rationale

Based on the above introduction the following aspects support the rationale behind the project:

- Small improvements in the accuracy of the estimation of the HETP can lead to large energy and capital savings due to the critical role that separation processes plays in the processing industry.
- Improvements in the HETP can be made by accurately predicting the mass transfer of the system and/or by accurately predicting the pressure drop and

liquid hold-up of a packed column system (as there is an increase in the HETP in the loading region).

- A few reliable models exist that predict the hydraulic capacity of structured packing. However, these models do not fully incorporate the effect of liquid viscosity and other physical properties.

- Structured and random packing has major advantages over tray columns in certain applications, thus it is necessary to be able to accurately measure the capacity of new random and structured packing materials. Such data can be used to extend the ranges and accuracy of existing models.

Thus, from the above it follows that large savings in terms of energy- and capital cost can be made if accurate models exist in the prediction of the capacity and efficiency of both random and structured packing. It can be reasoned as follow: the savings are directly related to the HETP of the column which in turn is related to the mass transfer occurring in the system. The HETP of a column determines the column diameter and height of a specific system. The mass transfer can be improved by optimizing the efficiency of the packing and by accurately predicting the different hydrodynamic regions of operability.

Reduction CO_2 emission is one of the major concerns in the industry today, and thus many process plants are exploring/implementing CO_2 sequestration options. To meet the goal of optimised CO_2 capture, modern packings with the following characteristics are required: high capacity, high mass transfer efficiency and low pressure drop [Schultes et. al, 2010]. Therefore it is necessary to be able to measure the hydraulic capacity of new packing materials accurately, as well as being able to predict their hydrodynamic/efficiency parameters.

1.6 Objectives

The aim of this project was to establish a facility that can measure the hydraulic capacity of both random and structured packing accurately. This has been achieved by accomplishing the following goals:

- Conduct a literature survey on current literature to gain insight into the field of hydrodynamics of packed columns.

- Design and construct a setup that can accurately measure the hydraulic capacity of both random and structured packing over a range of liquid and gas flow rates. The setup should be able to give visual insight into the classification of the three hydraulic operating regimes. Also, the setup should be able to investigate the influence of physical liquid and gas properties on

the pressure drop, liquid hold-up and entrainment on packing material. This is necessary for future research and will be covered in the literature review.

- The experimental setup should be commissioned with an air/water system and the accuracy of the results compared to a viable random packing predictive model(s).
- Measure the pressure drop and liquid hold-up of 1.5" Intalox® Ultra™. These characteristics should be measured with an air/water system with liquid ranges of 6 - 122 $m^3/(m^2 \cdot h)$. The vapour flow rates should cover the full hydraulic range of the packing (e.g. pre-loading, loading and flooding region).
- Compare the experimental data on 1.5" Intalox® Ultra™ to comparable older generations of random packing (1.5" Pall® Rings and IMTP® 40).
- Make meaningful conclusions on the data gathered and provide suggestions on the continuation of the current project.

The following objectives are beyond the scope of the project and are subject to future research:

- Measure the entrainment during experimental runs.
- Test the influence of viscosity and other liquid and gas properties on the hydraulic capacity of structured packing.
- Develop new correlations or improved modification of the existing correlations.

1.7 Plan of Development

The structure of the thesis is as follow:

A thorough literature review on the subject: Hydraulic capacity of random and structured packing follows in Chapter 2. The design and construction of the experimental setup is discussed in Chapter 3. Data validation and the experimental results obtained are discussed in Chapter 4. Next, conclusions are drawn regarding the results and given in Chapter 5. Finally, recommendations for future projects are made in Chapter 6.

2 Literature Review

The literature review consists of a basic introduction to the key terminology used in most of the literature. This facilitates a better understanding of them when they are used in the literature review. Next, the methods by which the hydraulic capacity of random and structured packing is predicted are discussed. These methods are subdivided into two categories, namely capacity charts and empirical correlations. Each one of these methods will be discussed with regard to their range of operability, strengths and weaknesses. Finally, conclusions are drawn on the literature review and the research strategy is defined.

It should be noted that since the facility is able to measure data for both random and structured packing, both packing-type models are covered in the literature review. Lastly, based on the strengths and weaknesses of the respective models reviewed throughout the literature review, the most appropriate model(s) are chosen to verify the experimental data against.

2.1 Key Theoretical Concepts

The capacity of a packed column is determined by its effective cross-sectional area open to vapour flow. Normally, a column will be designed to operate at the highest economical pressure drop to ensure good liquid- and gas distribution [Coulsen & Richardson, 1999]. Before the methods predicting the hydraulic capacity are discussed, a few concepts relating to the hydraulic capacity of structured packing need to be clarified. Two key concepts are the pressure drop over the packed column and the liquid hold-up. The pressure drop over the packed column is self-explanatory, but the liquid hold-up needs to be defined. The liquid hold-up is defined as the amount of liquid that is retained (held back) in the packing material after the liquid feed to the column has been cut [Kister, 1992]. Both these factors are influenced by the superficial vapour velocity and can be better understood by viewing Figure 2.1 and Figure 2.2.

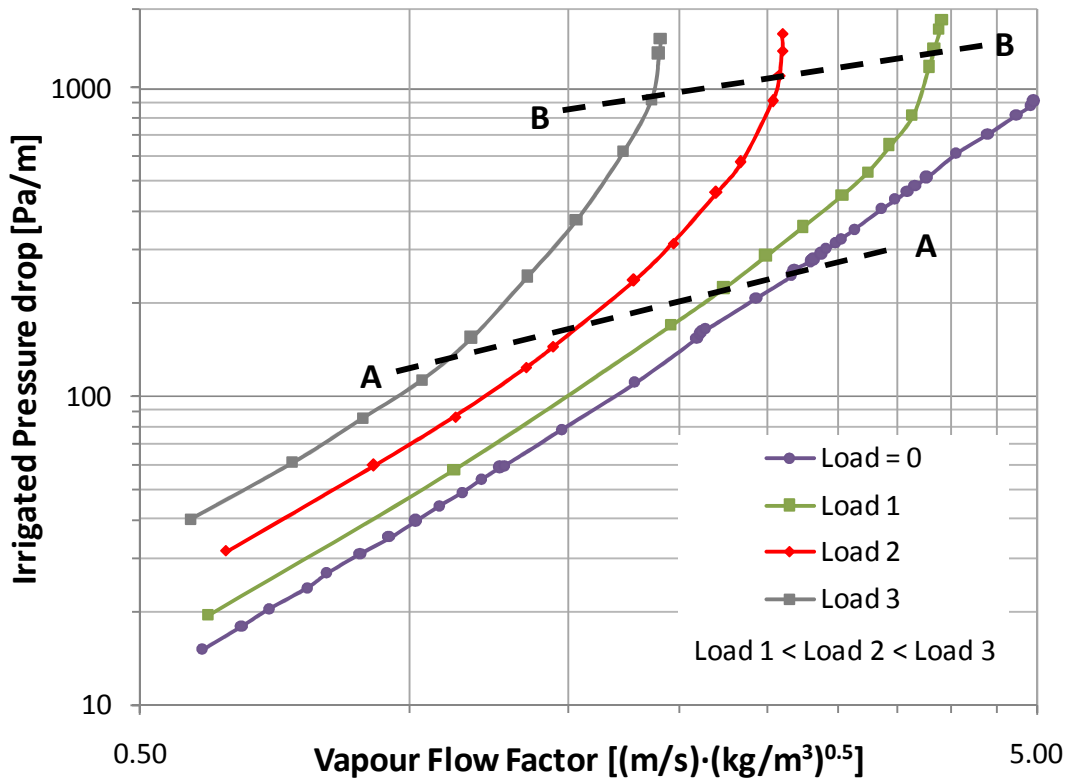

Figure 2.1: Irrigated pressure drop vs. Vapour flow factor

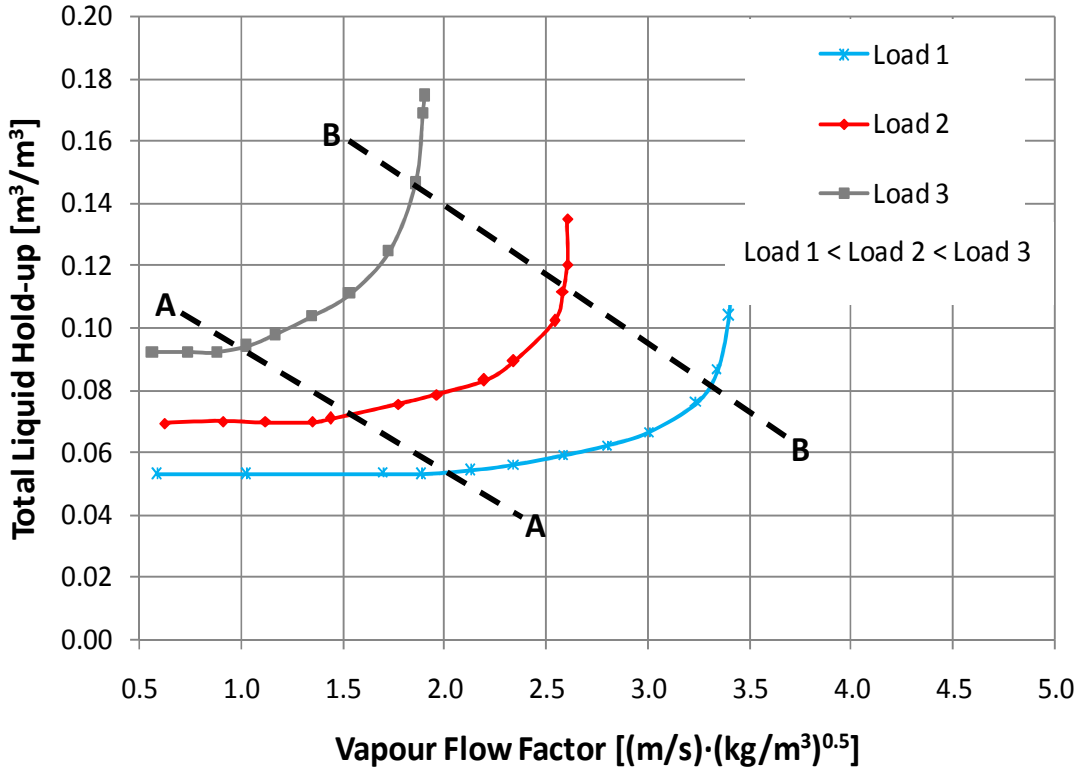

Figure 2.2: Liquid hold-up vs. Vapour flow factor

The values in the figures are used for explanatory purposes only and are generated from measured data. The typical pressure drop over a packed bed as a function of vapour flow factor is represented in Figure 2.1. Figure 2.2 represents a typical liquid hold-up profile for the same system and liquid loads. The vapour flow factor is a convenient way to describe the gas flow rate in a packed column that is adjusted for the density of the gas (as defined in the glossary). Figure 2.1's axes are log based to assist with interpolation between the pressure drop data points.

From the two figures above, three distinct regions can be identified and will be discussed accordingly. It should be noted that the total column hold-up is comprised of two contributing terms, namely the static hold-up and the dynamic hold-up. The dynamic hold-up is defined as the liquid that freely drains from a packed bed after the feed to the column has been cut off, and the static hold-up is defined as the remaining liquid in the packed bed after the bed has been allowed to drain for a prolonged time interval.

Other factors found throughout the literature that contribute to the hydraulic capacity are entrainment and the maximum operational capacity (MOC). Entrainment data in packed columns is hard to come across while flood point data are in abundance. According to Kister [1992], the MOC is defined as the "Maximum vapour rate that provides normal efficiency of a packing". Although this is a clear-cut definition, locating it is difficult and leaves much room for subjectivity due to the fact that accurate efficiency as well as pressure drop and liquid hold-up data is required [Kister, 1992].

Based on the discussion above the hydraulic capacity in this thesis is defined in terms of liquid hold-up and pressure drop only.

2.1.1 Pressure Drop Curve

Figure 2.1 shows that the pressure drop curve at a specific liquid load is parallel to the pressure drop curve of the dry packing up to a certain vapour flow factor (below line A-A). Beyond this point the pressure drop increases rapidly with an increase in vapour flow factor (between line A-A and B-B). Above line B-B, the pressure drop tends to infinity with a small increase in vapour flow factor.

2.1.2 Liquid Hold-up Curve

Figure 2.2 shows that the liquid hold-up, at a specific liquid load, is independent of the vapour flow factor up to a certain point (line A-A). Up to this point the liquid hold-up is only a function of liquid flow rate and liquid physical properties. Beyond this point an increase in the vapour flow rate would lead to an increase in the liquid hold-up until line B-B is reached. Beyond this point the liquid hold-up tends to infinity with an increase in

vapour flow factor. It should be noted that these regions coincide with the regions seen on the pressure drop curve.

Based on the above discussions, the three regions of operability can be defined. An on-going debate on the exact definition of these regions is evident throughout the literature, specifically with regards to the "flooding point" or onset of flooding conditions. Some of the industrial packing material suppliers don't even use the term, flooding point, due to its subjectivity. However, these regions are best described by the work of Billet & Schultes [1991; 1993; 1995] and Kister [1992]:

- The pre-loading region: This is the region in both figures before line A-A is reached. In this region the pressure drop of the packed bed is parallel to the dry bed pressure drop and thus the liquid hold-up is independent of the vapour flow factor and only dependent on the liquid load and liquid properties.

- The loading region: This is the region on both figures between lines A-A and B-B. In this region the pressure drop and liquid hold-up in the packed bed are functions of the vapour flow (the pressure drop trend deviates from the dry bed pressure drop). The point where the pressure drop as well as the liquid hold-up starts to be influenced by the vapour flow factor is known as the loading point (represented by line A-A). The point where the pressure drop as well as the liquid hold-up tends to infinity is known as the flooding point (represented by line B-B). According to Billet & Schultes [1995], the free cross-section for the gas flow is reduced by the column hold-up in this region. He also states that the shear forces between gas and liquid increases to a point where it is able to suspend the liquid in the column. Thus, the sharp increase in both pressure drop and liquid hold-up is noted.

- The flooding region: At and beyond the flooding point the vapour flow rate is large enough to prevent the liquid from flowing down the column. Also, according to Billet & Schultes [1995], the shear forces between the gas and liquid are larger than the gravitational force working in on the liquid and thus it is said that the liquid is entrained.

The hydraulic operating regime is closely related to the mass transfer efficiency of random and structured packing. Normally there is a gradual increase in the efficiency with an increase in liquid- and vapour flow rates. There is a sharp increase in efficiency in the loading region, followed by a sharp decrease in the efficiency as the flooding point is approached [Kister, 1992].

Based on the above discussion it is therefore extremely important to be able to predict the loading - and flooding point. There are two general methods where these parameters are predicted and they are discussed below. The first is empirical correlations and capacity charts and the second method is semi-theoretical modelling.

2.2 Empirical Correlations and Capacity charts

The following section is based on the work by Erasmus [2004] and Kister [1992], and is subdivided into sections of some of the researchers who made significant contributions (or modifications) to the empirical correlations and capacity charts in the literature.

Although empirical correlations and capacity charts have the advantage of being simple, they lack the ability to predict the liquid hold-up. For a given pressure drop, they only supply data on the liquid- and vapour flow rates [Kister, 1992]. The well-known GPDC charts (Generalized Pressure Drop Correlation) have been around for decades assisting with the design of random packing columns. This chart was initially developed by Sherwood et al. [1938] and was later modified by Lobo et al. [1945]. The chart initially consisted of a single curve that predicted packing flood points. Later on, Leva [1954] added curves onto the chart to predict packing pressure drop whilst still retaining the flood point curve. Eckert [1975] omitted the flood curve and only retained the pressure drop curve. Finally, Eckert's version was changed by Strigle [1994] to a semi-log plot to make interpolation between pressure drop curves easier.

The GPDC chart ordinate describes the balance between the vapour momentum force and the abscissa the ratio of liquid kinetic energy to the vapour kinetic energy [Kister, 1992]. The GPDC gives accurate predictions with aqueous systems, but deviates with average absolute errors of 60 % with non-aqueous systems [Heymes et al., 2006].

The following subsection describes the more recent modifications to the GPDC charts and/or empirical correlations derived from it.

2.2.1 McNulty and Hsieh

The first comprehensive structured packing study was done by McNulty & Hsieh and they also documented the history of modifications to the GPDC [McNulty & Hsieh, 1982]. The hydraulic performance and efficiency of the Flexipac range of structured packing was measured and characterised in a 0.91 m diameter column. The system used was air and water at ambient conditions. The GPDC method for random packing was found to be inadequate to predict the capacity and pressure drop of the Flexipac structured packing range.

They proposed the "CGCL" method to predict the flooding point of the structured packing that was investigated. This method uses capacity factors C_G and C_L to correlate the density and velocity dependence of pressure drop and flooding. However, viscosity and surface tension influences were not investigated at first. Efficiency tests were performed and showed that there was an increase in the efficiency if the liquid flow rate was increased due to the better spreading and wetting behaviour of structured packing at higher liquid flow rates. Up to a certain point, the efficiency was found to be moderately independent of the superficial vapour flow rate. Beyond this point the efficiency decreased sharply, thus this point was called the maximum design vapour velocity. This was found to be at approximately 80% of the flooding vapour flow rate. The capacity factor for the vapour- and liquid phase can be defined as follow:

$$C_G = u_{G,s}\sqrt{\frac{\rho_G}{\rho_L - \rho_G}} \qquad 2.1$$

$$C_L = u_{L,s}\sqrt{\frac{\rho_L}{\rho_L - \rho_G}} \qquad 2.2$$

The flood point correlation is as follow:

$$\left(\frac{C_G}{f}\right)^{1/2} + m \cdot C_L^{1/2} = \frac{c}{\mu^{0.03}} \qquad 2.3$$

Where:

m and c are taken from linear regression analysis of the data [McNulty & Hsieh, 1982].
f is the fraction of flooding (ratio of vapour flow factor to flooding vapour flow factor)
μ is the ratio of dynamic viscosity of the liquid to that of water [1 mPa·s]

The attempt by McNulty & Hsieh to apply the GPDC chart to structured packing was only partially successful [Erasmus, 2004].

2.2.2 Kister and Gill

Kister & Gill [1991] identified the limitations of the GPDC charts and proposed the following modifications to be made to include structured packing (in addition to the efforts of McNulty & Hsieh).

The abscissa is the flow parameter and is determined as follow:

$$X = \frac{L}{G}\left(\frac{\rho_G}{\rho_L}\right)^{1/2} \qquad 2.4$$

The ordinate is the capacity parameter and is determined as follow:

$$Y = C_S \cdot F_P^{0.5} \cdot v^{0.05} \quad 2.5$$

$$C_S = u_{G,s}\sqrt{\frac{\rho_G}{\rho_L - \rho_G}} \quad 2.6$$

Where:

F_p is an empirical factor that characterises the packing shape and size

C_S is the superficial vapour velocity corrected for density

v is the kinematic liquid viscosity (mm^2/s)

The proposed chart is called the GPDC (SP) interpolation chart and makes it possible to interpolate between the experimental values in operating regions where data is available. They also stated that all the pressure drop data has an accuracy of 15 %. Lastly, they correlated the pressure drop at flooding for a wide range of 2nd and 3rd generation random and structured packing materials in the form of the following equation:

$$\Delta P_{Fl} = 0.115 F_P^{0.7} \quad 2.7$$

This states that the pressure drop at flooding is a function of the packing factor alone. The packing factors are readily found throughout the literature. Kister [1992] states that the weak link in the correlation is the packing pressure drop prediction. Inaccurate pressure drop predictions will in turn result in inaccurate flood point predictions. Thus, he recommends that equation 2.7 be used with interpolated pressure drop data instead of predicted values.

2.2.3 Spiegel and Meier

Spiegel & Meier [1987] characterised the capacity of the Mellapak structured packing range. Their experimental setup consisted of chloro-/ethylbenzene and trans-/cis-decalin test mixtures at total reflux in a 1 m internal diameter column. Their results were plotted on both a Souders and a Wallis diagram (see glossary for definitions). This could be correlated in the following equation and could predict the capacity with an accuracy of 6 percent:

$$C_G^{1/2} + m \cdot C_L^{1/2} = c \quad 2.8$$

Where:

m and c are adjustable constants specific to each type of packing material

Initially, they also developed a pressure drop correlation which was valid for the 4 Mellapak types for liquid loads below 20 $m^3/(m^2 \cdot h)$ with an accuracy of about 10 % [Spiegel & Meier, 1987]. This model was later extended to a range of liquid loads up to 200 $m^3/(m^2 \cdot h)$ in an air/water system [Spiegel & Meier, 1992].

The pressure drop model consisted of 2 regions, namely 1) a region where the wet bed pressure drop is parallel to the dry bed pressure drop and, 2) the wet bed pressure drop increases with a larger slope than the dry bed pressure drop. The regions are based on the 45 % capacity and 100 % capacity limit as calculated by equation 2.8 with a pressure drop at flooding equal to 1200 Pa/m. The equations governing the model could be described as follow:

Wet Bed Pressure Drop in Region 1:

$$\frac{dP}{dz} = f_1 \cdot f_2 \left(\frac{dP}{dz} \right)_0 \qquad 2.9$$

$$f_1 = \left(1 - h_{L,s}\right)^{-2.5} \qquad 2.10$$

$$f_2 = \left(\frac{w_L' + w_G'}{w_G'} \right)^{1.8} \qquad 2.11$$

Where:

w_G' and w_L' are the effective vertical velocity components of the two phases

The subscript, 0, referring to the dry bed pressure drop

$$w_G' = \frac{F_V}{\left(\rho_G \cdot 0.5\left(1 - h_{L,s}\right)\right)} \qquad 2.12$$

$$w_L' = \frac{l}{\left(3600 h_{L,s}\right)} \qquad 2.13$$

Where:

$h_{L,s}$ is the liquid hold-up and is proportional to $0.25 \cdot \mu_L$

μ_L is the liquid dynamic viscosity [mPa·s]

F_V is the vapour flow factor [(m/s)·(kg/m^3)]

l is the liquid load [$m^3/(m^2 \cdot h)$]

Above liquid loads of 100 $m^3/(m^2 \cdot h)$ another correction factor f_3 (and is incorporated into eq. 2.9) is required. This factor is plotted against the transformed liquid hold-up:

$$h_L^{\ *} = \frac{\left(h_{L,s} \cdot \sigma^{0.8}\right)}{\left(a_i^{0.75} \cdot \mu_L^{0.25}\right)} \qquad 2.14$$

Where:

σ is the liquid surface tension [mN/m]

a_i is the geometric surface area [m^2/m^3]

μ_L is the dynamic liquid viscosity [mPa·s]

For values of $h_L^{\ *} < 0.0046$, f_3 is unity and for values of $h_L^{\ *} > 0.0046$ the f_3 is calculated by a linear function fitted to the data that can be found in Spiegel & Meier [1992].

Wet Bed Pressure Drop in Region 2:

A cubic polynomial describes the pressure drop curve in this region:

$$\log\left(\frac{dP}{dz}\right) = ax^3 + cx + d \qquad 2.15$$

$$x = \frac{\left(\log\left(F_V \middle/ F_{V,\max}\right) - \log(0.45)\right)}{-\log(0.45)} \qquad 2.16$$

$$a = \log(12) - m - \log\left(\frac{dP}{dz}\right)_A \qquad 2.17$$

$$d = \log\left(\frac{dP}{dz}\right)_A \qquad 2.18$$

Where:

$F_{v,max}$ is the F factor at 100 % capacity

The subscript, A, refers to the 45 % capacity point

$c = m$ in equation 2.8

The accuracy over the entire range is said to be within 20 %. However, it can be seen that this model is only suitable for the Mellapak structured packing types and is heavily empirical.

2.2.4 Robbins

Robbins [1991] derived an equation to predict the pressure drop for random and structured packing materials. It was based on the work of Leva [1954] that modified the dry bed pressure drop for irrigation to give:

$$\Delta P_d = C_0 \cdot 10^{(C_1 \cdot \mu_L)} \cdot \rho_G \cdot u_{G,s}^2 \qquad 2.19$$

This model was only applicable for gas-continuous operation. At low liquid loading, the pressure drop depends only on the superficial vapour flow rate and the geometry of the

packing. Robbins [1991] found that C_0 correlates directly to the packing factor and that C_1 correlates well to the square root of the packing factor and the liquid viscosity raised to the 0.1th power. This led to a new generalised pressure drop equation in the form of:

$$\Delta P = C_3 \cdot G_f^2 \cdot 10^{(C_4 \cdot L_f)} + 0.4\left(\frac{L_f}{20000}\right)^{0.1} \cdot \left(C_3 \cdot G_f^2 \cdot 10^{(C_4 \cdot L_f)}\right)^4 \qquad 2.20$$

$$G_f = G\left[\frac{0.075}{\rho_G}\right]^{0.5} \cdot \left[\frac{F_{pd}}{20}\right]^{0.5} \qquad \text{for P} \leq 1 \text{ atm} \qquad 2.21$$

$$G_f = G\left[\frac{0.075}{\rho_G}\right]^{0.5} \cdot \left[\frac{F_{pd}}{20}\right]^{0.5} \cdot 10^{(0.3 \cdot \rho_G)} \qquad \text{for P} \geq 1 \text{ atm} \qquad 2.22$$

$$L_f = L\left[\frac{62.4}{\rho_L}\right] \cdot \left[\frac{F_{pd}}{20}\right]^{0.5} \cdot \mu_L^{0.1} \qquad \text{for } F_{pd} \geq 15 \qquad 2.23$$

$$L_f = L\left[\frac{62.4}{\rho_L}\right] \cdot \left[\frac{20}{F_{pd}}\right]^{0.5} \cdot \mu_L^{0.1} \qquad \text{for } F_{pd} \leq 15 \qquad 2.24$$

Equation 2.20 can be reduced to the following dry bed pressure drop at atmospheric conditions [Kister, 1992]:

$$\Delta P_d = 0.00375 C_3 \cdot F_{pd}\left(\frac{G^2}{\rho_G}\right) \qquad 2.25$$

Where:

C_0 and C_1 are constants that characterises the packing shape and size

C_3 = 7.4 x 10^{-8}

C_4 = 2.7 x 10^{-5}

ΔP is the packing specific pressure drop [in. H_2O/ft packing]

ΔP_d is the dry bed packing specific pressure drop [in. H_2O/ft packing]

ρ_G is the gas density [lb/ft^3]

F_{pd} is the dry bed packing factor

ρ_L is the liquid density [lb/ft^3]

μ_L is the liquid dynamic viscosity [mPa·s]

G is the gas loading [lb/(ft^2·h)]

L is the liquid loading [lb/(ft^2·h)]

However, caution is required when using the above model as it has only been extensively tested on air/water systems. It was also concluded that this model should not be used at pressures above atmospheric as limited data above atmospheric pressures were used in the verification of the model [Kister, 1992].

2.3 Semi-theoretical Modelling

Quite a number of semi-theoretical models for random - and structured packing have been published. These models are in the form of equations and correlations that can be implemented into numerical solutions [Erasmus, 2004]. Semi-theoretical models can be subdivided into two categories, namely channel models and particle - or porous bed models. The aim of this section is to give a better understanding on the different models used, as well as their respective strengths and weaknesses.

Table 2.1 presents all the dimensionless numbers required in all the respective model calculations:

Table 2.1: Dimensionless numbers used in all the different modelling approaches

Dimensionless Number	*Definition*	*Calculation*
SRP Liquid Froude Number ($Fr_{L,S}$)	Ratio of the inertia and gravity forces	$\frac{u_{l,s}{}^2}{S \cdot g}$
SRP Gas phase Reynolds Number ($Re_{G,S}$)	Ratio of inertia and viscous forces	$\mathrm{Re}_{G,s} = \frac{u_{G,s} \cdot S \cdot \rho_G}{\mu_G}$
SRP Liquid phase Reynolds Number ($Re_{L,S}$)	Ratio of inertia and viscous forces	$\mathrm{Re}_{L,s} = \frac{u_{L,s} \cdot S \cdot \rho_L}{\mu_L}$
SRP Liquid Weber Number ($We_{L,S}$)	Ratio of inertia and surface tension forces	$We_{L,s} = \frac{u_{L,s}^2 \cdot S \cdot \rho_L}{\sigma}$
Delft Effective Gas phase Reynolds Number ($Re_{G,e}$)	Ratio of inertia and viscous forces	$\mathrm{Re}_{G,e} = \frac{\left(u_{G,e} + u_{L,e}\right) \cdot d_{hG} \cdot \rho_G}{\mu_G}$
Billet Gas phase Reynolds Number (Re_V)	Ratio of inertia and viscous forces	$\mathrm{Re}_V = \frac{u_V \cdot d_p}{(1-\varepsilon)\nu_G} \cdot K$
Billet Liquid Froude Number (Fr_L)	Ratio of the inertia and gravity forces	$Fr_L = \frac{u_L^2 \cdot a}{g}$
Billet Liquid Reynolds Number (Re_L)	Ratio of inertia and viscous forces	$\mathrm{Re}_L = \frac{u_L \cdot \rho_L}{a \cdot \eta_L}$
Maćkowiak Liquid Reynolds Number ($Re_{L,M}$)	Ratio of inertia and viscous forces	$\mathrm{Re}_{L,M} = \frac{u_L \cdot \rho_L}{a \cdot \mu_L}$

Table 2.1 continued

Brunazzi Gas Phase Reynolds Number (Re_G)	Ratio of inertia and viscous forces	$\mathrm{Re}_G = \frac{u_{G,e} \cdot \rho_G \cdot d_G}{\mu_G}$
Brunazzi Liquid Phase Weber Number (We_L)	Ratio of inertia and surface tension forces	$We_L = \frac{\rho_L \cdot u_{L,e} \cdot 4\delta}{\sigma_L}$
Brunazzi Liquid Phase Bond Number (Bo_L)	Ratio of gravitational and surface tension forces	$Bo_L = \frac{(4\delta)^2 \cdot g(\rho_L - \rho_G)}{\sigma_L}$
Woerlee Gas Phase Reynolds Number ($Re_{G,W}$)	Ratio of inertia and viscous forces	$\mathrm{Re}_{G,W} = \frac{\rho_G \left\lvert \left(\frac{u_{SG}}{\varepsilon \cdot \theta^2 \cdot \cos\alpha} \right) \right\rvert \cdot 2\theta \cdot r_0}{\mu_{SG}}$
Woerlee Liquid Phase Reynolds Number ($Re_{L,W}$)	Ratio of inertia and viscous forces	$\mathrm{Re}_{G,W} = \frac{4\rho_L \cdot u_{SL}}{\mu_L \cdot a}$
Woerlee Galileo Packing Number (Ga_p)	Ratio of gravity and viscous forces	$Ga_p = \frac{4\Delta\rho \cdot \rho_L \cdot g \cdot \cos\alpha}{3\mu_L^2 \cdot a^3}$
Illiuta Gas Phase Reynolds Number ($Re_{G,I}$)	Ratio of inertia and viscous forces	$\mathrm{Re}_{G,I} = \frac{u_{G,s} \cdot \rho_G \cdot d_e}{\mu_G}$
Illiuta Gas Phase Galileo Number ($Ga_{G,I}$)	Ratio of gravity and viscous forces	$Ga_{G,I} = \frac{d_e^3 \cdot g \cdot \rho_G^2}{\mu_G^2}$
Illiuta Interfacial Reynolds Number ($Re_{i,I}$)	Ratio of inertia and viscous forces	$\mathrm{Re}_{i,I} = \frac{\rho_G \cdot d_e \cdot u_{i,L} \cdot \cos\theta}{\mu_G}$
Illiuta liquid Phase Reynolds Number ($Re_{L,I}$)	Ratio of inertia and viscous forces	$\mathrm{Re}_{L,I} = \frac{u_{L,s} \cdot \rho_L \cdot d_e}{\mu_L}$
Illiuta Liquid Phase Galileo Number ($Ga_{L,I}$)	Ratio of gravity and viscous forces	$Ga_{L,I} = \frac{d_e^3 \cdot g \cdot \rho_L^2}{\mu_L^2}$
Stichlmair Gas Phase Reynolds Number ($Re_{G,S}$)	Ratio of inertia and viscous forces	$\mathrm{Re}_{G,S} = \frac{\rho_G \cdot d_p \cdot u_G}{\mu_G}$
Stichlmair Liquid Phase Froude Number ($Fr_{L,S}$)	Ratio of the inertia and gravity forces	$Fr_{L,S} = \frac{u_L^2 \cdot a}{g \cdot \varepsilon^{4.65}}$

2.3.1 Channel Models up to the Year 2000

In channel models the packed bed is modelled as a series of inclined wetted-wall channels where the liquid and the vapour is split up, uniformly or non-uniformly, between the different channels. The pressure drop that occurs is due to the following factors: i) skin friction, ii) drag and iii) abrupt changes in the flow path. The total area available to vapour flow is reduced as the hold-up in the bed causes the liquid films to become thicker. A brief history of the models is given along with an updated version of the model. Any shortcomings of the models are also discussed.

SRP II Model:

The SRP II model was developed at the University of Texas over several years [Bravo et al., 1985; Rocha et al., 1993; Rocha et al., 1996; Gualito et al., 1997; Verschoof et al., 1999]. The model can be used to predict the pressure drop, liquid hold-up and mass transfer in structured packed columns. The first SRP model [Bravo et al., 1985] was fitted on air-water pressure drop data (done at atmospheric conditions) for two types of packing, namely Flexipac [McNulty & Hsieh, 1982] - and Gempak range [Chen et al., 1982; Chen et al., 1983]. However, this model did not apply to conditions where loading caused significant liquid hold-up.

The model was then extended to include the prediction of the pressure drop and the liquid hold-up in the loading region (with a liquid - and vapour flow rate range of 0.0068 - 0.34 m/s and 0.461 - 4.368 m/s respectively) [Rocha et al., 1993]. Additional experimental data was used to verify the pressure drop data apart from that of McNulty & Hsieh [1982], as well as Chen et al. [1982] and Chen et al. [1983]. This was done in a 0.43 m ID packed column with a cyclohexane/n-heptane system at different pressures (called SRP II). However, it should be noted that no additional hold-up verification data was generated apart from that of McNulty & Hsieh and Chen and co-workers which was air/water data. The range of parameters investigated by Rocha et al. [1993] is presented in Table 2.2.

Table 2.2: Range of parameters investigated by Rocha et al., 1993

Parameter	*Units*	*Range*
System pressure	[bar]	0.33 - 4.14
Liquid density	[kg/m^3]	686 - 1000
Dynamic liquid viscosity	[mPa·s]	0.2 - 1
Surface tension	[mN/m]	10 - 73
Column diameter	[m]	0.43 - 1
Total surface area per unit volume	[m^2/m^3]	213 - 492
Void fraction	[m^3/m^3]	0.9 - 0.95
Vapour density	[kg/m^3]	1.1 - 11.7
Vapour viscosity	[mPa·s]	0.0074 - 0.0185

Refinements were made to improve the pressure drop and mass transfer at low and high pressures [Gualito et al., 1997]. The range of parameters investigated by Gualito et al. [1997] can be seen in Table 2.3.

Table 2.3: Range of parameters investigated by Gualito et al., 1997

Parameter	*Units*	*Range*
System pressure	[bar]	0.05 - 27.2
Liquid density	[kg/m^3]	383 - 1000
Dynamic liquid viscosity	[mPa·s]	0.049 - 1
Surface tension	[mN/m]	1.1 - 72
Column diameter	[m]	0.245
Total surface area per unit volume	[m^2/m^3]	101.7 - 282.15
Void fraction	[m^3/m^3]	0.7 - 0.95
Vapour density	[kg/m^3]	0.35 - 85
Vapour viscosity	[mPa·s]	0.0076 - 0.0185

The model was then changed by implementing the loading point correction and the model was renamed [Verschoof et al., 1999]. The change made by Verschoof et al. [1999] was a joint effort between TU Delft and the SRP in Texas to reliably predict the pressure drop under loading conditions by using either the SRP or Delft model's pre-loading pressure drop equations. The accuracy of this refinement can predict the pressure drop with an absolute average relative error (AARE) of 9.7 %.

It should be noted that the mass transfer section of the model is not be discussed as it is beyond the scope of the project. The following section describes the working of the refined hydrodynamic model:

Liquid Hold-up:

$$h_t = \left(4 \cdot \frac{F_t}{S}\right)^{2/3} \cdot \left(\frac{3\mu_L \cdot u_{L,s}}{\rho_L (\sin\theta) \cdot \varepsilon \cdot g_{eff}}\right)^{1/3} \quad 2.26$$

$$g_{eff} = g\left[\left(\frac{\rho_L - \rho_G}{\rho_L}\right)\left(1 - \frac{(\Delta p/\Delta z)_{preload}}{(\Delta p/\Delta z)_{flood}}\right)\right] \quad 2.27$$

$$F_t = \frac{29.12\left(We_{L,S} \cdot Fr_{L,S}\right)^{0.15}}{\mathrm{Re}_{L,S}^{0.2} \cdot \varepsilon^{0.6}\left(1 - 0.93\cos\gamma\right)(\sin\theta)^{0.3}} \quad 2.28$$

$$\cos\gamma = 0.9 \qquad \text{for } \sigma \leq 0.055 \text{ [N/m]} \quad 2.29$$

$$\cos\gamma = 5.211 \times 10^{-16.835 \cdot \sigma} \qquad \text{for } \sigma \geq 0.055 \text{ [N/m]} \quad 2.30$$

Where:

g_{eff} is the effective gravity
S is the side dimension of a corrugated passage
ε is the void fraction
F_t is the correction factor to account for under-wetting
ρ_L is the liquid density [kg/m^3]
ρ_G is the gas density [kg/m^3]
μ_L is the dynamic liquid viscosity [Pa·s]
$We_{L,S}$ is the liquid Weber number
$Fr_{L,S}$ is the liquid Froude number
$Re_{L,S}$ is the liquid Reynolds number
$u_{L,s}$ is the superficial liquid velocity [m/s]

Dry Bed Pressure Drop:

$$\frac{\Delta P_d}{\Delta z} = \frac{f \cdot \rho_G \cdot u_{G,e}^2}{S} \quad 2.31$$

$$f = A + \frac{B}{\mathrm{Re}_{G,S}} \quad 2.32$$

$$u_{G,e} = \frac{u_{G,s}}{\varepsilon\left(1 - h_t\right) \cdot \sin\theta} \quad 2.33$$

Where:

f is the friction factor
$u_{G,e}$ is the effective gas phase velocity
A and B are packing specific constants

Pressure drop in pre-loading region:

$$\left(\frac{\Delta P}{\Delta z}\right)_{preload} = \frac{\Delta P_d}{\Delta z}\left[\frac{1}{1-K_2 \cdot h_{t,s}}\right]^5 \quad 2.34$$

$$K_2 = 0.614 + 71.35S \quad 2.35$$

Total Pressure drop:

$$\frac{\Delta P}{\Delta z} = \left(\frac{\Delta P}{\Delta z}\right)_{preload} \cdot F_{load} \quad 2.36$$

$$F_{load} = 3.8\left(\frac{F_G}{F_{G,lp}}\right)^{2/\sin\theta} \cdot \left(\frac{u_{L,s}^2}{\varepsilon^2 \cdot g \cdot d_{hG}}\right)^{0.13} \quad 2.37$$

$$F_{G,lp} = \left(0.053\varepsilon^2 \cdot g \cdot d_{hG}\left(\rho_L - \rho_G\right)\left(\frac{u_{L,s}}{u_{G,s}} \cdot \sqrt{\frac{\rho_L}{\rho_G}}\right)^{-0.25} \cdot \left(\sin\theta\right)^{1.15}\right)^{0.5} \quad 2.38$$

$$d_{hG} = \frac{\left(\frac{\left(B \cdot h - 2\delta \cdot S\right)^2}{B \cdot h}\right)}{\left[\left(\frac{\left(B \cdot h - 2\delta \cdot S\right)^2}{2h}\right)^2 + \left(\frac{\left(B \cdot h - 2\delta \cdot S\right)^2}{B}\right)\right]^{0.5} + \left(\frac{\left(B \cdot h - 2\delta \cdot S\right)}{2h}\right)} \quad 2.39$$

Where:

$F_{G,lp}$ is the loading point F-factor [(m/s)·(kg/m^3)$^{1/2}$]
d_{hG} is the vapour phase hydraulic diameter
g is the gravitational acceleration [m/s^2]
B is the channel base dimension [m]
h is the channel crimp height [m]
δ is the liquid film thickness [m]

It should be noticed that the liquid hold-up presented in equation 2.34 is the liquid hold-up in the pre-loading region (which is not a function of the vapour velocity). This liquid hold-up can be calculated with the following equation:

$$h_t = C\left(Fr_{L,S}\right)^{0.5} \quad 2.40$$

SUMMARY:

In the SRP II model the pressure drop at flooding is required and in this model it is assumed to be constant and varies between 900 and 1200 Pa/m for different packing types [Rocha et al., 1993]. The liquid hold-up is calculated from the film thickness and the wetted area by utilising the effective gravity. This method for predicting hold-up was researched and refined by Shi & Mersmann [1985]. The parameter that needs to be determined is the dry pressure drop over the packing. All of the other parameters can be found in the literature or can be calculated.

A disadvantage of the SRP II model is the large number of packing specific constants that are required and the use of this model outside its application range can lead to sizable errors [Brunazzi & Paglianti, 1997]. Another problem could be in the prediction of the liquid hold-up, which was only verified against air/water data even though the model that it is based on is over a range of fluid properties. Fair et al. [2000] suggests that the liquid flow-related parameters are not represented accurately in the model.

Fair et al. [2000] indicates that the SRP II model over predicts the pressure drop. According to Erasmus [2004], the SRP II model performs relatively well in the prediction of the loading point of normal capacity packing (he used Flexipac 350Y and Flexipac 350Y HC). Also, the SRP II model should be used to predict the pressure drop in the pre-loading region, as it is more accurate than the other models investigated by Erasmus [2004].

Delft Model:

The Delft model was developed at the TU Delft by Olujic and co-workers [1997; 1999; 1999]. Like the SRP II model, it can be used to predict the pressure drop, liquid hold-up and mass transfer in structured packed columns. Olujic [1997] developed the complete simulation model by using previously generated experimental work from TU Delft in a 0.45 m ID column with air/water - and air/organic solvent systems. This was tested over a range of structured packing materials. Later, Olujic et al. [1999] refined this model by adding the influence of column diameter. Tests were done in Perspex columns ranging between 0.2 - 1.4 m with air/water systems. Finally, Olujic et al. [1999] improved this model to include a refined mass transfer model based on the corrugation geometry. This was done by incorporating the cyclohexane/n-heptane data at different pressures from the SRP in Texas. Table 2.4 summarises the system parameters investigated in the Delft model.

Table 2.4: Parameters investigated throughout the Delft model

Parameter	*Units*	*Range*
System pressure	[bar]	0.33 - 4.14
Liquid density	[kg/m^3]	561 - 1000
Dynamic liquid viscosity	[mPa·s]	0.161 - 1
Surface tension	[mN/m]	8 - 72
Column diameter	[m]	0.192 - 1.4
Total surface area per unit volume	[m^2/m^3]	244 - 394
Void fraction	[m^3/m^3]	0.96 - 0.98
Vapour density	[kg/m^3]	1.19 - 13.14
Vapour viscosity	[mPa·s]	0.0069 - 0.0185

The following section describes the working of the refined model, only the new parameters will be defined (if not already defined in the SRP II model) and it should be noted that the mass transfer will not be discussed as it's beyond the scope of this project.

In this model the corrugated sheets form triangular channels which in turn cause the vapour flow to have zig-zag flow channels with a corresponding hydraulic diameter at crossings of the corrugations. A Darcy type equation is used to predict the pre-loading region pressure drop with the pressure loss coefficient in the equation consisting of three different contributing terms. These contributions are:

- Overall vapour/liquid interaction (ζ_{GL})
- Vapour interaction between adjacent triangular channels (ζ_{GG})
- Directional changes of vapour- and liquid phases (ζ_{DC})

Pressure drop in pre-loading region:

$$\Delta P_{preload} = \left(\zeta_{GL} + \zeta_{GG} + \zeta_{DC}\right) \cdot \frac{\rho_G \cdot u_{G,e}^2}{2} \tag{2.41}$$

$$\zeta_{GL} = \varphi \cdot \xi_{GL} \cdot \frac{h_{pb}}{d_{hG} \cdot \sin\theta} \tag{2.42}$$

$$\xi_{GL} = \left\{-2\log\left[\frac{\delta / d_{hG}}{3.7} - \frac{5.02}{\mathrm{Re}_{G,e}} \cdot \log\left(\frac{\delta / d_{hG}}{3.7} + \frac{14.5}{\mathrm{Re}_{G,e}}\right)\right]\right\}^{-2} \tag{2.43}$$

$$\zeta_{GG} = \left(1-\varphi\right) \cdot 0.722 \left(\cos\theta\right)^{3.14} \cdot \frac{h_{pb}}{d_{hG} \cdot \sin\theta} \tag{2.44}$$

$$\zeta_{DC} = \frac{h_{pb}}{h_{pe}} \left(\xi_{bulk} + \psi \cdot \xi_{wall}\right) \tag{2.45}$$

Where:

ξ_{GL} vapour/liquid friction factor

φ is the fraction of the triangular passage occupied by the liquid

h_{pb} is the height of the packed bed [m]

Θ is the corrugation inclination angle [degrees]

δ is the liquid film thickness [m]

$Re_{G,e}$ is the effective gas phase Reynolds number

h_{pe} is the height of a packing element [m]

ξ_{bulk} is the direction change factor for the bulk zone

ξ_{wall} is the direction change factor for the wall zone

ψ is fraction of vapour channels ending at the wall

$$\xi_{bulk} = 1.76\left(\cos\theta\right)^{1.63} \tag{2.46}$$

$$\xi_{wall} = \frac{4092u_{L,s}^{0.31} + 4715\left(\cos\theta\right)^{0.445}}{\mathrm{Re}_{G,e}} + 34.19u_{L,s}^{0.44}\cdot\left(\cos\theta\right)^{0.779} \tag{2.47}$$

$$\psi = \frac{2h_{pe}}{\pi\cdot d_c^2\cdot\tan\theta}\left(d_c^2\cdot\frac{h_{pe}^2}{\left(\tan\theta\right)^2}\right)^{0.5} + \frac{2}{\pi}\cdot\arcsin\left(\frac{h_{pe}}{d_c\cdot\tan\theta}\right) \tag{2.48}$$

$$\varphi = \frac{2S}{\left(B+2S\right)} \tag{2.49}$$

The loading region pressure drop is calculated in the same way as the method described for the SRP II model. The liquid hold-up is calculated from the packing area and average liquid film thickness by assuming complete wetting of the metal surface by using the following expressions:

$$h_t = \delta\cdot a_p \tag{2.50}$$

$$\delta = \left(\frac{3\mu_L}{\rho_L\cdot g\cdot a_p\cdot\sin\theta}\right)^{1/3} \tag{2.51}$$

Where:

a_p is the geometric area of the packing [m^2/m^3]

Summary:

The liquid hold-up in the Delft model is straightforward to predict as it is simply calculated from the geometric area of the packing and the liquid film thickness. The liquid film thickness is calculated from the Nusselt formula for falling film with provision made for the inclination angle of the packing. This model is relatively simple as no

packing specific constants are needed. All the parameters required in this model can be calculated from the characteristic lengths of the corrugated structured packing.

The strong effect of corrugation angle on pressure drop is predicted fairly well with this model [Fair et al., 2000]. According to Erasmus [2004], the Delft model performs reasonably well in predicting the loading point of the normal capacity packing (he used Flexipac 350Y and Flexipac 350Y HC). Also, he concluded that the Delft model is more accurate than the SRP II and Billet models in predicting the liquid hold-up in the pre-loading region.

Billet Model:

A hydrodynamic model was developed by Billet & Schultes [1991; 1993; 1995, 1999] for both random and structured packing. Initially, Billet & Schultes [1991] modelled the pressure drop by using a large amount of random packing experimental data by adopting a fundamental approach. The range of parameters investigated in the modelling of pressure drop data is summarised in Table 2.5.

Table 2.5: Range of parameters investigated in the Billet pressure drop model

Parameter	*Units*	*Range*
Gas velocity	[m/s]	0.09 - 2.51
Liquid load	[$m^3/(m^2 \cdot h)$]	1.33 - 82.8
Column diameter	[m]	0.076 - 0.44
Total surface area per unit volume	[m^2/m^3]	59 - 772
Void fraction	[m^3/m^3]	0.57 - 0.99
Liquid density	[kg/m^3]	800 - 1810
Dynamic liquid viscosity	[mPa·s]	0.59 - 185
Surface tension	[mN/m]	20.8 - 86.3

The model was refined by Billet & Schultes [1993] to include the prediction of liquid hold-up in packed columns. The most recent version [Billet & Schultes, 1999] assumes non-uniform wetting of the packing material. Billet based his liquid hold-up modelling on a phenomenological approach applied to the curvatures of the liquid hold-up data. Table 2.6 provides the range of parameters investigated in generating the hold-up data.

Table 2.6: Range of parameters investigated in Billet the liquid hold-up model

Parameter	*Units*	*Range*
Vapour flow factor	$[(m/s)\cdot(kg/m^3)^{0.5}]$	0.21 - 5.09
Liquid load	$[m^3/(m^2\cdot h)]$	0.61 - 60.12
Column diameter	[m]	0.15 - 0.8
Packed bed height	[m]	0.76 - 3.95
Interfacial area	$[m^2/m^3]$	54 - 380
Void fraction	$[m^3/m^3]$	0.66 - 0.98

Mass transfer predictions were included in the model by Billet & Schultes [1995]. The range of parameters investigated in the development of the mass transfer equations is not included here. Finally, an updated summarised version of the model was published by Billet & Schultes [1999]. The following section describes the working of the refined model and only the parameters defined in it.

Pressure drop:

Billet assumed that the void fraction in a bed of packing could be represented by a multiplicity of vertical channels through which the liquid flows downwards in a film counter-current to the rising gas stream [Billet & Schultes, 1995]. The deviation of the real flow behaviour could then be accounted for by including a packing-specific shape constant. The dry bed pressure drop is calculated with the following expressions:

$$\left(\frac{\Delta P}{H}\right)_{dry} = \psi_0 \left(\frac{a}{\varepsilon^3}\right)\left(\frac{F_V^2}{2}\right)\left(\frac{1}{K}\right) \qquad 2.52$$

$$\left(\frac{1}{K}\right) = 1 + \left(\frac{2}{3}\right)\left(\frac{1}{1-\varepsilon}\right)\left(\frac{d_p}{d_s}\right) \qquad 2.53$$

$$\psi_0 = C_{P,0}\left(\frac{64}{\mathrm{Re}_V} + \frac{1.8}{\mathrm{Re}_V^{0.08}}\right) \qquad 2.54$$

$$d_p = 6\left(\frac{1-\varepsilon}{a}\right) \qquad 2.55$$

Where:

ε is the void fraction $[m^3/m^3]$

F_V is the vapour flow factor $[(m/s)\cdot(kg/m^3)^{0.5}]$

K is the wall factor

d_p is the packing element diameter [m]

d_s is the column diameter [m]

ψ_0 is the dry bed resistance coefficient

Re_V is the gas phase Reynolds number

$C_{P,0}$ is the pressure drop packing specific constant

The irrigated bed pressure drop is determined by including the column hold-up in the calculations. This is due to the reduction in free cross-section for gas flow (by the column hold-up) and the change in surface structure as a result of the film coating [Billet & Schultes, 1999]. Normally, the theoretical hold-up (by assuming uniform wetting) is used to predict the irrigated pressure drop. However, non-uniform wetting was introduced [Billet & Schultes, 1999] to calculate the real column hold-up and it will be used to calculate the irrigated pressure drop. Thus, the pressure over an irrigated packed bed can be calculated with the following expressions:

$$\left(\frac{\Delta P}{H}\right)_{irrigated} = \psi_L \left(\frac{a}{\left(\varepsilon - h_L\right)^3}\right)\left(\frac{F_V^2}{2}\right)\left(\frac{1}{K}\right) \qquad 2.56$$

$$\psi_L = C_{P,0}\left(\frac{64}{\mathrm{Re}_V} + \frac{1.8}{\mathrm{Re}_V^{0.08}}\right)\left(\frac{\varepsilon - h_L}{\varepsilon}\right)^{1.5}\left(\frac{h_L}{h_{L,S}}\right)\cdot \exp\left(C_1\sqrt{Fr_L}\right) \qquad 2.57$$

$$C_1 = \frac{13300}{a^{3/2}} \qquad 2.58$$

Where:

ψ_L is the irrigated bed resistance factor

Fr_L is the liquid Froude number

h_L is the total column hold-up [m^3/m^3]

$h_{L,S}$ is the column pre-loading hold-up [m^3/m^3]

$$h_L = h_{L,S} + \left(h_{L,Fl} - h_{L,S}\right)\left(\frac{u_V}{u_{V,Fl}}\right)^{13} \qquad 2.59$$

$$h_{L,Fl}^3\left(3h_{L,Fl} - \varepsilon\right) = \frac{6}{g}\cdot a^2 \cdot \varepsilon\left(\frac{\eta_L}{\rho_L}\right)\left(\frac{L}{V}\right)\left(\frac{\rho_V}{\rho_L}\right)\cdot u_{V,Fl} \qquad \text{for } \frac{\varepsilon}{3} \le h_{L,Fl} \le \varepsilon \qquad 2.60$$

$$h_{L,S} = \left(12\left(\frac{1}{g}\right)\left(\frac{\eta_L}{\rho_L}\right)\cdot u_L \cdot a^2\right)^{1/3}\left(\frac{a_h}{a}\right)^{2/3} \qquad 2.61$$

$$\frac{a_h}{a} = C_h\left(\frac{u_L \cdot \rho_L}{a \cdot \eta_L}\right)^{0.15}\left(\frac{u_L^2 \cdot a}{g}\right)^{0.1} \qquad \text{for } \mathrm{Re_L} \le 5 \qquad 2.62$$

$$\frac{a_h}{a} = 0.85C_h\left(\frac{u_L \cdot \rho_L}{a \cdot \eta_L}\right)^{0.25}\left(\frac{u_L^2 \cdot a}{g}\right)^{0.1} \qquad \text{for } \mathrm{Re_L} \ge 5 \qquad 2.63$$

Where:

$h_{L,Fl}$ is the liquid hold-up at flooding [m^3/m^3]

u_L is the liquid velocity [$m^3/(m^2 \cdot s)$]

u_V is the vapour velocity with reference to the free column cross-section [$m^3/(m^2 \cdot s)$]

$u_{V,Fl}$ is the vapour flooding velocity [$m^3/(m^2 \cdot s)$]

L is the liquid mass flow rate [kg/h]

V is the vapour mass flow rate [kg/h]

η_L is the liquid dynamic viscosity [Pa·s]

Re_L is the liquid Reynolds number

C_h is the liquid hold-up packing specific constant

It can be seen from the above that the vapour velocity at flooding needs to be calculated in order to calculate the hold-up at flooding, which in turn is solved iteratively and used together with the pre-loading hold-up to calculate the total column hold-up. The form of the real column hold-up was based on a phenomenological approach as mentioned earlier. All the hold-up data was fitted on an equation with the following form:

$$h_L = b + c\left(\frac{u_V}{u_{V,Fl}}\right)^d \qquad 2.64$$

The above equation represents the basic form of equation 2.59 with b representing equation 2.61 and c the difference between the flooding and pre-loading hold-up. Constant d was determined experimentally.

The total column hold-up is then used to calculate the irrigated pressure drop over the packed bed. Thus, the only remaining parameter that needs to be calculated is the vapour velocity at flooding:

$$u_{V,Fl} = \sqrt{2} \cdot \sqrt{\frac{g}{\psi_{Fl}}\left(\frac{\left(\varepsilon - h_{L,Fl}\right)^{3/2}}{\varepsilon^{1/2}}\right)} \cdot \sqrt{\frac{h_{L,Fl}}{a}} \cdot \sqrt{\frac{\rho_L}{\rho_V}} \qquad 2.65$$

$$\psi_{Fl} = \left(\frac{g}{C_{Fl}^2}\right)\left[\left(\frac{L}{V}\right)\sqrt{\frac{\rho_V}{\rho_L}}\left(\frac{\eta_L}{\eta_V}\right)^{0.2}\right]^{-2n_{Fl}} \qquad 2.66$$

$$u_{L,Fl} = \left(\frac{\rho_V}{\rho_L}\right)\left(\frac{L}{V}\right) \cdot u_{V,Fl} \qquad 2.67$$

$$n_{Fl} = -0.194 \qquad \text{for } \left(\frac{\mathrm{L}}{\mathrm{V}}\right)\sqrt{\frac{\rho_V}{\rho_L}} \leq 0.4 \qquad 2.68$$

$$n_{Fl} = -0.708; \quad C_{Fl}^{*} = 0.6244 \cdot C_{Fl} \qquad \text{for } \left(\frac{\mathrm{L}}{\mathrm{V}}\right)\sqrt{\frac{\rho_V}{\rho_L}} \geq 0.4 \qquad 2.69$$

Where:

ψ_{Fl} is the resistance coefficient at flooding

$u_{L,Fl}$ is the liquid flooding velocity [$m^3/(m^2 \cdot s)$]

η_V is the vapour dynamic viscosity [Pa·s]

C_{Fl} is the liquid hold-up packing specific constant at flooding

Another parameter that can be calculated is the loading point, where the shear forces between the vapour and liquid become large enough to suspend some of the liquid. At this point, the liquid hold-up is no longer independent of vapour velocity. However, the prediction of the loading point is not of concern in this project and will not be discussed any further. Billet & Schultes [1993; 1999] found that the theoretical liquid hold-up at flooding predicted by equations 2.60 and 2.65 diverged erratically from the experimentally measured values. Thus, the following empirical equation was derived to predict the real column liquid hold-up at flooding:

$$h_{L,Fl} = 2.2 h_{L,S} \left(\frac{\eta_L \cdot \rho_W}{\eta_W \cdot \rho_L} \right)^{0.05} \qquad 2.70$$

Where:

η_W is the dynamic liquid viscosity of water [Pa·s]

ρ_W is the density of water [kg/m^3]

Summary:

The Billet model involves many tedious calculations and a number of packing specific constants, which are in abundance in the literature for random packing. A limited number of structured packing constants are available in the literature. Apart from the tedious calculations, the model is accurate in predicting the hydrodynamic parameters such as dry and irrigated pressure drop, as well as liquid hold-up (the parameters which are of concern in this project).

All the experimental vs. predicted pressure drop data was compared on a 20 % parity plot with a mean relative deviation of 10.8 %. The hold-up data was compared in the same way on a 15 % parity plot with a mean relative deviation of 6.7 %.

Erasmus [2004] concluded that this model performed reasonably well in predicting the loading point of normal capacity packing (he used Flexipac 350Y and Flexipac 350Y HC). He also concluded this model was more accurate than the other models investigated in predicting the steep slope of the pressure drop curve in structured packing.

Maćkowiak:

A hydrodynamic model was developed by Maćkowiak [1990; 1991; 2009] for both random and structured packing. Initially, Maćkowiak [1990] derived a model to determine the flooding gas velocity, as well as the liquid hold-up in packed columns. Later, Maćkowiak [1991] developed a complete model to predict the hydrodynamic parameters (pressure drop and liquid hold-up over the entire operating range) in packed columns. This was verified for a number of different random and structured packing types. The range of parameters investigated is presented in Table 2.7.

Table 2.7: Range of parameters investigated in the Maćkowiak model

Parameter	*Units*	*Range*
Pressure drop range	[Pa/m]	2 - 4000
Liquid Reynolds number	-	0.3 - 200
Column diameter	[m]	0.1 - 1.4
Total surface area per unit volume	[m^2/m^3]	54 - 500
Void fraction	[m^3/m^3]	0.63 - 0.987
Liquid density	[kg/m^3]	660 - 1260
Dynamic liquid viscosity	[mPa·s]	0.2 - 8
Surface tension	[mN/m]	14 - 74.6
Vapour density	[kg/m^3]	0.03 - 3.6
Vapour viscosity	[mPa·s]	0.0065 - 0.0185

More recently, Maćkowiak [2009] extended his channel model to be able to predict the dry bed pressure drop for any type of random or structured packing. This is a general model that doesn't require any experimental evaluation of the packing type. However, the dry bed pressure drop is not of concern here (nor is it required in his hydraulic model). Thus, only his hydraulic model will be discussed in the section below:

Maćkowiak [1990] uses a bed of suspended droplets as modelling technique to predict the velocity of the gas, as well as the liquid hold-up at flooding:

$$u_{V,Fl} = C_{Fl} \cdot \varepsilon^{1.2} \cdot \left(\frac{d_h}{d_T}\right)^{1/4} \left(\frac{d_T \cdot \rho_L \cdot g}{\rho_V}\right)^{1/2} \left(1 - \frac{h_{L,Fl}}{\varepsilon}\right)^{7/2} \qquad 2.71$$

$$d_T = \sqrt{\frac{\sigma_L}{(\rho_L - \rho_V) \cdot g}} \qquad 2.72$$

$$h_{L,Fl} \cong \left(\frac{\varepsilon}{0.4(1-\lambda_0)}\right)\left[\left(1.44\lambda_0^2 + 0.8\lambda_0(1-\lambda_0)\right)^{0.5} - 1.2\lambda_0\right] \qquad \text{for } \mathrm{Re}_{L,M} \geq 2 \qquad 2.73$$

$$h_{L,Fl} \cong \left(\frac{\varepsilon}{0.24(1-\lambda_0)}\right)\left[\left(1.254\lambda_0^2 + 0.48\lambda_0(1-\lambda_0)\right)^{0.5} - 1.12\lambda_0\right] \qquad \text{for } \mathrm{Re}_{L,M} \leq 2 \tag{2.74}$$

$$\lambda_0 = \frac{u_L}{u_{V,Fl}} \tag{2.75}$$

Where:

C_{Fl} is the flooding point factor
d_h is the hydraulic diameter of the bed [m]
d_T is the diameter of the liquid droplets [m]
h_{Fl} is the liquid hold-up at flooding [m^3/m^3]
σ_L is the surface tension of the liquid [mN/m]
λ_0 is the phase flow ratio at the flooding point
$Re_{L,M}$ is the liquid Reynolds number
$u_{V,Fl}$ is the vapour velocity at the flooding point [m/s]

The above equations give two linked equations for the vapour flooding velocity and liquid hold-up at flooding. The total liquid hold-up can be calculated from the following equations:

$$h_L = h_{L,Fl} - (h_{L,Fl} - h_{L,S})\left[1 - \left(\frac{(F_V / F_{V,Fl}) - 0.65}{0.35}\right)\right]^{1/2} \tag{2.76}$$

$$h_{L,S} = 2.2\sqrt{B_L} \tag{2.77}$$

$$B_L = \left(\frac{\mu_L}{\rho_L \cdot g^2}\right)^{1/3}\left(\frac{u_L}{\varepsilon^3}\right)\left(\frac{1-\varepsilon}{d_p}\right) \tag{2.78}$$

Where:

$h_{L,S}$ is the pre-loading region liquid hold-up [m^3/m^3]
B_L is the non-dimensional liquid load
d_p is the particle (packing) diameter [m]
F_V is the vapour flow factor [(m/s)·$(kg/m^3)^{1/2}$]
$F_{V,Fl}$ is the vapour flow factor at the flooding point [(m/s)·$(kg/m^3)^{1/2}$]

Finally, the irrigated pressure drop can be calculated from liquid hold-up by means of a drag coefficient for two-phase flow:

$$\frac{\Delta P}{H} = 3.8\mu\left(\frac{1-\varepsilon}{\varepsilon^3}\right)\left(\frac{F_V^2}{d_p \cdot K}\right)\left(1 + \left(\frac{h_L}{1-\varepsilon}\right)\right)\left(1 - \frac{h_L}{\varepsilon}\right)^{-3} \tag{2.79}$$

$$K = \left(1 + \frac{2}{3}\left(\frac{1}{1-\varepsilon}\right)\left(\frac{d_p}{d_s}\right)\right)^{-1} \qquad 2.80$$

Where:

μ is the packing specific shape factor found in the literature

d_s is the column diameter [m]

K is the wall factor

SUMMARY:

The Maćkowiak model uses a relatively simple calculation procedure to obtain the hydraulic parameters. No experimental data on dry packing is required to implement this model. However, two constants are required, namely the flood point factor and a packing shape factor. Both these constants are available for a variety of packing materials [Maćkowiak, 1991].

The flooding point velocity and the liquid hold-up at flooding can be predicted with an average relative error of about 5 and 15 % respectively. The model predicts the dry bed pressure drop and the pressure drop below the loading point with an average relative error less than 10 % for both. The pressure drop prediction above the loading point is less accurate with an average error of about 15 % [Maćkowiak, 1991].

Heymes et al. [2006] did a comparative study on some of the reliable hydraulic models in the literature. He concluded that the model predicted the liquid hold-up at zero vapour velocity (pre-loading region) with an average relative error of 37 %. Heymes et al. [2006] also concluded that the model prediction has large errors when the viscosity of the system is varied significantly (absolute average relative errors, AARE, of 57 % in liquid hold-up and 25 % in pressure drop).

Brunazzi and Paglianti:

A mechanistic pressure drop model for structured packing was developed by Brunazzi & Paglianti [1997]. This model is based on solving mass and momentum conservation equations in an idealised wetted-wall arrangement approximating the actual geometry of the structured packing [Illiuta & Larachi, 2001].

Tests were done on the Mellapak and BX packing ranges in column diameters ranging between 50 and 100 mm. The systems investigated were primarily air/water, as well as air/Genosorb 300 and air/Genosorb 1843. Experimental data (on the same packing materials) from other authors were used to test the validity of the model over a wider range of column diameters. This included air/water data in columns ranging from 200 -

1000 mm. The liquid - and gas loadings ranged between 5 - 125 [$m^3/(m^2 \cdot h)$] and ± 0.3 - 5 [$(m/s) \cdot (kg/m^3)^{0.5}$].

The following section describes the working of the model and again the mass transfer will not be discussed as it is beyond the scope of this project.

The channels within the packing are viewed as a bundle of identical columns inclined with respect to the horizontal axis by an angle that is equal to the corrugation angle. The model is based on the following assumptions [Illiuta & Larachi, 2001]:

- The packing fractional wetted area is unaffected by the vapour load and the vapour-liquid interfacial shear stress.
- The interfacial shear stress is related to the effective liquid velocity and is not a function of the interfacial velocity.
- The dynamic liquid hold-up is known as a priori.

The total pressure drop is calculated as the sum of friction, gravitational and acceleration terms:

$$\left(\frac{dP}{dz}\right)_{Total} = \left(\frac{dP}{dz}\right)_F + \left(\frac{dP}{dz}\right)_G + \left(\frac{dP}{dz}\right)_A \qquad 2.81$$

The friction term is split up into distribution losses and concentrated losses. Distribution losses are due to the losses at the channel walls and vapour-liquid interface, and the concentrated losses are due to the changes in flow direction.

$$\left(\frac{dP}{dz}\right)_F = \left(\frac{dP}{dz}\right)_{F,d} + \left(\frac{dP}{dz}\right)_{F,c} \qquad 2.82$$

The following equations describe the dry bed pressure drop terms used in the model:

$$\left(\frac{dP}{dz}\right)_A = \rho_G \cdot u_{G,s}\left(\frac{du_{G,e}}{dz}\right) \qquad 2.83$$

$$\left(\frac{dP}{dz}\right)_G = \pm \rho_G \cdot g \qquad 2.84$$

$$\left(\frac{dP}{dz}\right)_{F,d} = \left(\frac{1}{A_G \cdot \sin\theta}\right)\left(\tau_{w,G} \cdot S_G\right) \qquad 2.85$$

$$\left(\frac{dP}{dz}\right)_{F,c} = 4 f_G \cdot N_C \left(\frac{L_{eq}}{d_e}\right)\left(\frac{\rho_G \cdot u_{G,e}^2}{2}\right) \qquad 2.86$$

Where:

A_G is the cross-sectional area of the channel available to vapour flow [m^2]

$\tau_{w,G}$ is the shear stress at the channel wall relative to vapour flow by itself in the channel

S_G is the channel perimeter wetted by the gas

N_c is the number of flow direction changes in a unit height of packing

f_G is the gas friction factor

L_{eq} is the channel length equivalent to a single bend pressure drop [m]

$$A_G = \frac{\pi \cdot d_e^2}{4} \quad 2.87$$

$$S_G = \pi \cdot d_e \quad 2.88$$

$$\tau_{w,G} = \frac{1}{2} f_G \cdot \rho_G \cdot u_{G,e}^2 \quad 2.89$$

$$f_G = B_1 + \frac{B_2}{\mathrm{Re}_G} \quad 2.90$$

$$N_C = \frac{1}{H} \quad 2.91$$

$$d_G = \frac{4A_G}{\pi \cdot d_e} \quad 2.92$$

Where:

B_1 is a packing specific constant

B_2 is a packing specific constant

d_e is the equivalent channel diameter

d_G is the equivalent diameter for gas flow

$$d_e = \frac{4\varepsilon}{a} \quad 2.93$$

The irrigated pressure drop can be calculated in the same way as the dry bed pressure drop, but also accounting for the part of the structured packing that is wetted. This wetted area can be calculated from the following equation:

$$\frac{a_e}{a} = \left(\frac{d_e \cdot \sin\theta}{4\varepsilon} \right) \cdot h_t^{1.5} \left(\frac{\rho_L \cdot g}{3\mu_L \cdot u_{L,s}} \right)^{0.5} \quad 2.94$$

Where:

h_t is the dynamic liquid hold-up [m^3/m^3]

$u_{L,s}$ is the superficial liquid velocity [$m^3/(m^2 \cdot s)$]

The dynamic liquid hold-up for the Mellapak range can be calculated by the correlation proposed by Suess & Spiegel [1992]:

$$h_t = C \cdot a^{0.83} \left(3600 u_{L,s}\right)^x \left(\frac{\mu_L}{\mu_{W,20^oC}}\right)^{0.25} \quad 2.95$$

$$C = 0.0169 \qquad \text{for liquid load} \leq 40\ [\mathrm{m^3/(m^2 \cdot h)}] \quad 2.96$$

$$C = 0.0075 \qquad \text{for liquid load} > 40\ [\mathrm{m^3/(m^2 \cdot h)}] \quad 2.97$$

$$x = 0.37 \qquad \text{for liquid load} \leq 40\ [\mathrm{m^3/(m^2 \cdot h)}] \quad 2.98$$

$$x = 0.59 \qquad \text{for liquid load} > 40\ [\mathrm{m^3/(m^2 \cdot h)}] \quad 2.99$$

Next, the friction factors need to be adjusted for the presence of liquid:

$$\left(\frac{dP}{dz}\right)_{F,d} = \left(\frac{1}{A_G \cdot \sin\theta}\right)\left(\tau_{w,G} \cdot S_{G^*} + \tau_i \cdot S_i\right) \quad 2.100$$

$$\left(\frac{dP}{dz}\right)_{F,d} = 4 f_m \cdot N_C \left(\frac{L_{eq}}{d_e}\right)\left(\frac{\rho_G \cdot u_{G,e}^2}{2}\right) \quad 2.101$$

$$\tau_i = \frac{1}{2} f_i \cdot \rho_G \left(u_{G,e} + u_{L,e}\right)^2 \quad 2.102$$

$$S_i = \frac{a_e}{a} \cdot \pi \cdot d_e \quad 2.103$$

$$S_{G^*} = \pi \cdot d_e - S_i \quad 2.104$$

Where:

f_m is a mean friction factor, weighed on the wetted area and calculated from the wall - and interfacial friction factors

f_i is the interfacial friction factor

τ_i is the interfacial shear stress

S_i is the interfacial chord

$$f_i = f_G \left[1 + B_3 \cdot Bo_L^{0.3} + B_4 \left(\frac{\delta - \delta_0}{d_e}\right)\left(\frac{\mu_L}{\mu_{L,0}}\right)^{0.1} \left(We_L\right)^{\alpha}\right] \quad 2.105$$

$$\delta = \frac{\pm\left(\frac{\tau_i}{2\mu_L}\right) + \sqrt{\left(\pm\frac{\tau_i}{2\mu_L}\right)^2 + 4\left[\rho_L \cdot g \cdot \sin\theta - \left(\frac{dP}{dz}\right)_{channel}\right]\left(\frac{u_{L,e}}{3\mu_L}\right)}}{\left(\frac{2}{3\mu_L}\right)\left[\rho_L \cdot g \cdot \sin\theta \pm \left(\frac{dP}{dz}\right)_{channel}\right]} \quad 2.106$$

$$\left(\frac{dP}{dz}\right)_{channel} = \left(\frac{dP}{dz}\right)_{F,d} \cdot \sin\theta \pm \rho_G \cdot g \cdot \sin\theta \qquad 2.107$$

SUMMARY:

The mechanistic model proposed by Brunazzi & Paglianti [1997] can predict the irrigated pressure drop of the Mellapak and BX structured packing ranges with a mean square error of 20 %. This model was verified over the following liquid property ranges: Liquid - vapour loads of 5 - 125 [$m^3/(m^2 \cdot h)$] and ± 0.3 - 5 [$(m/s) \cdot (kg/m^3)^{0.5}$] respectively, dynamic viscosity between 1 - 7.7 mPa·s and surface tension between 34 - 72 mN/m and the column diameters ranged between 50 and 1000 mm. Six packing constants are needed in the model predictions and they are published for the two packing ranges [Brunazzi & Paglianti, 1997]. However, this model mainly focuses on the pressure drop prediction and not the liquid hold-up (liquid hold-up implemented by using correlation from Suess & Spiegel [1992]). Also, the range of application is limited although the authors state that the method can be implemented easily on other structured packing types.

2.3.2 Recent Channel Models (2000-Present)

A few more models have been developed recently that are of the channel type. These models are more fundamental in nature and have been developed to predict the pressure drop and liquid hold-up in the pre-loading region. Since these models are fundamental in nature, they are quite complex and only have a limited range of application. In this section the models will not be discussed in full detail due to their complex nature and their limited range of application. A discussion on the basic structure of the models, the range of applicability, as well as the assumptions is given below (where applicable).

Woerlee Model:

Woerlee et al. [2001] developed a fundamental model to predict the pressure drop in both random and structured packing. They used a macroscopic approach to describe the hydrodynamics of two-phase counter-current flow in packed beds. This was done by viewing the bed as a number of inclined tubes where the flow is assumed to be annular. The liquid is modelled as a laminar falling film that completely wets the tubes. The model was verified over a number of packing materials, fluid ranges, fluid systems and column diameters as shown in Table 2.8. The data used was from other author's work found in the open literature.

Table 2.8: Range of parameters investigated in the Woerlee model

Parameter	*Units*	*Range*
Liquid density	[kg/m^3]	826 - 1090
Vapour density	[kg/m^3]	1.21 - 27.39
Column diameter	[m]	0.038 - 0.79
Total surface area per unit volume	[m^2/m^3]	78.7 - 375
Void fraction	[m^3/m^3]	0.59 - 1
Dynamic liquid viscosity	[mPa·s]	1 - 8.1
Gas viscosity	[mPa·s]	0.015 - 0.018
Surface tension	[mN/m]	26 - 73
Effective inclination angle	[degrees]	0 - 58.5

The pressure drop comprises of two terms: the frictional losses at the vapour/liquid interface and frictional losses due to the geometry:

$$\left(\frac{dP}{dz}\right)_{total} = \left(\frac{dP}{dz}\right)_{f} + \left(\frac{dP}{dz}\right)_{g} \qquad 2.108$$

The friction factor for a smooth liquid interface is calculated with the Blasius equation and can be used to calculate the friction factor for turbulent flow [Woerlee et al., 2001]:

$$4f = 0.3168\left(\mathrm{Re}_{G,W}\right)^{0.25} \qquad 2.109$$

The pressure drop due to geometry and interfacial losses are combined by using the Ergun equation:

$$\begin{aligned} 4f_p &= 4\left(f + f_g\right) \\ &= 4\left|\frac{dP}{dz}\right|_{total} \cdot \frac{\Theta \cdot r_0}{\rho_G\left(\left(\frac{u_{SG}}{\varepsilon \cdot \Theta^2}\right) - u_{\mathrm{int}} \cdot \cos\alpha\right) \cdot \Theta \cdot r_0} \\ &= \left(\frac{600}{9}\right)\left(\frac{\mu_G}{\rho_G\left(\left(\frac{u_{SG}}{\varepsilon \cdot \Theta^2}\right) - u_{\mathrm{int}} \cdot \cos\alpha\right) \cdot \Theta \cdot r_0}\right) + \left(\frac{28}{12}\right) \\ &= \left(\frac{600}{\mathrm{Re}_p}\right) + 2.33 \end{aligned} \qquad 2.110$$

$$\mathrm{Re}_p = \mathrm{Re}_{G,W} \cdot \cos\alpha \qquad 2.111$$

Where:

f is the smooth pipe friction factor

f_p is the packing specific friction factor

f_g is a geometrical friction factor

u_{SG} is the superficial vapour velocity [m/s]

Θ is the relative interface position defined as $\Theta = (r_{int}/r_0)$

α is the effective inclination angle [^{o}]

u_{int} is the interface velocity [m/s]

r_0 is the hydraulic radius [m]

r_{int} is the interface radius [m]

$$u_{\text{int}} = -\left[\begin{array}{l} \Theta^2 \cdot \ln(\theta)\left(\Delta\rho \cdot g + \left(\frac{dP}{dz}\right)_{total}\right)\cdot\cos\alpha \\ +\left(\frac{1-\Theta^2}{2}\right)\left(\Delta\rho \cdot g + \left(\frac{dP}{dz}\right)_{total}\right)\cdot\cos\alpha \end{array}\right]\left(\frac{r_0^2}{2\mu_L}\right) \qquad 2.112$$

The characteristic friction factors need to be determined from dry bed experimental data by fitting an Ergun type relation in the form of:

$$4f_p = \left(\frac{4F_1}{\text{Re}_p}\right) + 4f_\infty \qquad 2.113$$

Where:

F_1 is the laminar coefficient of the packing friction

f_∞ is the packing friction factor at an “infinite” Reynolds number

The above friction factor equation is also adapted to include the “effective” inclination angle of the packing material. It is calculated from dry bed pressure drop data, as well as from a smooth pipe geometry friction factor.

$$4f_\infty = \left(\frac{0.6556 \cdot \tan^2\alpha + 0.0142}{\cos\alpha}\right) \qquad 2.114$$

Thus, by combining all the above equations, the pressure drop over a dry packed bed can be calculated as:

$$\left(\frac{dP}{dz}\right)_{total} = -f_p\left(\frac{\rho_G\left(\frac{u_{SG}}{\varepsilon}\right)\left|\frac{u_{SG}}{\varepsilon}\right|}{r_0}\right) \qquad 2.115$$

$$4 f_p = \left[\left(\frac{83.5}{\mathrm{Re}_p \cdot \cos\alpha} \right) + \left(\frac{0.6556 \tan^2 \alpha + 0.0142}{\cos\alpha} \right) \right] \quad 2.116$$

Next, the effect of column diameter on pressure drop is included for both random and structured packing. This is done by adjusting the packing friction factor and the effective inclination angle used in equation 2.116.

$$f_p^* = f_p \left(1 + \left(\frac{2.5 \cdot \varepsilon \cdot \alpha \cdot \sin\alpha}{a \cdot d_c} \right) \right) \quad 2.117$$

$$\frac{\alpha}{\alpha_0} = \frac{1}{1 + \left(\frac{4}{a \cdot d_c} \right)} \quad 2.118$$

Where:

f_p^* is the adjusted packing friction factor

α_0 is the effective inclination angle at infinite column diameter

d_c is the column diameter [m]

Finally, the increase in the pressure drop due to the presence of a disturbed liquid film is accounted for by defining a vapour-liquid interaction coefficient. Thus, the pressure drop over the entire bed is the non-disturbed pressure drop multiplied by the vapour-liquid interaction:

$$\left(\frac{dP}{dz} \right)_{total} = -f_p \left(1 + \psi_{G-L} \right) \left[\frac{\rho_G \left(\frac{u_{SG}}{\Theta^2 \cdot \varepsilon} - u_{\mathrm{int}} \cdot \cos\alpha \right) \left| \frac{u_{SG}}{\Theta^2 \cdot \varepsilon} - u_{\mathrm{int}} \cdot \cos\alpha \right|}{\Theta \cdot r_0} \right] \quad 2.119$$

$$\psi_{G-L} = \sinh \left[\left(\frac{34 \times 10^{-15}}{(\cos\alpha)^9} \right) \left(\frac{a \cdot h}{\varepsilon^7} \right) \left(\frac{h}{h_0} \right)^6 \cdot \mathrm{Re}_{L,W} \cdot \mathrm{Re}_{G,W}^{1.5} \left(\frac{\rho_L \cdot \mu_L}{\rho_G \cdot \mu_G} \right) \right] \quad 2.120$$

$$a \cdot h_0 = \left(Ga_p^{-1} \cdot \mathrm{Re}_{L,W} \right)^{0.33} \quad 2.121$$

Where:

$\psi_{G\text{-}L}$ is the vapour-liquid interaction parameter

h is the liquid film thickness [m]

h_0 is the free falling liquid film thickness [m]

SUMMARY:

The mechanistic model proposed by Woerlee et al. [2001] can predict the irrigated pressure drop of random and structured packing materials. The accuracy of the

predicted irrigated pressure drop in randomly packed column is reasonable. The structuredly packed irrigated pressure drop is not predicted well at all, especially for packing materials with an inclination angle of 30°. This deviation is thought to be due to liquid entrainment [Woerlee et al., 2001].

This model was verified over the following liquid and vapour property ranges: density between 826 - 1090 kg/m^3 for the liquid and 1.21 - 27.39 kg/m^3 for the vapour. Viscosity ranged between 1 - 8.1 mPa·s for the liquid and between 0.015 - 0.018 mPa·s for the vapour. Surface tension was varied between 26 and 73 mN/m and the column diameters ranged between 38 and 790 mm.

As this model is of a fundamental nature, the complexity of the calculations is quite cumbersome to perform. Each packing has to be evaluated first to obtain the dry bed friction factors needed in the calculations. Lastly, the equations are all linked to each other, and thus an iterative method is required to find a stable solution.

Illiuta and Larachi:

Illiuta & Larachi [2001] developed a mechanistic model for columns containing structured packing in the pre-loading region. The model is based on the well-known single-slit mechanistic approach used in co-current, down-flow trickle bed reactors. The model gives three interlinked non-linear algebraic equations that need to be solved iteratively and thus predicting the pressure drop, liquid hold-up and fraction wetted area at the same time. The model was developed by using experimental data from other authors found throughout the literature and the range of packing materials used can be seen in Table 2.9. The liquid velocity ranged between 0.6 and 50 mm/s and the superficial vapour velocity between 0.1 and 2.6 m/s.

Table 2.9: Range of packing parameters investigated in the Illiuta and Larachi model

Packing Type	*a [m^2/m^3]*	*ε [%]*	*Inclination Angle [°]*	*Column ID [m]*
Flexipak 1Y	443	91	45	0.914
Flexipak 2Y	223	95	45	0.914
Flexipak 3Y	223	96	45	0.914
Gempak 1A	115	96	45	0.914
Gempak 2A	223	95	45	0.914
Gempak 4A	453	91	45	1
Mellapak 250X	250	98	60	1
Mellapak 250Y	250	95	45	1.2, 0.295
Montz-Pak B1-250	244	98.5	60	0.8
Montz-Pak B1-400	394	96	60	0.43
Coiled screen Packing	628	83.6	61.7	0.105

The refined model equations can be described by the following equations:

$$\psi_G = \left(\frac{32}{\cos^2\theta}\right)\left(\frac{1-\eta_e}{\varepsilon - h_L}\right)\left[1+\left(\frac{f_W \cdot \mathrm{Re}_{G,I}}{8\varepsilon \cdot \cos\theta}\right)\right]\left(\frac{\mathrm{Re}_{G,I}}{Ga_{G,I}}\right)$$

$$= \left(\frac{32}{\cos^2\theta}\right)\left(\frac{\varepsilon^2 \cdot \eta_e^2}{(\varepsilon - h_L)(\eta_e \cdot \varepsilon - h_L)^2}\right)$$

$$\times\left[1+\left(\frac{f_W\left(\eta_e \cdot \mathrm{Re}_{G,I} + (\eta_e \cdot \varepsilon - h_L)\cdot \mathrm{Re}_{G,I}\right)}{8\eta_e \cdot \varepsilon \cdot \cos\theta}\right)\right]\left(\frac{\eta_e \cdot \mathrm{Re}_{G,I} + (\eta_e \cdot \varepsilon - h_L)\cdot \mathrm{Re}_{G,I}}{Ga_{G,I}}\right) \quad 2.122$$

$$\psi_L = \left(\frac{32\eta_e^2}{\cos^2\theta}\right)\left(\frac{\varepsilon^2}{h_L^3}\right)\left(1+\left(\frac{f_W \cdot \mathrm{Re}_{G,I}}{8\eta_e \cdot \varepsilon \cdot \cos\theta}\right)\right)\left(\left(\frac{\mathrm{Re}_{L,I}}{Ga_{L,I}}\right)\right) - \psi_G\left(\frac{\rho_G}{\rho_L}\right)\left(\frac{\varepsilon \cdot \eta_e}{h_L} - 1\right) \quad 2.123$$

$$\eta_e = -\left[\left(\frac{h_L^2 \cdot \cos^2\theta}{64\varepsilon}\right)\left(\frac{\rho_G}{\rho_L}\right)\left(\frac{Ga_{L,I}}{\mathrm{Re}_{L,I}}\right)\right] + \left[\left(\frac{h_L^2 \cdot \cos^2\theta}{8\varepsilon}\right)\left(\frac{Ga_{L,I}}{\mathrm{Re}_{L,I}}\right)^{1/2}\right]$$

$$\times\sqrt{\left[\left(\frac{4}{3h_L}\right)\left(1+\frac{3}{2}\left(\frac{\rho_G}{\rho_L}\right)\right)\right] + \left[\left(\frac{\cos^2\theta}{64}\right)\left(\frac{\rho_G}{\rho_L}\right)^2\left(\frac{Ga_{L,I}}{\mathrm{Re}_{L,I}}\right)\right]} \quad 2.124$$

Where:

ψ_G is the gas phase dimensionless body force
ψ_L is the liquid phase dimensionless body force
$Re_{G,I}$ is gas phase Reynolds number
$Ga_{G,I}$ is the gas phase Galileo number
$Re_{i,I}$ is the interfacial Reynolds number
$Re_{L,I}$ is the liquid phase Reynolds number
$Ga_{L,I}$ is the liquid phase Galileo number
f_W is the wall friction factor
η_e is packing fractional wetted area
h_L is the liquid hold-up [m^3/m^3]
θ is the slit inclination angle [^{o}]
$u_{i,L}$ is the liquid phase interfacial velocity [m/s]

Finally, the irrigated pressure drop can be calculated from the following relation:

$$-\frac{\Delta P}{H} + \rho_L \cdot g = \rho_G \cdot g \cdot \psi_L \quad 2.125$$

The mapping between the slits and the structured packing column is based on the following assumptions [Illiuta & Larachi, 2001]:

- The slits have identical half-wall thicknesses S, half-void thicknesses w, and stream wise slit lengths l.

- The packing surface area per packing volume is uniform across the two slits and equal to that of the bed.
- The void-to-solid and liquid-to-solid volume fractions within the slits and the whole packed bed are identical.
- The slits are inclined by an angle Θ corresponding to the corrugation angle of the structured packing.

The following assumptions are made with respect to the nature of the vapour-liquid flow [Illiuta & Larachi, 2001]:

- The packing is partially wetted with a smooth, stable liquid film.
- The dominant liquid texture components are contributed by films and rivulets which are referred to as the liquid film.
- The liquid film - and vapour flow remain acceleration-free and at steady state.
- The average phase interstitial velocities in the bed and the slits are assumed to be identical.
- The friction factor (f_i) at the vapour-liquid interface and wall friction factor (f_W) at the fluid-solid interface are equal.
- There are no discontinuities in the velocity and shear stress profiles at the vapour-liquid interface.
- The total pressure gradient is the same across the bed and the idealised slit network.

Summary:

The mechanistic model proposed by Illiuta & Larachi [2001] can predict the irrigated pressure drop, liquid hold-up and effective wetted packing area of structured packing materials within the pre-loading region. The model can predict the irrigated pressure drop with an AARE of 25 %. The liquid hold-up can be predicted with an AARE of 13.8 % and the effective wetted packing area with an AARE of 15 % [Illiuta & Larachi, 2001].

This model was verified over a number of structured packing materials with liquid and vapour flow rates between 0.6 - 50 mm/s and 0.1 - 2.6 m/s respectively. Data from various liquid/vapour systems were used found throughout the literature.

Although this model is fundamental in nature, the calculations are quite easy to perform. No additional constants are needed in this, only the dry bed pressure drop is required. The only draw-back of this model is that it is only valid for the pre-loading region, thus limiting its usefulness in general.

Ranke Model:

In 2000, Ranke et al. [2000] developed a physically based model that could predict the pressure drop and liquid hold-up of structured packing. Due to the nature of equations presented in the model (using Gaussian distribution functions), the equations will not be included in this section. However, a discussion of the model is presented below:

In this model the pressure drop, film thickness and radial liquid distribution are correlated as a function of column load up to the flooding point. This was done by using a quadratic diameter column (400 x 400 mm) and tested with a low boiling hydrocarbon (LBH) as liquid, nitrogen (saturated with the LBH) as vapour. The densities were 1.7 and 650 kg/m^3 respectively for the vapour and liquid. The dynamic viscosities were 0.31 and 0.012 mPa·s for the gas and liquid and the LBH had a surface tension of 18 mN/m. The maximum vapour flow factor tested was below 1.8 [(m/s)·(kg/m^3)]. Lastly, two structured packing types were investigated, both with a specific packing area of 750 m^2/m^3 but with different crimp geometries.

In developing the model the following is assumed:

- The vapour follows the channels within the packing elements.
- The liquid stays on a single corrugated sheet and follows a path of steepest inclination angle down the plane.
- The interfacial shear stress at the vapour-liquid interface influences the angle at which the liquid flows down the plane.
- The packing is completely wetted.

The dry pressure drop is calculated by splitting the friction factor into 3 factors, namely: 1.) contributions from interfacial friction, 2.) losses due to changes in direction in the between packing elements, and 3.) losses due to the outflow of vapour from a packing element. Shear forces at the vapour-liquid interface are taken into account by conducting a force balance over the liquid film. This yields an equation for the velocity distribution and the liquid film thickness.

The liquid hold-up is determined from the average film thickness and the geometric area of the packing material. The irrigated pressure drop is calculated from the dry bed pressure drop and an adjustment made for the available cross-sectional flow area. Lastly, a radial distribution model of the liquid phase is introduced. This means that at each contact point (between sheets in the packing material) a portion of the liquid flows to the adjacent sheet. Apart from the radial distribution, lateral distribution is generated in the troughs of the channels.

SUMMARY:

This model contains three fitting parameters that have to be determined for each type of packing. Only the two packing materials investigated have the necessary constants published. The problem is that radial distribution is not measured easily, and thus limits the extension of this model to other packing material types.

2.3.3 Particle - or Porous bed Models

In particle - or porous bed models, the column is modelled as a packed bed using the Ergun equation. The pressure drop is accounted for by the drag associated with the particles. The void fraction in the bed is reduced by the liquid hold-up in the bed. However, structured packing has a close resemblance to a series of inclined wetted-walls and thus only a few particle- or porous bed models are available in the literature [Erasmus, 2004]. One of the well-known models is the Stichlmair model and will be discussed in the next section.

Stichlmair model:

A generalised model to predict the pressure drop and capacity of columns containing random and structured packing was developed by Stichlmair et al. [1989]. Fundamental studies on capacity and pressure drop in porous beds were done to develop the model.

No experimental work was done by Stichlmair [1989], however, he used a set of pooled data from various authors to verify his model. This included a combination of 19 random and structured packing materials over a range of air/water experiments, as well as a limited number of systems that were non-aqueous. The following section describes the working of the model:

An expression is developed based on the Richardson Zaki relationship between vapour velocity and fluidised bed porosity to give the following:

$$\frac{(\Delta P)_{dry}}{Z} = \frac{3}{4} f_0 \left[\frac{(1-\varepsilon)}{\varepsilon^{4.65}} \right] \left(\frac{\rho_G \cdot u_G^2}{d_p} \right) \qquad 2.126$$

$$f_0 = \frac{C_1}{\mathrm{Re}_{G,S}} + \frac{C_2}{\mathrm{Re}_{G,S}^{0.5}} + C_3 \qquad 2.127$$

Where:

f_0 is the friction factor for flow over a single particle

u_G is the superficial vapour velocity through a packed bed [m/s]

$\mathrm{Re}_{G,S}$ is gas phase Reynolds number

C_1, C_2, C_3, are packing specific constants

ε is the bed porosity

The packing constants are readily available [Stichmair et al., 1989] for random packing, but only a few are available for structured packing. The irrigated pressure drop can be calculated by accounting for the decrease in bed porosity due the liquid being held back in the bed. The friction factor is modified to include the liquid hold-up and thus the ratio of irrigated pressure drop to dry pressure drop is given by:

$$\frac{(\Delta P)_{irrigated}}{(\Delta P)_{dry}} = \left[\frac{\left(1-\varepsilon\left(1-\frac{h_L}{\varepsilon}\right)\right)}{(1-\varepsilon)}\right]^{\left(\frac{2+c}{3}\right)} \left(1-\frac{h_L}{\varepsilon}\right)^{-4.65} \qquad 2.128$$

$$c = \frac{\left[-\left(C_1 / \mathrm{Re}_{G,S}\right)-\left(C_2 / \left(2\,\mathrm{Re}_{G,S}^{0.5}\right)\right)\right]}{f_0} \qquad 2.129$$

The only factor left to calculate is the total liquid hold-up in the packed bed (h_L). A correlation was derived from experimental air/water hold-up data below the loading point:

$$h_{L,s} = 0.555 Fr_{L,S}^{1/3} \qquad 2.130$$

Equation 2.130 does not take into account any properties of the liquid and has been validated for air/water only [Stichmair et al., 1989]. The hold-up above the loading point is calculated from an expression that accounts for the gas friction as well as the pressure gradient in a single dimensionless pressure drop term:

$$h_L = h_{L,s}\left[1+20\left(\frac{(\Delta P)_{irrigated}}{Z\cdot\rho_L\cdot g}\right)^2\right] \qquad 2.131$$

Where:

Z is the packed bed height [m]

The flooding point is defined as the point where the irrigated pressure drop increases infinitely with a small increase in vapour load. This means differentiating the irrigated pressure drop equation yields the pressure drop at flooding:

$$\left(\frac{(\Delta P)_{irrigated}}{Z\cdot\rho_L\cdot g}\right)_{Fl}^{-2}=\left[\frac{40\left(\frac{2+c}{3}\right)\cdot h_{L,s}}{1-\varepsilon+h_{L,s}\left[1+20\left(\frac{(\Delta P)_{irrigated}}{Z\cdot\rho_L\cdot g}\right)\right]_{Fl}^{2}}\right]+\left[\frac{186h_{L,s}}{\varepsilon-h_{L,s}\left[1+20\left(\frac{(\Delta P)_{irrigated}}{Z\cdot\rho_L\cdot g}\right)\right]_{Fl}^{2}}\right] \quad 2.132$$

SUMMARY:

The fundamental model proposed by Stichlmair et al. [1989] can predict the irrigated pressure drop, liquid hold-up and flooding pressure drop of structured - and random packing materials over the whole operating region. The model was verified over a range of random and structured packing experimental data found throughout the literature.

The model pressure drop predictions compared reasonably well with the experimental data for random packing, but deviated substantially in the case of structured packing. Stichlmair et al. [1989] concluded that this model should not be used in systems with liquid viscosities higher than 5 mPa·s. The liquid hold-up was not verified experimentally, only an empirical correlation (tested only on air/water) was used in the irrigated pressure drop prediction.

In this model the irrigated pressure drop, as well as the pressure drop at the flooding point are heavily dependent on an accurate representation of the liquid hold-up in the column. Since the hold-up prediction is based on an empirical correlation and not verified experimentally, large errors are possible when this model is used in systems with liquid properties differing substantially from that of water.

2.3.4 Other Hydrodynamic Modelling Approaches

This section deals with modelling approaches not specified in the above sections. Both of the models included here are in the form of a simulation package and will merely be discussed with respect to their inputs, outputs and accuracy.

KG-Tower®:

As most of the random packing materials supplied in this project were from the manufacturer Koch-Glitsch, it would thus be sensible to include their software package as a possible verification tool as it was developed on data obtained from the respective packing materials. The software package is known as KG-TOWER®. The software package predicts the pressure drop over a packed bed by incorporating the following inputs:

- Liquid density
- Vapour density
- Dynamic liquid viscosity
- Liquid surface tension
- Kinematic vapour viscosity
- Liquid flow rate
- Packed bed height
- Vapour flow rate
- Packing type

The outputs are the pressure drop in mbar/m as well as the capacity constant (L/V) as a percentage. The system limit for the given L/V ratio is also given so that the user is notified when he/she is working outside the range of application of the system.

Piché ANN-DA Model:

Artificial neural network and dimensional analysis (ANN-DA) was used by Piché and co-workers [2001; 2001; 2001] to model the hydrodynamics and mass transfer of randomly packed columns. This model can predict the following hydraulic parameters over the entire operating range of randomly packed columns: loading and flooding capacities, total liquid hold-up, irrigated pressure drop and the packing fractional wetted area.

The general methodology surrounding the application of neural network computing as well as the data mining procedure used for the extraction of the best set of dimensionless groups involved are summarised in the section below as described by Piché and co-workers [2001].

A multiple decision procedure was developed to prune, within optimal sets of ∏ dimensionless groups, the 15 natural factors having a potential impact on the fluid dynamics and inter-phase mass transfer. The procedure is built around the following steps:

- Input/Output cross-correlation analysis
- ∏-group generation and pruning
- Artificial neural network modelling
- Analysis of variance
- Data reconciliation
- Model physical likeliness

This procedure was implemented over the entire range of experimental data found in the open literature over the past 70 years. Table 2.10 indicates the range of hydraulic parameters covered in the ANN-DA model.

Table 2.10: Range of parameters investigated in the ANN-DA model

Parameter	*Units*	*Range*	*Range Median*
Pressure	[atm]	0.066 - 102	1
Temperature	[^{o}C]	-27 - 728	22
Column diameter	[m]	0.03 - 1.4	0.3
Packing Diameter	[mm]	3.2 - 88.9	25
Void fraction	[m^3/m^3]	0.4 - 0.987	0.725
Bed specific area	[m^2/m^3]	57 - 1148	260
Bed height	[m]	0.1 - 5.9	1.3
Liquid density	[kg/m^3]	486 - 13350	1000
Liquid viscosity	[mPa·s]	0.0995 - 50	1
Surface tension	[mN/m]	11.5 - 73	48.7
Liquid velocity	[m/s]	$1.1x10^{-4}$ - $8.92x10^{-2}$	$7x10^{-3}$
Vapour density	[kg/m^3]	0.082 - 541	1.19
Vapour viscosity	[mPa·s]	$6.55x10^{-3}$ - $3.3x10^{-2}$	$1.75x10^{-2}$
Vapour velocity	[m/s]	$5x10^{-4}$ - 7.02	0.65
Liquid hold-up	[%]	0.5 - 52.2	7.5
Irrigated pressure drop	[Pa/m]	15 - 7765	723

It should be noted that the model used to predict the pre-loading region pressure drop is an extended double-slit mechanistic model, and is based on the work done by Illiuta & Larachi [2001]. The ANN-DA model requires no adjustable parameters giving it a wide range of applicability. A user friendly spread sheet is available from http://www.gch.ulaval.ca/~grandjea for further use of the model. The mass transfer part of this model will not be discussed.

SUMMARY:

The ANN-DA model can predict the liquid hold-up and irrigated pressure drop with an AARE of 13.8 % and 20 % respectively. The superficial vapour velocity at loading and flooding can also be predicted with an AARE of 21 % and 15.7 % respectively. This compares favourably to the model proposed by Billet & Schultes [1999].

2.4 Literature Review Evaluation

The section below summarises the range of applicability, as well as their accuracy (where possible) of each of the predictive models included in this literature review (see Table 2.11). An evaluative discussion then follows to determine the best predictive model(s) to validate and compare the experimental data against. Finally, a discussion on both random and structured packing models is included, specifically referring to future work.

Table 2.11: Summary the semi-theoretical models overall performance characteristics found throughout the literature

Model	*Column Parameters*					*Prediction of Correlation Parameters [Accuracy, AARE %]*			*Fluid Property Range*						
	Column ID [m]	*Packing Type*	*a* $[m^2/m^3]$	*ε [fraction]*	*z [m]*	$\left(\frac{\Delta P}{\Delta z}\right)_d$	$\left(\frac{\Delta P}{\Delta z}\right)$	h_L	ρ_L $[kg/m^3]$	*Liquid Load*	μ_L *[mPa·s]*	*σ [mN/m]*	ρ_V $[kg/m^3]$	*Vapour Load*	μ_V *[mPa·s]*
SRP II	0.245–1	Structured	101–492	0.7–0.98	2.7–4	Yes [N/A]	Yes [9.7]	Yes [N/A]	383–1000	0.0068–0.34 [m/s]	0.049–1	1.1–73	0.35–85	0.46–4.37 [m/s]	0.0076–0.018
Delft	0.192–1.4	Structured	244–394	0.96–0.98	2	Yes [N/A]	Yes [N/A]	Yes [N/A]	561–1000	1.5–69.8 $[m^3/(m^2 \cdot h)]$	0.161–1	8–72	1.19–13.14	0.25–4.7 $[(m/s)\cdot(kg/m^3)^{0.5}]$	0.0069–0.018
Billet	0.076–0.8	Both - mainly Random	54–772	0.57–0.99	0.76–3.95	Yes [N/A]	Yes [10.8]	Yes [6.7]	800–1810	0.61–82.8 $[m^3/(m^2 \cdot h)]$	0.59–185	20.8–86.3	N/A	0.21–5.09 $[(m/s)\cdot(kg/m^3)^{0.5}]$	N/A
Maćkowiak	0.1–0.4	Both	54–500	0.63–0.98	N/A	Yes [10]	Yes [15]	Yes [N/A]	660–1260	0.3–200 $[Re_L]$	0.2–8	14–74.6	0.6–3.6	2–4000 [Pa/m]	0.0065–0.018

Table 2.11 continued

Brunazzi & Paglianti	0.05–1	Structured	125–500	0.9–0.95	N/A	Yes [20]	Yes [20]	Yes [N/A]	N/A	5–125 [$m^3/(m^2 \cdot h)$]	1–7.7	34–72	N/A	±0.3–5 [$(m/s)\cdot(kg/m^3)^{0.5}$]	N/A
Woerlee	0.038–0.79	Both	78–375	0.59–1	N/A	Yes [N/A]	Yes [N/A]	No –	826–1090	N/A	1–8.1	26–73	1.21–27.39	N/A	N/A
Illiuta & Larachi	0.295–1.2	Structured (pre-load)	115–628	0.83–0.98	N/A	No –	Yes [25]	Yes [13.8]	N/A	0.0006–0.05 [m/s]	N/A	N/A	N/A	0.1–2.6 [m/s]	N/A
Ranke	0.4 (quadratic)	Structured	750	N/A	N/A	Yes [N/A]	Yes [N/A]	Yes [N/A]	650	8 [$m^3/(m^2 \cdot h)$]	0.31	18	1.7	0–1.8 [$(m/s)\cdot(kg/m^3)^{0.5}$]	0.012
Stichlmair	N/A	Both - mainly Random	71–472	0.56–0.99	N/A	Yes [N/A]	Yes [N/A]	Yes [N/A]	N/A	N/A	up to 5	N/A	N/A	N/A	N/A
Piché et al.	0.03–1.4	Random	57–1148	0.4–0.98	0.1–5.9	No –	Yes [20]	Yes [13.8]	486–13350	0.11–89.2 [mm/s]	0.099–50	11.5–73	0.082–541	0.0005–7.02 [m/s]	0.0065–0.033

2.4.1 Viable Verification Model(s)

Kister [1992] recommends that pressure drop data (if available) should be used by interpolation to determine the pressure drop in a column. If no pressure drop data is available, then empirical correlations should be used to determine the pressure drop and flooding point of a packed column. The problem is that these correlations only give information about the pressure drop; they provide no additional information on the local fluid properties. Thus, all of the empirical correlations and capacity charts will not be considered as a viable experimental data verification tools in this project.

Quite a number of semi-theoretical models can be found throughout the literature with varying degrees of complexity, accuracy and range of application. The classic channel models contain a fair amount of empiricism, with the more recent models becoming more fundamental in nature. However, the more recent models do not predict all the variables required in the hydraulic operating regime (irrigated pressure drop and liquid hold-up in the pre-loading -, loading - and flooding region) as of yet.

It is important that a model is validated over a large experimental database, as well as being able to predict all the hydraulic parameters (since it improves its general application range). The models found in the literature that comply with these conditions are the following models: SRP II, Delft, Billet & Schultes [1999], Stichlmair et al. [1989], Maćkowiak [1991] and the ANN-DA model by Piché et al. [2001]. In this project the prediction of random packing hydraulics are of importance since one of the objectives is to characterise the hydraulic capacity of Intalox® Ultra™, which is a random packing. Thus, the SRP II -, Delft models are excluded as viable verification tools.

The possible remaining models are the following: Billet -, Stichlmair -, Maćkowiak - and the ANN-DA model. Of these remaining possibilities the most accurate model is needed to verify the experimental data against. Based on the summary in Table 2.11 the above mentioned models should perform favourably over the entire hydraulic operating range for an air/water system. To evaluate the relative accuracies of each model, two figures (Figure 2.3 and Figure 2.4) were constructed where these models are compared to each other (referring to irrigated pressure drop and liquid hold-up) at a typical random packing operating load. The liquid load was chosen at 49 $m^3/(m^2 \cdot h)$ since random packing is favoured above structured packing at similar rates and above.

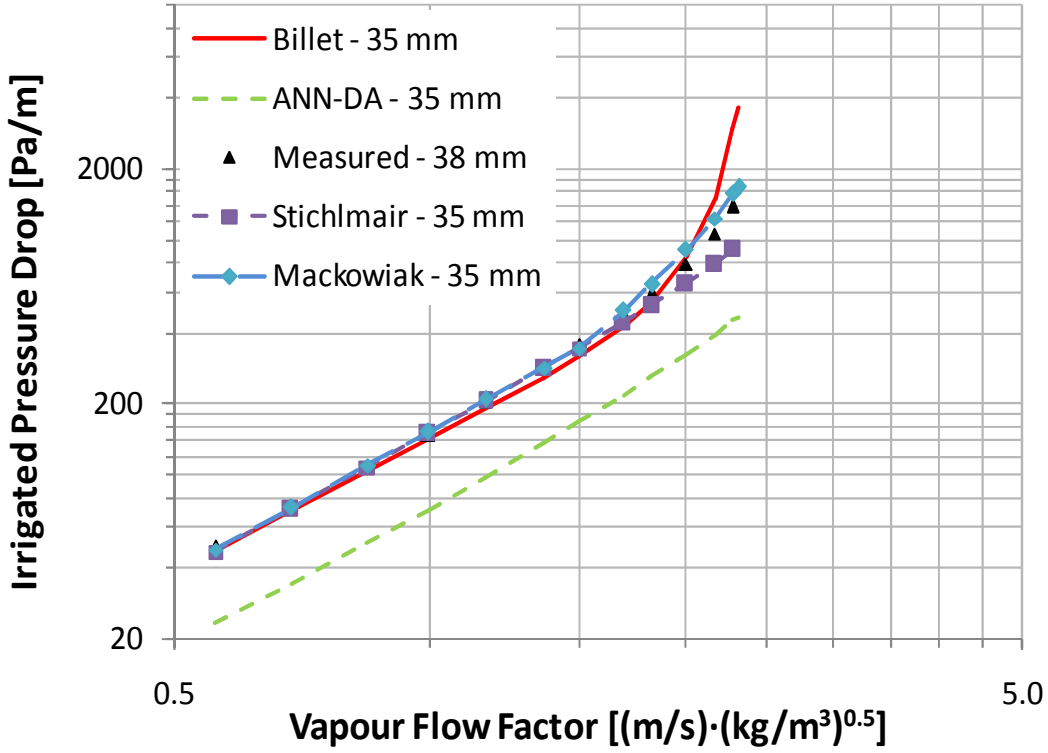

Figure 2.3: Pall® Ring predictive pressure drop modelling comparison with air/water at a liquid rate of 49 $m^3/(m^2 \cdot h)$

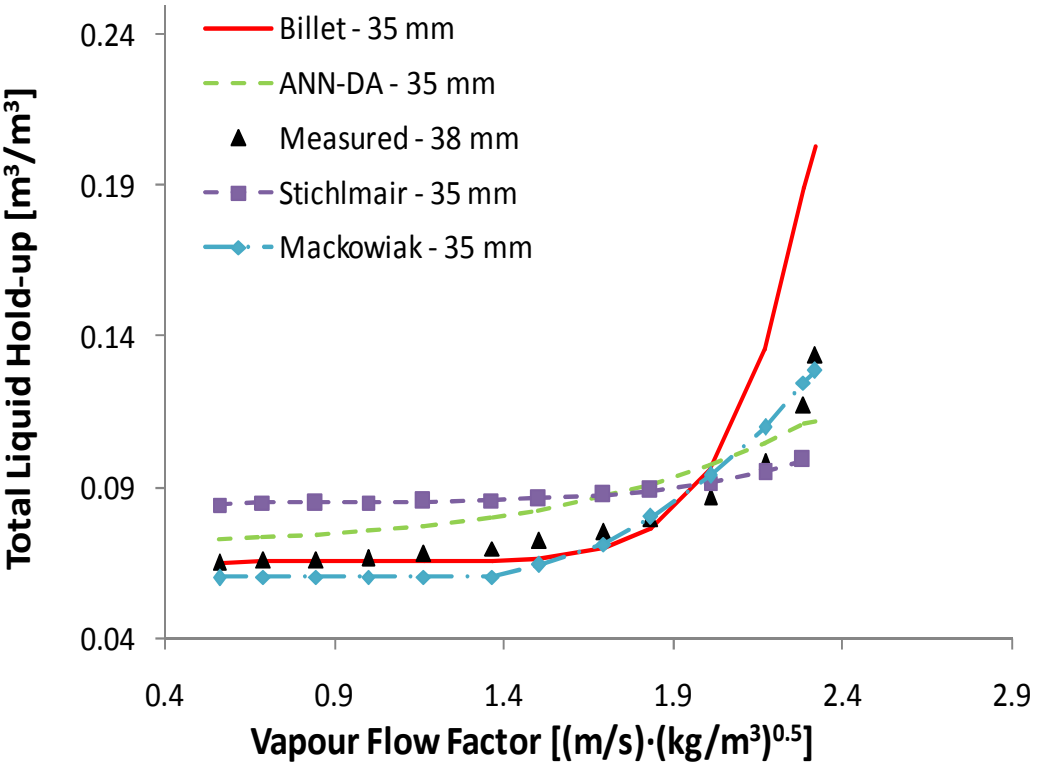

Figure 2.4: Pall® Ring predictive liquid hold-up modelling comparison with air/water at a liquid rate of 49 $m^3/(m^2 \cdot h)$

Experimentally measured data was included in both the figures to illustrate the relative accuracies of each of the predictive models. Even though the experimental data was measured with 38 mm Pall® Rings, the only packing size available in all the above mentioned models was 35 mm Pall® Rings. The difference between the 35 mm and 38 mm parameters should be marginal and thus would give a good general indication of each of the model's performance.

From Figure 2.3 and Figure 2.4 it is evident that the ANN-DA model under-predicts the pressure drop and over predicts the liquid hold-up at moderate liquid rates. This model also fails to predict the sharp increase in both pressure drop and liquid hold-up in the late loading to flooding region. The model proposed by Stichlmair [1989] predicts the pressure drop in the pre-loading and loading region accurately, but also fails to predict the sharp increase in pressure drop near the flooding region. The liquid hold-up is severely over-predicted at this moderately high liquid rate and this model again fails to predict the sharp increase in liquid hold-up near the flooding region.

The two best performing models are the models proposed by Billet [1999] and Maćkowiak [1990]. Both models predict the correct trend of the pressure drop over the entire hydraulic operating range. The model proposed by Billet [1999] predicts the sharp increase in both the pressure drop and liquid hold-up curves slightly better, as the experimentally measured data should be marginally lower in both cases due to the enlarged packing element size. Of these two models, the model by Billet [1999] has been acknowledged as a better model for industrial scale-up [Heymes et al., 2006]. Thus, based on this notion the Billet model will be used to verify the accuracy of the experimental data. The simulation package KG-TOWER® will also be used as back-up verification tool for the pressure drop of the experimental data. It would be sensible to use the random packing manufacturer's own simulation package as well to verify the experimental data.

2.4.2 Scope for Work

Structured packing models:

Based on the literature review above and the work done by Erasmus [2004] it is evident that the models (structured packing) that were validated over a wide range of experimental data, predict a conservative dependence of capacity on liquid viscosity. The models in question are the following: SRP II, Delft, Stichlmair et al. [1989] and Billet & Schultes [1999]. In the SRP II model, Fair et al. [2000] indicates that the pressure drop in the loading region is over predicted and he also suggests that liquid flow-related parameters are not represented accurately. This over prediction is most likely due to the fact that the influence of viscosity isn't accounted for properly (as the effects of under wetting aren't a factor in the loading region, which is due to surface tension).

From Table 2.11 the limited range of liquid viscosities that were investigated in the Delft model can be seen. Based on the work of Erasmus [2004], the Delft model did not predict the liquid hold-up accurately in the loading region and thus the conclusion is made that a conservative dependency on viscosity is implemented in the model. The model by Stichlmair et al. [1989] is mostly based on random packing experimental data and thus, is not of a big concern here. However, this model's liquid hold-up prediction is verified on only air/water data and the author states that the models should not be used in systems where the liquid viscosity is higher than 5 mPa·s. The model by Billet & Schultes [1999] is also mainly for random packing, and has a sound fundamental basis for its pressure drop correlation, thus it will not be discussed further in this structured packing evaluation.

Some of the more recent models have a fundamental approach to the modelling of the liquid hold-up and pressure drop in the pre-loading region, but there still is not a model for structured packing that fully incorporates the effect of liquid viscosity at high flow rates (loading region). If the liquid hold-up can be predicted accurately, the effective phase velocities can be determined more accurately which in turn would lead to better mass transfer estimations. New modelling methods such as ANN-DA might prove to be successful as well in the case of structured packing, only if a substantial and reliable database of experimental data is accessible.

Random packing models:

To further evaluate the more reliable random packing models found throughout the literature, these models are compared in an air/water hybrid scenario where the dynamic viscosity is increased significantly (25 mPa·s). Based on the work done by Schultes [2010], there is a need to be able to predict the hydraulic parameters in extreme distillation applications. This refers to high liquid rates (> 80 $m^3/(m^2 \cdot h)$) and extreme fluid properties. He also indicated that there is need to predict the hydraulic operating parameters of modern high capacity packings [Schultes, 2010].

Figure 2.5 and Figure 2.6 illustrates the predictive performance of current random packing models at an elevated dynamic viscosity:

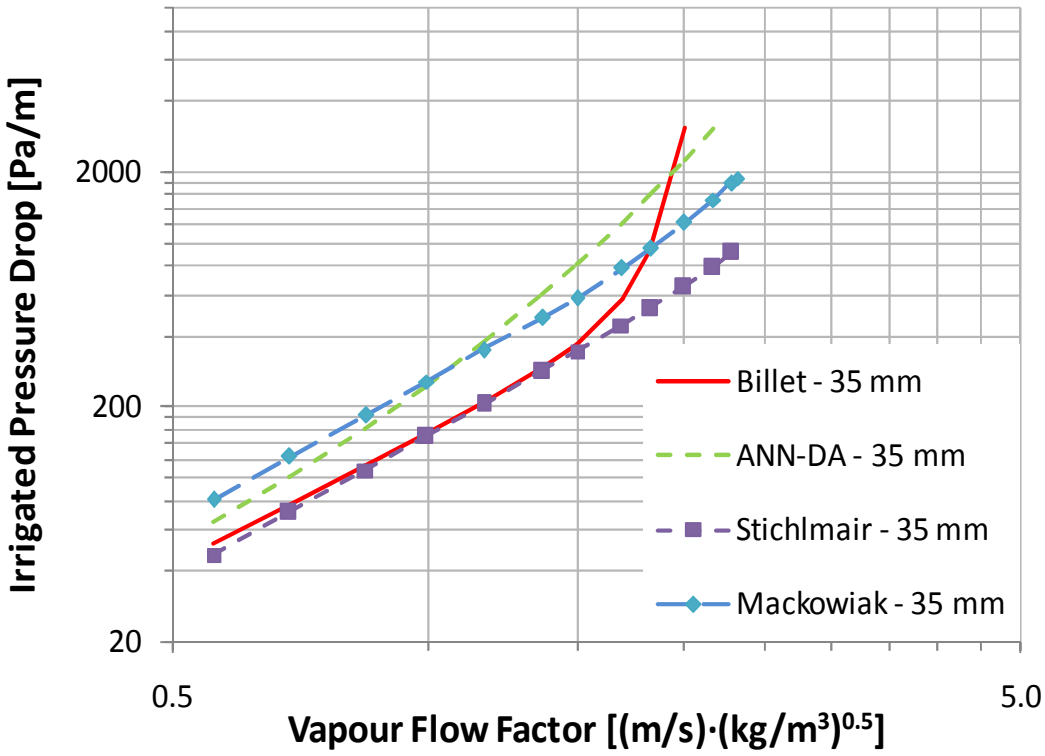

Figure 2.5: Pall® Ring predictive pressure drop modelling comparison at a liquid rate of 49 $m^3/(m^2 \cdot h)$ and dynamic viscosity of 25 mPa·s

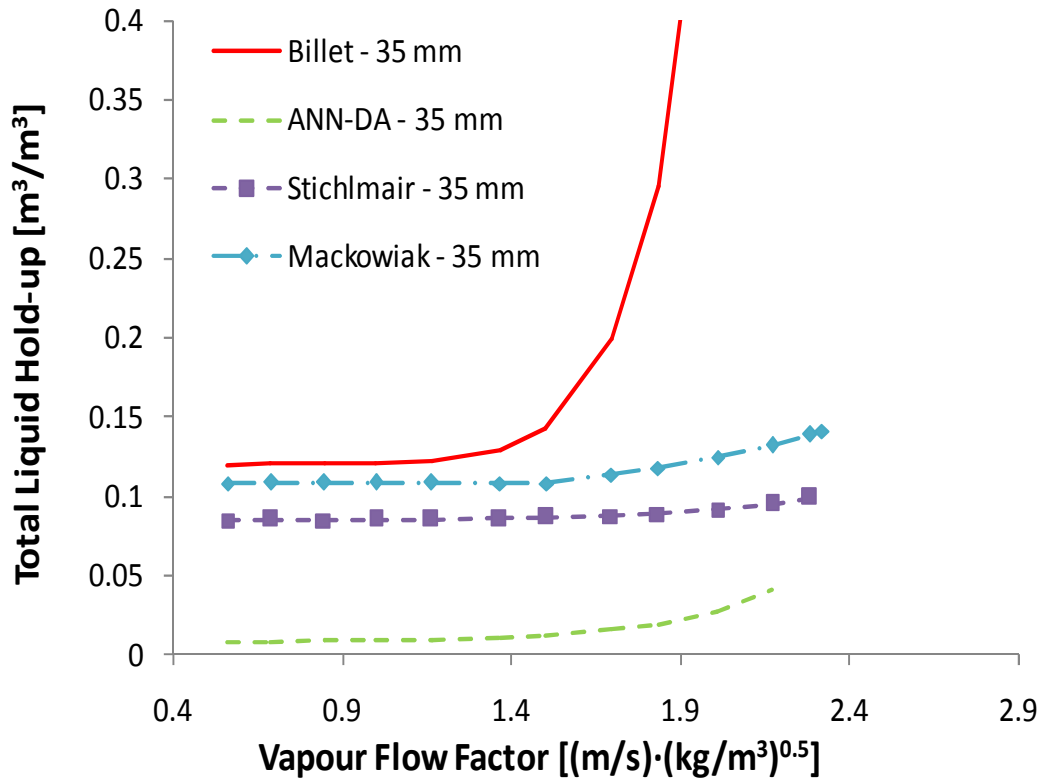

Figure 2.6: Pall® Ring predictive liquid hold-up modelling comparison at a liquid rate of 49 $m^3/(m^2 \cdot h)$ and dynamic viscosity of 25 mPa·s

From Figure 2.5 and Figure 2.6 it is evident that the models proposed by Maćkowiak [1990] and Stichlmair [1989] fail to predict the correct pressure drop and liquid hold-up trends. This is attributed to the fact that these models have only been verified up to a dynamic viscosity of 8 and 5 mPa·s respectively (see Table 2.11) and is to be expected. The ANN-DA model [Piché et al., 2001] also fails to predict the correct pressure drop and liquid hold-up trends even though it was verified up to a dynamic viscosity of 125 mPa·s. The only model that shows the correct general trends is the model proposed by Billet [1999]. The accuracy of these predictions can only be verified with further research at these elevated fluid properties. Lastly, none of the random packing predictive models were verified at liquid rates above 90 $m^3/(m^2 \cdot h)$ (see Table 2.11) and thus have to be extrapolated at these high liquid rates which could lead to severe errors.

Thus, to conclude, a need for structured packing models over the entire hydraulic range emerged from this literature study. The lack of proper validation of fluid property influences on the hydraulic parameters is also of concern here. This, in turn, leads to a need of experimental data to supplement the current databanks where future models can be derived from (or extension of current models).

From the literature a need for high liquid rate data, as well as increased fluid property data arose. This data could be used to either supplement the current models, or lead to new models that are specifically aimed at predicting the hydraulic parameters of the new high capacity random packings (4^{th} generation and onwards).

3 Experimental Methods and Design

A need arose from the literature for a test system that can characterise the hydraulic performance of random and structured packing. In order to test over a wide range of liquid and vapour rates, a normal distillation column under total reflux cannot be used. Most of the test systems in the literature were either a total reflux column, or a normal industrial column that supplied the data. In the case of a total reflux column the system is bound to the specific liquid to vapour ratio (L/V), meaning that it's impossible to vary the vapour rate freely without altering the liquid rate as well. In the case of industrial columns it won't be feasible to deviate from the specification rates for research purposes. Thus, a non-reacting, non-foaming system with no mass transfer is required where the liquid and vapour flow rates can be varied independently from each other, and where the fluid properties can be varied to study their respective effects. By eliminating the mass transfer, the data collected will be a simplified version of what's happening in an industrial column. In industrial columns the fluid properties change between each stage, where in this system the liquid and vapour will have constant densities.

Since one of the main objectives in this project is to measure the pressure drop and liquid hold-up of 1.5" Intalox® Ultra™ (4^{th} generation), as well as compare it to older generations of random packing (section 1.6), it is essential to verify the system with a well-established random packing frequently used in the industry. The random packings chosen for verification/comparative purposes are 38 mm Pall rings (2^{nd} generation) and 1.5" IMTP (Intalox® Metal Tower Packing, 3^{rd} generation).

This section is divided into the following sub-sections: the design objectives are discussed first with the scope and limitations following thereafter. Next, the concept design of the system is discussed followed by the detailed design. The experimental method is then discussed followed, lastly, by the limitations on measurement accuracy.

3.1 Design Objectives

One of the main objectives of this project is to design and construct a setup that can accurately measure (and aid in the visual classification of) the hydraulic capacity of both random and structured packing over a wide range of liquid and gas flow rates. Also, the setup should be able to investigate the influence of physical liquid and gas properties on the pressure drop, liquid hold-up and entrainment (for future research) of packing material (as found in section 1.6). The liquid properties include density, viscosity and surface tension. The gas properties include density and, to a lesser extent, viscosity.

3.2 Scope and Limitations

Various limitations defined the scope of the construction of the packed column. These limitations are discussed individually below:

3.2.1 Fluid Properties

In order to accomplish the task of eliminating mass transfer in the system, care was taken with the selection of the liquid and gas systems. If the flashpoint is low or if the vapour pressure is high, evaporation of the liquid is inevitable, this would mean that mass transfer is taking place. In addition, if this is the case then there's a risk of explosion due to the flammable liquid in the vapour phase (only when flammable liquids are used). Therefore, pure, inert, technical grade gasses should be used to lower the risk of explosion.

Thus, based on the above limitations the liquid and gas systems depend on the availability, cost, corrosive properties and most importantly, safety.

3.2.2 Range of Operability

Based on the literature review summary in Table 2.11, the liquid and vapour rates that were investigated ranged (on average) between 1.5 - 90 [$m^3/(m^2 \cdot h)$] and 0.3 - 5 [$(m/s) \cdot (kg/m^3)^{0.5}$] respectively. With new high capacity packings entering the market, these rates may be higher than the above mentioned. Another factor limiting the liquid rate is the minimum liquid wetting rate for random and structured packing respectively. Kister [1992] suggests that the minimum wetting rate for structured packing is around 0.2445 [$m^3/(m^2 \cdot h)$] due to the capillary action that promotes self-wetting. The minimum wetting rate for random packing is 10 times higher than that equating to a rate of roughly 2.45 [$m^3/(m^2 \cdot h)$]. However, at these low rates liquid distribution tends to become a problem. Thus, the liquid range in this design is chosen to be between 0 - 122 [$m^3/(m^2 \cdot h)$]. Since random packing is evaluated in this project the measuring range is 6 - 122 [$m^3/(m^2 \cdot h)$].

3.2.3 Materials of Construction

Most organic solvents have corrosive properties that dissolve seals and polymeric compounds. To counteract this, polytetrafluoroehtylene (PTFE) or a fluoropolymer elastomer (Viton) seals were used. Any viewing ports throughout the column should be properly specified to be resistant to the organic solvents. Thus, borosilicate glass was selected as viewing ports as well as for the packed bed sections. Borosilicate glass is known for its universal resistance to corrosion as well as its extremely low thermal expansion coefficient. This relates to a reduced chance of the column cracking during sizable temperature differences between summer and winter. Since water will be used as test system, stainless steel 304 should be the material of construction for the additional packed column sections.

3.2.4 Safety

In order to cover a wide range of liquid and gas properties, the use of flammable liquids and gasses are necessary. With the use of flammable liquids and gasses special rules and legislation apply. Precautions regarding sensor - and electronic device selection as well as their placement have to be made based on the material safety data sheet (MSDS) and operating conditions of the liquids and gasses.

Safe operation is still of concern, thus a Hazard and Operability Study (HAZOP) was conducted in conjunction with the original one conducted by Uys [2010] and is discussed in section 3.4.8. Lastly, air leaking into the system could result in fires and/or explosions. To eliminate this risk the column should be operated at pressures slightly higher than atmospheric and the surrounding areas should be well ventilated.

3.3 Process Concept

The process concept is present in Figure 3.1. The following units are incorporated into this system:

1. A column that can characterise the hydrodynamic behaviour of random and structured packings.
2. Vessels to measure the liquid hold-up and entrainment rate in the packed column.
3. A liquid pump to circulate the liquid and thus replace the need for a condenser that is usually present in a distillation column.
4. A blower to circulate the gas and in the process remove the need for a reboiler that is usually present in a distillation column.

5. A surge tank to act as a dampener to possible system pressure fluctuations. Another purpose of this tank is to act as a droplet settling tank to remove the excess liquid droplets carried over by the vapour from the de-entrainment section of the column.
6. A heat exchanger to control the operating temperature of the system.
7. A range of well calibrated sensors to measure the flow rates, temperatures, absolute pressure and pressure drops.
8. A control system to control the temperature, pressure and flow rates as well as logging the data continuously.

It should be noted that points 3 - 8 have already been established by Uys [2010]. Thus, only additional sensors and modifications to the control system are required and their seamless integration to the existing system. A brief description of the main circulation lines follows after the flow diagram with a detailed discussion of each unit in section 3.4 (and the specifications of each unit in section 8.1 of the Appendix).

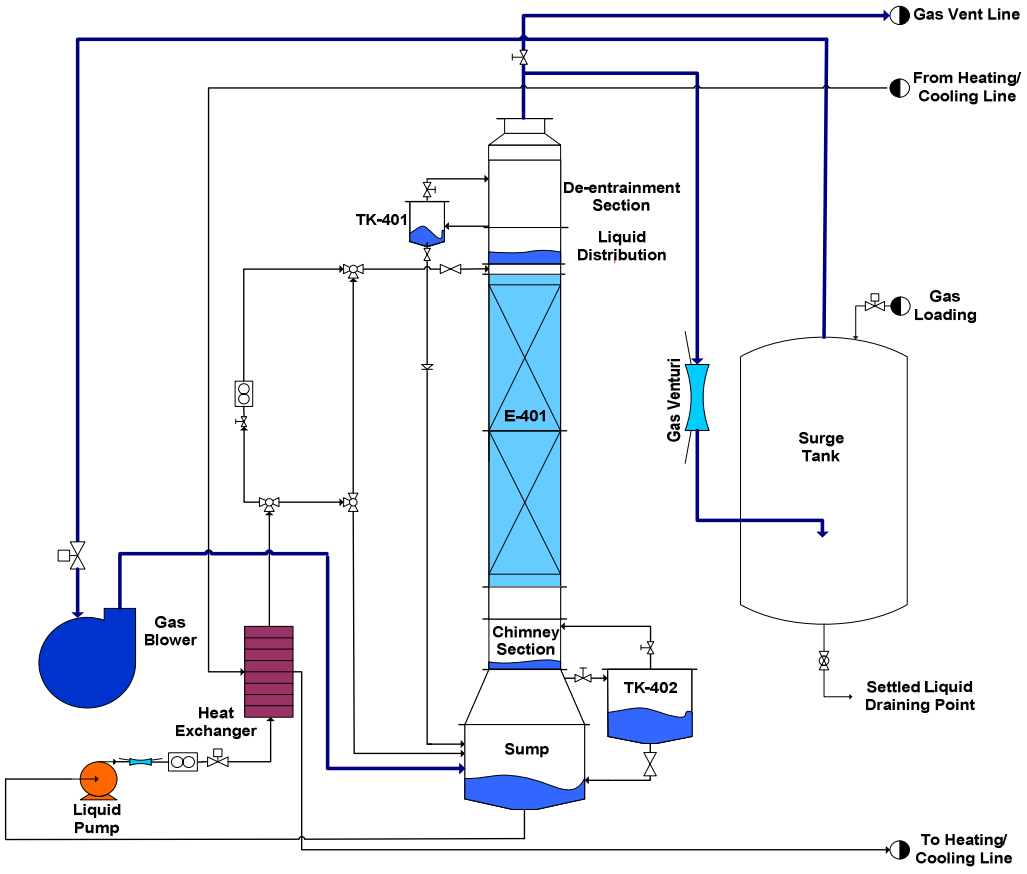

Figure 3.1: Packed column flow diagram

3.3.1 Liquid Circulation Loop

The liquid from the sump is circulated via a centrifugal pump through a venturi - and a liquid flow meter (medium to high liquid rates) and control valve to a heat exchanger where the excess process heat is removed. From the heat exchanger the liquid can be diverted in two directions via a 3-way valve:

1.) Into a low liquid flow line (< 2 m^3/h) where a needle valve and another flow meter is situated or,
2.) Into a high liquid flow line (2 - 15 m^3/h) where the flow can again be diverted (via another 3-way valve) directly to the sump (to heat up the liquid to operating conditions), or to another 3-way valve where the low and high flow lines meet before the liquid enters at the top of the packed column.

The liquid enters the packed column via the liquid distribution section and flows down the column where it is brought into contact with the gas. The liquid is then collected in the chimney section where it's diverted to the sump via the liquid hold-up tank (TK-402[1]). The dynamic hold-up is measured by cutting the feed directly before it enters at the top of the column via a pneumatic valve, as well as closing the pneumatic valve at the bottom of TK-402. The remaining liquid in the column drains into the hold-up tank and the amount is measured over time (more details in section 3.4). Entrained liquid during normal operation is collected in the de-entrainment section and measured over time in the de-entrainment tank (TK-401[1]).

3.3.2 Gas Circulation Loop

The gas is fed to the column via a centrifugal blower and enters at the top section of the sump. The gas is then evenly distributed by a gas distributor which is located in the chimney section and then travels upwards through the column where it passes through the liquid distribution section as well as the de-entrainment section. The gas exits at the top of the column where it passes through a venturi gas flow meter before it enters a surge tank, which is connected to the suction side of the blower.

[1] Refer to Figure 3.1

3.4 Detailed Design

The detailed design section consists of a P&ID (Figure 3.2), followed in depth discussion on each of the various selection processes that were made during the design, construction and commissioning phases of the experimental setup. Any additional specifications can be found in section 8.1 and 8.2 in the appendix. Based on the detail design requirements and control objectives, the original P&ID of the system was reconstructed and modified with permission from Mr. E.C Uys to accompany the packed column. The P&ID was adapted to conform to the original equipment and line numbers used. A P&ID of the heating and cooling system is included in section 8.3 of the Appendix as it was reprinted with permission from Uys [2010]. It should be noted that all the subsequent numbers and annotations from here on refer to Figure 3.2, unless stated otherwise.

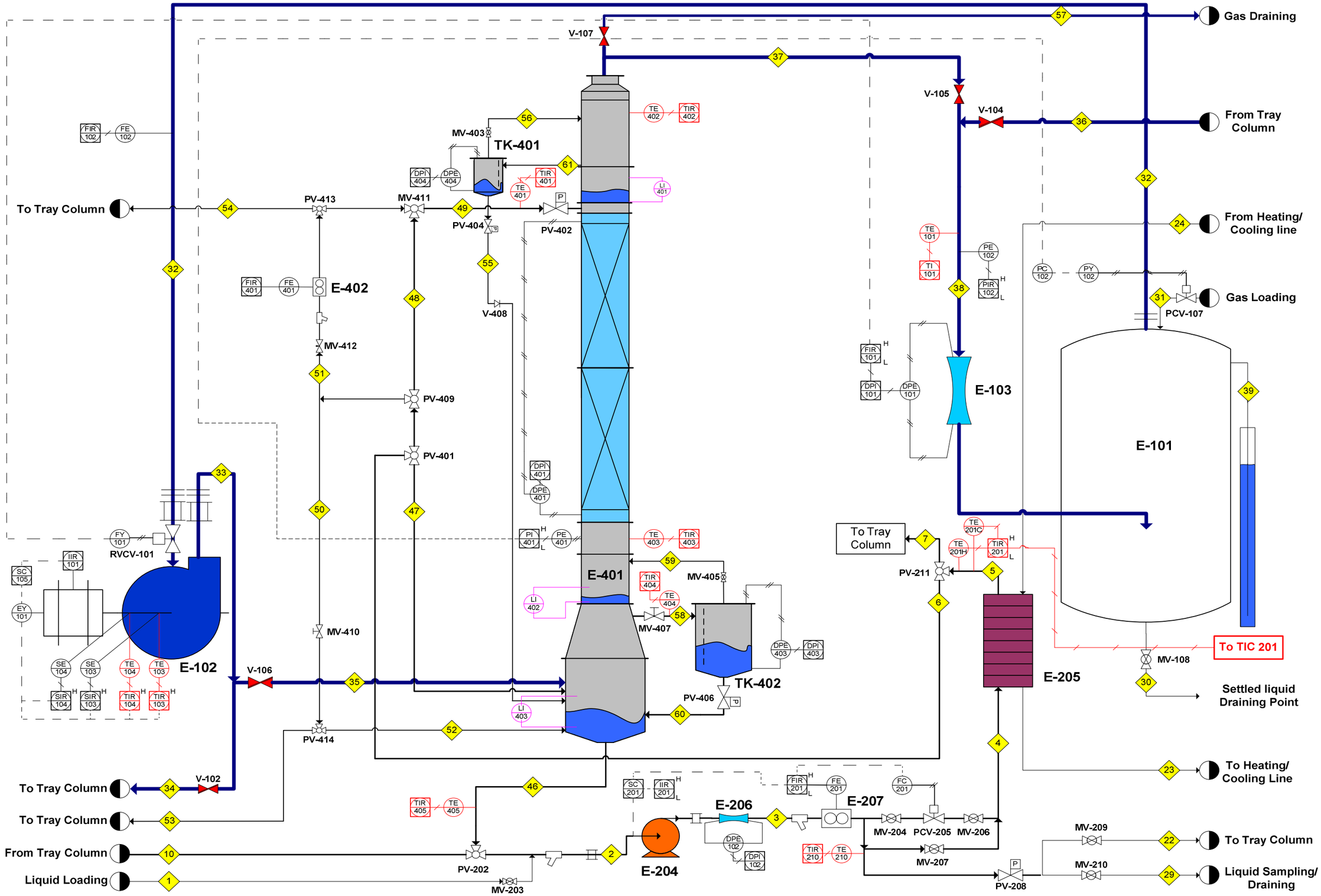

Figure 3.2: P&ID of packed column hydrodynamic characterisation setup

3.4.1 Suitable Liquid and Gas Systems

Before any sizing of units, sensors or piping can be done, the range of liquid and gas physical properties needs to be defined. It is important to extend the range of properties as wide as possible whilst still remaining within the property range found in commercial distillation applications. Probably one of the most common applications of distillation is the separation of crude oil into its components. The main products are: liquid petroleum gas (LPG), gasoline, naphtha (and its derivatives), kerosene, fuel oil (light to heavy oils), lubricating oils, paraffin wax, asphalt and tar. A wide range of hydrocarbons are covered in this process ranging up to C_{12} for gasoline. The other "heavier" products with higher boiling points range up to C_{70} in some cases for heavy fuel oils. The higher boiling point products increase in viscosity as the boiling point increases. Another common application of distillation is the separation of air into its components: oxygen, liquid nitrogen and ultra-pure argon. Thus, Table 3.1 gives an indication of the physical property range found in some of the more common distillation applications:

Table 3.1: Property range of common distillation applications (modified with permission from Uys, [Uys, 2010])

Compound	*Formula*	*Boiling Point Temp [^oC]*	*Absolute Pressure [kPa]*	*Liquid Density [kg/m^3]*	*Vapour Density [kg/m^3]*	*Liquid Viscosity [mPa·s]*	*Surface Tension [mN/m]*
Methane	CH_4	-162	100	422	1.8	0.12	13
Butane	C_4H_{10}	-0.8	100	602	2.7	0.20	15
Pentane	C_5H_{12}	36	100	610	2.9	0.20	14
Octane	C_8H_{18}	125	100	612	3.7	0.20	12
Decane	$C_{10}H_{22}$	174	100	604	4.1	0.20	11
Dodecane	$C_{12}H_{26}$	216	100	595	4.5	0.20	9
Oxygen	O_2	-183	100	1142	4.4	0.20	13
Oxygen	O_2	-153	1000	976	38.5	0.10	6
Cyclohexane	C_6H_{12}	80.	100	720	2.97	N/A	18
Water	H_2O	100	100	958	0.59	0.28	59
Water	H_2O	20	2.3	998	0.017	1.00	73
Water	H_2O	25	3.2	997	0.023	0.89	72
Silicone Oil	$(C_2H_6OSi)_n$	140	<1	965	>1	50	19

The silicone oil was added to the table to give an example of the viscosities that can be encountered with lubricant oils. In an effort to eliminate mass transfer, evaporation of the liquids into the vapour phase needs to be avoided. The operating temperature is chosen to be at 25°C as this requires no excessive heating or cooling for temperature control. Based on the operating temperature, the liquids should have a low vapour pressure to minimise the possibility of evaporation. At a constant temperature and with a closed gas loop, evaporation occurs initially until the gas is saturated (which relates to a no mass transfer system). The range of properties tested throughout the literature is shown in Table 2.11. The range of fluid - and gas properties are found in Table 3.2 and Table 3.3, this includes the range for future work as well.

Table 3.2: Gas physical properties at 25°C and 1 atm (obtained mostly from www.nist.gov)

Gas	*Molecular Weight [kg/kmol]*	*Density [kg/m³]*	*Dynamic Viscosity [mPa·s]*
Air	29	1.18	1.82×10^{-2}
He	4	0.16	1.98×10^{-2}
CO_2	44	1.78	1.49×10^{-2}
SF_6	146	5.96	1.53×10^{-2}

Table 3.3: Liquid physical properties at 25°C and 1 atm (obtained mostly from www.nist.gov)

Liquid	*Molecular Weight [kg/kmol]*	*Density [kg/m³]*	*Dynamic Viscosity [mPa·s]*	*Surface tension [mN/m]*	*Vapour Pressure [mm Hg]*
Water	18	997	0.89	73	23.36*
n-Butanol	74	810	2.6	24.9	6.64*
Isopar G	Not specified	748	0.84	23.1	Not specified
Silicone Oil	74	963	50	19	<5
Ethylene Glycol	62	1113	15.4*	48	0.12 [hPa]

The values that were not available from NIST were estimated from Perry et al. [1999] (these values are marked with an *). These values will be verified for each test system by physically measuring the properties of interest. Isopar G is an Isoparaffinic hydrocarbon product from Exxon Mobil.

3.4.2 Existing Setup

The bulk of the utility system was designed and built by Uys [2010] in an attempt to design and construct a facility to characterise the hydrodynamic behaviour of tray columns. These units are of concern in this project and will be discussed accordingly. The existing system includes the following: Gas blower, surge tank, heat exchanger, gas venturi flow meter and finally the pressure control. The description below (remainder of section 3.4.2) is adapted from the work of Uys [2010].

Gas Blower (E-102):

A centrifugal blower was chosen to circulate the gas through the pilot plant. The blower was placed in an acoustic enclosure (to reduce noise levels) outside the laboratory on a specially designed plinth to support these units. An inverter was connected to the blower to control the gas flow rate, especially at low volumetric rates. The design specifications of the gas blower can be seen in section 8.1 of the Appendix.

Liquid Pump (E-204):

A centrifugal pump with a delivery side pressure of 10 bar was chosen to circulate the liquid through the system. The full design specifications of the liquid pump can be seen in section 8.1 of the Appendix.

Surge Tank (E-101):

A surge tank was designed and constructed to act as a dampener against any system pressure oscillations. Another purpose of the surge tank is to improve the efficiency of the de-entrainment (in the columns) by providing sufficient residence time for the liquid droplets to settle out. The design specifications of the surge tank can be seen in section 8.1 of the Appendix.

Heat Exchanger (E-205):

A heat exchanger was designed and constructed to 1) remove the excess heat from the system, or 2) raise the temperature of the system to the desired operating temperature. The operating temperature was chosen as 25^{o}C with a maximum 80^{o}C (for future research if needed). A net energy value of 17.55 kW needed to be removed from the system based on an energy balance. The design specifications of the heat exchanger can be seen in section 8.1 of the Appendix.

Gas Venturi Flow Meter (E-103):

A gas venturi flow meter was designed and constructed as the use of a single flow meter to cover the whole operating range (as stated in section 3.2.2) was impossible. A venturi was found to be more accurate than a Pitot tube and an Orifice plate, as the discharge coefficient has a more linear relationship to the Reynolds number over the operating range. The design specifications of the gas venturi can be seen in section 8.2.1 of the Appendix.

Pressure Control:

As mentioned in section 3.2.4 the system should be operated at pressures slightly above atmospheric when using flammable liquids. To achieve this, a pressure control valve (PCV-107) was placed between the regulator valve of the gas cylinder and the surge tank (E-101). A liquid seal (in line 39) was constructed and attached to the surge tank to prevent the system from over-pressurising. A limit of 10 kPa above atmospheric was used to determine the liquid height of the seal.

3.4.3 Packed Column Design (E-401)

The packed column design was done with the aid from industry experts from both Sasol and Koch-Glitsch. As shown in Figure 3.1, gas enters at the bottom of the column where it passes through a chimney section to distribute it evenly. The gas then passes through the packed bed, liquid distributing section and finally the de-entrainment section before it exists at the top of the column. The liquid is fed to the column via the liquid distribution section from where it flows downwards through the packed bed to the chimney section where it's collected and bypassed to the sump via the liquid hold-up tank. Based on this process, the column design can be categorised into the following main subsections:

1.) Column shape and size
2.) Liquid distribution section
3.) Gas distribution section
4.) De-entrainment section
5.) Visibility
6.) Liquid sump

Column Shape and Size:

The column was chosen to have a diameter of 400 mm (the inner diameter has a tolerance of 6 mm) because in practice, research column diameters have to be around 400 mm ID or larger to be of industrial value. This is based on research showing that

wall-effects become too prominent at smaller diameters. The diameter chosen was due to the fact that industrial packing experts produce a standard size structured packing in the above mentioned range (for future research). The packed bed height was chosen as 3 m due to height restrictions in the construction area. It also falls well within the recommended height by Kister [1992] of ±6 m before re-distribution of the liquid is required. The random packing support plate and hold-down grid was supplied and tested by Koch-Glitsch. The hold-down grid is used to prevent the packing material from becoming fluidised at high gas velocities.

Figure 3.3 shows a detailed drawing of the packed column with the sections included and Figure 3.4 shows some of the most important dimensions of the column. The packing materials used and their specifications are discussed in section 3.5.

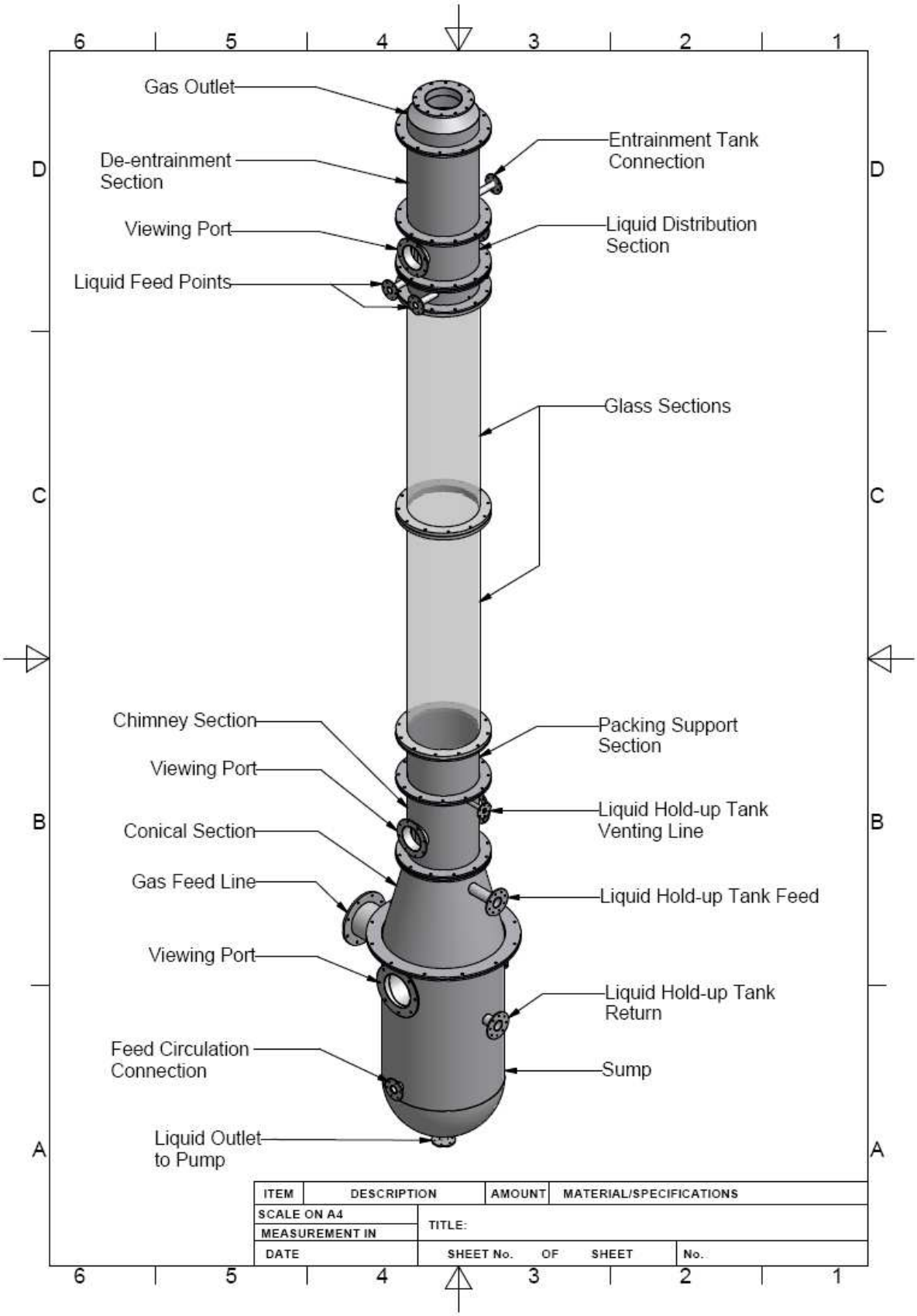

Figure 3.3: Detailed packed column with components

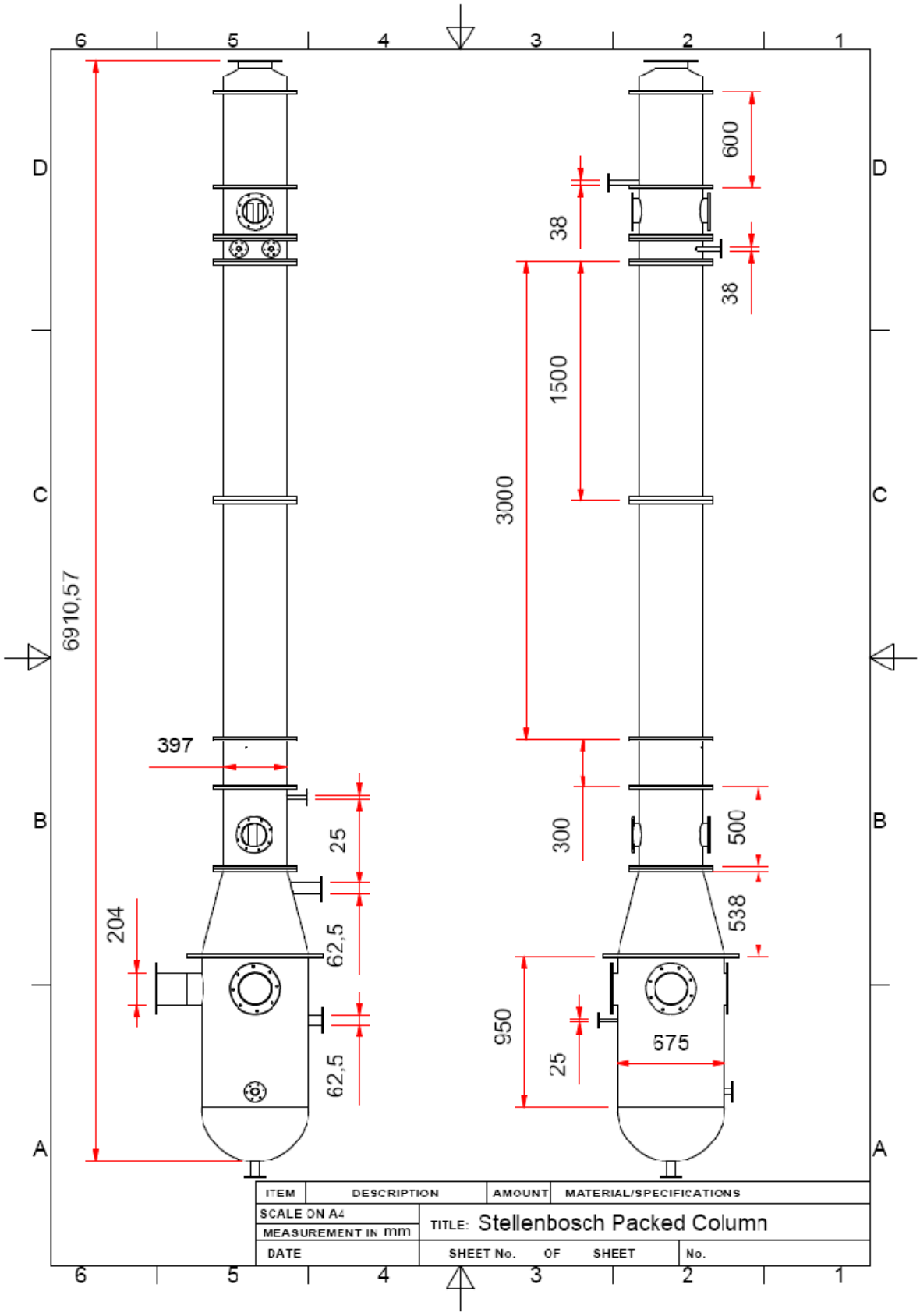

Figure 3.4: Detailed packed column with dimensions

Liquid Distribution Section:

Liquid distribution in packed columns (especially structured packing) is critical, thus special attention was given to the design of the liquid distributors. The operating range of the system is 6 - 122 $m^3/(m^2 \cdot h)$ and no single distributor would cover the whole operating range. Thus, 3 distributors were designed and built to cover the following ranges: Low flow - up to 20 $m^3/(m^2 \cdot h)$, medium flow - 20 - 80 $m^3/(m^2 \cdot h)$ and high flow - above 80 $m^3/(m^2 \cdot h)$. These designs were done with guidance from Dr. A.B Erasmus from Sasol. The distributors have 19 drip pipes, each relating to a drip point density of 157 per m^2. Figure 3.5 - Figure 3.7 shows a basic design drawing of the different distributors. The detailed drawings are included on the CD attached to this thesis.

The liquid enters the distributing plate from below (see Figure 3.4 and Figure 3.5) through 2 x 1.5" pipes. The liquid is fed to the top of the column via a 2" pipe which is then divided into the two 1.5" pipes. This is to reduce the velocity of the liquid before entering the distributor. The distributing pipes have annular caps (2" caps with 5 mm spacing between the pipe outlet and the annular cap) on them to prevent liquid from jetting into the distributing section, to slow down the liquid velocity and to prevent unnecessary splashing. The gas risers prevent contact with the liquid to ensure a smooth, even liquid distribution.

The main differences between the three distributors are: 1) the low flow distributor has ½" drip pipes that extend upwards to a height that is almost equal to the gas risers. Small orifices (of increasing size) are drilled into the pipes to promote even distribution at low liquid rates, 2) the medium flow liquid distributor also has ½" drip pipes, but they are only level with the base plate, and 3) the high flow liquid distributor has ¾" drip pipes that are also level with the base plate.

Gas Distribution Section:

As noted before, a centrifugal blower circulates the gas through the pilot plant. The gas enters the column just above the maximum liquid level (see Figure 3.3 and Figure 3.4). It is then distributed on the chimney plate, which is bolted between the conical and chimney section. Figure 3.8 shows a basic design drawing of the gas distributor. The design was done with guidance from Dr. A.B Erasmus from Sasol. The detailed drawings can be found on the CD attached to this thesis. Figure 3.8 shows that chimney hats are implemented to cover the gas risers in an effort to prevent the liquid from flowing down into the gas risers. A vortex breaker is also inserted at the bottom of the chimney plate to prevent vortex formation in the liquid.

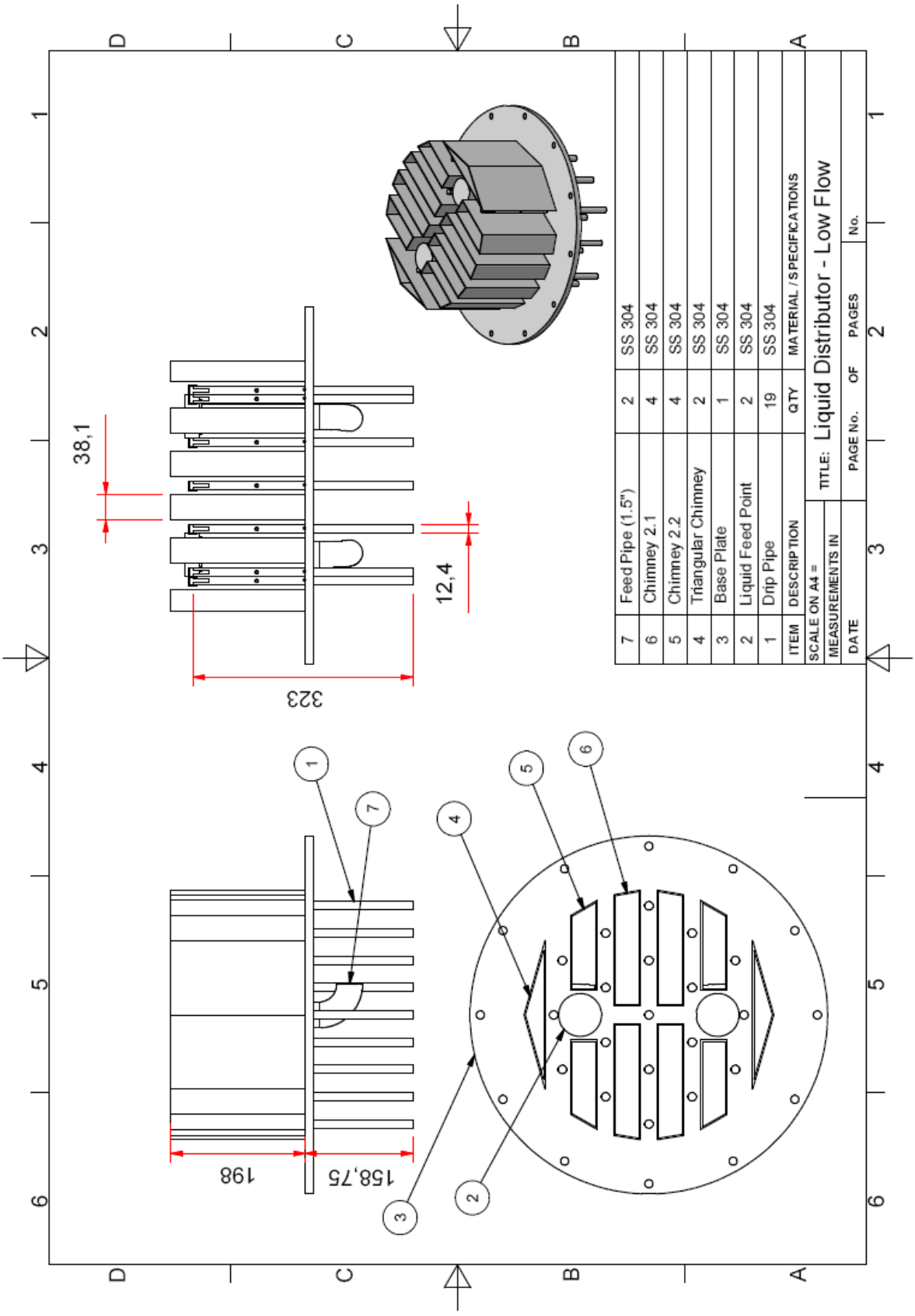

Figure 3.5: Low flow liquid distributor

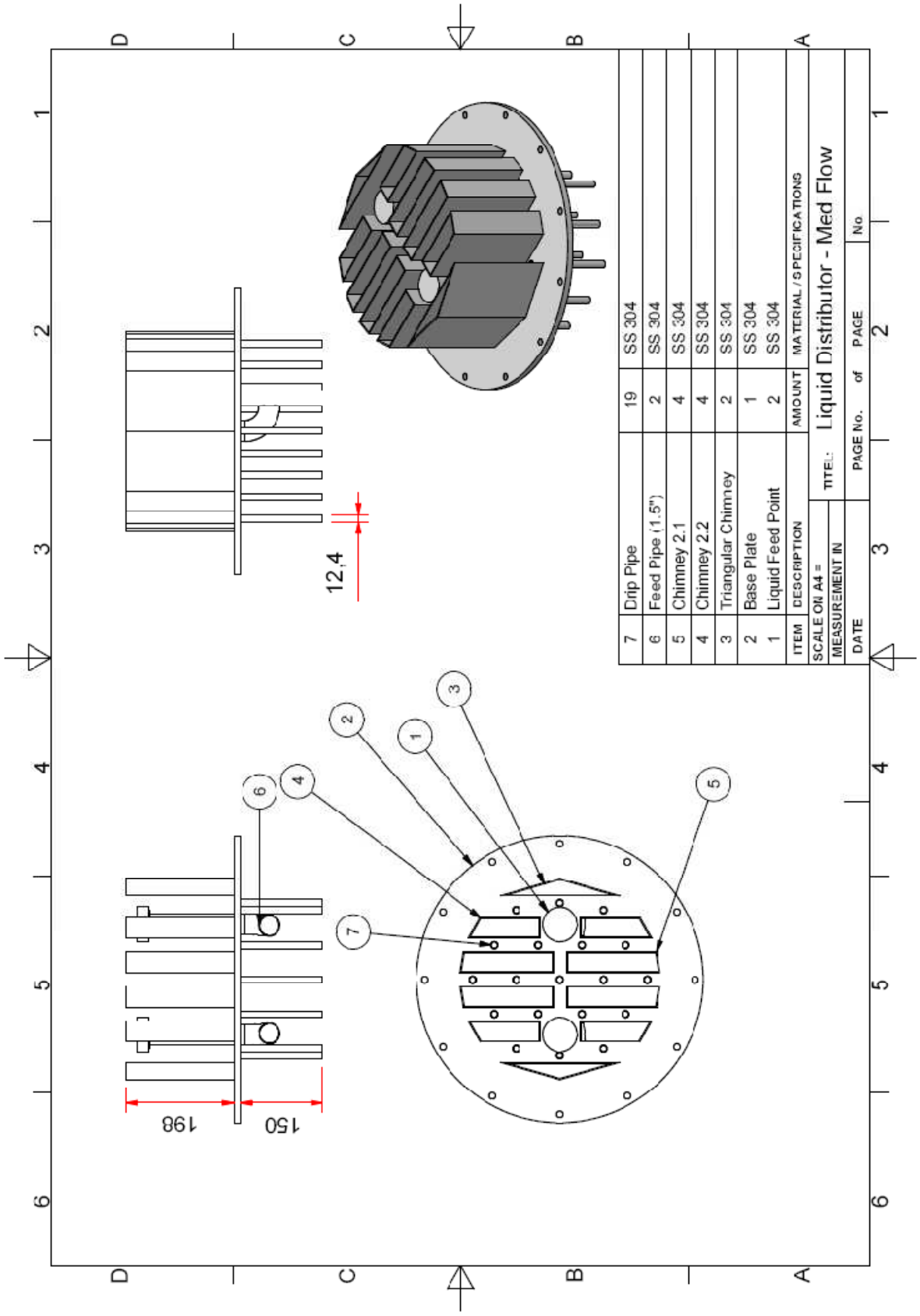

Figure 3.6: Medium flow liquid distributor

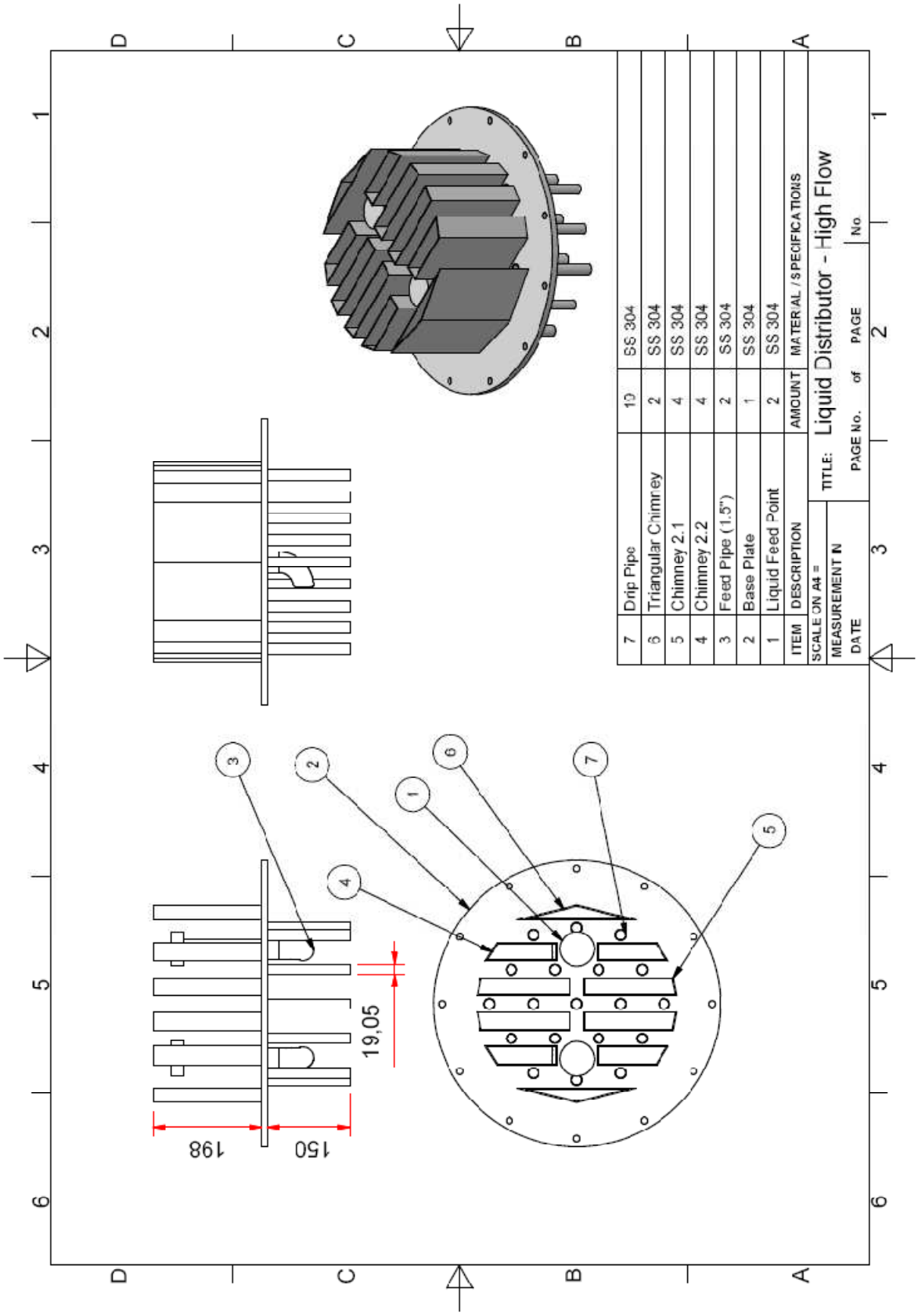

Figure 3.7: High flow liquid distributor

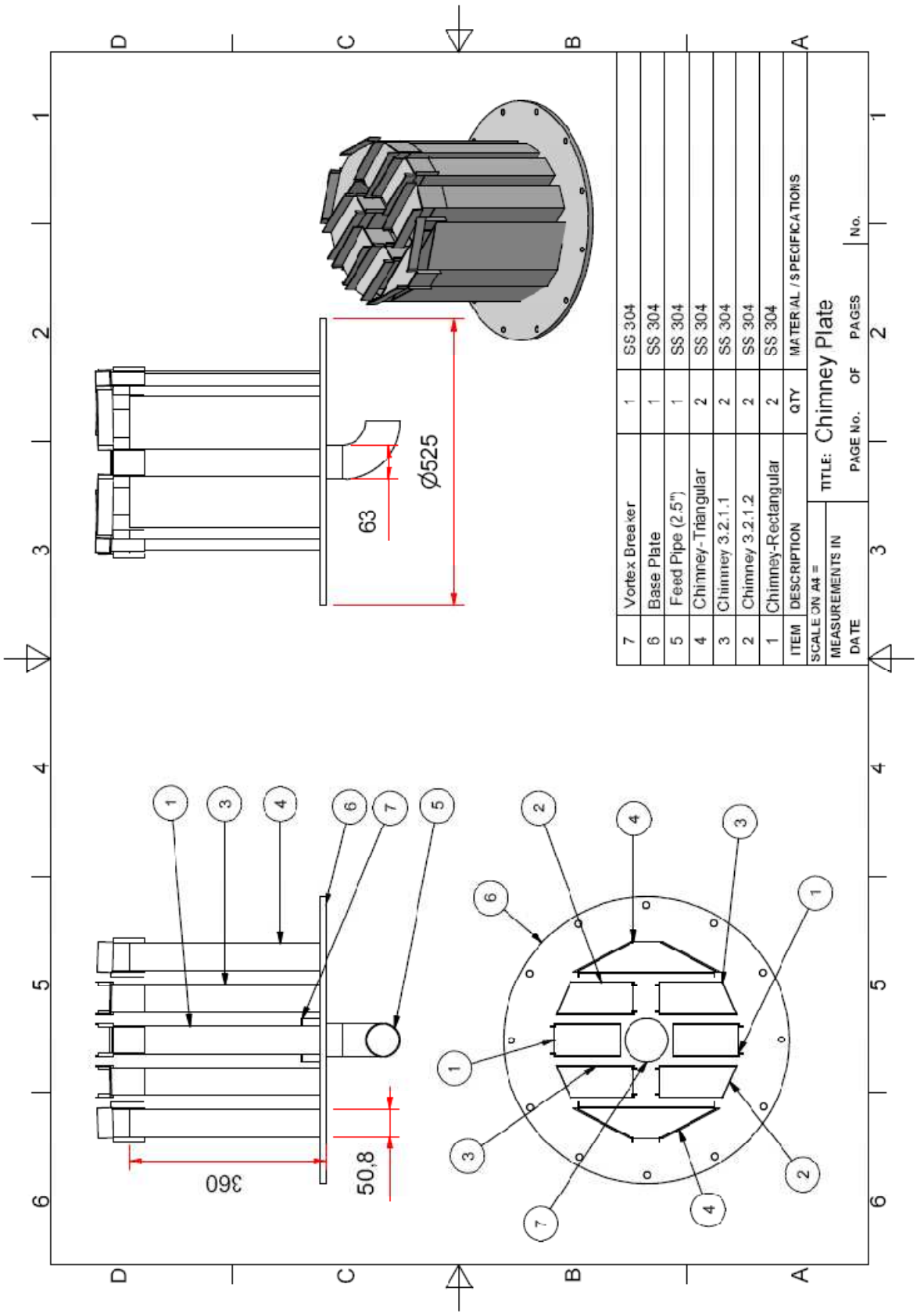

Figure 3.8: Gas distributor

De-entrainment Section:

The de-entrainment section consists of a de-entrainment plate which is bolted in between the liquid distributing and de-entrainment section. The de-entrainer was supplied and tested by Koch-Glitsch. The de-entrainer induces a centrifugal force on the gas that contains the entrained liquid, from where the heavier particles (liquid) settle out on the sides of the de-entrainer and then collect in the entrainment tank (more about the entrainment tank in section 3.4.4).

Visibility:

One of the main objectives in this project is to be able to visually identify the three hydraulic operating regimes. This is obtained by constructing the packed bed sections from borosilicate glass. Ports with sight glass clamped between two flanges are inserted in the following locations throughout the column (refer to Figure 3.3):

- In the sump above the splash deck (more about the splash deck in the sump section below). This is to check if any liquid is leaking through the chimney plate and thus affecting hold-up measurements.
- In the chimney plate to monitor stability of the liquid level. Another glass tube is inserted at the side of the chimney plate to measure the level of the liquid on the chimney plate (for liquid hold-up measurements).
- In the liquid distributing section to monitor the stability of the liquid level and a glass tube is inserted at the side of the distributor plate to measure the liquid level (same as for the chimney plate).
- In the gas line exiting the column to monitor whether or not the de-entrainer is working properly.
- In each measuring tank (hold-up and entrainment) two viewing ports are inserted to check for level stability during operation and sampling.

Liquid Sump:

The liquid sump was elevated to enable the pump to provide a net positive head of 4.2 m (at maximum liquid flow equating to a minimum liquid level in the sump). A splash deck was inserted between the blower inlet and the liquid return (from the hold-up tank) in the sump. This is to eliminate the possibility of liquid droplets being entrained prematurely, which would also disrupt the gas distribution. In the case where bubbles of other gases are present, the splash deck would serve as barrier between the liquid return and gas feed to promote disengagement from the liquid. Lastly, a vortex breaker is inserted in the sump exiting line to prevent vortex formation that could result in pump cavitation due to gas entering the liquid line. A translucent silicone hose is connected

between two fittings at the bottom of the sump and above the maximum liquid level to serve as a level indicator.

3.4.4 Hold-up and Entrainment Measuring Tanks (TK-402, TK-401)

The use of hold-up and entrainment tanks was selected as the most suitable method of measuring the column hold-up and entrainment rate. This required vessels of accurate volume to measure the absolute liquid hold-up and the entrainment rate. Differential pressure transmitters were used to measure the mass (and inherently the volume) in both tanks. This method can be derived from the static pressure head equation:

$$\Delta P = \rho_L \cdot g \cdot \Delta h \qquad 3.1$$

Since the area of each vessel is known (the tanks are calibrated to resemble a constant area), the mass can be easily calculated from the differential pressure reading without requiring the density of the liquid:

$$\Delta M_L = \frac{\Delta P \cdot A}{g} \qquad 3.2$$

By using differential pressure transmitters instead of absolute pressure transmitters the effect of pressure fluctuations in the system is filtered out. A baffle was inserted into each tank to negate the momentum effect of the liquid entering tank on the pressure drop reading. The static vapour head in each tank was negated with the calibration and setup of each tank (see section 8.4.2 the Appendix). The following subsections describe the placement and sizing of the hold-up - and entrainment tank (Figure 3.9 and Figure 3.10):

Liquid Hold-up Tank:

The liquid hold-up tank (see Figure 3.9) was designed to accommodate 10 % of the packed bed volume filled with liquid, as well as any additional liquid head encountered during normal operation (eg. liquid on distributor plate, liquid on chimney plate and the liquid level in the tank during normal operation). This equates to a measuring volume of roughly 90 litres. The valve in line 58 is a knife-gate valve (MV-407) that can control the liquid level on the chimney plate as a constant level is required for liquid hold-up calculations. A dished end was used as the bottom of the tank to promote gravity draining and this standard sizing fixed the diameter of the tank. A smaller diameter tank with a larger height would lead to more accurate measuring of the liquid height, but due to height restrictions a nominal diameter of 450 mm was used. Line 59 is used as a venting line to equalise the pressure between the tank and the column.

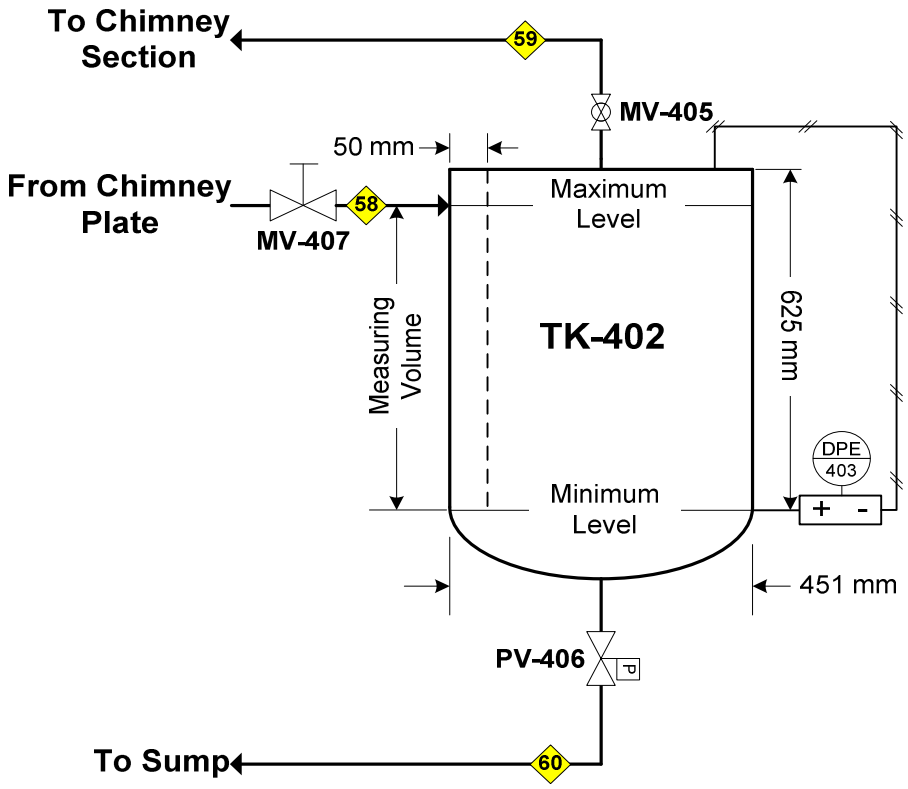

Figure 3.9: Liquid hold-up tank

Entrainment Tank:

The entrainment tank (see Figure 3.10) was designed to accommodate an entrainment rate of 10 % (flooding rate) of the feed liquid (at maximum load). The maximum flow rate is 14 m^3/h which relates to a maximum entrainment rate of 3.88 l/s. The sampling time is a minimum of 10 seconds which gives a total measuring volume of roughly 40 litres. A non-return valve is placed in line 55 below PV-404 to prevent any gas flow from the sump into the entrainment tank. A dished end was used as the bottom of the tank to promote gravity draining back to the sump. Also, due to the same restrictions as mentioned in the section above a nominal diameter of 300 mm was chosen. Line 56 is used as a venting line to equalise the pressure between the tank and the column.

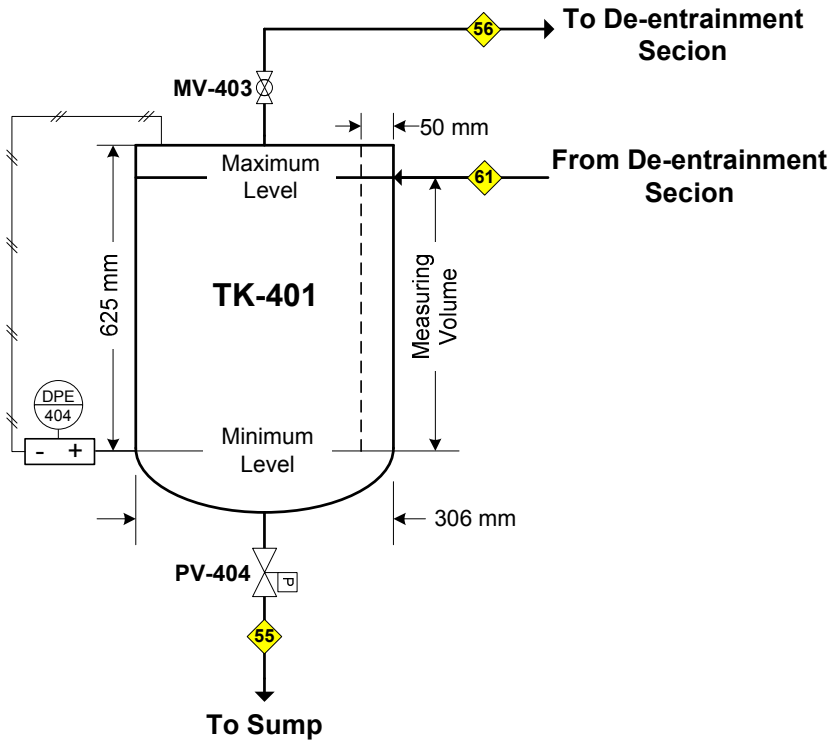

Figure 3.10: Entrainment tank

3.4.5 Liquid Venturi Flow Meter (E-206)

A liquid venturi flow meter was designed (flow rates between 0 - 20 m^3/h) and installed in line with the high rate liquid flow meter (E-207) as a backup and flow rate verification tool. A detailed drawing with design specifications and calculations is included in section 8.2.2 of the Appendix.

3.4.6 Sensor Placement

The sensors in the existing setup are the high rate liquid flow meter, gas venturi, gas flow meter, various temperature probes and an absolute pressure transmitter. The high rate liquid flow meter and the gas venturi were placed in their respective positions due to space limitations [Uys, 2010], however, the temperature probe - and absolute pressure transmitter positions are explained again (only those sensors that overlap with the current project). The remaining sensors are discussed individually below:

Temperature Probes:

The following temperature probes were placed throughout the system to monitor the temperature (see Figure 3.2):

1.) At the exit of the heat exchanger to control the liquid temperature (TE-201)
2.) At the high rate liquid flow meter to convert volumetric flow to mass flow is needed (TE-210)
3.) At the gas venturi flow meter inlet to compensate for temperature (TE-101)

The above probes were already in the existing setup designed by Uys [Uys, 2010].

4.) At the liquid feed point to the packed column (TE-401)
5.) At the top of the de-entrainment section to measure the gas temperature exiting the column (TE-402)
6.) At the top of the packing support section to measure the temperature of the gas entering the packed bed (TE-403)
7.) In the liquid line feeding the liquid hold-up tank to measure the liquid hold-up temperature (TE-404)
8.) At the bottom of the sump to measure the temperature of the liquid exiting the column (TE-405).

Absolute Pressure Transmitters:

The existing pressure transmitter (PE-102) is placed at the inlet of the gas venturi flow meter to determine the density of the gas. An additional absolute pressure transmitter (PE-401) is placed at the top of the packing support section to measure the absolute pressure of the column directly below the packed bed.

Differential Pressure Transmitters:

The pressure drop over a packed bed is one of the variables that define the hydraulic operating regime, but it can also be used to determine the stability of the column. When measuring the liquid hold-up, the pressure drop in the hold-up tank gives an indication whether the column is drained of all its liquid (apart from the static hold-up). Thus, differential pressure transmitters were placed in the following locations:

1.) Over the packed bed (DPE-401)
2.) Over the pressure tappings of the liquid venturi flow meter (DPE-102)
3.) Over the pressure tappings of the gas venturi flow meter (DPE-101)
4.) At the bottom of the liquid hold-up tank (DPE-404)
5.) At the bottom of the entrainment tank (DPE-403)

Liquid Flow Meter (Low Flow):

A liquid flow meter (E-407) was placed in the low rate liquid flow line (line 51) to measure liquid rates (< 2 m^3/h). Sufficient space (> 10 pipe diameters) was allowed for fully developed flow.

Liquid Venturi Flow Meter:

The liquid venturi flow meter (E-206) was inserted in line with the high rate flow meter (E-207) and with sufficient pipe length to allow for fully developed flow.

Gas Flow Meter:

A CO_2 mass flow meter (FE-102) was inserted in the gas line (line 32) to calibrate the gas venturi flow meter for other gasses (for future research and inserted by Uys [2010]).

3.4.7 Sensor Sizing

The sensor specifications in the existing setup are included in section 8.2 of the Appendix and include the following sensors: the high rate liquid flow meter, the gas venturi flow meter as well as the gas flow meter. The additional sensors will be discussed below as they overlap with some of the existing system's sensors:

Temperature Probes:

PT-100 (Platinum Resistance Thermometers) probes were used instead of thermocouple type sensors since accuracy is preferred over measuring range and response time (see section 8.2.3 of the Appendix for probe accuracy).

Absolute Pressure Transmitters:

As specified earlier, the operating conditions are close to atmospheric (slightly above 1 atm), thus the pressure transmitter that would operate in this region has a range of 0 - 200 kPa (abs). The accuracy of the transmitter can be increased by scaling the transmitter between 80 - 120 kPa and thus increasing the measurement resolution.

Differential Pressure Transmitters:

From the observations made by Rocha et al. [1993], the pressure drop at the flooding point in packed beds varies, on average, between 900 - 1200 Pa/m (this value might

change depending on the system specific parameters). Since the packed bed is 3 m in height, a simple calculation reveals that the maximum pressure drop over the packed bed (DPE-401) could vary between 4 - 4.5 kPa. Thus, a suitable pressure drop range would be 0 - 5 kPa. The liquid hold-up (DPE-403) and entrainment (DPE-404) tanks have a measurable volume height of roughly 500 mm, implying that, with water, the pressure drop at maximum volume will be 5 kPa in both cases. Since all the above differential pressure transmitters should have a range of 0 - 5 kPa, transmitters with a range of 0 - 10 kPa were used and scaled down using their 15:1 turndown ratio, once again increasing the measuring resolution. This 0 - 5 kPa range can be converted by the PLC (see section 3.4.9) analog card to give a 0 - 4000 digital range, resulting in a measuring resolution of 1.25 Pa in the specified range.

The liquid venturi flow meter required a pressure drop range of 0 - 85 kPa based on the values summarised in section 8.2.2 of the Appendix. Thus, a 0 - 100 kPa differential pressure transmitter was used.

Liquid Flow Meter (Low Flow):

Based on the liquid range found in Table 3.3, the only viable flow meter is a positive displacement flow meter (E-402). An oval gear type flow meter measuring between 0 - 2 m^3/h was used. A detailed specification sheet is included in section 8.2.3 of the Appendix.

3.4.8 HAZOP and Control Philosophy

Before a control philosophy can be derived, a hazard and operability study (HAZOP) needs to be conducted. The primary HAZOP for the system was done by Uys [2010]. He then derived an interlock strategy to reduce the probability of equipment failure in the existing system when operating at limiting design conditions. A short summary of the HAZOP, interlock strategy and control philosophy for both the existing, as well as the packed column setup, is included in section 8.3 of the Appendix.

The HAZOP on the packed column identified the following additional main control objectives: The liquid flow rate of the low rate flow meter and the liquid level in the hold-up tank.

3.4.9 Control System and Data Logging

The control system and data logging is discussed as a general overview of the existing systems inner workings, followed by the additional work that was required for the packed column setup.

The control system can be divided into three categories: 1) the control panel with the controllers and switch gear 2) the human machine interface (HMI) that enables communication between the operator and the control panel 3) the software with the automation and control loops.

The primary control system was designed and implemented by Uys [2010], however all the additional equipment of this project had to be integrated seamlessly into the existing control system. A programmable Logic Controller (PLC) with temperature controllers, analog to digital conversion cards, digital to analog conversion cards, and frequency inverters were used to control the tray column pilot plant [Uys, 2010]. The analog to digital conversion cards have a 12 bit resolution, meaning it can measure the 4 - 20 mA range with a 5 µA resolution.

A touch panel was used as HMI as it can be used for data logging and inexpensive compare to other systems. Special software was purchased to record the data. This software requires communication between the PLC and a desktop computer. It will then monitor the appointed data registers and then log the data in interchangeable time intervals (from 1 second intervals and upwards in second increments). This data can then be accessed using Microsoft Excel [Uys, 2010].

Thus, any additional analog to digital (and *visa* versa) cards, as well as frequency inverters needed for the packed column operation were assembled in a different control box. A single HMI was shared between the control boxes of the two columns, with different programmed layers to meet each system's operating demands. The necessary control integration for the shared equipment was completed with the aid of an industry professional.

3.5 Experimental Method

The experimental method will be discussed chronologically according to the following: start-up procedure, pressure drop measurement, liquid hold-up measurement, entrainment measurement and finally the shut-down procedure. All the discussions refer to Figure 3.2. Before any experimental work on the pilot plant commences, 3 static hold-up tests are done on the packing material in question to determine the static hold-up (more on this matter in section 3.6). Detailed information on the packing materials used can be found in section 8.5 of the Appendix.

The procedures below are only for the operation of the column during experimental runs. The procedures for changing the packing material (the column is dry-packed with the packing material washed beforehand with a solvent to remove production oil and grease), loading the system with liquids and gasses, flushing the system with a suitable solvent, as well as drying the column are assumed to be have been completed before attempting procedures 3.5.1 - 3.5.3.

Three Packing materials (40 mm Intalox® Ultra™, 40 mm Pall® Rings and 1.5" IMTP®) were characterised and compared in this study. Pall® Rings were chosen as it is one of the most common 2nd generation random packings found throughout the literature, as well having been investigated thoroughly by different authors [Billet, 1999 for example]. IMTP® was chosen as it is from the same packing family as Intalox® Ultra™ and would serve as a good comparison.

The characterisation procedure was to determine the pressure drop and liquid hold-up of the packing materials over 8 liquid rates, namely 6, 12, 24, 37, 49, 73, 98 and 122 $m^3/(m^2 \cdot h)$. Each liquid rate was characterised by increasing the gas flow rate in sequential, incremental steps (as described by the procedures below) until flooding was reached. The number of gas velocity points measured per liquid rate varied between 10-13 (3-4 points in the pre-loading, 4-7 points in the loading region and 3 points in the flooding region). Lastly, the entrainment rate was not measured in this study, but only the liquid hold-up and the pressure drop over the packed bed.

It should be noted that, during the measuring of the liquid hold-up, only the liquid in the packed bed is of concern and that the liquid on the distributor and chimney plate (which also drains into the hold-up tank), should be accounted for. Both the liquid distribution and chimney sections have level sensors (LI-401 and LI-402). These level sensors consist of drilled 6 mm holes on the flanges which are connected with glass tubes, indicating the liquid level. Since the area occupied by the liquid on both plates can easily be determined, the volume of liquid is obtained from the product of the area and the measured level height. These volumes are subtracted from the total measured in the hold-up tank to

determine the dynamic liquid hold-up. The static liquid hold-up is then added to give the total liquid hold-up.

The entrainment was omitted from this study as initial tests revealed that the pressure drop over the liquid distributor was too high to give a progressive entrainment rate curve (e.g. no entrainment was observed up to certain gas velocity rate, above this gas rate the entrainment rate was more than 10 %. Thus, no useful entrainment data could be generated with the current liquid distributors. However, with the replacement of liquid distributors, the system would be capable of measuring the entrainment rate as well.

3.5.1 Start-up Procedure

The start-up procedure of the packed column can be described by the following steps (the numbers below refer to the P&ID shown in Figure 3.2):

1.) Switch on the control panel.
2.) Select the packed column configuration.
3.) Input all the required system parameters into the touch panel (such as packed bed height, gas universal constant etc.).
4.) Switch the three way valve (PV-401) to circulate the liquid through the sump.
5.) Enter a liquid flow rate set value on the touch panel (preferably high rate). Wait approximately 30 seconds for PCV-205 to open. After it has opened, the liquid pump can be started (E-204).
6.) Switch on the cooling/heating water system and enter a set point of 25^{o}C. This start-up procedure is to ensure that the liquid temperature is close to the operating temperature before the column is operated.
7.) When the liquid temperature is close to 25 ^{o}C, ensure that MV-411 is positioned to divert the liquid flow from line 48 to line 49. Then select on the touch panel to operate the column at high liquid rates. Next switch PV-401 so that liquid is diverted through the column. Keep running the liquid-only cycle for at least an hour to ensure proper wetting of the packing material.
8.) Start the blower (E-102) with the frequency of the inverter set to 28 Hz. As soon as the blower start-up cycle is finished, open the radial control valve to 30 %. At this setting, small fluctuations in the valve position will not affect the gas flow rate by a significant amount. Keep running the gas-liquid cycle in the column until the gas temperature is close to the operating temperature.
9.) Shut-down the liquid pump and the gas blower when the operating conditions are reached.

3.5.2 Operating Procedure

The experimental procedure below describes the measuring process of the pressure drop and the liquid hold-up of the packed column. As mentioned above the measurement of the entrainment rate is not one of the main objectives of this project, but is still described briefly (section 8.6 of the Appendix) in the interest of a complete operating procedure. The numbers below refer to the P&ID shown in Figure 3.2:

1.) Flush all the differential pressure lines to remove any condensate build-up from previous runs.
2.) Set the liquid circulation loop to the desired flow path on the touch panel (low or high liquid rates).
3.) Set the minimum measuring volume in the hold-up tank to 308 Pa on the touch panel (to account for the dished end dead volume and time delay before the valves are fully closed).
4.) Repeat steps (5) and (8) from section 3.5.1.
5.) Set the liquid flow rate to the desired rate. To ensure a constant liquid flow rate the control valve should be fully opened by setting the liquid flow rate to a value of 14 m^3/h. The rotational speed of the pump should then be increased by changing the inverter output frequency of the pump (15 - 50 Hz) until the liquid rate is approximately 0.5 m^3/h above the desired rate. The liquid rate set point can then be lowered to the desired rate to ensure continuous control via PCV-205. Note that point (5) only applies to flow rates above 2 m^3/h.
6.) In the case of low liquid rates (below 2 m^3/h) repeat steps (2) and (4) of section 3.5.2. Lower the inverter frequency to 25 Hz and then adjust the needle valve (MV-412) until the desired liquid flow rate is reached.
7.) Set the gas flow rate to the desired rate by changing the blower rotational speed on the touch panel.
8.) Check that a stable liquid level develops on the chimney plate (LI-402) by adjusting the knife-gate valve (MV-407).
9.) To measure the pressure drop, check that the pressure drop as well as the liquid and gas flow rates have stabilised in the column (hydrodynamic equilibrium). This is done by monitoring the respective graphs on the touch panel as a function of time (normally between 5-10 minutes after point (8) in section 3.5.2).
10.) Measure the liquid level on the distributor (LI-401).
11.) Measure the liquid level on the chimney plate (LI-402).
12.) Press the liquid hold-up sample button on the touch panel which closes PV-406 first, until the measurement starting volume is reached, and then close PV-402. Note the time that it takes PV-402 to fully close as this results in an additional amount of liquid that enters the column before the feed is completely shut-off.
13.) Switch off the blower.

14.) The liquid is left to drain from the column into the hold-up tank. The end of the sampling period can be seen on the touch panel by monitoring the liquid hold-up vs. time curve. When a zero gradient is achieved, the sampling button is reset (normally between 12-20 minutes).
15.) Repeat steps (1) - (14) of section 3.5.2 for all the desired liquid and gas rates.

3.5.3 Shut-down Procedure

The emergency shut-down procedures are described in sections 8.3.2 and 8.4.1 of the Appendix. The operational shut-down procedure is described below:

1.) Switch off the blower.
2.) Switch off the liquid pump.
3.) Switch off the cooling/heating water system.
4.) Switch off the control panel.

3.6 Limitations on Measurement Accuracy

Certain factors may influence the accuracy of the experimental data. The factors that could influence the accuracy of the experimental data are the following:

- System leakages
- Calibration of the control system
- Calibration of the hold-up - and entrainment tank
- Sensor measurement verification
- Hydrodynamic Equilibrium
- Measurement repeatability
- Experimental error

These factors are discussed individually and can be seen in section 8.4 of the Appendix. The following table summarises the maximum possible experimental error incurred in the operational parameters:

Table 3.4: Experimental measurements maximum deviation summary

Parameter	Measurement Accuracy	Maximum Deviation
Vapour flow factor	± 2.6 %	0.026 x 4.0 = 0.104 [(m/s)·(kg/m^3)]
Liquid rate (low flow meter)	± 0.75 %	2 x 0.0075 = 0.015 [m^3/h]
Liquid rate (high flow meter)	± 0.75 %	15 x 0.0075 = 0.113 [m^3/h]
Liquid rate (venturi flow meter)	± 3.8 %	15 x 0.038 = 0.57 [m^3/h]
Packed bed pressure drop	± 0.75 %	1600 x 0.0075 = 12 [Pa/m]
Liquid hold-up	± 1.25 %	0.140 x 0.0125 = 0.00175 [m^3/m^3]
Entrainment rate	± 1.05 %	3.88 x 0.0105 = 0.041 *l*/s

4 Results and Discussion of Results

Experimental runs were successfully performed over the range of liquid loads described in section 3.5 on the 3 random packing materials mentioned in section 3.5. In this section the accuracy of the system is firstly discussed in general and then compared to the predictive models identified in section 2.4.1. Next, the capacity of Intalox® Ultra™ is characterised according to typical methods found in the literature. Finally, a capacity comparison between the Pall® Rings, IMTP® and Intalox® Ultra™ random packings is made and commented on.

4.1 System Data Verification

One of the main objectives of this project was to establish a facility that can accurately characterise the hydraulic capacity of both random and structured packing. Since it was decided to verify the experimental data with random packing, Pall® Rings were chosen because predictive model packing constants are available for Pall® Rings in the model proposed by Billet & Schultes [1999]. No packing constants are available for the other two random packing materials in question. A first verification test is to see if the correct general trends for the pressure drop and liquid hold-up are achieved as described in the literature. The pressure drop - and total liquid hold-up curves for the 38 mm Pall® Rings are shown in Figure 4.1 and Figure 4.2.

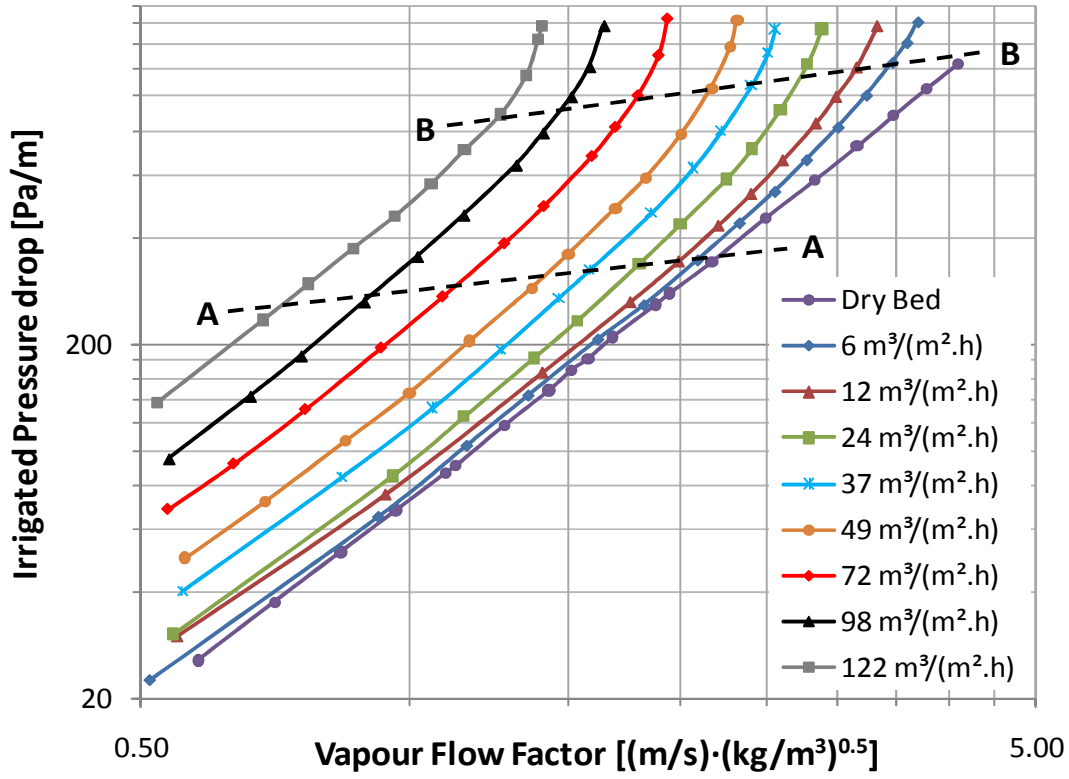

Figure 4.1: Pall® Ring pressure drop vs. vapour flow factor

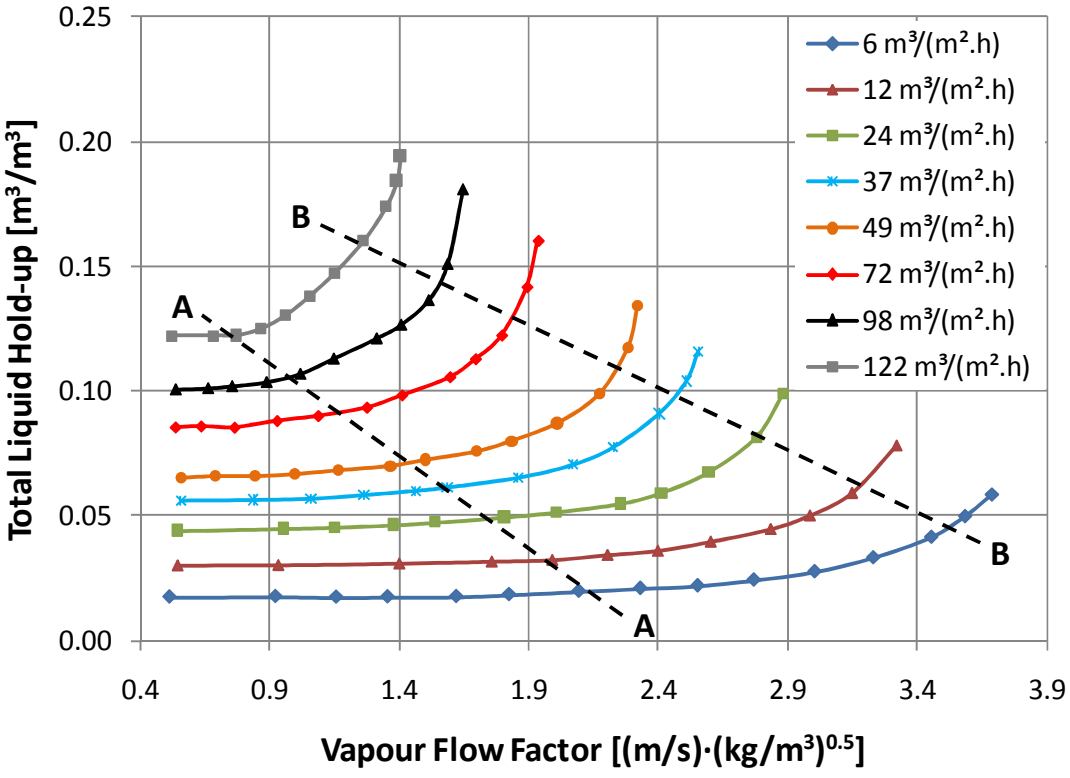

Figure 4.2: Pall® Ring total liquid hold-up vs. vapour flow factor

According to Figure 4.1, all the pressure drop curves follow the dry bed pressure drop curve in the loading region (below line A-A) and the only difference is the influence of liquid load as described by Kister [1992]. This is also confirmed in Figure 4.2, where the liquid hold-up is independent of the vapour flow factor. In the loading region, the shear forces between the liquid and gas increase relative to the gravitational forces to enable the suspension of some of the liquid between the packing elements (between line A-A and B-B). Thus, an increase in liquid hold-up causes a larger increase in pressure drop due to the reduced area available for gas flow. This relates to the loading region as described by Kister [1992]. Finally, the flooding region (above line B-B) is reached where a small increase in vapour flow factor results in a large increase in both pressure drop and liquid hold-up (Figure 4.1 and Figure 4.2).

The general trends of the experimental data conform to the trends found in the literature and thus, it was concluded that the system does not contain any severe irregularities. The repeatability of the experimental measurements was good (Figure 8.4 and Figure 8.5 which can be found in section 8.4.5 of the Appendix). This is confirmed by the small variance in data points that were measured over different days. Also, based on the maximum experimental error incurred for each measured parameter (Table 3.4 found in section 3.6), the pressure drop measurements have a maximum deviation of 0.75 %. Similarly, the liquid hold-up measurements have a maximum deviation of 1.25 %. It should be noted that the deviations in the liquid and gas flow rate measurement will have an effect on the overall accuracy of the above mentioned parameters. Having validated the general trends of the hydrodynamic data sets, the next step is to validate their reliability, and is as follow:

4.1.1 Billet Model Comparison

The model proposed by Billet & Schultes [1999] can predict the dry bed, irrigated pressure drop as well as the total liquid hold-up in the column. The accuracies from Table 2.11 are 10.8 % for the irrigated pressure drop and 6.7 % for the liquid hold-up (AARE). However, the parity plots used for the respective parameters are 20 % for the pressure drop [Billet & Schultes, 1991] and 15 % for the liquid hold-up [Billet & Schultes, 1993]. To account for this difference in parity plots and AARE, a 10 % upper - and lower limit parity plot on both parameters is constructed and compared to the experimental data. It should be noted that only packing constants for 35 mm and 50 mm Pall® Rings were available in the literature. To counter this, a 10 % upper limit on the 50 mm Pall® Rings and a - 10 % lower limit on the 35 mm Pall® Rings were constructed to form a bandwidth in which the experimentally measured data points should fall in between.

Billet Dry Bed Comparison:

Figure 4.3 illustrates the comparison between the experimental dry bed pressure drop and the dry bed pressure drop predicted by the model of Billet & Schultes [1999] as a function of gas flow.

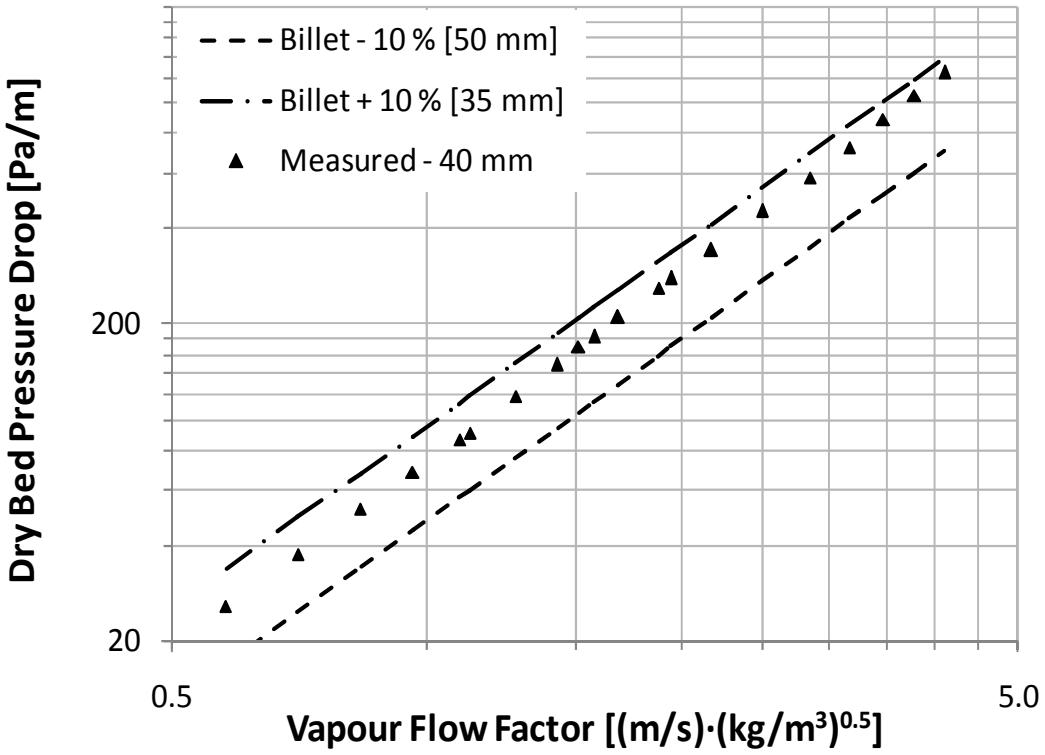

Figure 4.3: 38 mm Pall® Ring experimental dry bed pressure drop vs. Billet model prediction

From Figure 4.3, the dry bed pressure drop compares well to the model proposed by Billet & Schultes [1999]. The data is closer to the upper limit of the 35 mm Pall® Rings as the 40 mm rings used in this study are closer to 35 mm than to 50 mm. The smaller the diameter, the larger the pressure drop due to the reduced area open to gas flow (compared to larger diameter random packing elements in the same column size) and thus a larger friction factor experienced by the gas. The next step is to compare the irrigated pressure drop and liquid hold-up against the experimental data. Since the model of Billet & Schultes [1999] requires the liquid hold-up to be calculated first and then the irrigated pressure drop, the liquid hold-up comparison will be discussed below followed by the irrigated pressure drop comparison.

Billet Liquid Hold-up Comparison:

Figure 4.4 (a)-(f) illustrates the comparison between the experimental liquid hold-up data and the total hold-up predicted by the Billet model [Billet & Schultes, 1993] at a range of different liquid loads.

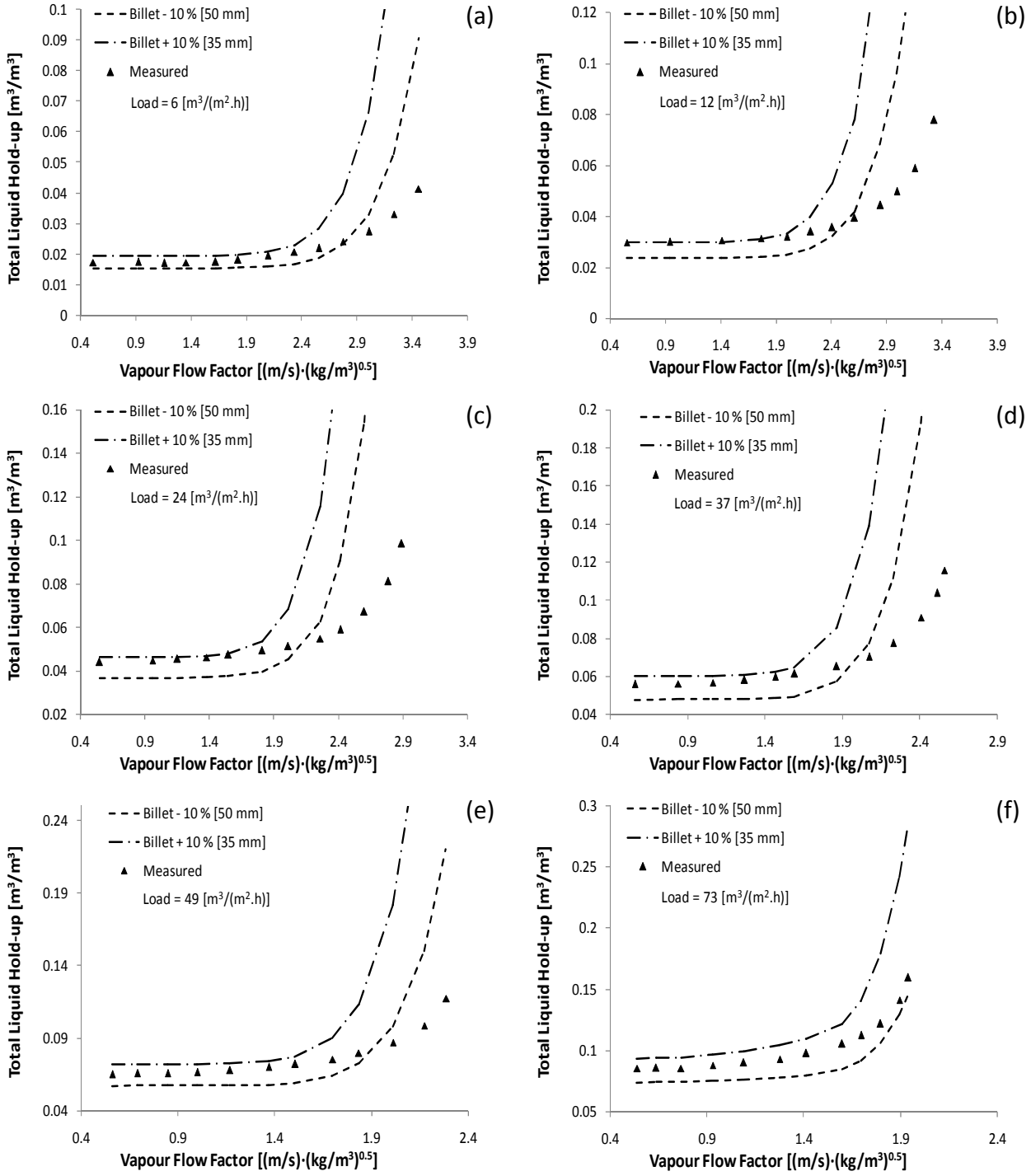

Figure 4.4: Pall® Ring experimental liquid hold-up vs. Billet model prediction

The liquid hold-up falls within the allocated boundaries up to the early loading region for all the liquid loads (see Figure 4.4). The deviation that is present occurs from the loading region onwards. This can be partially explained by the fact that Billet & Schultes [1993] modelled the liquid hold-up from a phenomenological approach as described by equation 2.64. This equation states that the gradient of the increase in liquid hold-up is a function of the pre-loading hold-up, the hold-up at flooding and the ratio of gas velocity to the flooding velocity raised to a constant power (as can be seen in equation

2.59). Also, the boundary condition stipulating the theoretical hold-up at the flood point, (which states that the change in vapour flow factor vs. the change in hold-up equals zero [Billet, 1993]) could be severely over-predicted compared to the real column hold-up at flooding. At liquid rates between 25-40 $m^3/(m^2 \cdot h)$ and below, no vertical hold-up line is reached at flooding [Nieuwoudt, 2010].

The method used to predict the real column hold-up was the step-by-step example found at the end of his liquid hold-up paper [Billet & Schultes, 1993]. Due to this discrepancy in theoretical hold-up at flooding, the hold-up equation (2.64) could have large errors in predicting the total column hold-up from the loading region onwards. An attempt to rectify the difference above is discussed in section 4.1.2.

The experimental data was measured up to a liquid load of 122 $m^3/(m^2 \cdot h)$, but the comparison is only up to a load 72 $m^3/(m^2 \cdot h)$. This is due to the fact that the liquid hold-up prediction in the model proposed by Billet was only verified up to a liquid load of 82 $m^3/(m^2 \cdot h)$, and the next experimental liquid rate is at 98 $m^3/(m^2 \cdot h)$. Thus, a comparison at 98 and 122 $m^3/(m^2 \cdot h)$ would be irrelevant.

Billet Irrigated Pressure Drop Comparison:

Figure 4.5 (a)-(f) illustrates the comparison between the experimental pressure drop data and the pressure drop predicted by the Billet model [Billet & Schultes, 1999] at various liquid loads.

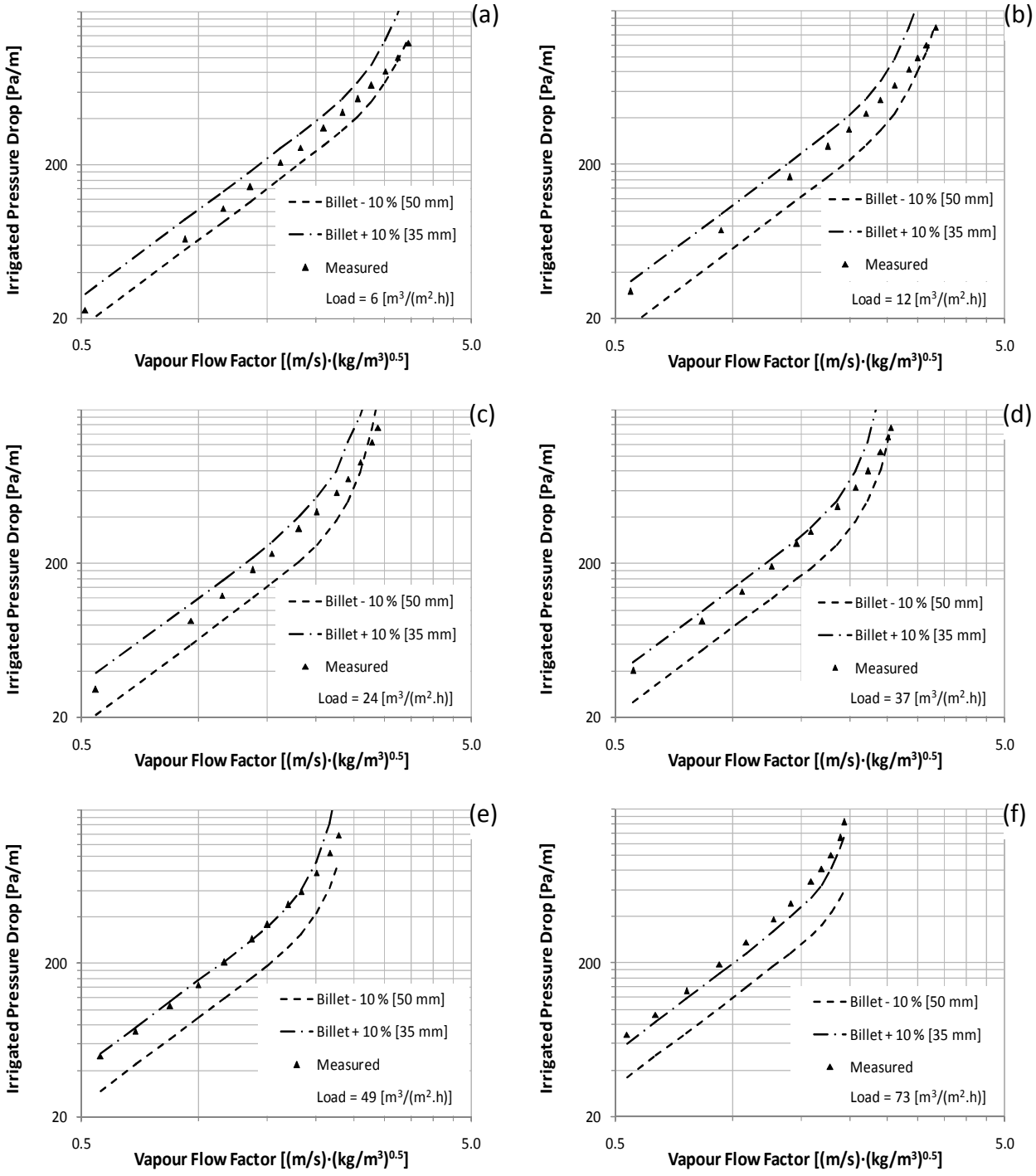

Figure 4.5: Pall® Ring experimental pressure drop vs. Billet model prediction

The comparison between the experimental data and the predictive model by Billet & Schultes [1999] is good (see Figure 4.5). The pressure drop prediction in the predictive model is dependent on the accurate prediction of the liquid hold-up, as indicated by equations 2.56 and 2.57. Thus, an inaccurate prediction of the hold-up would inevitably lead to a deviation in the irrigated pressure drop prediction. This deviation is evident in Figure 4.5 (a)-(f) in the mid loading to flooding region. In Figure 4.5 (f) the pressure drop

trend is correct, since Figure 4.4 (f) coincides with the general hold-up equation as explained in the section above. However, the absolute values fall outside the ± 10 % range. This is partly due to the fact that the predictive model could possibly under-predict the pressure drop at higher liquid loads. Another attributing factor could be that 10 % parity plots were used in this comparison, while a 20 % parity plot was used by Billet [1991]. The pressure drop model was only verified up to a liquid load of 60 $m^3/(m^2 \cdot h)$ [Billet & Schultes, 1991].

Referring back to section 2.4.1, the model proposed by Billet [1999] performed the best compared to the other predictive models that were evaluated. Also, from Figure 2.3 and Figure 2.4 it is evident that the values predicted by this model are close to the absolute values and would serve as a good reference to compare the experimentally measured data against.

From the above sections, the experimentally measured dry bed pressure drop coincides with Billet's predictive model. The liquid hold-up compares well up to the mid loading to flooding region within the range of applicability of the model. The pressure drop follows the same trend. The deviations are possibly due to the deviation in real column hold-up vs. the theoretical column hold-up at flooding, which refers to the theoretical liquid hold-up boundary condition at flooding, which will be discussed shortly. An attempt to characterise the differences between the experimental data and the above mentioned predictive model follows in the section below.

4.1.2 Billet Model Deviation

Further investigation into the papers by Billet & Schultes [1991; 1993; 1995; 1999] revealed that the real column hold-up (at flooding) and the theoretical hold-up (at flooding) diverged erratically from each other as the flooding region was approached. This was countered by using equations 2.70 and 2.65 (real column hold-up at flooding) in equation 2.59 instead of the theoretical hold-up (at flooding) predicted by the model (from equations 2.60 and 2.65). In other words this means that:

$$h_L = h_{L,S} + \left(h_{L,Fl} - h_{L,S}\right)\left(\frac{u_V}{u_{V,Fl}}\right)^{13} \qquad 2.59$$

with $h_{L,FL}$ calculated as:

$$h_{L,Fl} = 2.2 h_{L,S}\left(\frac{\eta_L \cdot \rho_W}{\eta_W \cdot \rho_L}\right)^{0.05} \qquad 2.70$$

and

$$u_{V,Fl} = \sqrt{2} \cdot \sqrt{\frac{g}{\psi_{Fl}} \left(\frac{\left(\varepsilon - h_{L,Fl}\right)^{3/2}}{\varepsilon^{1/2}} \right)} \cdot \sqrt{\frac{h_{L,Fl}}{a}} \cdot \sqrt{\frac{\rho_L}{\rho_V}} \qquad 2.65$$

Instead of

$$h_{L,Fl}^3 \left(3h_{L,Fl} - \varepsilon\right) = \frac{6}{g} \cdot a^2 \cdot \varepsilon \left(\frac{\eta_L}{\rho_L}\right)\left(\frac{L}{V}\right)\left(\frac{\rho_V}{\rho_L}\right) \cdot u_{V,Fl} \qquad \text{for } \frac{\varepsilon}{3} \le h_{L,Fl} \le \varepsilon \qquad 2.60$$

and equation 2.65.

Table 4.1 indicates the % difference between the two different methods presented by Billet & Schultes [1993; 1999] of calculating the total column hold-up at various vapour flow factors:

Table 4.1: Difference between Billet's model prediction of theoretical and real column hold-up at flooding (at a liquid load of 24 $m^3/(m^2 \cdot h)$)

	Theoretical Column Hold-up (calculated with eq.2.60 and 2.65)		***Real Column Hold-up (Calculated with eq. 2.70)***		
u_v [m/s]	**$h_{L,Fl}$ [m^3/m^3]**	**$h_{L,Total}$ [m^3/m^3]**	**$h_{L,Fl}$ [m^3/m^3]**	**$h_{L,Total}$ [m^3/m^3]**	**$h_{L,Total}$ [% difference]**
0.50	0.320	0.0449	0.099	0.0449	0
0.88	0.319	0.0450	0.099	0.0450	0
1.06	0.319	0.0448	0.099	0.0448	0
1.26	0.318	0.0451	0.099	0.0450	0.3
1.42	0.318	0.0457	0.099	0.0452	1
1.68	0.318	0.0487	0.099	0.0459	6
1.86	0.318	0.0567	0.100	0.0478	19
2.07	0.318	0.0779	0.099	0.0514	51
2.20	0.318	0.1097	0.100	0.0582	89
2.36	0.318	0.1860	0.100	0.0737	153
2.51	0.318	0.3502	0.101	0.1080	224
2.60	0.318	0.4767	0.100	0.1322	261

From the above table the % difference in total hold-up diverges as the gas flow rate is increased and as it approaches the flooding region and beyond. Thus, a possible solution would be to calculate this empirical, real column hold-up at flooding (eq. 2.70) and re-calculate the total column hold-up (even though this is not the suggested method as prescribed by the author in his hold-up paper [Billet & Schultes, 1993]).

To simplify the comparison (resulting in a narrower comparison band) between the experimental data and the predictive model, packing constants were derived from the experimental data for the 38 mm Pall® Rings used in the experimental runs. Thus, instead of using 35 mm and 50 mm Pall® Ring data, 38 mm data points can be predicted. The section below describes the method used in determining the packing specific constants for the 38 mm Pall® Rings.

Packing Constant Determination in Billet Model:

The following table represents the packing specific constants needed to determine the 35 mm and 50 mm Pall® Ring predictive values [Billet, 1991; 1993; 1999]:

Table 4.2: Billet model packing specific constants for 35 mm and 50 mm Pall® Rings

35 mm Pall® Rings			***50 mm Pall® Rings***		
$C_{p,0}$	C_h	C_{Fl}	$C_{p,0}$	C_h	C_{Fl}
0.967	0.644	1.679	0.763	0.784	1.580

Thus, in order to be able to use a single packing size to compare against, the dry bed packing factor ($C_{p,0}$), pre-loading hold-up packing factor (C_h) and the flooding packing factor (C_{Fl}) need to be determined for the 38 mm Pall® Rings. Table 8.30 illustrates the additional parameters found in the literature. The method of determination is as follows:

- Solve equations 2.52 to 2.54 to determine the dry bed packing factor (experimental dry bed pressure drop data is substituted into eq. 2.52).
- Determine the flooding velocity at each respective liquid rate by using the statistical method described in section 4.2.1.
- For each liquid rate, calculate the pre-loading hold-up packing factor by solving equations 2.61 to 2.63. The pre-loading hold-up is replaced with experimentally measured data in the pre-loading region.
- Determine the onset of flooding velocity and liquid hold-up with the method described in section 4.2.1 for each liquid rate. Next, solve equations 2.65 and 2.66 to calculate the flooding packing factor by replacing the flooding velocity and liquid hold-up with the experimentally determined values.
- Lastly, average all the different liquid rate packing factors and recalculate the parameters in question.

Table 4.3 represents the revised Billet model packing specific constants for 38 mm Pall® Rings:

Table 4.3: Revised Billet model packing specific constants for 38 mm Pall® Rings

38 mm Pall® Rings		
$C_{p,0}$	C_h	C_{Fl}
0.965	0.721	1.689

Revised Liquid Hold-up Comparison:

Figure 4.6 illustrates the comparison between the experimental hold-up data and the data from the revised liquid hold-up model.

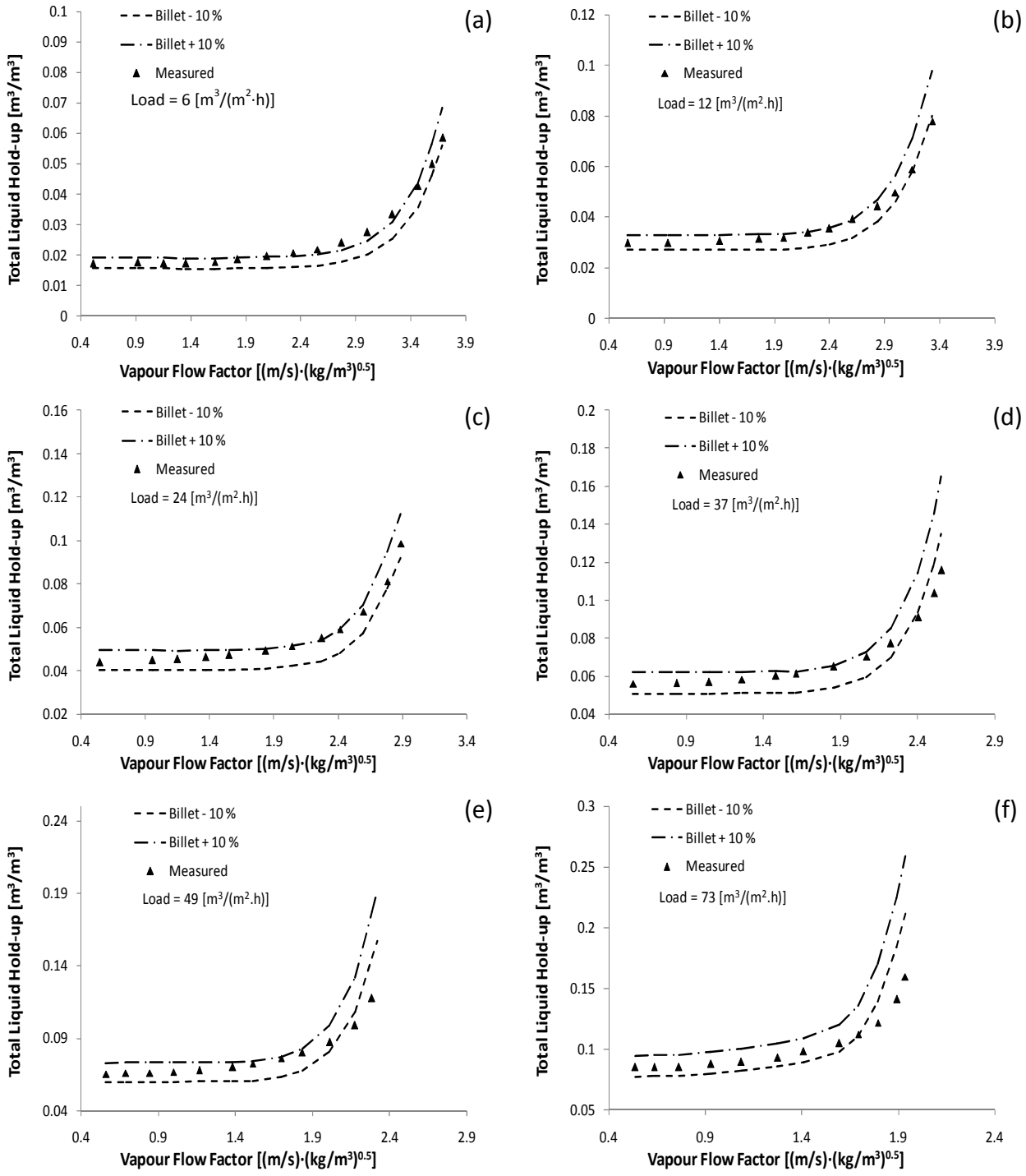

Figure 4.6: Pall® Ring experimental hold-up vs. revised liquid hold-up prediction

A much better comparison between the experimental - and predictive data is evident (see Figure 4.6). Slight differences are still noticeable in or near the flooding region. These differences are attributed to the fact that experimental flooding data is extremely difficult to measure due to the pronounced non-steady state behaviour in the flooding range [Billet & Schultes, 1993]. As already mentioned, numerous sets of hydrodynamic data were generated from industrial columns. The pronounced non-steady state behaviour is more likely due to pressure control difficulties in the boil-up of the liquid than anything else. Hydrodynamic steady state as per definition is when both gas and liquid flow rates are stable, resulting in a stable pressure drop over the packed bed. By doing an error analysis on a typical flooding data point (experimentally measured at a vapour flow factor of 4.98 $[(m/s)\cdot(kg/m^3)^{0.5}]$ for Intalox® Ultra™ and at a liquid rate of 6 $m^3/(m^2\cdot h)$), the average value over a sample time of 198 seconds is 1626 Pa/m with a standard deviation of 5.87 Pa/m.

Theoretically, if hydrodynamic equilibrium has been attained there would be little or no deviation in the pressure drop (and liquid hold-up for that matter) over a prolonged time interval. The above standard deviation is 0.36 % of sample mean, indicating that the pressure drop is stable in the flooding region. It should be noted, however, that due to the mechanisms present in the flooding region (resulting in the rapid increase in pressure drop and hold-up) that any small variations in the vapour flow factor would result in significant changes in both the pressure drop and hold-up. The standard deviation of a typical vapour flow factor at flooding is calculated for IMTP® at a liquid rate of 2.91 $m^3/(m^2\cdot h)$ in Table 8.60 (section 8.8.2 of the Appendix).

Based on the above observations, all of the differences in liquid hold-up between the experimental - and predictive data are accounted for. Since the irrigated pressure drop of the model proposed by Billet & Schultes [1991] is inherently linked to accurate liquid hold-up measurements, the experimental pressure drop data will be further compared to the KG-TOWER® simulation package.

Lastly, the significant differences between the total column hold-up by using the theoretical and real column hold-up (at flooding) in the predictive model proposed by Billet & Schultes [1993], should be noted for future use as this could lead to confusion for prospective users.

4.1.3 KG-TOWER® Comparison

Based on the literature study, the predictive model developed by Koch-Glitsch was used as an alternative verification test of the experimental data. The random packing 1.5" IMTP® was used in this comparison (as it was produced and supplied by Koch-Glitsch). Figure 4.7 illustrates the comparison between the experimental data and KG-TOWER®

simulations at different loads with ± 10 % reliability limits. This simulation package is semi-empirical in nature and fitted on experimentally measured data of all of Koch-Glitsch's available packing materials.

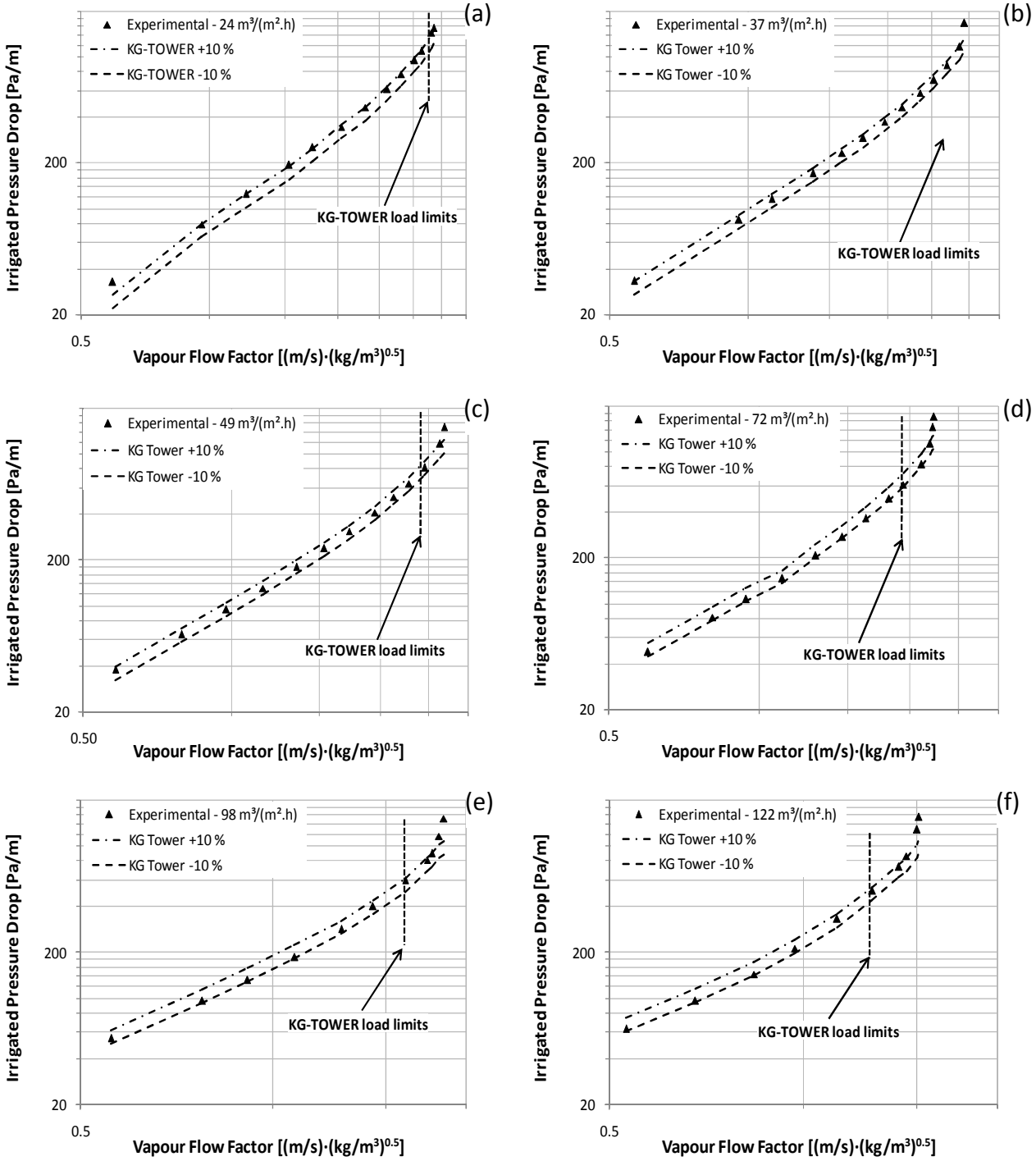

Figure 4.7: IMTP® experimental pressure drop vs. KG-TOWER®

Figure Figure 4.7 shows that the experimental data falls within the ± 10 % reliability limits of KG-TOWER® results, within its operating limits over all the liquid loads. The vertical lines refer to the limiting loads, which correspond to the maximum operable capacity, or the onset of the flooding region. It can be seen that the model does not describe the pressure drop in the flooding region well. The aim is to compare the experimental data over a wide as possible operating range. Thus, the figure below (Figure 4.8) represents a 10 % parity plot where data falling outside the load limits of KG-TOWER® (6 and 12 $m^3/(m^2 \cdot h)$) are neglected.

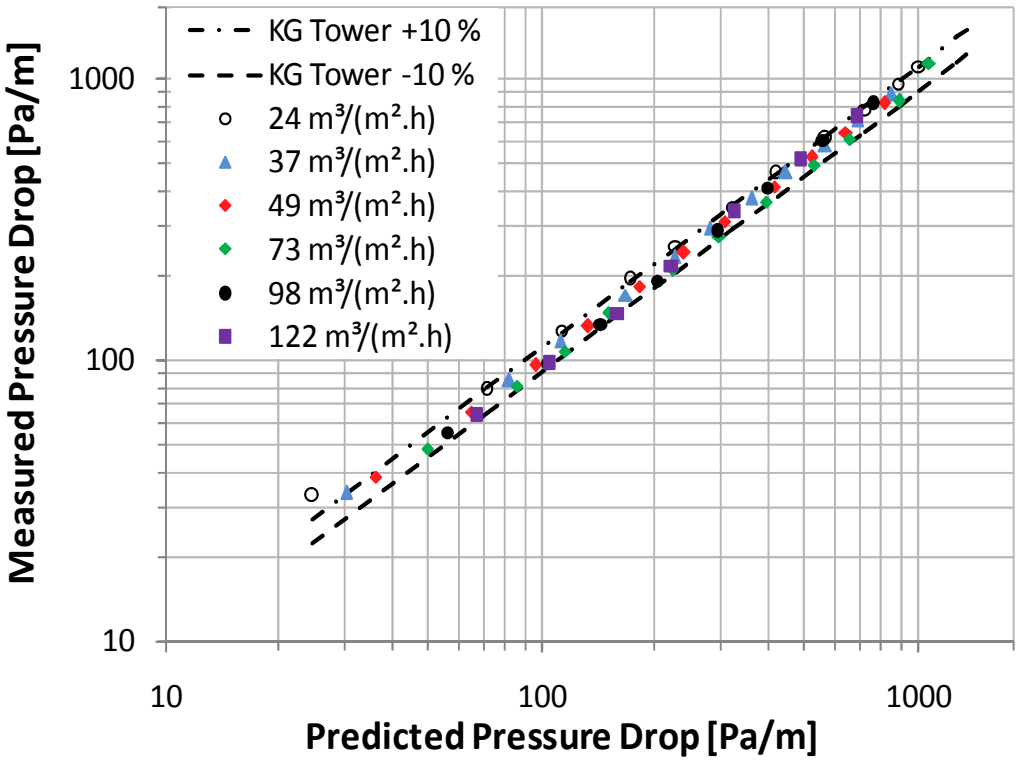

Figure 4.8: 10 % Parity plot between IMTP® experimental pressure drop data and KG-TOWER®

Figure 4.8 shows that the comparison between KG-TOWER® predictions and the experimental data is good. It can be concluded that the packed column's experimental data follows the trends of predictive models found in the literature, as well as falling within their reliability limits (with a small error in the experimental measurements as already stated). Thus, it is likely that the measurements from the packed column setup are close to other experimentally measured data points over the entire operating regime.

4.2 Intalox® Ultra™ Capacity Quantification

After verifying the repeatability of the experimental setup as well as the verification of the experimentally measured data sets, the last main objective was to quantify the capacity of 1.5" Intalox® Ultra™ over all the experimentally measured conditions. To do this, data was compared to similar older generations of random packing (1.5" IMTP® to be more specific, as the 1.5" Pall® Rings do not come from the same packing family and do not share the same packing properties). Before any of these comparisons could be made, a reliable, repeatable method of determining the loading and flooding points of the experimentally measured data had to be developed, as follow:

4.2.1 Experimental Loading and Onset of Flooding Determination

Three distinct regions are present in any packed column hydrodynamic curve and each has a distinct curve trend (be it pressure drop or hold-up curves). From the experimental data it is possible to observe these three regions seen in Figure 4.1 and Figure 4.2. The transition from the pre-loading region to the loading region is when the gas velocity becomes large enough (relative to the liquid load) to increase the interfacial shear forces between the liquid and the gas. This counteracts the gravitational forces and results in more liquid being retained on the surface of the packing material. This, in turn, results in a higher pressure drop due to the reduced gas flow area. Empirically, this split point should be where the pressure drop curve starts to deviate from the dry bed pressure drop curve (see theory below). The dry bed pressure drop curve should be normalised to negate the effect of liquid load on the dry bed pressure drop in the pre-loading region (which is what the irrigated pressure drop is comprised of).

In the case of flooding, the situation becomes a bit more delicate as most of the flooding point definitions are vague (such as, where the pressure drop and liquid hold-up increase to infinity with a small increase in vapour flow factor [Kister, 1992]). However, it is still possible to determine the point where the loading region ends and a new regime (flooding) starts. Instead of trying to define the flooding point, defining the onset of the flooding region would be applicable to this project. This region is initiated where the pressure drop increases sharply relative to the trend at lower vapour flow factors. Thus, the flooding points determined below are closer to the last point in the loading regime than the true flood point (see theory below).

An ideal verification tool would be to compare the HETP/vapour flow factor curve to the pressure drop and hold-up curves. The onset of the loading regime would relate to a decrease in the HETP from where it would reach a local minimum before it starts to rise again rapidly. This local minimum would relate to the transition point between the

empirically fitted curves (between loading and flooding regimes). Since no mass transfer is present in this project, the HETP method is unfortunately not available.

In the absence of mass transfer data the above mentioned points (loading point and onset of flooding) were determined statistically by fitting empirical curves on the regions in question. This was done on the pressure drop curves due to the simplicity by which the pressure drop measurements are done and due to the dry bed pressure drop which can be used as a reference line. Error analysis was then done on these curves as well as determining their confidence prediction intervals. These intervals where then compared to each other with a 95 % confidence interval and where a significant difference was observed, it was flagged as the first point in the flooding regime.

To better clarify the above mentioned method, the section below describes the statistical theory found in Ostle [1966] as well as a step-by-step method in determining the loading and onset of flooding point. The experimental data used as an example is IMTP® at a liquid rate of 2.91 m^3/h.

Confidence Prediction Interval Theory in Simple Linear Regression:

The 100·γ percent prediction interval can be calculated by the following equations:

$$L', U' = \hat{Y} \pm t_{\left[(1+\gamma)/2\right](n-2)} \cdot s_{\hat{Y}} \quad 4.1$$

$$s_{\hat{Y}}^2 = s_E^2 \left[1 + \frac{1}{n} + \frac{\left(X - X_{ave}\right)^2}{\sum \left(X - X_{ave}\right)^2} \right] \quad 4.2$$

$$s_E^2 = \frac{\sum \left(Y - \hat{Y}\right)^2}{\left(n-2\right)} \quad 4.3$$

Where:

L' is the lower value of the predicted interval

U' is the upper value of the predicted interval

$\hat{Y}$ is the predicted value given an input X

n is the number of measured observations in the population sample (eq. 4.1 & 4.3)

n is the number of generated observations in the population sample (eq. 4.2)

$s_{\hat{Y}}^2$ is the estimated variance of predicted individual $\hat{Y}$ for a given X

s_E^2 is the residual mean square

t is the confidence interval

X_{ave} is the mean value of X for the given population sample

Thus, based on the equations above the lower and upper “reliable limit” point of an individual sample point can be calculated by choosing a confidence interval. This interval

is normally chosen as 95 % in statistical calculations. The above prediction interval is also the most accurate for X values close to the mean value of X. The only assumption that is made in these calculations is that the residual mean square is constant for the sample size (and for extrapolation purposes). So, in short what happens is that an upper and lower limit (to account for errors in the data) is assigned to each data point based on an average residual mean square of the data points in the sample. This assumption is not necessarily true when extrapolating as the incremental increase between data points (on the y-axis) could be larger than the upper limit value of the previous data point. Thus, a constraint is placed on this method: the predicted value should be less than the upper limit of the previous data point when extrapolating. If this constraint is not met, the residual mean square should be calculated for each individual sequential point and not assumed to be constant. It should be noted that in the figures below, in the loading point determination and onset of flooding sections, the abscissa represents x and the ordinate y on the empirical curves.

Loading Point Determination:

As said earlier, the loading point can be described as the point where the experimental pressure drop data trend starts to deviate substantially from the dry bed pressure drop trend. Figure 4.9 shows the experimental pressure drop data for IMTP® at a liquid load of 2.91 $m^3/(m^2 \cdot h)$.

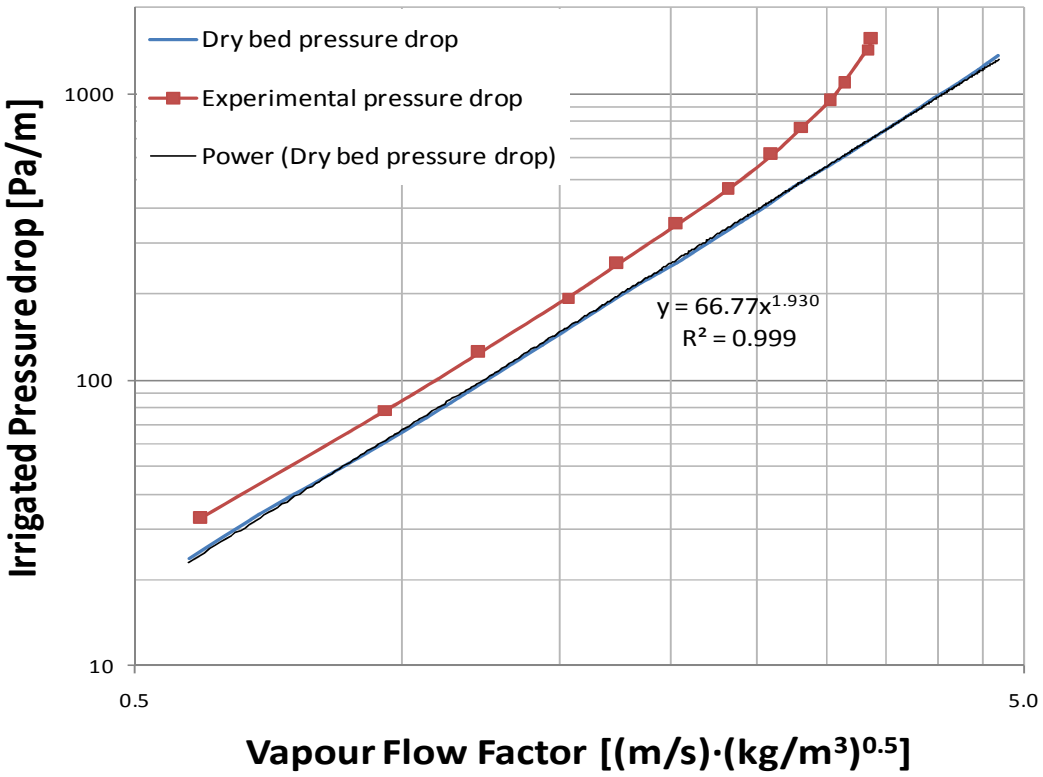

Figure 4.9: IMTP® experimental pressure drop data at a liquid rate of 2.91 m^3/h

First off, the dry bed pressure drop needs to be normalised so that the vapour flow factors coincide with those of the irrigated pressure drop data. The difference between the dry bed pressure drop and the irrigated pressure drop is negated by adjusting the dry bed pressure drop curve. This is done by calculating an average % difference between the irrigated and dry bed pressure drop. This average is calculated up to the first point of significant deviation (the row that is shaded) from the rest of the averages and is shown in the table below:

Table 4.4: Adjusted dry bed pressure drop summary

Column Pressure Drop [Pa/m]	Normalised Dry Bed Pressure Drop [Pa/m]	Dry Bed Pressure Drop Difference [%]	Average Dry Bed Pressure Drop Difference in Pre-Load [%]	Adjusted Dry Bed Pressure Drop [Pa/m]
0	0	0	29	0
33	24	30		32
78	62	27		80
125	98	27		127
194	153	27		197
255	196	30		253
351	264	33		341
463	340	36		439
614	424	45		548
767	494	55		638
948	565	68		730
1094	607	80		785
1435	683	110		882
1550	700	122		904

This adjusted dry bed pressure drop is then plotted on a figure to fit a curve through the adjusted as shown in Figure 4.10.

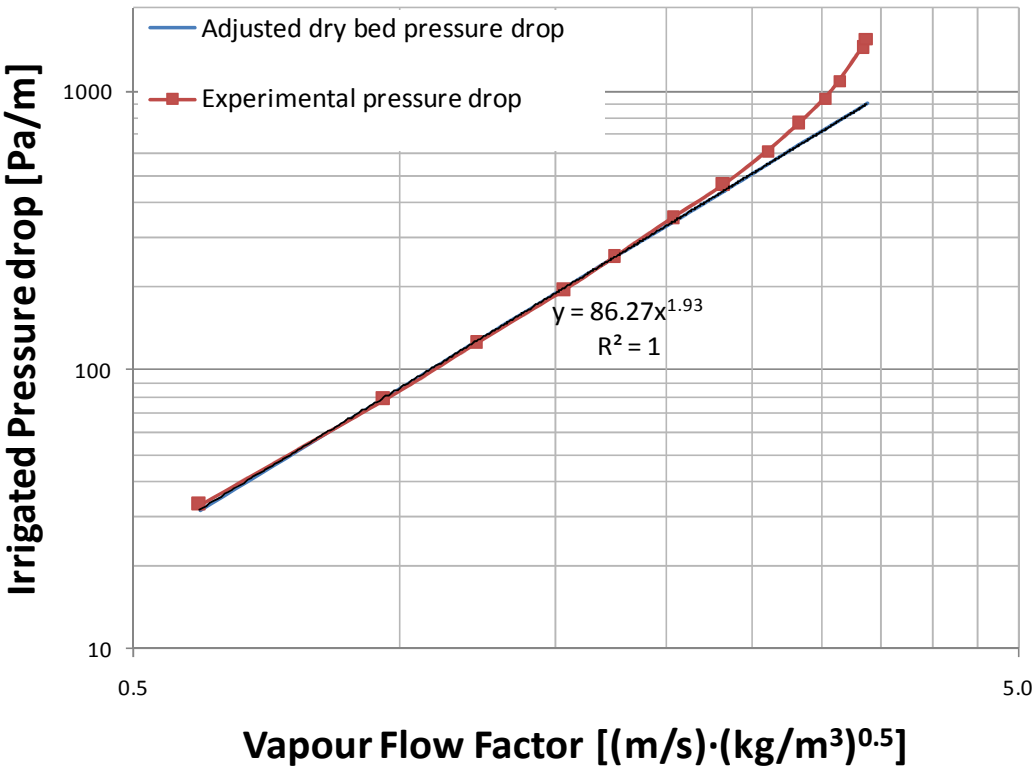

Figure 4.10: IMTP® adjusted dry bed pressure drop data at a liquid rate of 2.91 m^3/h

Next, a polynomial curve is fitted on 4 points in the experimental pressure drop data near the region where the two curves start to deviate in Figure 4.10. These are points 4 - 7 and the region is marked in Figure 4.11.

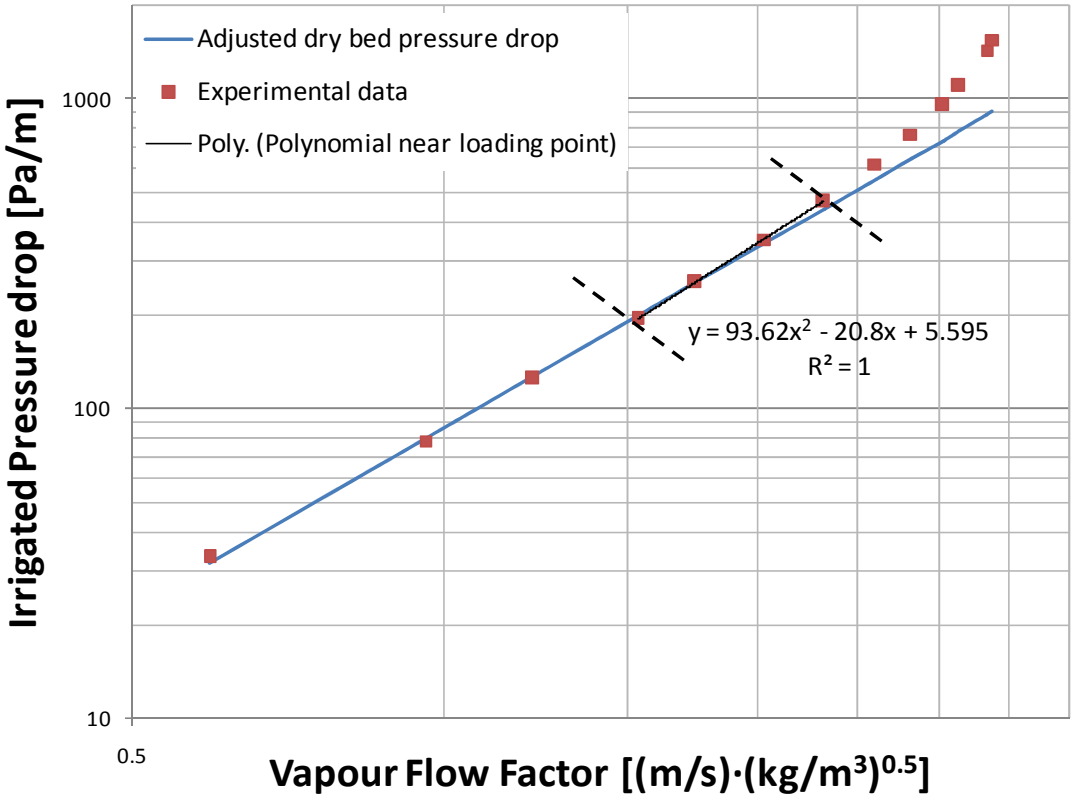

Figure 4.11: IMTP® polynomial near loading point at a liquid rate of 2.91 m^3/h

In order to increase the resolution of the statistical analysis (and since we're interpolating), artificial data is required for both the adjusted pressure drop curve and the polynomial near the loading point. However, the minimum incremental step at which the data can be generated is dependent on the standard deviation of the experimental data. Thus, the steps cannot be smaller than one standard deviation as the generated data would then be irrelevant. The relationship between the sample time and the data points are as follow: The data logger logs a data point every 2 seconds (can be changed to 1 second as well), and the sample time of each experimental point is 2 minutes once steady state has been reached. Thus, every data point on Figure 4.11 is an average of a group of at least 60 individual data points. These sample sizes are used to determine the standard deviation incurred on each of the axes in the respective figures. Table 8.55 shows this calculation (section 8.8.1 of the Appendix). The raw data sheets are included on the CD attached to this thesis.

Once the incremental steps have been determined (vapour flow factor of 0.006), artificial data is generated for both the adjusted pressure drop curve (between data points 1 - 7, see Figure 4.10) and the polynomial near the loading point (between data points 4 - 7, see Figure 4.11). Equations 4.1 - 4.3 are then applied to both the adjusted pressure drop curve and the polynomial near the loading point to calculate the confidence prediction interval of each data set. In the equations X is the vapour flow

factor and Y is the pressure drop. A simple logical test then determines at what maximum vapour flow factor the loading point is at. The logical test is true if the upper limit of the adjusted pressure drop curve is above the lower limit of the polynomial near the loading point and false if it is above it. The tables showing these results are found in section 8.8.1 of the Appendix.

It should be noted that the data tables in section 8.8.1 are truncated to only show the values up to the loading point. The original tables can be found on the CD attached to this thesis. From the tables the loading point is predicted at a vapour flow factor of 1.87. The corresponding pressure drop and liquid hold-up is then calculated from experimentally fitted curves that yield 293 Pa/m and 0.0464 m^3/m^3 respectively.

Onset of Flooding Determination:

The onset of flooding can be determined by applying the same principles of confidence prediction intervals that were applied in the determination of the loading point. There is, however, a subtle difference which is described below:

A consistent curve trend is required to represent the experimental data in the loading region. By trial and error an exponential curve trend was successfully fitted to all the experimental data sets within the loading region as shown in Figure 4.12.

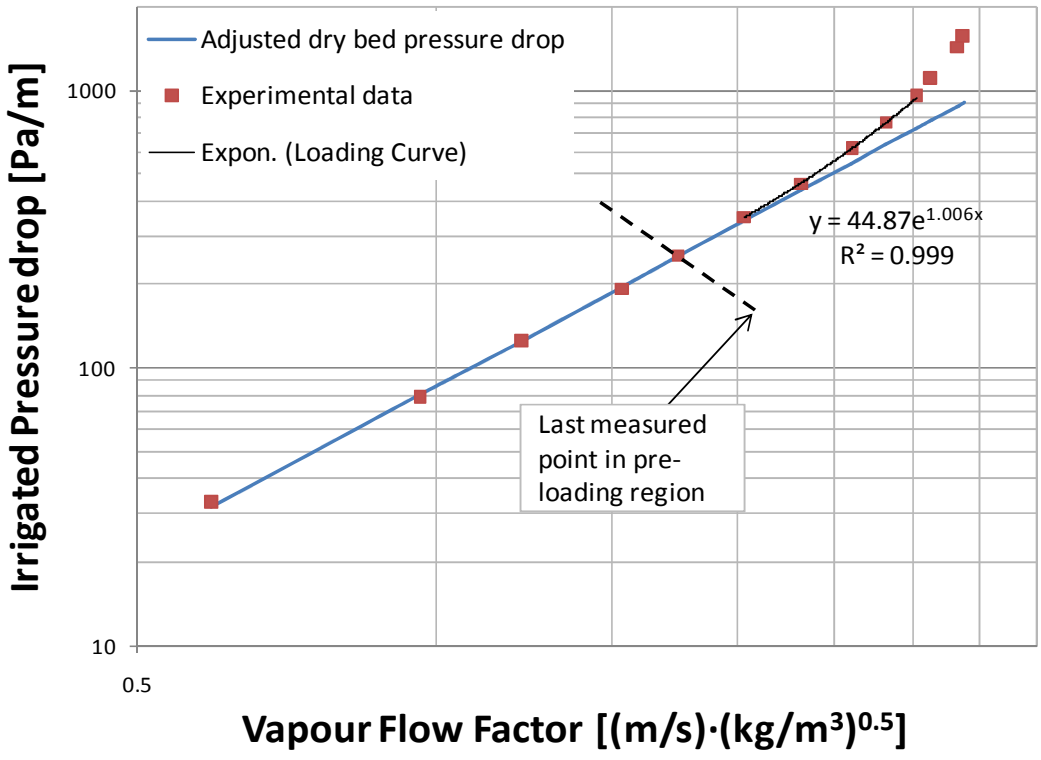

Figure 4.12: IMTP® initial loading curve fit at a liquid rate of 2.91 m^3/h

From the loading point discussion in the section above it was found that point 5 was the last measured point in the pre-loading region. Thus, the first point of the loading region curve is the next data point in line or point 6 (the difference by using data point 5 or 6 as the starting point of the loading curve in the determination of the onset of flooding is less than 3 %; however, the loading point is in-between data points 5 and 6 and thus by using data point 5 would still refer to the pre-loading region).

The next step is to determine where the regime transition from loading to flooding occurs (between which data points). By sequentially adding a data point to the curve sample size, refitting the exponential curve and evaluating its R^2 value, the point where the exponential curve is no longer valid (and thus the onset of a new regime) can be determined. Figure 4.12 - Figure 4.14 illustrates this sequential method by noting the R^2 values.

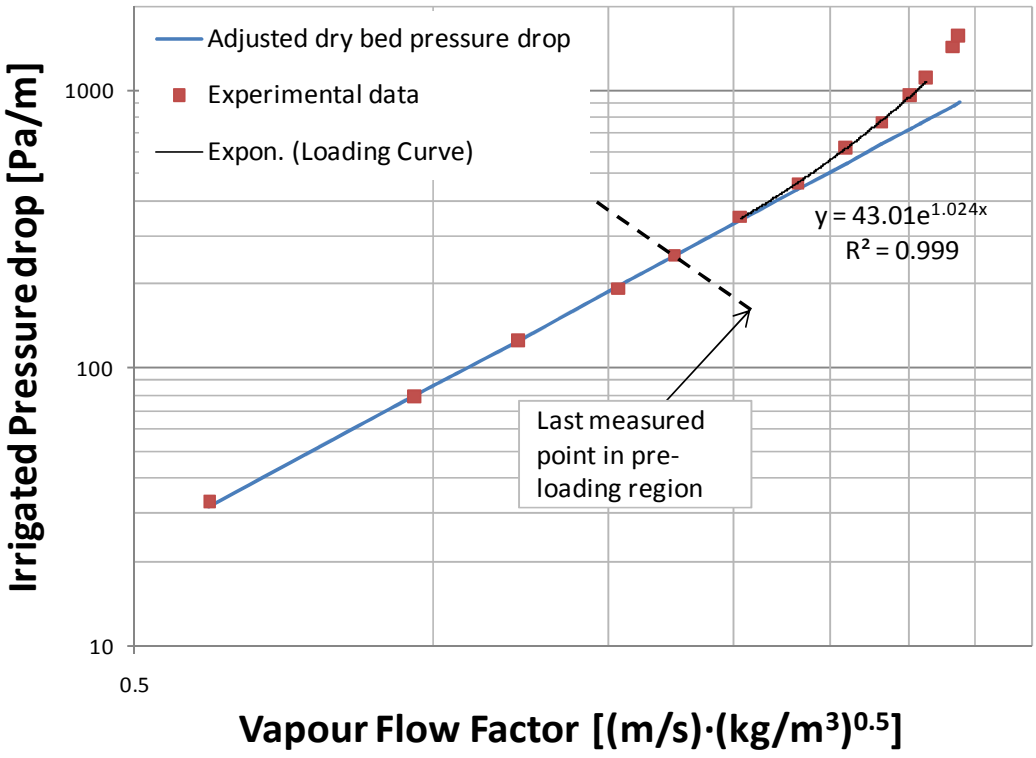

Figure 4.13: IMTP® intermediate loading curve fit at a liquid rate of 2.91 m^3/h

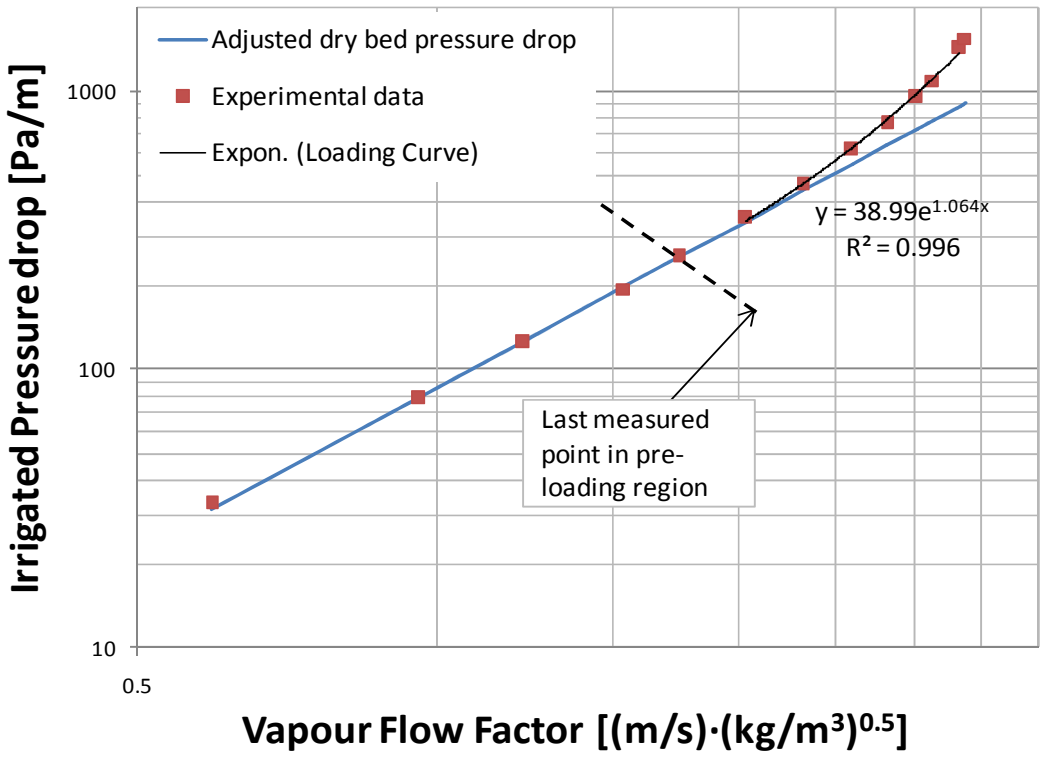

Figure 4.14: IMTP® final loading curve fit at a liquid rate of 2.91 m^3/h

The benchmark R^2 value was determined to be 0.999. Thus, anything below an R^2 value of 0.999 would signify the end of the loading region. This is shown in Figure 4.14 where the pen-ultimate data point was added to the loading curve which gave an R^2 value of 0.996 (all the other data points gave a value of at least 0.999). Thus, the loading curve has a R^2 value of 0.999 or more between data points 6 and 11.

In order to apply the same logical test used in the loading point determination (confidence interval prediction), another comparative trend is required. A polynomial was fitted on data points 10 - 13. The reason why two of the loading region points were included in this trend is to have at least two over-lapping data points where the trends are the same as shown in Figure 4.15.

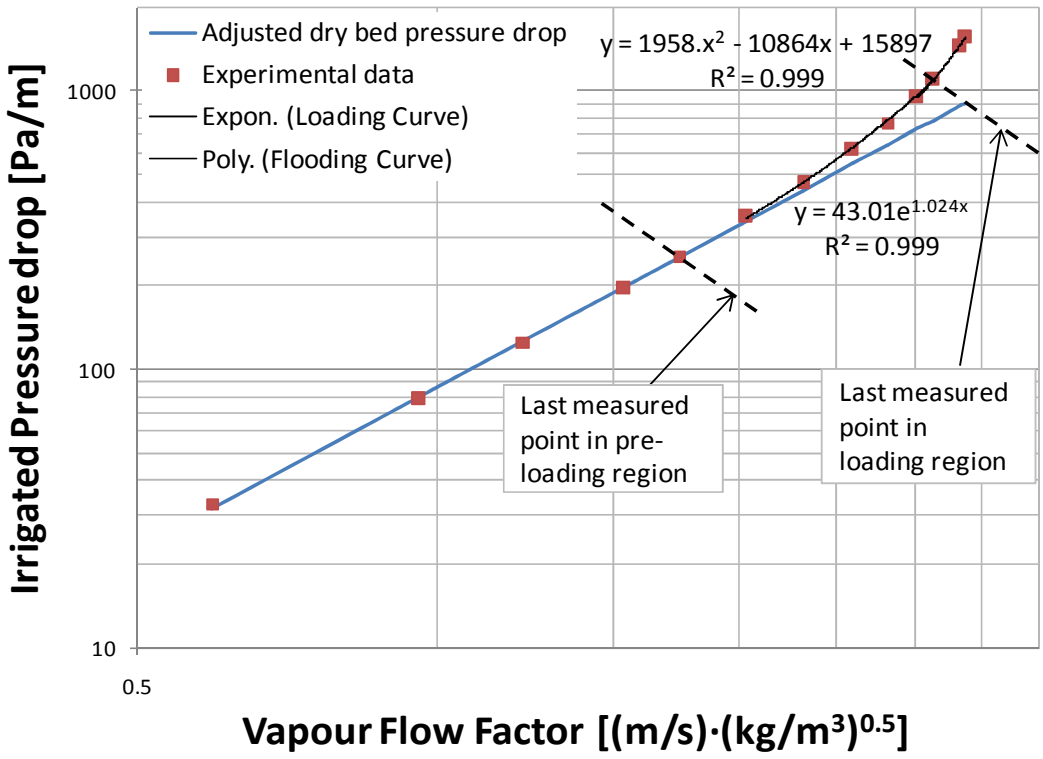

Figure 4.15: IMTP® loading and flooding curve fit at a liquid rate of 2.91 m^3/h

In order to increase the resolution of the statistical analysis artificial data is required for both the loading and flooding curve. Once again the minimum incremental step at which the data can be generated is required before the artificial data can be generated. The sample times are exactly the same as the loading point determination section (2 minutes). The standard deviation of the flooding region is shown in Table 8.60 (section 8.8.2 of the Appendix).

Once the incremental steps have been determined (vapour flow factor of 0.008), artificial data is generated for the loading (between data points 6 - 13) and flooding curve (between data points 10 - 13). Equations 4.1 - 4.3 are then applied to the loading and flooding data to calculate the confidence prediction interval of each data set. In the equations X is the vapour flow factor and Y is the pressure drop.

A simple logical test then determines at what maximum vapour flow factor the onset of flooding begins. The logical test is true if the upper limit of the loading curve is above the lower limit of the flooding curve and false if it is above it. As mentioned before, when extrapolating an additional constraint is placed on the model indicating that the upper limit of the data point in question should be higher than the next data points predicted value. If not, the residual mean square should be calculated individually. The tables showing these results can be found in section 8.8.2 of the Appendix.

The data tables in section 8.8.2 are truncated to only show the values up to the onset of flooding. The original tables can be found on the CD attached to this thesis. From the tables the onset of flooding is predicted at a vapour flow factor of 3.21. The corresponding pressure drop and liquid hold-up is then calculated from experimentally fitted curves that yield 1151 Pa/m and 0.0725 m^3/m^3 respectively.

The vapour flow factor at which the model breaks down is 3.61, which is higher than the onset of flooding value. The other value of importance in Table 8.65 (section 8.8.2 of the Appendix) is the measured limiting value. This value (along with the absolute test value) confirms the deviation point between the two regimes as the experimentally measured data point falls outside the upper limit of the predicted value at the same vapour flow factor. This indicates that at a vapour flow factor of 3.34 the exponential curve is no longer valid (meaning a change in regimes has occurred).

4.2.2 Hydraulic Capacity of Intalox® Ultra™

Since the method for determining the loading point as well as the onset of flooding conditions has been explained, the hydraulic capacity of Intalox® Ultra™ can be quantified from the pressure drop and hold-up curves. Figure 4.16 and Figure 4.17 represent the pressure drop and liquid hold-up curves over the entire testing range specified in section 3.5.

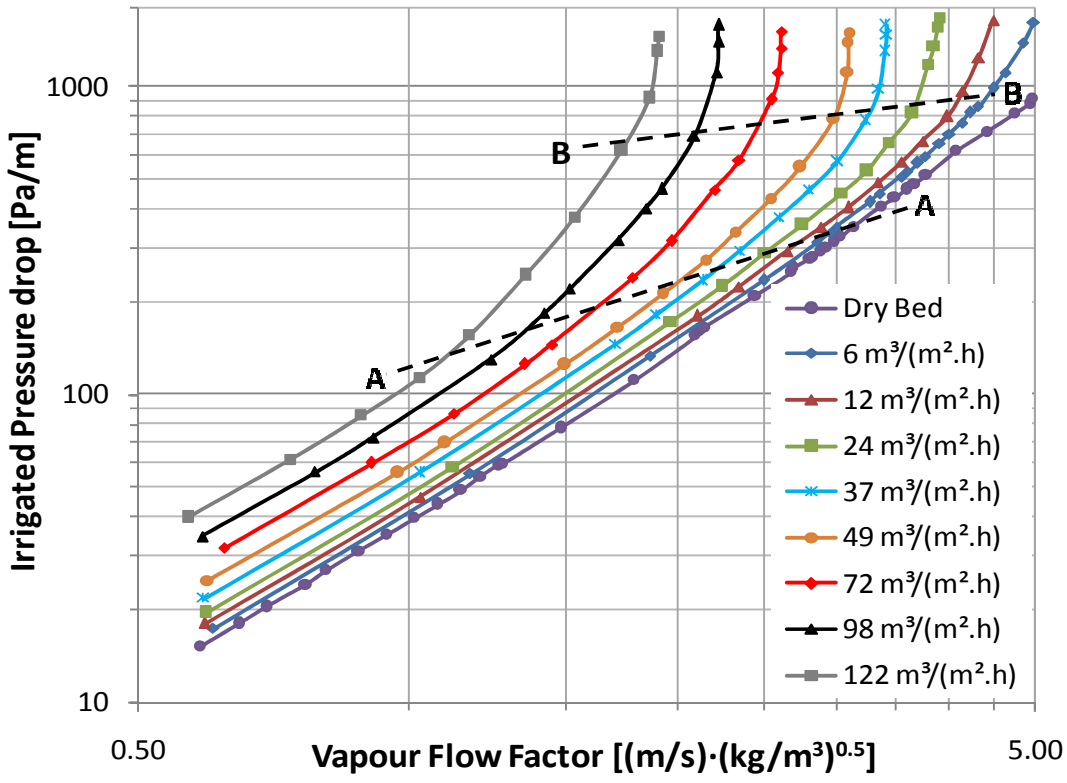

Figure 4.16: Intalox® Ultra™ pressure drop capacity regime at various liquid loads

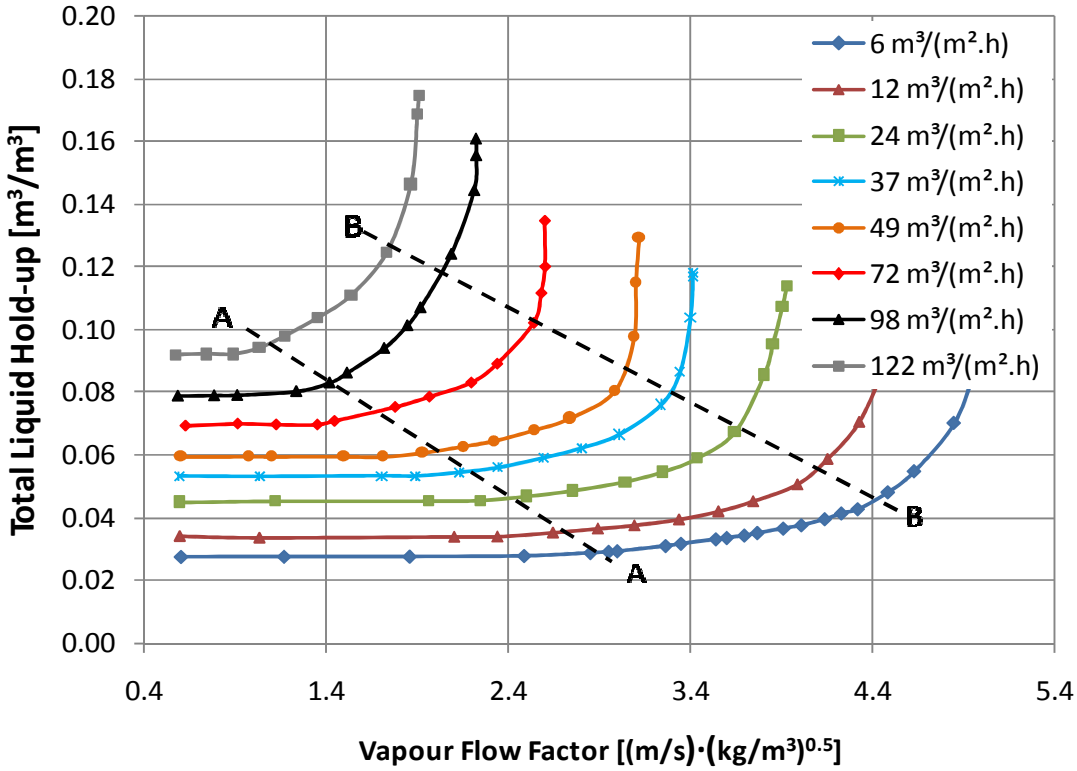

Figure 4.17: Intalox® Ultra™ liquid hold-up capacity regime at various liquid loads

In the above figures the loading point and onset of flooding was determined for every liquid load. These points were then marked on the respective curve from where the average loading and flooding curves were constructed from. Referring back to the section 1.2.2, improved packed column capacity can have the following benefits:

1.) A low pressure drop per theoretical stage results in less severe column pressure drop constraints which become critical in vacuum operations.
2.) Adequate liquid hold-up at low liquid rates resulting in a lower chance of under-wetting of the packing material.
3.) At high liquid rates low liquid hold-up values (whilst still being adequate for proper wetting) resulting in a lower pressure drop, which in turn results in a larger operating range before flooding is reached.
4.) A larger operating range (up to line B-B) results in a larger throughput capacity.
5.) In the loading region the HETP decreases, which means there's an increase in the efficiency of the packing. Thus, a better separation split is possible if operating in the loading region compared to the pre-loading region. However, the risk of entering the flooding region due to system disturbances if operating close to the flooding point.

To better understand the hydraulic capacity of Intalox® Ultra™, a comparison between it and a similar type of packing is required.

4.2.3 Comparison between different Random Packing Generations

One of the main objectives of this thesis was to quantify the hydraulic operating regime of 1.5" Intalox® Ultra™ packing material and compare it to that of older generations of random packings. Pall® Rings were chosen as benchmark, and served as a good reference to illustrate the performance of Intalox® Ultra™ and 1.5" IMTP®. Figure 4.18 illustrates the increase in pressure drop performance between the latter random packing generations (IMTP® and Intalox® Ultra™) compared to the 2nd generation Pall® Rings. It should be noted that the figures below are specifically sized for comparison purposes. The full data tables are included in section 8.7 of the Appendix.

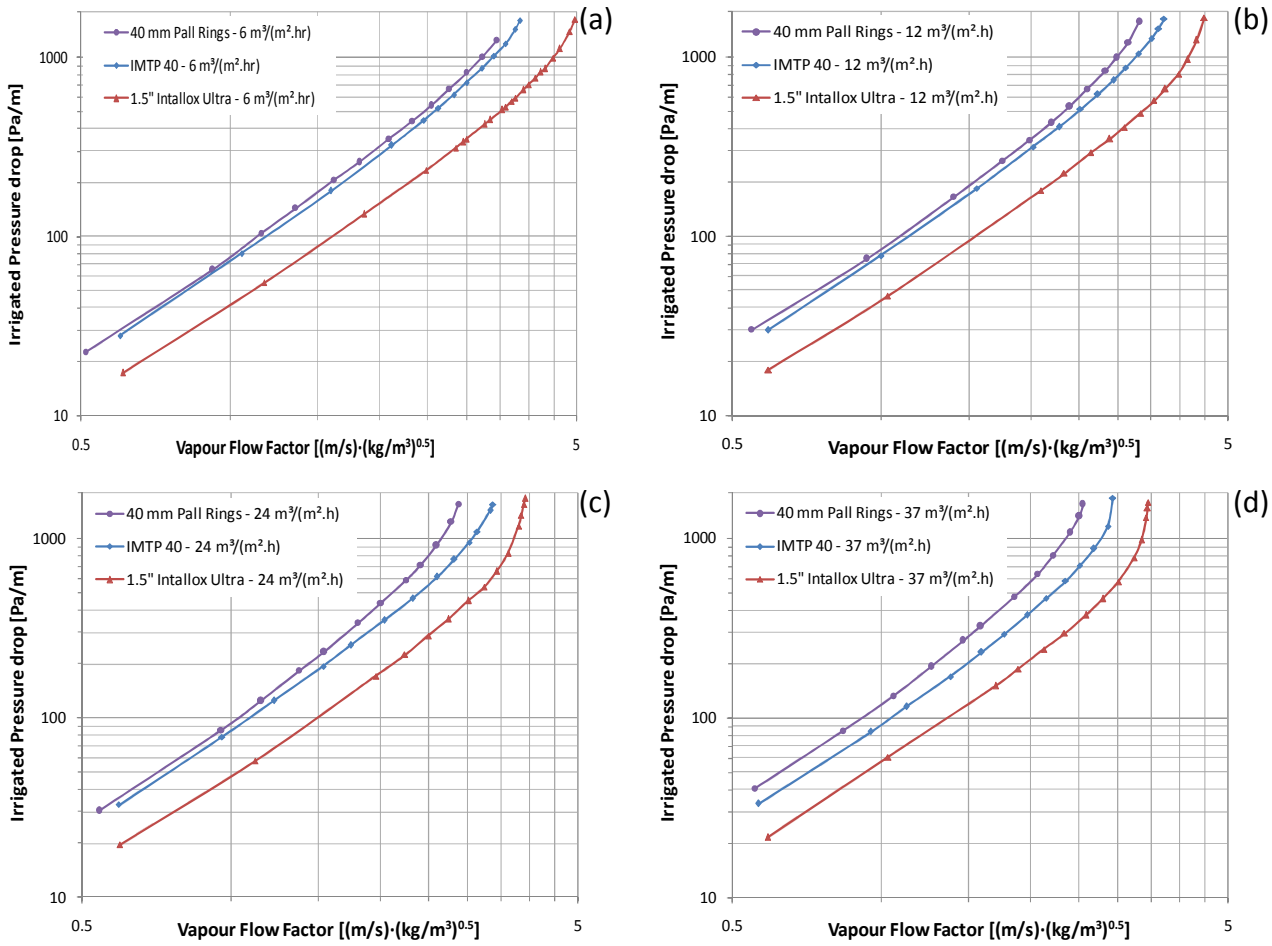

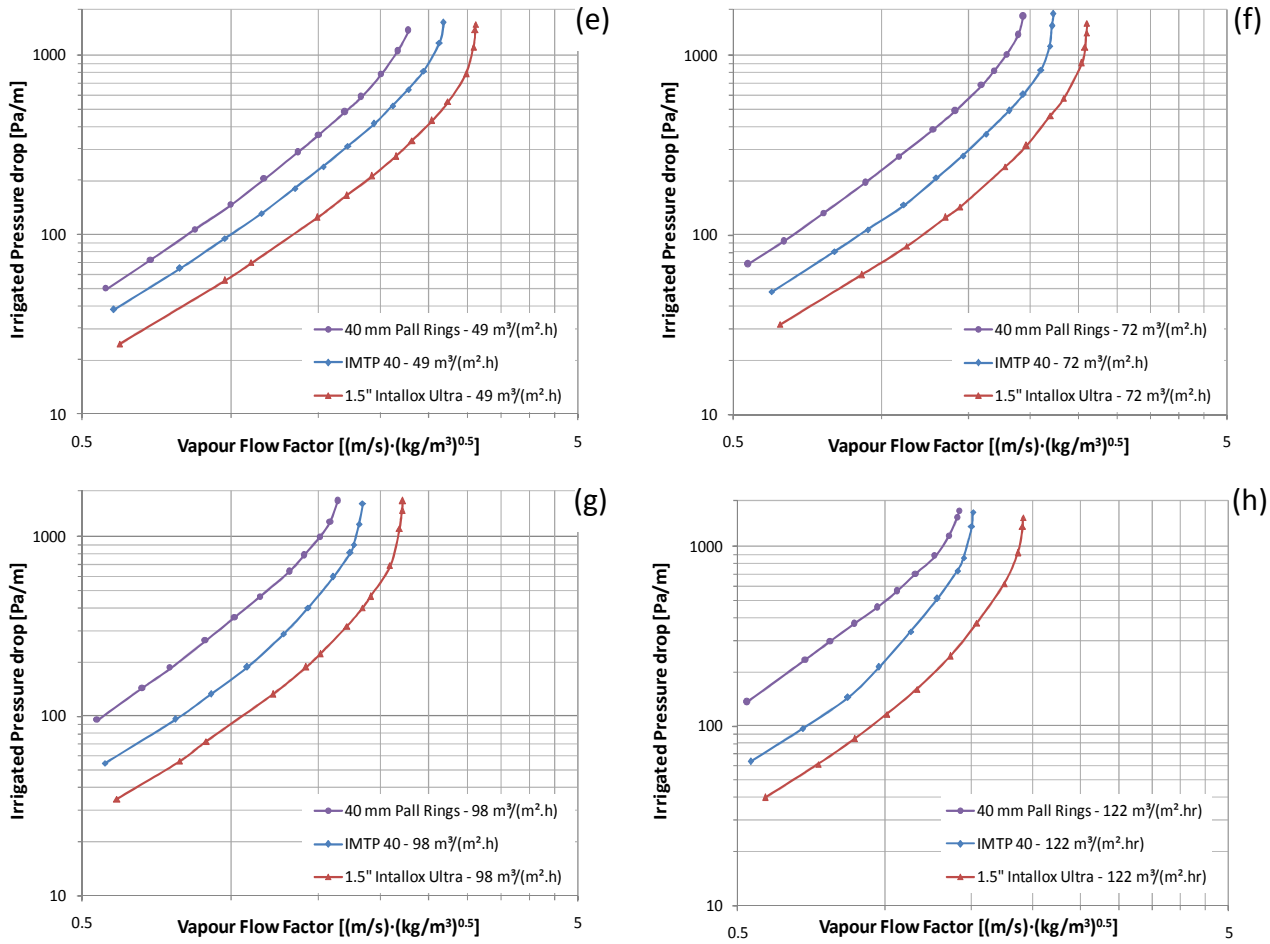

Figure 4.18: Pressure drop comparison between random packing generations

Figure 4.18 (a)-(c) shows that the pressure drop of the IMTP® is close to that of the Pall® Rings at low liquid rates (< 24 $m^3/(m^2 \cdot h)$). At higher liquid rates the pressure drop difference (between Pall® Rings and IMTP®) increases up to a maximum of 44 % at 122 $m^3/(m^2 \cdot h)$. The pressure drop of Intallox® Ultra™ is consistently lower than both Pall® Rings and IMTP® (on average 20 % lower than that of IMTP®) over all the liquid rates. The operating range (i.e. vapour flow factor at onset of flooding) of the Intalox® Ultra™ packing material is significantly larger than the other two at all the measured liquid rates. More will be said on the operating ranges in the next section.

Figure 4.19 illustrates the liquid hold-up performance comparison between the different random packing generations:

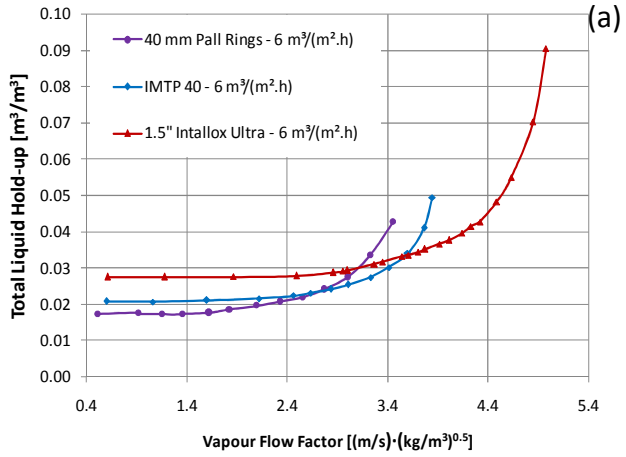
(a)
40 mm Pall Rings - 6 m³/(m².h)
IMTP 40 - 6 m³/(m².h)
1.5" Intallox Ultra - 6 m³/(m².h)
Total Liquid Hold-up [m³/m³]
Vapour Flow Factor [(m/s)·(kg/m³)^0.5]

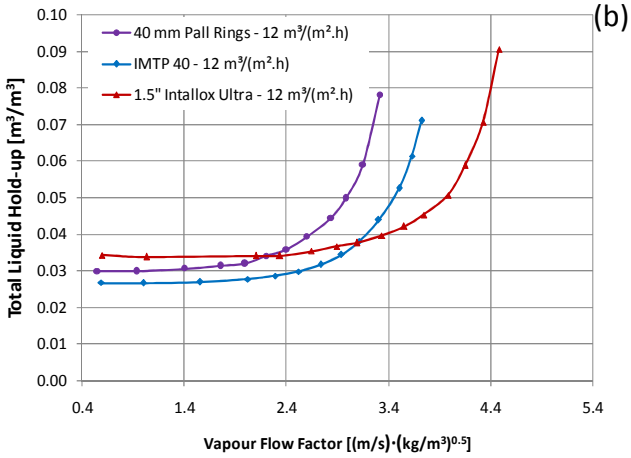
(b)
40 mm Pall Rings - 12 m³/(m².h)
IMTP 40 - 12 m³/(m².h)
1.5" Intallox Ultra - 12 m³/(m².h)
Total Liquid Hold-up [m³/m³]
Vapour Flow Factor [(m/s)·(kg/m³)^0.5]

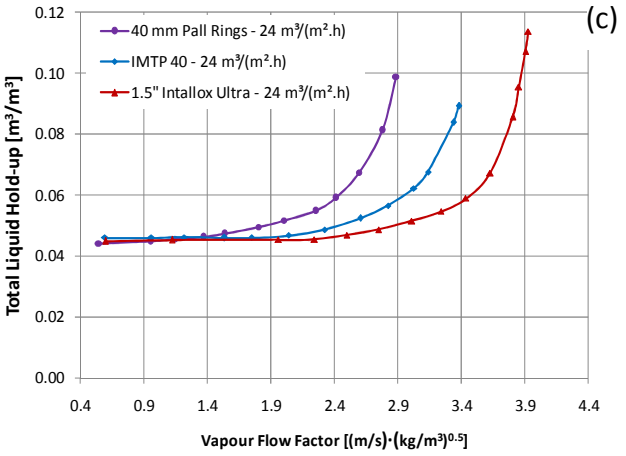
(c)
40 mm Pall Rings - 24 m³/(m².h)
IMTP 40 - 24 m³/(m².h)
1.5" Intallox Ultra - 24 m³/(m².h)
Total Liquid Hold-up [m³/m³]
Vapour Flow Factor [(m/s)·(kg/m³)^0.5]

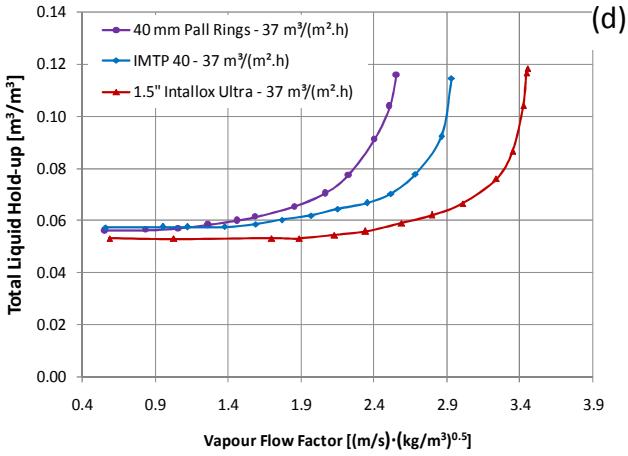
(d)
40 mm Pall Rings - 37 m³/(m².h)
IMTP 40 - 37 m³/(m².h)
1.5" Intallox Ultra - 37 m³/(m².h)
Total Liquid Hold-up [m³/m³]
Vapour Flow Factor [(m/s)·(kg/m³)^0.5]

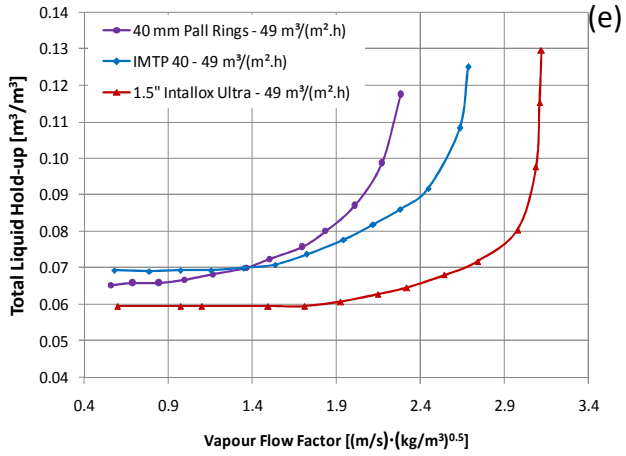
(e)
40 mm Pall Rings - 49 m³/(m².h)
IMTP 40 - 49 m³/(m².h)
1.5" Intallox Ultra - 49 m³/(m².h)
Total Liquid Hold-up [m³/m³]
Vapour Flow Factor [(m/s)·(kg/m³)^0.5]

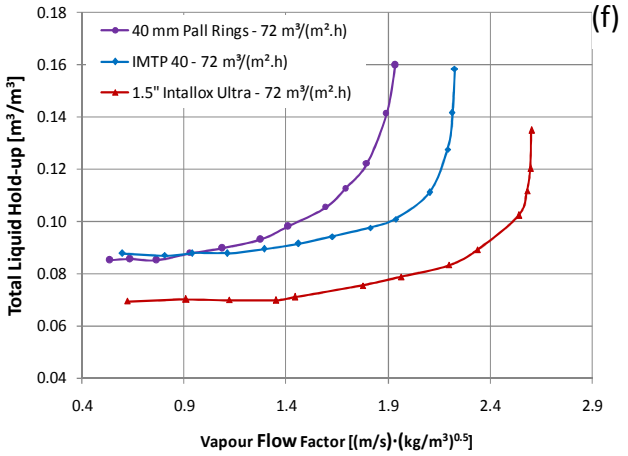
(f)
40 mm Pall Rings - 72 m³/(m².h)
IMTP 40 - 72 m³/(m².h)
1.5" Intallox Ultra - 72 m³/(m².h)
Total Liquid Hold-up [m³/m³]
Vapour Flow Factor [(m/s)·(kg/m³)^0.5]

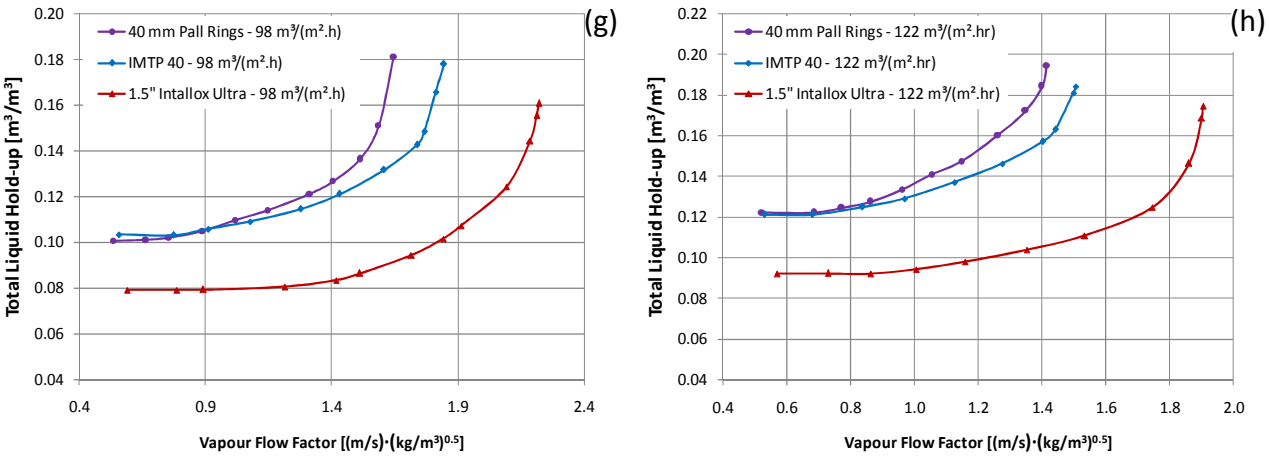

Figure 4.19: Liquid Hold-up comparison between different random packing generations

Figure 4.19 shows that the liquid hold-up of IMTP® is comparable to that of Pall® Rings. The only noticeable difference between the two is the increased capacity range for IMTP® before the onset of flooding. At low liquid rates (< 37 $m^3/(m^2 \cdot h)$) the liquid hold-up of Intalox® Ultra™ is slightly higher than the other two packing types and decreases with an increase in vapour flow factor. This relates to a reduced chance of under-wetting at these rates. As the liquid rate increases, the increase in liquid hold-up of Intalox® Ultra™ is lower compared to the increase experienced by the other two packing materials. This results in a larger capacity range as there is still adequate hold-up for proper wetting, but not sufficient to restrict the flow area open to gas flow significantly. The reduced Intalox® Ultra™ liquid hold-up reaches a maximum value of 24 % lower than that of IMTP® at flooding and at a liquid rate of 122 $m^3/(m^2 \cdot h)$.

Table 4.5 summarises the capacity of all the random packing materials investigated:

Table 4.5: Loading and flooding point summary of the three packings investigated

		Loading Point			Onset of Flooding		
	Liquid Rate $[m^3/(m^2 \cdot h)]$	Flow Factor $[(m/s)\cdot(kg/m^3)^{0.5}]$	Pressure Drop [Pa/m]	Hold-up $[m^3/m^3]$	Flow Factor $[(m/s)\cdot(kg/m^3)^{0.5}]$	Pressure Drop [Pa/m]	Hold-up $[m^3/m^3]$
1.5" Intalox® Ultra™	6	2.89	320	0.0291	4.39	914	0.0447
	12	2.66	294	0.0351	4.02	823	0.0521
	24	2.36	252	0.0461	3.58	786	0.0645
	37	2.20	212	0.0546	3.23	731	0.0763
	49	1.86	197	0.0603	3.01	776	0.0820
	72	1.52	159	0.0716	2.42	651	0.0931
	98	1.30	153	0.0816	2.04	587	0.1195
	122	1.05	127	0.0951	1.75	628	0.1251
1.5" IMTP®	6	2.10	316	0.0216	3.70	1317	0.0370
	12	2.04	317	0.0279	3.55	1309	0.0556
	24	1.87	293	0.0464	3.21	1151	0.0725
	37	1.62	239	0.0588	2.83	1087	0.0901
	49	1.49	218	0.0709	2.58	978	0.1037
	72	1.30	205	0.0900	2.15	970	0.1186
	98	1.09	192	0.1071	1.78	923	0.1519
	122	0.85	151	0.1239	1.45	856	0.1646
1.5" Pall® Rings	6	2.14	367	0.0199	3.53	1323	0.0461
	12	2.02	353	0.0321	3.13	1155	0.0578
	24	1.71	281	0.0478	2.69	1030	0.0738
	37	1.58	321	0.0576	2.35	975	0.0854
	49	1.43	299	0.0716	2.10	912	0.0916
	72	1.11	285	0.0911	1.75	906	0.1160
	98	0.91	275	0.1043	1.46	872	0.1292
	122	0.71	268	0.1233	1.25	899	0.1596

Based on data presented in Table 4.5, the capacity range (vapour flow factor up to the onset of flooding) of Intallox® Ultra™ compares to the other two packing materials as follow:

Table 4.6: Intalox® Ultra™ capacity range increase summary

Liquid Rate $[m^3/(m^2 \cdot h)]$	% Increase relative to Pall® Rings	% Increase relative to IMTP®
6	24	19
12	28	13
24	33	12
37	37	15
49	43	17
72	38	13
98	40	15
122	40	21

Based on the discussion above, Intalox® Ultra™ is hydrodynamically superior to the other two packing materials tested with reference to the pressure drop, liquid hold-up and operating range. Based on Table 8.30 (see section 8.5 in the Appendix), only IMTP® can be compared to Intalox® Ultra™ as they both have similar packing element diameters, densities, surface areas and void fractions. Pall®Rings have a lower void fraction and higher packing density, which leads to higher pressure drops as was shown in Figure 4.18.

The lower pressure drop and increased capacity of Intalox® Ultra™ compared to IMTP® would make it an attractive packing material when smaller diameter columns are needed (as these packing materials have similar packing efficiencies). This low pressure drop would also reduce the energy consumption if a column is to be retrofitted with this packing material. An interesting comparison would be between Intalox® Ultra™ and the other 4th generation packing material Raschig Super-Rings. There is unfortunately no experimental air/water data available on the 1.5" rings and should be investigated in future research.

5 Conclusions

Based on the literature review of this report, the following conclusions are drawn:

1.) The operating regime of a packed column can be divided into three distinct regions, namely the pre-loading region, the loading region and the flooding region. Although a general consensus has been reached on the definition of the loading point, most definitions for the flooding point are vague and subjective leaving room for improvement.

2.) A number of semi-theoretical models can be found throughout the literature with varying degrees of complexity, accuracy and range of application (see Table 2.11). The channel models (up to the late 1990's) are fairly empirical, with the more recent models becoming more fundamental in nature. However, the more recent models still do not predict all the parameters required in the hydraulic operating regime (irrigated pressure drop and liquid hold-up in the pre-loading -, loading - and flooding region).

3.) A large amount of the data used in the modelling approaches (see section 2) was collected from industrial distillation applications and total reflux research columns. This inherently limited data either to a fixed L/V ratio (in the case of total reflux research columns), or to a fixed system composition and operating point (in the case of industrial data). The other experimental test facilities collected large amounts of air/water data which, together with the limitations of industrial applications and total reflux columns, limited a thorough investigation of the influence of fluid properties (especially liquid viscosity) on the hydrodynamics of packed columns.

4.) Care should be taken when using of the model proposed by Billet & Schultes [1993] as large errors are possible if the use of the model is misunderstood due to the differences in the theoretical and real column hold-up at flooding (both predicted by the model). However, this model is still excellent in predicting the pressure drop and hold-up of a large number of random packings over the entire operating range.

5.) By comparing some of the random packing models found in the literature, it can be concluded that no random packing model can reliably predict the hydraulic parameters at a liquid rate in excess of 90 $m^3/(m^2 \cdot h)$. It can also be concluded that under extreme fluid property variations, the only model that gives the general correct trends, is the model proposed by Billet [1999] as the other models were not verified in these extreme cases. Lastly, it can be concluded that there is a lack of predictive models that include modern random packings (4^{th} generation).

Due to the shortcomings in current understanding of packed column behaviour, a 400 mm diameter packed column setup with a packed bed height of 3000 mm was designed, constructed and commissioned to accurately measure the following with good repeatability (see Figure 8.4 and Figure 8.5):

1.) Measure the pressure drop and liquid hold-up (pre-loading -, loading - and flooding region) of both random and structured packing over a range of liquid and gas properties (see Table 3.2 and Table 3.3).

2.) The gas flow rate covering the entire operating range (0 – 5 $[(m/s)\cdot(kg/m^3)^{0.5}]$) and the liquid rates are between 6 - 122 $m^3/(m^2\cdot h)$.

3.) Measure entrainment for future research.

Tests were conducted with an air/water system using 1.5" Pall® Rings, as well as 1.5" IMTP® as packing material and compared to the predictive model proposed by Billet & Schultes [1991; 1993; 1995; 1999]. Correct general trends for both the pressure drop and the liquid hold-up curves were observed and based on the discussion of the results on the accuracy of the system, the following conclusions are drawn:

1.) The Pall® Ring experimental dry bed pressure drop data fell between the reliable limits (± 10 %) of the Billet model. The comparison between the experimental irrigated pressure drop data and the predicted values were reasonable (± 10 %) in the pre-loading and loading regions, but with deviations in the flooding region. At higher liquid rates (> 70 $m^3/(m^2\cdot h)$) the Billet model under-predicted the irrigated pressure drop, which was partly attributed to the fact that the model was close to its validation limit and that extrapolation could lead to these errors.

2.) Initially, the experimental liquid hold-up deviated substantially from of the predictive model. An in-depth investigation revealed a substantial difference between the theoretical hold-up (at flooding) and the real column hold-up (at flooding) predicted by the Billet model (see Table 4.1). By substituting these different hold-up approaches, a satisfactory comparison (within a ± 10 % error margin) was obtained between the experimental and predicted hold-up values up to the flooding region. The differences in the flooding region were attributed to the difficulty of obtaining accurate industrial flooding data.

3.) The IMTP® pressure drop data was compared to the KG-TOWER® simulation package and the experimental data fell between the 10 % error margins over the entire liquid range (whilst omitting the simulation package loading limits). From the experimental data it is concluded that the experimental setup is thus capable of measuring packed column

pressure drop with a maximum deviation of 0.75 % and the liquid hold-up with a maximum deviation of 1.25 %. The maximum error involved with the liquid and gas flow rate accompanying these measurements is, 0.75 % (if the liquid flow meter is used), 3.8 % (if the liquid venturi is used) and 2.6 % for the gas venturi.

Additional tests were conducted with an air/water system with 1.5" Intalox® Ultra™ as packing material and results were compared to the data obtained from 1.5" IMTP®, as well as 1.5" Pall® Rings. The following conclusions can be drawn:

1.) A maximum reduction in pressure drop of up to 44 % was obtained between the pressure drop of IMTP® and that of Pall® Rings. The pressure drop of Intalox® Ultra™ was on average 20 % lower than the pressure drop of IMTP® over all the liquid rates.

2.) Based on the liquid hold-up data, Intalox® Ultra™ had a slightly higher liquid hold-up value at lower liquid rates (< 24 $m^3/(m^2 \cdot h)$) that results in a reduced chance of under-wetting. At higher rates Intalox® Ultra™ yielded a lower liquid hold-up than the other two packing materials with a maximum reduction of up to 22 % at 122 $m^3/(m^2 \cdot h)$ compared to that of IMTP®.

3.) A comparison of the operating ranges of the packing materials revealed that Intalox® Ultra™ was hydrodynamically superior to Pall® Rings™ and IMTP®. The operating range of Intalox® Ultra was found to be, on average, 35 % and 16 % larger than those of Pall® Rings and IMTP® respectively.

4.) Since IMTP® and Intalox® Ultra™ are of similar void fraction, packing density and size, it can be concluded that Intalox® Ultra™ would be a better option if a smaller, more energy efficient column was desired due to the lower pressure drop.

6 Recommendations

The following recommendations are made:

1.) Further testing should be done to investigate the influence of fluid properties (specifically liquid viscosity and, to a lesser extent, surface tension), as well as gas properties on the hydraulic capacity of packed columns.

2.) More reliable, accurate data should be generated in the loading to late loading region in order to assist in the further development of the recent hydrodynamic models. This is true for both random and structured packing models. The latest structured packing models are fundamental in nature, but lack the necessary experimental validation from the pre-loading region onwards. This modelling approach is likely to continue in the fundamental direction as more data becomes available. Eventually, these fundamental hydrodynamic models could be extended to be included in rate-based models. It is also recommended that high liquid/gas rate tests be conducted in random packing towers, as well as systems with extreme fluid property variation (from that of air/water) to improve the current models. These fundamental/semi-empirical models should be revised (or new ones derived) to include the modern high capacity packings.

3.) The generation of mass transfer data in conjunction with hydrodynamic data to test the validity of the statistical method in the determination of the onset of flooding conditions.

4.) The use of Intalox® Ultra™ would be far more beneficial from a hydrodynamic perspective than some of its 2^{nd} and 3^{rd} generation predecessors as it is hydrodynamically superior, but more characterisation work is required in terms of its separation efficiency. It is also recommended that comparative characterisation work be done between the two 4^{th} generation random packing materials (Intalox® Ultra™ and Raschig Super-Rings).

5.) Entrainment rate data should be generated alongside the pressure drop and liquid hold-up data. As none of the predictive models in the literature give any information on the entrainment rate at or near flooding, this data could be extremely useful in improving the understanding of the mechanisms involved under flooding conditions.

7 References

Billet, R. and Schultes, M., (1991) "Modelling of Pressure Drop in Packed Columns", *Chem. Eng. Tech*, 14. 89-95.

Billet, R. and Schultes, M., (1993) "A Physical Model for the Prediction of Liquid Hold-up in Two-phase Countercurrent Columns", *Chem. Eng. Tech*, 16. 370-375.

Billet, R. and Schultes, M., (1995) "Fluid Dynamics and Mass Transfer in the Total Capacity Range of Packed Columns up to the Flood Point", *Chem. Eng. Tech*, 18. 371-379.

Billet, R. and Schultes, M., (1999) "Prediction of Mass Transfer Columns with dumped and Arranged Packings: Updated Summary of the Calculation Method of Billet and Schultes", *Trans. IChemE*, 77. Part A. 498-504.

Billet, R., (1995) "Packed Towers in Processing and Environmental Technology", VCH, Weinheim.

Bravo, J.L., Rocha, J.A. and Fair, J.R., (1985) "Mass Transfer in Gauze Packings", *Hydrocarbon Process*, 64, 91.

Brunazzi, E. and Paglianti, A., (1997) "Mechanistic Pressure Drop Model for Columns Containing Structured Packings", *AIChE Journal*, 43, 317.

Chen, G.K., Kitterman, L. and Shieh, J.H., (1982) "Development of a New Generation of High Efficiency Packing for Mass Transfer Operations", *Chem. Eng. Progr.,* 79(9).

Chen, G.K., Kitterman, L. and Shieh, J.H., (1983) "Glitsch High Efficiency Packings - Preliminary Design Information", *Addendum to Glitsch Publication No. 40283,* Glitsch Inc.: Dallas, Texas.

Clayton T. Crowe, Donald F. Elger and John A. Robertson., (2001) "Engineering Fluid Mechanics", 7th Edition. Wiley & Sons.

Coulson, J.M. Richardson, J.F., (2004) "Chemical Engineering", Volume 6. Fourth edition.

Eckert, J.S., (1975) "How Tower Packings Behave", *Chem. Eng.,* April 14, 70-76.

Erasmus, A.B., (2004) "Mass Transfer in Structured Packing", PhD dissertation at the University of Stellenbosch. Stellenbosch.

Fair, J.R., Seibert, A.F., Behrens, M., Saraber, P.P. and Olujic, Z., (2000) "Structured Packing Performance – Experimental Evaluation of Two Predictive Models", *Ind. Eng. Chem. Res*, 39, 1788-1796.

Gualito, J.J., Cerino, F.J., Cardenas, J.C., Rocha, J.A., (1997) "Design Method for Distillation Columns Filled with Metallic, Ceramic, or Plastic Structured Packings", *Ind. Eng. Chem. Res*, 36, 1747-1757.

Heymes, F., Demouster, P.M., Charbit, F., Fanlo, J.L., Moulin, P., (2006) "Hydrodynamics and mass transfer in a packed column: Case of toluene absorption with a viscous absorbent", *Chem. Eng. Sci.,* 61, 5094-5106.

Humphrey, J.L., (1995) "Separation Processes: Playing a critical role", *Chem. Eng. Progr.,* 87(10), 31-41.

Kister, H.Z., (1992) "Distillation Design", McGraw-Hill. New York.

Kister, H.Z. and Gill, D.R., (1992) "Distillation and Absorption", Vol. 1. Hemisphere. Birmingham. pp. A109.

Krishnamurthy, R. and Taylor, R., (1985) "A Nonequilibrium Stage Model of Multicomponent Separation Processes. Part 1: Model Description and Method of Solution", *AIChE*, 31, 449-456.

Larachi, F., Cassanello, M., and Laurent, A., (2001) "Gas-liquid interfacial mass transfer in trickle-bed reactors at elevated pressures", *Chem. Eng. Chem. Res.*, 40, 993-1008.

Lobo, W.E., Friend, L., Hashmall, H., and Zenz, F.A., (1945) "Limiting the Capacity of Dumped Tower Packings", *Trans. AIChE.,* 41, 693-710.

Lockett, M.J., (1986) "Distillation Tray Fundamentals", Cambridge Univ. Press, Cambridge. U.K.

Leva, M., (1954) "Flow Through Irrigated Dumped Packings", *Chem. Eng. Prog.,* 50, 51-59.

Maćkowiak, J., (1990) "Determination of Flooding Gas Velocity and Liquid Hold-up at Flooding in Packed Columns for Gas/Liquid Systems", *Chem. Eng. Technol.*, 13, 184-196.

Maćkowiak, J., (1991) "Pressure Drop in Irrigated Packed Columns", *Chem. Eng. Process.*, 29, 93-105.

Maćkowiak, J., (2009) "Extended channel model for prediction of pressure drop in single-phase flow in packed columns", *Chem. Eng. Res. and Des.*, 87, 123-134.

Nieuwoudt, I., R&D Director at Koch-Glitsch (2010), Personal communication.

McNulty, K.J. and Hsieh, C.L., (1982) "Hydraulic Performance and Efficiency of Koch Flexipac Structured Packings", *AIChE Annual Meeting*, Los Angeles, California.

Olujic, Z., (1997) "Development of a Complete Simulation Model for Predicting the Hydraulic and Separation Performance of Distillation Columns Equipped with Structured Packings", *Chem. Biochem. Eng. Quarterly*, 11, 31-46.

Olujic, Z., Kamerbeek, A.B. and De Graauw, J., (1999) "A corrugation geometry based model for the efficiency of structured distillation packing", *Chem. Eng. Process.,* 38, 683-695.

Olujic, Z., (1999) "Effect of Column Diameter on Pressure Drop of a Corrugated Sheet Structured Packing", *Trans. Inst. Chem. Eng.,* 77(Part A), 505-510.

Olujic, Z., Jödecke, M., Skilkin, A., Schuch, G., Kaibel, B., (2009) "Equipment improvement trends in distillation", *Chem. Eng. Process.,* 48, 1089-1104.

Ostle, Bernard, (1966) "Statistics in Research", 2nd Edition. The Iowa State University Press. Iowa.

Piché, S., Illiuta, I., Grandjean, B.P.A., Larachi, F., (2001) "A unified approach to the hydraulics and mass transfer in randomly packed towers", *Chem. Eng. Sci.,* 56, 6003-6013.

Piché, S., Larachi, F., Grandjean, B.P.A., (2001) "Flooding capacity in packed towers: Database, correlations, and analysis", *Ind. Eng. Chem. Res.,* 40, 476-487.

Perry, R.H. and Green, D.W., (1999) "Perry's Chemical Engineer's Handbook", Seventh Edition. McGraw-Hill, Inc.

Ranke, H., Lerzer, R., Becker, O., (2001) "Hydraulic Calculations of Cross-channeled Packings in Distillation Units Based on a Physical Model", *Chem. Eng. Tech.,* 23, 691-699.

Robbins, L.A., (1991) "Improve Pressure-Drop Prediction With a New Correlation", *Chem. Eng. Prog.,* 87.

Rocha, J.A., Bravo, J.L. and Fair, J.R., (1993) "Distillation Columns Containing Structured Packings: A Comprehensive Model for Their Performance. 1. Hydraulic Models", *Ind. Eng. Chem. Res.,* 32, 641-651.

Rocha, J.A., Bravo, J.L., (1996) “Distillation Columns Containing Structured Packings: A Comprehensive Model for Their Performance. 2. Mass-Transfer Model”, *Ind. Eng. Chem. Res.,* 35, 1660.

Schultes, M., (2010) ”Research on Mass Transfer Columns: Old Hat or Still Relevant”, *Presentation at D&A Conference, de Haan, A.B., Kooijman, H., Górak (Eds.), Eindhoven*, *12 – 15 September*, ISBN 978-90-386-2215-6.

Schultes, M., Chambers, S., Fleming, B., (2010) ”Commercial Scale Test Validation of Modern High Performance Random and Structured Packings for CO_2 Capture Ranking”, *Presentation at D&A Conference, de Haan, A.B., Kooijman, H., Górak (Eds.), Eindhoven, 12 – 15 September,* ISBN 978-90-386-2215-6.

Seader, J.D. and Henley, E.J., (1998) “Separation Process Principles”, John Wiley & Sons, Inc.

Sherwood, T.K., Shipley, G.H., and Holloway, F.A.L., (1938) ”Flooding Velocities in Packed Columns”, *Ind. Eng. Chem.,* 30(7), 765-769.

Spiegel, L. and Meier, W., (1987) “Correlations of the performance characteristics of the various Mellapak types”, *Inst. Chem. Eng. Symp. Ser*., 104, A203-A215.

Spiegel, L. and Meier, W., (1992) “A Generalized Pressure Drop Model for Structured Packings”, *Inst. Chem. Eng. Symp. Ser*., 128, B85-B94.

Spiegel, L. and Meier, W., (2003) “Distillation Columns with Structured Packings in the Next Decade”, *Trans. Inst. Chem. Eng.,* 81(Part A), 39-47.

Strigle, R.F., Jr., (1994) “Packed Tower Design and Applications”, 2nd Ed., Gulf Publishing, Houston, Texas.

Suess, P. and Spiegel, L., (1992) “Hold-up of Mellapak structured packings”, *Chem. Eng. Process.*, 31, 119-124.

Woerlee, G.F., Berends, J., Olujic, Z., de Graauw, J., (2001) “A comprehensive model for the pressure drop in vertical pipes and packed columns”, *Chem. Eng. Journal*, 84, 367-379.

Uys, E.C., (2010) “Entrainment in an Air/water System Inside a Sieve Tray Column”, Master’s thesis at the University of Stellenbosch, Stellenbosch.

8 Appendix

8.1 Equipment Design Specifications

The equipment design specifications consist of the equipment from the existing setup as the additional equipment was already discussed in the main body of this thesis. The existing setup specifications were adapted and reprinted with permission from Uys [2010]. The following tables give the design specifications for the gas blower, liquid pump, surge tank and the heat exchanger:

Table 8.1: Gas blower specifications

Gas types	Flow Rate [m^3/h]	Delivery Pressure [kPa]
Air	5600	12
CO_2	2100	15
SF_6	900	16
System pressure (max)	1.2 atm	
Design Specifications		
Operating temp. range	5 - 80 ^oC	
Inlet and exit pipe diameter	203 mm	
Motor should be spark proof		
Radial vane control valve at inlet to control gas flow rate		
Safety sensors should be provided (vibration, bearing temp.)		

Table 8.2: Liquid pump specifications

Liquid types	Flow Rate [m^3/h]	Delivery Pressure [kPa]
Water	20	600
Ethylene Glycol	20	600
Silicone Oil	20	600
n-Butanol	20	600
Isopar G	20	600
The worst component of the cleaning agent is Methanol		
Design Specifications		
Operating temp. range	5 - 80 ^oC	
Inlet and exit pipe diameter	50.8 mm	
Motor should be spark proof		

Table 8.3: Surge tank geometry

Description	Values	Units
Unit design was based on a vertical liquid-vapour separator		
Vessel diameter	1.6	m
Height	2.8	m
Volume	5	m^3
Inlet Height	0.8	m

Table 8.4: Heat exchanger specifications

Description	Inlet Temperature [°C]	Outlet Temperature [°C]	Flow rate [m^3/h]
Liquid side (based on water)	25.7	25	20
Cooling water side	20	22	8
Design Specifications			
Heat exchanger type	Plate		
Operating temperature range	20 - 85 °C		
Inlet and outlet pipe diameters	50.8 mm		
Maximum pressure drop	2 bar gauge		
Maximum pressure	6 - 7.5 bar gauge		
Materials of construction	Stainless steel with compatible seals		
Operating liquids	See Table 3.3		

8.2 Sensor Design Specifications

The sensor design specifications are divided firstly into the existing setup sensors which had to be designed (gas venturi). Next, the current system sensors (liquid venturi) are discussed followed by all the remaining sensors which were merely specified.

8.2.1 Gas Venturi

The gas venturi was designed and constructed by Uys [2010]. He derived an equation to measure the gas mass flow rate based on the equation by Euler for compressible flow by assuming isothermal conditions.

$$G = C_D A_0 P_2 \sqrt{\frac{2\ln\left(\frac{P_1}{P_2}\right)}{RT}} \qquad 8.1$$

The physical design was based on the British Standards Institution section 1.1 [1981] for flow in closed conduits. Uys [2010] sized the venturi so that the discharge coefficient would be almost linear as a function of the Reynolds number as well as having a value close to unity. This leads to a discharge coefficient that ranged between 1 - 1.02 in value. The following figure illustrates the dimensions of the gas venturi and was reprinted with permission from Uys [2010].

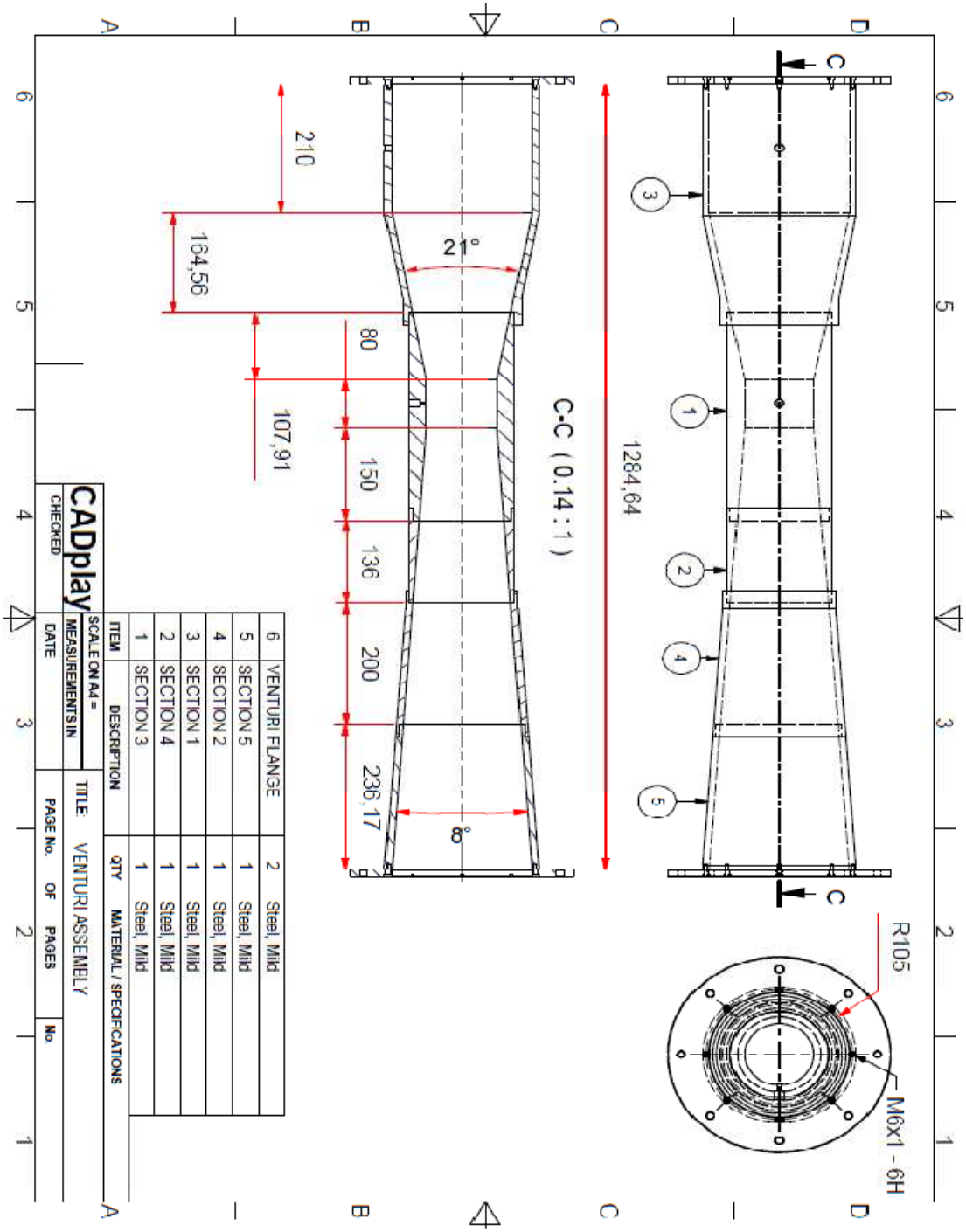

Figure 8.1: Gas venturi physical dimensions

8.2.2 Liquid Venturi

According to Crowe et al. [2001] the following equation can be derived to calculate the volumetric rate for incompressible flow in closed conduits (by assuming isothermal conditions):

$$Q = KA_0\sqrt{2\left(\frac{\Delta P}{\rho_L}\right)} \qquad 8.2$$

The above equation is useful as the volumetric flow rate of the liquid can be calculated by specifying the liquid density, contraction area (A_0) and discharge coefficient (K) and also continuously measuring the pressure drop. The physical design of the venturi was based on the British Standards Institution section 1.1 [1981] for flow in closed conduits. The K-value was sized to be as close to unity as possible whilst still remaining a linear function of the Reynolds number.

Since the specific K value between the minimum and maximum liquid rates differ, an average value was used to cover the operating range for each individual liquid. The use of this average value simplifies the computing requirements during experimental runs. The difference between the calculated and true values for water is given in the table below:

Table 8.5: Difference between average and true K-values for liquid venturi

	ΔP [Pa]	K	A_0 [m^2]	ρ_L [kg/m^3]	Q [m^3/h]	% Difference
Water [max]	73552	1.011	0.000452	997	20.000	0
	73552	1	0.000452	997	19.782	-1.088
	73552	0.9905	0.000452	997	19.594	-2.028
Water [min]	784	0.98	0.000452	997	2.002	0
	784	1	0.000452	997	2.042	2.041
	784	0.9905	0.000452	997	2.023	1.071

From the above table it can be seen that a maximum uncertainty of roughly 2 % is present due to the use of an average K-value. This is in conjunction with the 1 % uncertainty stated by the British Standards Institution for a classical venturi tube with a machined convergent section. The maximum pressure drop was calculated for silicone oil to be 85 kPa. The figures below illustrate the physical dimensions of the liquid venturi meter:

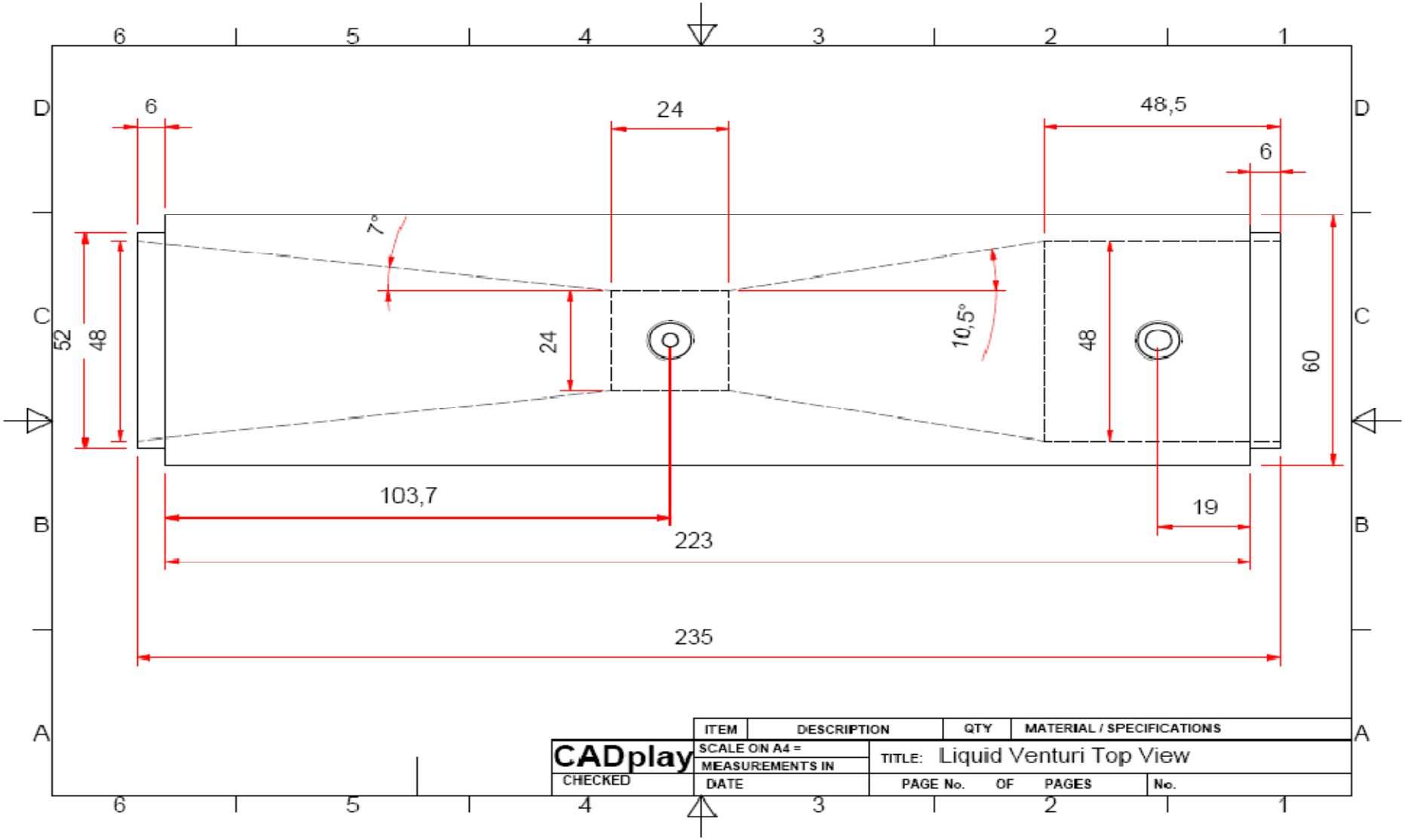

Figure 8.2: Liquid venturi physical dimensions

8.2.3 Sensor Specification Tables

Table 8.6: Absolute pressure transmitter specifications

Sensor Specifications	
Make	Endress & Hauser
Measuring range	0 - 200 kPa absolute
Turn down ratio	15:1
Measuring accuracy	± 0.05 %
Special Classification	ATEX II 2G EEx d IIC T6
Membrane Material	316 L
Fill fluid	Silicone oil
Output	0 - 20 mA

Table 8.7: Differential pressure transmitter specifications

Sensor Specifications	
Make	Endress & Hauser
Measuring range	0 - 10 kPa; 0 - 100 kPa (liquid venturi)
Turn down ratio	15:1
Measuring accuracy	± 0.05 %
Special Classification	ATEX II 2G EEx d IIC T6
Membrane Material	316 L
Seal	Viton
Output	0 - 20 mA

Table 8.8: Low liquid rate flow meter specifications

Sensor Specifications	
Make	Flowmec
Measuring range	0 - 2 m^3/h
Zero & span	Adjustable
Analog output	4 - 20 mA
Analog output accuracy	± 0.25 % full scale
Special classification	IECEX & ATEX approved intrinsically safe RT 12

Table 8.9: High liquid rate flow meter specifications

Sensor Specifications	
Make	Flowmec
Measuring range	1.7 - 20 m^3/h
Zero & span	Adjustable
Analog output	4 - 20 mA
Analog output accuracy	± 0.25 % full scale
Special classification	IECEX & ATEX approved intrinsically safe RT 12

Table 8.10: Gas mass flow meter specifications

Sensor Specifications	
Make	Sierra
Type	Hot wire anemometer
Measuring range	200 - 2100 kg/h
Analog output	4 - 20 mA
Repeatability	± 0.2 % full scale

8.3 HAZOP, Safety Interlocks and Control Philosophy

Each of the subsections will be subdivided into two parts, namely the work that was done in the existing setup (and that is relevant to this project) by Uys [2010] and the additional work that was required in the packed column setup. The existing HAZOP, safety interlocks as well as the control philosophy was modified and reprinted with permission from Uys [2010]. This author does not take any credit for the work already done; however, the work is included for completion of this thesis as a document on its own and to give readers complete access to all the relevant information regarding the system as a whole.

The following figure represents the P&ID of the heating and cooling section (reprinted with permission from Uys [2010]:

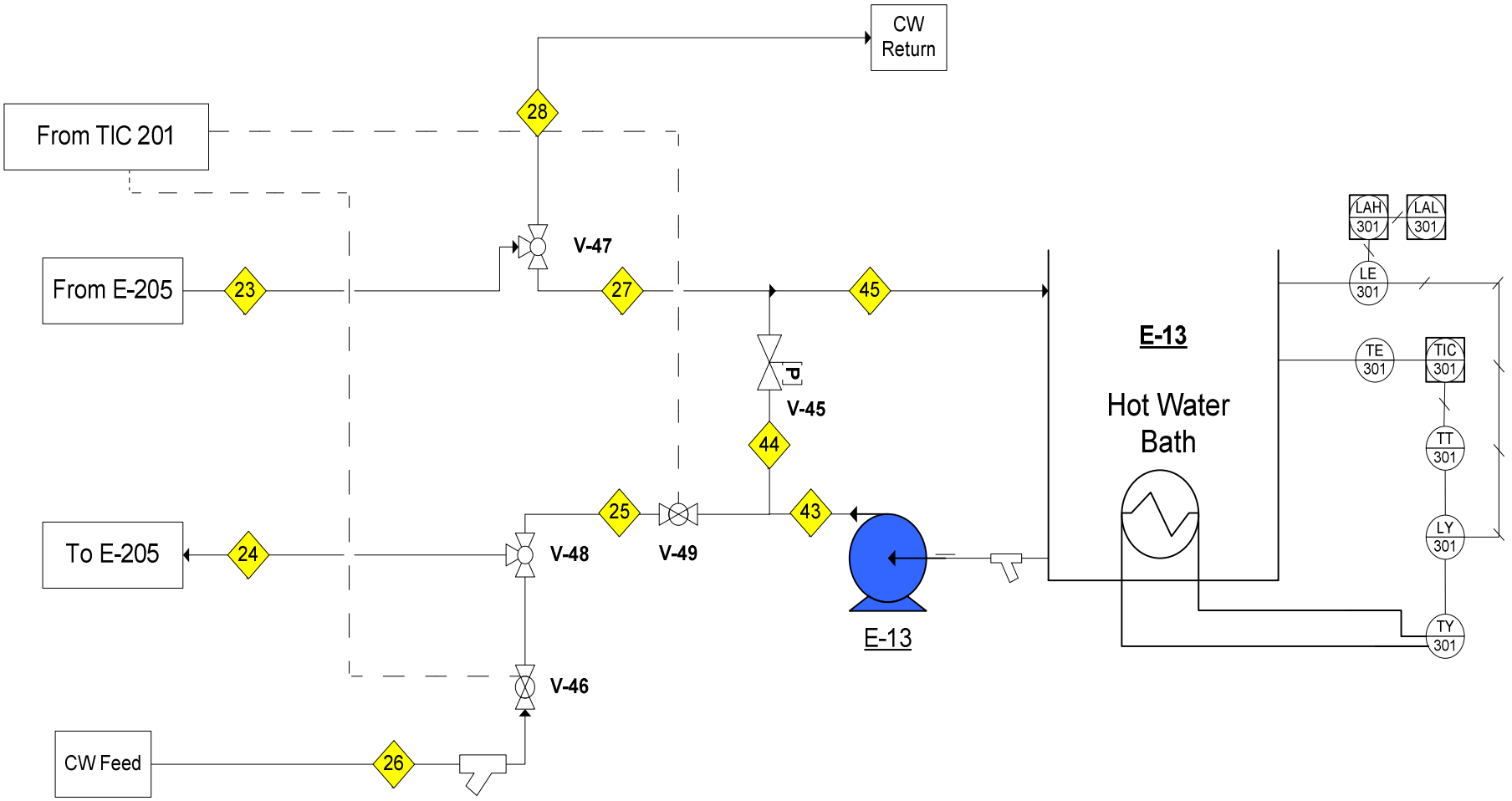

Figure 8.3: P&ID of heating and cooling system

8.3.1 Hazard and Operability Table

Existing Setup Hazard and Operability Table:

Table 8.11: Existing setup Hazard and Operability table

Equipment	Gas blower (E-102)
Intention	Supply packed column (E-401) with gas at the required pressure (100 - 110 kPa) and flow rate (up to 5000 m^3/h based on air)
Line Number	32, 33, 35, 37, 38
Intention	Transfer gas to packed column (E-401)

Guide Word	Deviation	Cause	Consequences	Action
No	Flow	RVCV-101 stuck or closed	No gas flow in column	Trigger (FAL-101), Stop Blower, inspect RVCV-101 air supply, actuator to valve connection, actuator feedback
	Flow	Blower motor failure, Bearing Temp High, Excessive Vibration interlocks	No gas flow in column	Shut system down, inspect control loop, Blower bearing temps and vibration level (Trigger Alarms), blower motor
	Flow	Duty exceeds blower motor size (high gas densities)	No gas flow in column	Close RCVC - 101
Less	Flow	RVCV-101 stuck	Less flow through column	Stop Blower, inspect RVCV-101, air supply, actuator to valve connection, actuator feedback
	Flow	Blower Inverter communication failure	Less flow through column	Restart Inverter, check inverter error messages
More	Flow	RVCV-101 stuck	Excessive flooding in column	Stop Blower, inspect RVCV-101, air supply, actuator to valve connection, actuator feedback

Table 8.11 continued

Equipment	Surge tank (E-101)
Intention	Dampening of gas pressure fluctuations and settling of liquid droplets in gas line
Line Number	30,31
Intention	Load system with gas and maintain operating pressure

Guide Word	Deviation	Cause	Consequences	Action
No	Pressure	PCV-107 stuck closed	Drop in system pressure Gas leak into the surroundings that could lead to fire and or explosion	Trigger the system pressure alarm Low (PAL-102), Close regulator on gas bottle, inspect PCV-107, air supply, actuator to valve connection, actuator feedback
	Pressure	Feed Bottle empty	Drop in system pressure	Close bottle pressure regulator valve, change feed bottle
	Pressure	MV-108 open	Drop in system pressure, gas leakage into environment, fire hazard	Close MV-108, ventilate surroundings
More	Pressure	PCV-107 stuck open	Rise in system pressure	Trigger (PAH -102) close PCV-107 and bottle pressure regulator valve, inspect control valve

Table 8.11 continued

Equipment	Liquid pump (E-204)
Intention	Circulate liquid at 0 - 15 m^3/h via heat exchanger at 4 - 6 bar to packed column (E-401)
Line Number	2
Intention	Transfer liquid to pump

Guide Word	Deviation	Cause	Consequences	Action
No	Flow	Pump stoped, valves switched to closed lines, low liquid level in sump	No Flow, possible pump cavitation and rise in liquid temp	Trigger FAL-201, stop pump, re-fill liquid sump in E-401
Less	Flow	Strainer blocked, low liquid level in sump	Debris in liquid line	Trigger FAL-201, stop pump, clean strainer, re-fill liquid sump in E-401
Line Number	3			
Intention	Transfer liquid to heat exchanger (E-205)			

Guide Word	Deviation	Cause	Consequences	Action
No	Flow	Strainer blocked, or PCV-205 stuck close, or manual valves closed	Liquid temp & pressure build-up in pump	Trigger FAL-201, stop pump, clean strainer
	Flow	Flow meter (FE-201) rotor failure	Liquid temp & pressure build-up in pump	Trigger FAL-201, stop pump, open flow meter, inspect strainer
More	Flow	Pump (P-201) failure	-	Trigger FAL-201, stop pump, inspect control loop and pump

Table 8.11 continued

Line Number	4
Intention	Transfer liquid to heat exchanger (E-205)

Guide Word	Deviation	Cause	Consequences	Action
No	Flow	PCV-205 stuck closed	Liquid temp & pressure build-up in pump	Trigger FAL-201, stop pump, use bypass line 21, inspect valve
More	Flow	PCV-205 stuck open	Flooding of column	Trigger FAH-201, reduce inverter frequency, inspect valve

Equipment	Heat exchanger (E-205)
Intention	Control liquid temperature entering packed column
Line Number	23, 24
Intention	Supply heating or cooling water to heat exchanger

Guide Word	Deviation	Cause	Consequences	Action
Less	Flow	cooling tower operation failed	Liquid temp build-up	Trigger TAH-201, stop pump, check cooling tower outlet temp
	Flow	blocked strainer	Liquid temp build-up	Trigger TAH-201, stop pump, inspect strainer,
	Flow	control valve failure	Liquid temp build-up	Trigger TAH-201, stop pump, check cooling line control valve (V-47, V-48)

Packed Column Hazard and Operability Table:

Table 8.12: Packed column Hazard and Operability table

Equipment	Packed column (E-401)
Intention	Simulating hydrodynamic distillation behaviour at atmospheric conditions
Line Number	35, 37, 46, 47, 48, 49, 52, 55, 56, 57, 58, 59, 60, 61
Intention	Simulate distillation hydrodynamics

Guide Word	Deviation	Cause	Consequences	Action
No	Gas flow	V-106 closed and/or V-105 closed	No gas flow in column	Open V-106 and/or V-105
	Liquid flow	PV-402 closed, PV-202 closed, PV-211 closed, PV-406 closed, MV-407 closed, PV-401 closed, MV-412 closed, PV-409 closed	No liquid flow in column	Trigger (FAL-201), check liquid circulation loop and open: PV-402, PV-202, PV-211, PV-406, MV-407, PV-401, MV-412, PV-409
Less	Gas flow	V-106 partially closed and/or V-105 partially closed	Reduced gas flow in column	Open V-106 and/or V-105
	Gas pressure	V-106 closed and/or V-105 open, V-107 open	No gas flow in column, reduced pressure in column	Trigger (PAL-401), Open V-106, close V-107
More	Gas pressure	V-106 open and/or V-105 closed	No gas flow in column, pressure build-up	Trigger (PAH-401), Open V-105

8.3.2 Safety Interlocks

Existing Setup Safety Interlocks:

Table 8.13: Existing safety interlocks

Equipment	Monitor	Situation	Action
Blower (E-102) [37 kW motor]	Bearing temp Axle vibration Motor current	> 70 ^{o}C > 7 mm/s > 64 A	Stop motor, Stop motor and close RVCV-101, Stop motor and trigger alarm
Pump (E-204) [5.5 kW motor]	Motor load	Too high	Stop pump
Surge tank (E-101)	Pressure	< 96 kPa < 93 kPa	Open PCV-107 Stop blower
Hot water bath (E-301)	Level	Too low (< 100 mm)	Disable heating elements

Packed Column Safety Interlocks:

Table 8.14: Packed column safety interlocks

Equipment	Monitor	Situation	Action
Packed column (E-401)	Pressure	> 110 kPa > 115 kPa < 98 kPa < 95 kPa	Close PCV-107, Stop blower, Open PCV-107, Stop Blower

8.3.3 Control Philosophy

Existing Setup Control Philosophy:

Table 8.15: Existing control philosophy

Controlled Variable	Manipulated Variable	Type of Control
TI-401 (column temperature)	CV-301 (heating) CV-302 (cooling) PV-303 (switch between heating and cooling)	Continuous PID Continuous PID Switch, comparative control
TI-301	Heating elements (TY-301)	Continuous PID
FI-201 (liquid flow rate)	PCV-205 SC-201 (motor frequency)	Continuous PID Set point
FIR-101 (gas flow rate)	RVCV-101 SC-105 (motor frequency)	Fixed setting Set point

Packed Column Control Philosophy:

Table 8.16: Packed column control philosophy

Controlled Variable	Manipulated Variable	Type of Control
DPI-404 (entrainment sampling)	PV-404	Comparative automation
DPI-403 (hold-up sampling)	PV-402 PV-406	Comparative automation
LI-402 (chimney liquid level)	MV-407	Manual

8.4 Experimental Setup Commissioning and Calibration

8.4.1 Control System Commissioning and Calibration

The following sequential system was used during the commissioning and calibration of the packed column: Firstly, the analog channels were calibrated followed by automation sequence testing. Next, the safety interlocks were tested which was followed by the equipment operation.

Analog Channels:

Analog channels convert analog signals from sensors to digital values as well as the other way around. Each channel was calibrated by changing the offset and gain value so that the converted digital value would match the value measured by the sensor. This was done with the help of a CALOG-PRO and a CALOG-TEMP calibrator. Typically, the accuracy between a conversion from analog to digital or visa versa is 0.5%. The following tables provide the measuring and sourcing specifications of the two calibrators:

Table 8.17: CALOG-PRO specifications

	Analog Input Ranges	Accuracy [%]	Resolution
Measure	0 – 24mA	0.01	1µA
	0 – 32V	0.005	1mV
	-10 – 100mV	0.005	1µV
	0.5 – 100Hz	0.001	0.1Hz
	1 – 20 000Hz	0.001	1Hz
	Analog Output Ranges	**Accuracy [%]**	**Resolution**
Source	0 – 24mA	0.01	1µA
	0 – 12V	0.01	1mV

Table 8.18: CALOG-TEMP specifications

	Analog Input Ranges	Accuracy [%]	Resolution
Measure	0 – 24mA	0.02 FS	1µA
	-10 – 100mV	0.01 FS	1µV
	RTD Type Pt 100	0.05 FS	0.01°C
	Analog Output Ranges	**Accuracy [%]**	**Resolution**
Source	0 – 24mA	0.02 FS	1µA
	-10 – 100mV	0.01 FS	1µV
	RTD Type Pt 100	0.05 FS	0.01°C

Automation Sequences:

Quite a number of automation sequences had to be tested in the commissioning of the packed column. These were:

- At start-up there is a choice between low and high liquid rate operation. Each of these has a specific valve configuration.
- At the high liquid rate setting there is also the option to circulate the fluid via the sump to assist with the heating of the liquid. This also has a unique valve configuration.
- The liquid hold-up sampling has an automation sequence that needed to be tested.
- The entrainment sampling also has an automation sequence that needed to be tested.

All of these automation sequences were individually tested by entering artificial values into the algorithm (in the case of the sampling sequences) to test their functionality and adjust accordingly. The first two sequences were tested by manipulating an input signal to test their functionality.

Interlocks:

Most of the safety interlocks were successfully tested by Uys [2010] and were not tested again. However, the additional packed column interlocks were tested by manually sourcing the interlock activation pressures with a calibrator to see if the interlock would activate. The main emergency stop interlock was tested after the packed column integration into the system. This interlock constitutes of 4 emergency stops placed throughout the pilot plant. Activating any one of these stops are activated any and all operations would stop.

Equipment Operation:

After all the above steps were done, the system was filled with water as the utilities were fully tested and operational. The automation sequences were tested again once the system was filled with water.

8.4.2 Hold-up and Entrainment Tank Calibration

The liquid hold-up and entrainment tanks were calibrated by means of their cross sectional area. By entering the area into equation 3.2 would give the change in mass if there is a change in pressure in the tank. The following method was used to determine the vessel cross sectional area:

1.) Calculate the geometrical cross sectional area of the vessel in question.
2.) Insert the calculated area into equation 3.2 which is programmed on an external computer (not the PLC).
3.) Fill the vessel with water up to the adjustable minimum level which is the zero reference point. See Figure 3.9 and Figure 3.10 for the specific minimum levels.
4.) Zero the differential pressure transmitter (for the vessel in question) at the minimum level to negate the static vapour head.
5.) To calibrate the liquid hold-up tank (TK-402 in Figure 3.9), the following was done:
    - A 25 litre vessel should be cleaned and the dry mass zeroed on a previously calibrated electronic balance.
    - Fill this vessel with exactly 20 kg of water.
    - Empty the contents into the hold-up tank through an access hole on top of the tank and note the change in pressure.
    - Change the value of the cross sectional area in equation 3.2 so that the output equals the mass added to the tank.
    - Add two more incremental 20 kg steps to the tank by following the previous four steps.
    - Empty the system and refill the tank to the minimum level.
    - Repeat all 6 of the above steps as final verification of the tank area.

6.) To calibrate the entrainment tank (TK-401 in Figure 3.10), the following was done:
    - A 20 litre vessel should be cleaned and the dry mass zeroed on a previously calibrated electronic balance.
    - Fill this vessel with exactly 10 kg of water.
    - Empty the contents into the hold-up tank through an access hole on top of the tank and note the change in pressure.
    - Change the value of the cross sectional area in equation 3.2 so that the output equals the mass added to the tank.
    - Add two more incremental 10 kg steps to the tank by following the previous four steps.
    - Empty the system and refill the tank to the minimum level.
    - Repeat all 6 of the above steps as final verification of the tank area.

Even with thorough calibration small differences exist between the measured and added mass. The following tables show the measuring accuracy of each of the measuring vessels:

Table 8.19: Liquid hold-up vessel (TK-402) calibration results

Mass Added	Measured Mass	Difference	% Difference
20.00 kg	20.06 kg	0.06 kg	± 0.3
40.00 kg	40.36 kg	0.36 kg	± 0.9
60.00 kg	60.18 kg	0.18 kg	± 0.3

Table 8.20: Entrainment vessel (TK-401) calibration results

Mass Added	Measured Mass	Difference	% Difference
10.00 kg	10.02 kg	0.02 kg	± 0.2
20.00 kg	20.06 kg	0.06 kg	± 0.3
30.00 kg	30.09 kg	0.09 kg	± 0.3

From Table 8.19 and Table 8.20 the average difference is 0.5 % and 0.3 % for the liquid hold-up and entrainment tank respectively. So the true % difference would equal the sum between the tank and the PLC (0.5 %) conversion error. Thus, the total differences are 1 % for the liquid hold-up tank and 0.8 % for the entrainment tank.

8.4.3 System Leakages

Only the packed column was tested for any leakages as the utility system was already tested by Uys [2010]. The packed column was placed under a pressure of 5 - 10 kPa gauge from where a soap and water mixture was systematically sprayed over. Any leakages were marked until the whole column was inspected and only then remedial action was taken. After the leakages were fixed the same method was used to check for additional leakages until there were none.

8.4.4 Verification of Sensor Measurements

To ensure that all of the sensors measure close to their intended values, all of the sensors used were either evaluated quantitatively or by spot checks.

High Rate Liquid Flow Meter:

The high rate liquid flow meter was already verified by Uys [2010]. However, spot checks were done by noting the change in sump volume over time as liquid is pumped from the system at a specified rate. This only gives an order of magnitude check. The following table shows the high rate liquid flow meter spot check results:

Table 8.21: High rate liquid flow meter verification results

Sample Volume [L]	Time [s]	Estimated Rate [m^3/h]	Flow Meter Rate [m^3/h]
± 100	± 70.6	± 5.1	5.05
± 100	± 35.9	± 10.02	9.97
± 100	± 24.2	± 14.88	14.98

From the above it is evident that the spot check was satisfactory in the verification of the high rate flow meter measurement.

Low Rate Liquid Flow Meter:

The low rate liquid flow meter was scaled correctly by inputting the specific values into the flow meter display. A manual draining valve was inserted into line 51 after the flow meter (E-402) in Figure 3.2). Thus, the measurement accuracy could be verified by noting the mass of liquid that entered a 10 l measuring vessel over time and comparing that to the rate indicated on the flow meter. The vessel was cleaned and dried before each sample as well as being zeroed on an electronic balance. The following table shows the low rate liquid flow meter spot check results:

Table 8.22: Low rate liquid flow meter verification results

Mass Added [kg]	Time [s]	Estimated Rate [m^3/h]	Flow Meter Rate [m^3/h]
11.52	± 60.3	± 0.688	0.682
11.61	± 29.5	± 1.417	1.379
11.65	± 30.07	± 1.398	1.371

The small differences between the two values are attributed to experimental error in the spot check method. Good hand-eye coordination is required when measuring with a stopwatch and a bucket. Even so, the spot check was satisfactory in the verification of the low rate flow meter measurement.

Liquid Venturi:

The liquid venturi meter was designed as back-up to the high rate liquid flow meter. The venturi measurement verification was done by comparing the venturi measured rates to the other two flow meters (low and high) at three intervals. By doing this it is assumed that the other measure correctly, as they have been shown to do in the sections above. The following table shows the results obtained by comparing the liquid venturi rates to those from the flow meters.

Table 8.23: Liquid venturi meter verification results

Liquid Venturi Rate [m^3/h]	Low Flow Meter Rate [m^3/h]	High Flow Meter Rate [m^3/h]	% Difference
1.865	1.851	-	0.8
7.154	-	7.133	0.3
11.65	-	11.81	- 1.4

The values in the above table agree well with the % error trend that is likely with this liquid venturi since an average K-value is used (referring back to Table 8.5). Thus, the order of magnitude measurement of the liquid venturi was verified.

Gas Venturi:

The gas venturi was verified by Uys [2010], thus a single pitot tube, order of magnitude spot check was done. The method used is to determine the average volumetric flow rate

by integrating (area under the graph) the velocity profiles over the entire radial distance of the gas venturi. This is accomplished by taking several measurements at specified intervals from the tube centre to construct the velocity profile. The average mass flow rate is then calculated with the following equation:

$$\dot{m} = \int (\rho \cdot V) \cdot 2\pi r \cdot dr \qquad 8.3$$

The density was obtained from measuring the absolute pressure 1 m behind Pitot tube measurements. This pressure was then converted to density by using the ideal gas law. The following table shows the spot check results:

Table 8.24: Gas venturi meter verification results

Gas Venturi Rate [kg/h]	Pitot Tube Rate [kg/h]	% Difference
1231	1215	1.3

The result in the table above verified the order of magnitude measurement of the gas venturi meter.

Differential Pressure Transmitter:

Another spot check at the minimum and maximum measurement values of the digital pressure transmitters was done as verification. Since the range of most of the digital pressure transmitters is 0 - 10 kPa, they were scale to a maximum value of 5 kPa. The zeroed value was verfied by opening the pressure taps to the atmosphere while keeping the taps level horizontally. The maximum value was checked by adding a vertical tube filled with roughly 510 mm of water and checked if 5 kPa was reached.

Temperature Sensors:

A CALOG-TEMP calibrator was used to verify the measurement accuracy of the temperature probes. They were tested between 20 ^{o}C and 80 ^{o}C (same as heat exchanger specs) and the measurements were ± 1 ^{o}C accurate.

8.4.5 Air/water System Testing

Before experimental data can be generated the experimental error needs to be determined as well as the systems measurement repeatability. Lastly, the data samples need to be checked if they're at hydrodynamic equilibrium or not otherwise the data would be useless.

Experimental Error:

The error involved in the measurements when recording data is of utmost importance. The following parameters will have % error in their measurement and will be calculated and discussed individually:

- Gas mass flow rate (which directly relates to the vapour flow factor)
- Liquid flow rate
- Pressure drop measurements over the packed bed
- Liquid hold-up measurements
- Entrainment measurements

The gas mass flow rate is influenced by the following errors (based on equation 8.1): The discharge coefficient (C_D, which has a maximum deviation of 0.02 or 2 % in this operating range); the pressure taps (P_1 and P_2 which have maximum deviations of 0.25 %); the temperature (T which has a maximum deviation of 1 ^{o}C). The following table summarises the maximum deviation of the gas mass flow rate at atmospheric conditions:

Table 8.25: Gas mass flow rate maximum deviation

Parameter	Value	Deviation	Adjusted Value
C_D	1	0.02	1.02
P_1 [Pa]	101325	0.25 %	101578
P_2 [Pa]	99000	0.25 %	99248
T [K]	298	1 ^{o}C	299
G [kg/h]	2062.1	2.1 %	2104.8

Thus, the maximum deviation in the gas mass flow rate is ± 2.6 % by adding the 0.5 % uncertainty of the PLC conversion. There are three possible liquid flow rates: the low rate liquid flow meter which has a maximum deviation value of 0.75 %. This is also valid for the high rate flow meter (0.75 %). The liquid venturi error is based on the discharge coefficient (K which has a maximum deviation of 2 % as seen in Table 8.5) and the pressure measurements via the differential pressure transmitters (P_1 and P_2 which have a maximum deviation of 0.25 %). Lastly, the contraction area can have a maximum deviation of 1 %. The following table summarises the maximum deviation in the flow rate measured by the liquid venturi:

Table 8.26: Liquid venturi maximum deviation

Parameter	Value	Deviation	Adjusted Value
K	0.9905	0.0205	1.011
P_1 [Pa]	50000	0.25 %	50125
P_2 [Pa]	20000	0.25 %	20050
A_0 [m^2]	0.00050671	1 %	0.00051178
Q [m^3/h]	13.97	3.3 %	14.45

Thus, the maximum deviation in the liquid venturi flow rate is 3.8 % by adding the 0.5 % uncertainty with the PLC conversion.

The maximum pressure drop deviation over the packed bed is 0.75 % (0.25 % from differential pressure transmitter + 0.5 % from PLC conversion).

The liquid hold-up measurements have a maximum deviation of 1.25 %. 0.25 % is from the differential pressure transmitter, 0.5 % from the calibration uncertainty (from Table 8.19) and another 0.5 % from the PLC conversion.

Lastly, the entrainment measurements have a maximum deviation of 1.05 %. 0.25 % is from the differential pressure transmitter, 0.3 % from the calibration uncertainty (from Table 8.20) and another 0.5 % from the PLC conversion.

System Repeatability:

The system repeatability in terms of pressure drop and liquid hold-up measurements was verified by doing repeated runs at four specified flow rates on different days.

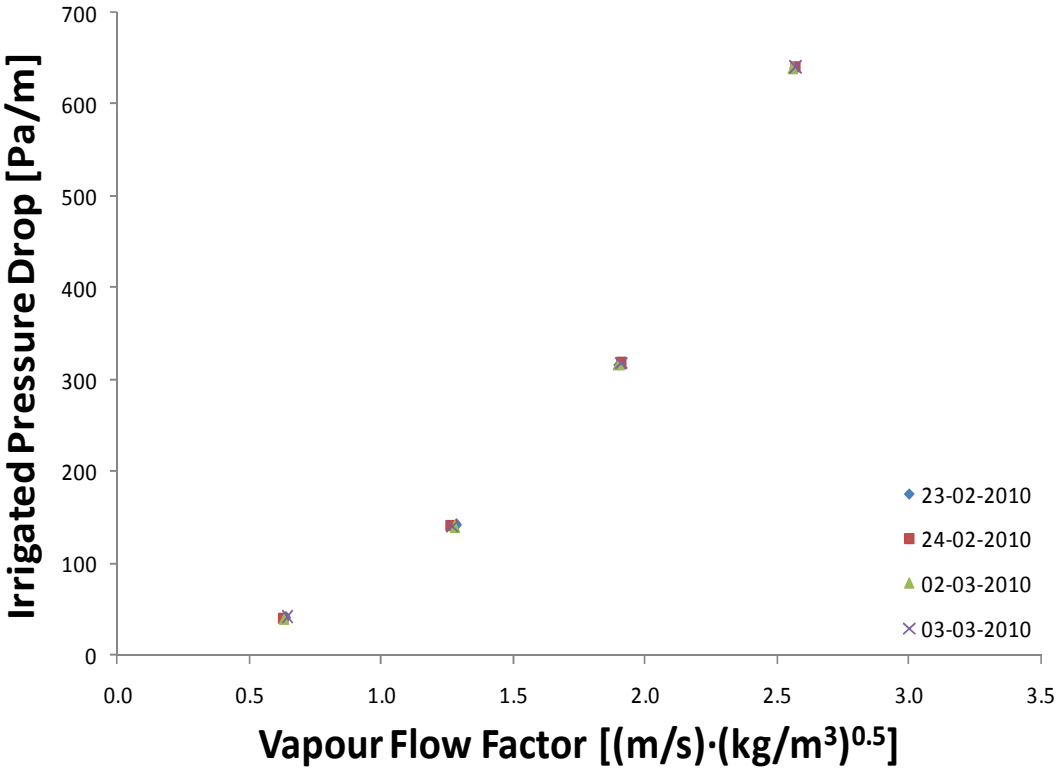

Figure 8.4: System pressure drop repeatability

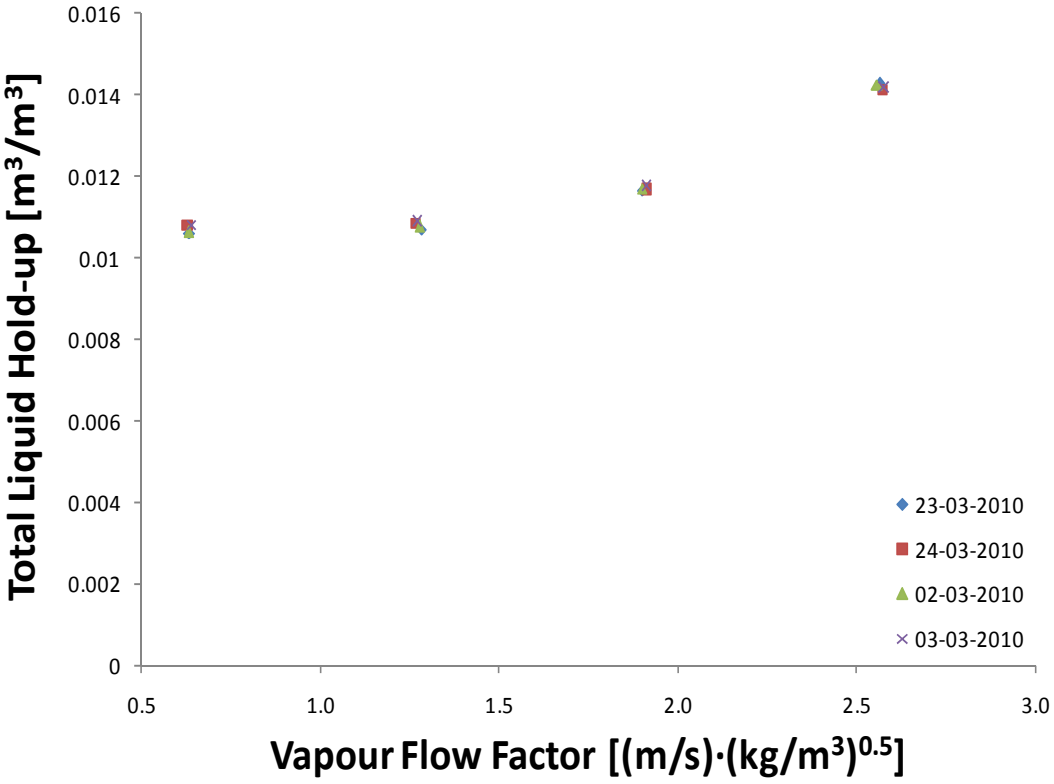

Figure 8.5: System liquid hold-up repeatability

From Figure 8.4 and Figure 8.5 it is evident that the system shows good repeatability with reference to the pressure drop and liquid hold-up measurements. In order to perform a proper statistical analysis, more data points would be required.

Hydrodynamic Equilibrium:

It is of utmost importance to know whether or not the system is at steady state (hydrodynamic equilibrium) when the samples are taken. This equilibrium is reached when the following is true:

- When the liquid rate is constant over time
- When the gas rate is constant over time
- When the pressure drop over the packed bed is constant over time

On the touch screen of the control panel these variables are plotted against time and serve as a reference when to take samples. To verify this, the logged raw data can be analysed by doing simple linear regression on each variable during the sampling period. Theoretically speaking, if a straight line is fitted through the data points the resulting coefficients should have an intercept with a very small gradient (if at all). Pressure drop is the variable of choice as it directly relates to the gas-liquid interaction in the packed bed.

The experimental data set of Intalox® Ultra™ at a liquid rate of 0.73 m^3/h and at a gas mass flow rate of 2401 kg/h will be used as an example. The following ANOVA tables show the variables for the linear model fitted on the data. The reason why a data set is referred to is that the sample time is 120 seconds with a data point logged every 2 seconds. Thus, every data point consists of a set 60 averaged points.

Table 8.27: Gas mass flow rate regression summary

	Coefficients	*Standard Error*	*t Stat*	*P-value*
Intercept	2470.384	1.0221	2416.984	6.4E-105
X Variable 1	-0.225	0.0414	-5.421	3.07E-06

Table 8.28: Liquid flow rate regression summary

	Coefficients	*Standard Error*	*t Stat*	*P-value*
Intercept	0.7399	0.00219	338.313	1.04E-98
X Variable 1	-2.697E-05	6.135E-05	-0.440	0.662

Table 8.29: Pressure drop regression summary

	Coefficients	*Standard Error*	*t Stat*	*P-value*
Intercept	1617.842	1.188	1361.855	2.4E-132

X Variable 1	0.243	0.034	7.165	1.55E-09

In all of the above tables the X Variable 1 (gradient) has a small value. A statistical way of determining how much weight the different parameters have in the model is by looking at the P-value. Normally, at a 95 % confidence level any P-value below 0.05 is significant. However, the smaller the P-value the more significant that parameter is in the model fit. Thus, by evaluating the P-values between the gradient and the intercept (for all three instances), it is evident that the gradient has almost no significance in the regression fit. It can thus be said that the system is at hydrodynamic equilibrium when sampling is done.

8.5 Packing Material Data

This section consists of the packing material physical data such as voidance, density, static hold-up etc. and it also states how these values were obtained. All of the parameters of concern were determined experimentally apart from the packing voidance. The density was calculated as follow:

A representative 1:10 scale section of the test column was constructed. This included a stainless 304 cylindrical section of 400 mm x 300 mm. The bottom of this section was covered with a coarse grid (welded on) to prevent the random packing pieces from falling out. Two handles were attached for easy transport and handling. The method to determine the packing density will be discussed first followed by the static hold-up method.

1.) Determine the dry mass of the 1:10 test section on a previously zeroed electronic balance.
2.) Fill the test section with the packing in question until the top is level with the packing material. Try to fill the section as randomly as possible (or as close to how an industrial column would be packed).
3.) Weigh the test section and determine the total mass of the packing material.
4.) Take 10 elements and weigh them individually on a suitable, pre-zeroed electronic balance.
5.) Count all the packing elements (including the 10 representative elements) in the test section.
6.) Repeat steps 1 - 5 three times until 30 individual elements have been weighed.
7.) Determine the average element weight (from the sample of 30) as well as the total mass of the packing material that was in each batch (there should be 3 batches). Note the number of elements that was in each batch.
8.) Determine the volume of the test section with the following: Volume = $pi*((0.400)^2/4)*0.3$

9.) Calculate the density of each batch by dividing the total packing mass by the section volume.
10.) Calculate the amount of pieces per batch (by dividing the total packing mass by the average element mass) and compare to the number of elements that were counted.

The static hold-up is determined with the following method:

1.) Measure the dry test section on an electronic balance.
2.) Fill a container (that is large enough to completely submerge the test section) with water and submerge the test section until all packing elements are wet.
3.) Place the wetted section on a surface where it can drain freely for 15 minutes (15 minutes was chosen as this is the draining time limit on the experimental hold-up samples).
4.) Carefully measure (do not collide with any obstacles as this would lead to unnecessary liquid draining) the section weight after the elapsed time and determine the amount of liquid on the packing elements.
5.) Clean and dry test section and repeat points 1 - 5 for a total of 3 times.
6.) Calculate the static hold-up per batch by dividing the total water mass by the known volume of the test section.

Table 8.30 summarises all of the necessary packing material data required in the experimental calculations and discussion:

Table 8.30: Packing material data

Packing Material	Particle Diameter [mm]	Void Fraction	Density [kg/m^3]	Static Hold-up [kg/m^3]	Piece Count [Pieces/m^3]
Pall® Rings	38 mm	0.952	181	11.36	12393
IMTP®	40 mm	0.98	106	8.85	49823
Intalox® Ultra™	38 mm	0.98	106	9.91	28184

8.6 Measurement of Entrainment

If the entrainment rate is to be measured (if required), the following steps would be inserted into the experimental procedure (section 3.5.2) between points 9 and 10:

1.) Set the minimum and maximum measuring volumes in the entrainment tank, TK-401 (to account for the dished end dead volume and time delay before the valves are fully closed).

2.) Entrainment can be measured at any time during the operation of the column by pressing the sampling button. PV-404 closes and the entrained liquid fills up TK-401 until the maximum measuring volume is reached from where sampling button is automatically reset. The rate is then calculated as a function of time.

8.7 Experimental Data at Atmospheric Conditions

The processed experimental data is inserted below. The raw data can be found on the CD attached to this thesis.

8.7.1 Pall® Rings Experimental Data

Table 8.31: 1.5" Pall® Ring experimental data at a liquid rate of 0.73 m^3/h

Gas Venturi dP [Pa]	T101 [^oC]	T403 [^oC]	$T_{air, ave}$ [^oC]	System Pressure [kPa]	$\rho_{Air, ave\ T}$ [kg/m^3]	Gas Flow [kg/h]	Area of Column [m^2]	Vapour Flow Factor [$(m/s)\cdot(kg/m^3)^{0.5}$]	Liquid Rate [m^3/h]	Liquid Rate [$m^3/m^2\cdot h$]
-	-	-	-	-	-	-	-	-	-	-
226	21.18	21.35	21.27	100.28	1.187	243	0.1213	0.51	0.74	6
653	21.51	22.59	22.05	100.25	1.183	437	0.1213	0.92	0.74	6
1037	22.05	23.48	22.76	100.22	1.180	548	0.1213	1.16	0.74	6
1439	23.05	25.36	24.20	100.21	1.174	641	0.1213	1.35	0.74	6
2064	24.68	25.39	25.03	100.21	1.171	765	0.1213	1.62	0.74	6
2579	20.00	21.03	20.52	100.05	1.187	867	0.1213	1.82	0.75	6
3454	20.62	22.22	21.42	100.06	1.184	994	0.1213	2.09	0.75	6
4388	21.35	23.21	22.28	100.10	1.181	1106	0.1213	2.33	0.75	6
5379	21.31	22.71	22.01	100.16	1.182	1212	0.1213	2.55	0.75	6
6604	22.53	23.92	23.23	100.20	1.178	1313	0.1213	2.77	0.75	6
8169	23.38	25.20	24.29	100.22	1.174	1421	0.1213	3.00	0.75	6
10040	24.07	26.11	25.09	100.29	1.172	1527	0.1213	3.23	0.75	6
12435	24.43	26.58	25.51	100.41	1.172	1633	0.1213	3.46	0.75	6
14132	17.39	19.51	18.45	106.50	1.273	1767	0.1213	3.59	0.74	6
16166	18.10	20.16	19.13	107.16	1.277	1821	0.1213	3.69	0.74	6

Table 8.31 continued

Liquid Density [kg/m^3]	Liquid Viscosity [mPa·s]	Surface Tension [mN/m]	Liquid Venturi dP [Pa]	K-factor	T401 [^{o}C]	T405 [^{o}C]	T404 [^{o}C]	Column Pressure Drop [Pa/m]	Static Hold-up [m^3/m^3]	Dynamic Hold-up [m^3/m^3]	Total Hold-up [m^3/m^3]
-	-	-	-	-	-	-	-	0	0	0	0
1033	0.811	64.7	-	0.9905	21.33	19.09	21.69	23	0.011	0.00634	0.01733
1033	0.801	64.7	-	0.9905	21.81	19.88	22.72	65	0.011	0.00654	0.01753
1033	0.791	64.7	-	0.9905	22.42	20.61	23.61	104	0.011	0.00628	0.01727
1033	0.770	64.7	-	0.9905	23.58	22.17	25.46	144	0.011	0.00640	0.01739
1033	0.761	64.7	-	0.9905	24.79	23.40	25.68	207	0.011	0.00652	0.01752
1033	0.819	64.7	-	0.9905	20.70	18.35	21.31	258	0.011	0.00730	0.01829
1033	0.808	64.7	-	0.9905	21.15	19.10	22.41	345	0.011	0.00865	0.01964
1033	0.796	64.7	-	0.9905	21.83	19.94	23.37	439	0.011	0.00983	0.02083
1033	0.795	64.7	-	0.9905	22.42	20.30	22.98	538	0.011	0.01089	0.02188
1033	0.782	64.7	-	0.9905	23.09	21.18	24.19	660	0.011	0.01320	0.02419
1033	0.769	64.7	-	0.9905	23.83	22.16	25.46	817	0.011	0.01653	0.02752
1033	0.757	64.7	-	0.9905	24.65	22.97	26.41	1004	0.011	0.02219	0.03318
1033	0.751	64.7	-	0.9905	25.11	23.46	26.91	1243	0.011	0.03047	0.04146
1033	0.849	65.7	-	0.9905	18.03	16.44	19.79	1413	0.011	0.03884	0.04984
1033	0.838	66.7	-	0.9905	18.88	17.21	20.42	1616	0.011	0.04752	0.05852

Table 8.32: 1.5" Pall® Ring experimental data at a liquid rate of 1.46 m^3/h

Gas Venturi dP [Pa]	T101 [^oC]	T403 [^oC]	$T_{air, ave}$ [^oC]	System Pressure [kPa]	$\rho_{Air, ave\ T}$ [kg/m^3]	Gas Flow [kg/h]	Area of Column [m^2]	Vapour Flow Factor [$(m/s)\cdot(kg/m^3)^{0.5}$]	Liquid Rate [m^3/h]	Liquid Rate [$m^3/m^2\cdot h$]
-	-	-	-	-	-	-	-	-	-	-
274	22.90	23.99	23.44	100.33	1.179	260	0.1213	0.55	1.47	12
721	23.31	24.12	23.71	100.49	1.179	445	0.1213	0.94	1.47	12
1633	23.38	24.46	23.92	100.77	1.182	667	0.1213	1.40	1.47	12
2625	23.35	24.18	23.77	101.28	1.189	838	0.1213	1.76	1.48	12
3335	23.38	24.12	23.75	101.64	1.193	951	0.1213	1.99	1.48	12
4309	23.18	23.64	23.41	101.78	1.196	1054	0.1213	2.21	1.48	12
5293	23.26	24.04	23.65	102.13	1.199	1148	0.1213	2.40	1.48	12
6583	21.99	23.86	22.92	103.44	1.217	1255	0.1213	2.61	1.47	12
8361	22.30	23.27	22.78	103.46	1.218	1367	0.1213	2.84	1.47	12
9935	22.38	23.90	23.14	103.97	1.223	1443	0.1213	2.99	1.47	12
12015	22.81	24.70	23.75	104.70	1.229	1525	0.1213	3.15	1.47	12
15710	23.38	25.52	24.45	105.85	1.239	1615	0.1213	3.32	1.48	12

Table 8.32 continued

Liquid Density [kg/m^3]	Liquid Viscosity [mPa·s]	Surface Tension [mN/m]	Liquid Venturi dP [Pa]	K-factor	Venturi Liquid Rate [m^3/h]	T401 [^{o}C]	T405 [^{o}C]	T404 [^{o}C]	Column Pressure Drop [Pa/m]	Static Hold-up [m^3/m^3]	Dynamic Hold-up [m^3/m^3]	Total Hold-up [m^3/m^3]
-	-	-	-	-	-	-	-	-	0	0	0	0
1033	0.776	64.7	459	0.9905	1.49	23.84	22.24	24.28	30	0.0110	0.01882	0.02981
1033	0.775	64.7	444	0.9905	1.55	24.01	22.36	24.38	75	0.0110	0.01893	0.02993
1033	0.773	64.7	400	0.9905	1.53	23.99	22.52	24.65	166	0.0110	0.01957	0.03057
1033	0.773	64.7	472	0.9905	1.57	24.15	22.62	24.50	262	0.0110	0.02036	0.03135
1033	0.775	64.7	474	0.9905	1.54	23.91	22.38	24.36	342	0.0110	0.02099	0.03199
1033	0.779	64.7	472	0.9905	1.56	23.84	22.22	23.95	431	0.0110	0.02296	0.03395
1033	0.778	64.7	400	0.9905	1.53	23.71	22.22	24.21	529	0.0110	0.02468	0.03568
1033	0.782	64.7	453	0.9905	1.45	23.24	21.39	24.11	658	0.0110	0.02835	0.03935
1033	0.786	64.7	454	0.9905	1.49	23.19	21.36	23.50	837	0.0110	0.03338	0.04438
1033	0.781	64.7	495	0.9905	1.51	23.27	21.68	24.11	994	0.0110	0.03886	0.04986
1033	0.772	64.7	482	0.9905	1.56	23.94	22.41	24.90	1202	0.0110	0.04791	0.05890
1033	0.762	64.7	438	0.9905	1.54	24.55	23.11	25.74	1571	0.0110	0.06699	0.07798

Table 8.33: 1.5" Pall® Ring experimental data at a liquid rate of 2.91 m^3/h

Gas Venturi dP [Pa]	T101 [^oC]	T403 [^oC]	$T_{air, ave}$ [^oC]	System Pressure [kPa]	$\rho_{Air, ave\ T}$ [kg/m^3]	Gas Flow [kg/h]	Area of Column [m^2]	Vapour Flow Factor [$(m/s)\cdot(kg/m^3)^{0.5}$]	Liquid Rate [m^3/h]	Liquid Rate [$m^3/m^2\cdot h$]
-	-	-	-	-	-	-	-	-	-	-
304	21.28	22.01	21.64	100.02	1.182	258	0.1213	0.54	2.88	24
851	21.28	21.93	21.61	100.16	1.184	454	0.1213	0.96	2.89	24
1251	21.79	22.44	22.11	100.29	1.183	546	0.1213	1.15	2.88	24
1829	21.87	22.73	22.30	100.44	1.184	654	0.1213	1.38	2.87	24
2338	22.11	22.78	22.44	100.78	1.188	733	0.1213	1.54	2.88	24
3375	22.00	22.57	22.29	101.12	1.193	861	0.1213	1.80	2.86	24
4363	22.13	22.64	22.39	101.50	1.197	958	0.1213	2.01	2.88	24
5831	22.28	22.86	22.57	101.98	1.202	1080	0.1213	2.26	2.91	24
7104	22.48	23.40	22.94	102.43	1.205	1156	0.1213	2.41	2.91	24
9199	22.77	23.59	23.18	103.10	1.212	1247	0.1213	2.59	2.91	24
12337	22.54	23.65	23.10	104.15	1.225	1343	0.1213	2.78	2.93	24
15493	23.32	24.50	23.91	105.14	1.233	1399	0.1213	2.88	2.93	24

Table 8.33 continued

Liquid Density [kg/m^3]	Liquid Viscosity [mPa·s]	Surface Tension [mN/m]	Liquid Venturi dP [Pa]	K-factor	Venturi Liquid Rate [m^3/h]	T401 [^{o}C]	T405 [^{o}C]	T404 [^{o}C]	Column Pressure Drop [Pa/m]	Static Hold-up [m^3/m^3]	Dynamic Hold-up [m^3/m^3]	Total Hold-up [m^3/m^3]
-	-	-	-	-	-	-	-	-	0	0	0	0
1033	0.803	64.7	1687	0.9905	2.93	21.90	20.44	22.37	31	0.0110	0.03315	0.04415
1033	0.804	64.7	1685	0.9905	2.93	21.82	20.35	22.29	85	0.0110	0.03397	0.04497
1033	0.798	64.7	1652	0.9905	2.92	22.15	20.75	22.76	125	0.0110	0.03448	0.04548
1033	0.795	64.7	1664	0.9905	2.94	22.35	20.96	23.02	183	0.0110	0.03540	0.04639
1033	0.793	64.7	1654	0.9905	2.96	22.53	21.20	23.09	234	0.0110	0.03646	0.04746
1033	0.795	64.7	1641	0.9905	2.96	22.46	21.11	22.93	338	0.0110	0.03848	0.04947
1033	0.795	64.7	1736	0.9905	3.00	22.47	21.09	22.98	436	0.0110	0.04052	0.05151
1033	0.792	64.7	1720	0.9905	2.94	22.72	21.30	23.15	583	0.0110	0.04397	0.05496
1033	0.787	64.7	1700	0.9905	2.99	23.00	21.73	23.63	711	0.0110	0.04821	0.05920
1033	0.784	64.7	1761	0.9905	3.01	23.17	21.86	23.88	919	0.0110	0.05634	0.06734
1033	0.784	64.7	1718	0.9905	3.07	23.09	21.84	23.88	1234	0.0110	0.07036	0.08135
1033	0.773	64.7	1750	0.9905	3.03	23.95	22.70	24.75	1551	0.0110	0.08776	0.09875

Table 8.34: 1.5" Pall® Ring experimental data at a liquid rate of 4.49 m^3/h

Gas Venturi dP [Pa]	T101 [^oC]	T403 [^oC]	$T_{air, ave}$ [^oC]	System Pressure [kPa]	$\rho_{Air, ave\ T}$ [kg/m^3]	Gas Flow [kg/h]	Area of Column [m^2]	Vapour Flow Factor [$(m/s)\cdot(kg/m^3)^{0.5}$]	Liquid Rate [m^3/h]	Liquid Rate [$m^3/m^2\cdot h$]
-	-	-	-	-	-	-	-	-	-	-
402	24.37	25.07	24.72	99.79	1.167	263	0.1213	0.56	4.47	37
844	24.32	24.75	24.54	99.94	1.170	396	0.1213	0.84	4.47	37
1327	24.07	24.56	24.31	100.10	1.173	501	0.1213	1.06	4.46	37
1943	23.82	24.41	24.11	100.28	1.175	598	0.1213	1.26	4.48	37
2706	24.26	25.26	24.76	101.27	1.184	696	0.1213	1.46	4.50	37
3244	24.11	24.73	24.42	100.93	1.182	753	0.1213	1.59	4.44	37
4698	23.69	24.09	23.89	101.27	1.188	885	0.1213	1.86	4.49	37
6279	22.86	23.25	23.06	101.85	1.198	989	0.1213	2.07	4.50	37
8005	22.27	22.77	22.52	102.51	1.208	1069	0.1213	2.23	4.51	37
10769	21.86	22.35	22.11	103.38	1.220	1160	0.1213	2.40	4.54	37
13308	21.51	22.34	21.93	104.16	1.230	1215	0.1213	2.51	4.57	38
15484	21.53	22.20	21.86	104.72	1.237	1241	0.1213	2.55	4.59	38

Table 8.34 continued

Liquid Density [kg/m^3]	Liquid Viscosity [mPa·s]	Surface Tension [mN/m]	Liquid Venturi dP [Pa]	K-factor	Venturi Liquid Rate [m^3/h]	T401 [^{o}C]	T405 [^{o}C]	T404 [^{o}C]	Column Pressure Drop [Pa/m]	Static Hold-up [m^3/m^3]	Dynamic Hold-up [m^3/m^3]	Total Hold-up [m^3/m^3]
-	-	-	-	-	-	-	-	-	0	0	0	0
1033	0.761	64.7	4010	0.9905	4.56	25.00	23.82	25.42	40	0.0110	0.04518	0.05617
1033	0.766	64.7	4020	0.9905	4.58	24.66	23.43	25.11	85	0.0110	0.04542	0.05641
1033	0.768	64.7	4042	0.9905	4.55	24.43	23.24	24.90	133	0.0110	0.04593	0.05693
1033	0.771	64.7	4015	0.9905	4.59	24.26	23.03	24.73	194	0.0110	0.04738	0.05837
1033	0.761	64.7	4043	0.9905	4.59	24.91	23.24	25.51	271	0.0110	0.04911	0.06010
1033	0.765	64.7	4054	0.9905	4.59	24.68	23.25	25.11	325	0.0110	0.05044	0.06143
1033	0.773	64.7	4090	0.9905	4.56	24.14	22.67	24.46	470	0.0110	0.05431	0.06531
1033	0.785	64.7	4036	0.9905	4.62	23.23	21.84	23.61	628	0.0110	0.05949	0.07049
1033	0.792	64.7	4066	0.9905	4.61	22.68	21.28	23.11	801	0.0110	0.06648	0.07748
1033	0.798	64.7	4066	0.9905	4.57	22.24	20.77	22.66	1077	0.0110	0.08006	0.09105
1033	0.800	64.7	4116	0.9905	4.64	22.02	20.63	22.60	1331	0.0110	0.09292	0.10392
1033	0.802	64.7	4097	0.9905	4.65	21.90	20.53	22.51	1548	0.0110	0.10489	0.11588

Table 8.35: 1.5" Pall® Ring experimental data at a liquid rate of 5.94 m^3/h

Gas Venturi dP [Pa]	T101 [°C]	T403 [°C]	$T_{air, ave}$ [°C]	System Pressure [kPa]	$\rho_{Air, ave\ T}$ [kg/m^3]	Gas Flow [kg/h]	Area of Column [m^2]	Vapour Flow Factor [$(m/s)\cdot(kg/m^3)^{0.5}$]	Liquid Rate [m^3/h]	Liquid Rate [$m^3/m^2\cdot h$]
-	-	-	-	-	-	-	-	-	-	-
498	25.02	25.45	25.24	99.60	1.163	264	0.1213	0.56	5.92	49
721	24.76	25.37	25.07	99.64	1.164	325	0.1213	0.69	5.97	49
1066	24.94	25.41	25.17	99.74	1.165	399	0.1213	0.85	5.95	49
1460	24.46	24.96	24.71	99.97	1.169	472	0.1213	1.00	5.95	49
2044	24.26	24.78	24.52	100.28	1.174	552	0.1213	1.17	5.96	49
2885	24.37	24.88	24.62	100.65	1.178	648	0.1213	1.37	5.93	49
3593	24.65	25.26	24.95	100.90	1.179	713	0.1213	1.50	5.92	49
4835	24.93	25.41	25.17	101.10	1.181	805	0.1213	1.70	5.91	49
5866	24.80	25.40	25.10	101.51	1.186	872	0.1213	1.83	5.91	49
7794	24.92	25.41	25.16	102.07	1.192	958	0.1213	2.01	5.95	49
10543	24.87	25.52	25.19	102.95	1.202	1040	0.1213	2.17	5.98	49
13742	24.93	25.60	25.27	103.93	1.213	1099	0.1213	2.28	6.05	50
15345	25.02	25.77	25.40	105.43	1.230	1124	0.1213	2.32	5.94	49

Table 8.35 continued

Liquid Density [kg/m^3]	Liquid Viscosity [mPa·s]	Surface Tension [mN/m]	Liquid Venturi dP [Pa]	K-factor	Liquid Rate [m^3/h]	T401 [^{o}C]	T405 [^{o}C]	T404 [^{o}C]	Column Pressure Drop [Pa/m]	Static Hold-up [m^3/m^3]	Dynamic Hold-up [m^3/m^3]	Total Hold-up [m^3/m^3]
-	-	-	-	-	-	-	-	-	0	0	0	0
1033	0.757	64.7	7057	0.9905	6.04	25.30	24.28	25.80	50	0.0110	0.05431	0.06530
1033	0.758	64.7	7025	0.9905	6.08	25.22	24.14	25.72	72	0.0110	0.05493	0.06592
1033	0.758	64.7	6988	0.9905	6.03	25.23	24.14	25.73	107	0.0110	0.05496	0.06596
1033	0.763	64.7	7028	0.9905	6.09	24.83	23.65	25.30	146	0.0110	0.05572	0.06672
1033	0.766	64.7	7028	0.9905	6.06	24.57	23.48	25.10	204	0.0110	0.05727	0.06826
1033	0.765	64.7	6989	0.9905	6.04	24.66	23.56	25.19	288	0.0110	0.05905	0.07004
1033	0.761	64.7	7018	0.9905	6.03	24.94	23.87	25.58	359	0.0110	0.06146	0.07246
1033	0.758	64.7	7018	0.9905	6.05	25.23	24.07	25.73	483	0.0110	0.06478	0.07577
1033	0.759	64.7	7077	0.9905	6.05	25.15	24.02	25.71	587	0.0110	0.06904	0.08003
1033	0.758	64.7	7053	0.9905	6.09	25.16	24.05	25.74	780	0.0110	0.07611	0.08711
1033	0.757	64.7	7149	0.9905	6.08	25.26	24.12	25.82	1054	0.0110	0.08775	0.09875
1033	0.758	64.7	7272	0.9905	6.13	25.01	24.35	25.87	1375	0.0110	0.10655	0.11755
1033	0.757	65.7	-	0.9905	6.09	25.22	24.49	25.91	1634	0.0110	0.12306	0.13406

Table 8.36: 1.5" Pall® Ring experimental data at a liquid rate of 8.86 m^3/h

Gas Venturi dP [Pa]	T101 [^oC]	T403 [^oC]	$T_{air, ave}$ [^oC]	System Pressure [kPa]	$\rho_{Air, ave\ T}$ [kg/m^3]	Gas Flow [kg/h]	Area of Column [m^2]	Vapour Flow Factor [$(m/s)\cdot(kg/m^3)^{0.5}$]	Liquid Rate [m^3/h]	Liquid Rate [$m^3/m^2\cdot h$]
-	-	-	-	-	-	-	-	-	-	-
687	24.97	25.53	25.25	99.62	1.163	253	0.1213	0.54	8.80	73
921	24.98	25.58	25.28	99.79	1.165	300	0.1213	0.64	8.84	73
1312	24.95	25.58	25.26	99.97	1.167	361	0.1213	0.76	8.78	72
1960	24.96	25.45	25.20	100.18	1.170	439	0.1213	0.93	8.81	73
2727	25.03	25.61	25.32	100.44	1.173	514	0.1213	1.09	8.81	73
3854	25.07	25.55	25.31	100.82	1.177	604	0.1213	1.27	8.82	73
4908	25.09	25.45	25.27	101.11	1.181	669	0.1213	1.41	8.78	72
6790	25.02	25.49	25.25	101.69	1.187	759	0.1213	1.60	8.86	73
8196	25.00	25.52	25.26	102.06	1.192	808	0.1213	1.69	8.87	73
10062	25.08	25.54	25.31	102.65	1.198	858	0.1213	1.80	8.87	73
13059	25.12	25.61	25.36	103.46	1.208	908	0.1213	1.89	8.84	73
16552	25.14	25.66	25.40	104.50	1.220	934	0.1213	1.94	8.84	73

Table 8.36 continued

Liquid Density [kg/m^3]	Liquid Viscosity [mPa·s]	Surface Tension [mN/m]	Liquid Venturi dP [Pa]	K-factor	Venturi Liquid Rate [m^3/h]	T401 [°C]	T405 [°C]	T404 [°C]	Column Pressure Drop [Pa/m]	Static Hold-up [m^3/m^3]	Dynamic Hold-up [m^3/m^3]	Total Hold-up [m^3/m^3]
-	-	-	-	-	-	-	-	-	0	0	0	0
1033	0.756	64.7	15197	0.9905	8.85	25.37	24.16	25.87	69	0.0110	0.07424	0.08524
1033	0.755	64.7	15266	0.9905	8.91	25.42	24.26	25.93	92	0.0110	0.07466	0.08565
1033	0.756	64.7	15315	0.9905	8.93	25.43	24.19	25.87	131	0.0110	0.07421	0.08521
1033	0.757	64.7	15357	0.9905	8.90	25.32	24.12	25.75	196	0.0110	0.07681	0.08780
1033	0.756	64.7	15379	0.9905	8.93	25.38	24.31	25.92	273	0.0110	0.07885	0.08984
1033	0.756	64.7	15411	0.9905	8.92	25.41	24.28	25.86	385	0.0110	0.08218	0.09317
1033	0.757	64.7	15333	0.9905	8.94	25.33	24.21	25.79	491	0.0110	0.08707	0.09806
1033	0.757	64.7	15390	0.9905	8.96	25.33	24.20	25.82	679	0.0110	0.09434	0.10534
1033	0.757	64.7	15511	0.9905	8.96	25.30	24.23	25.82	820	0.0110	0.10163	0.11262
1033	0.757	64.7	15457	0.9905	8.96	25.25	24.31	25.87	1007	0.0110	0.11104	0.12203
1033	0.756	64.7	15651	0.9905	9.04	25.30	24.34	25.91	1306	0.0110	0.13037	0.14137
1033	0.756	64.7	15561	0.9905	8.97	25.27	24.36	25.93	1656	0.0110	0.14889	0.15989

Table 8.37: 1.5" Pall® Ring experimental data at a liquid rate of 11.89 m^3/h

Gas Venturi dP [Pa]	T101 [°C]	T403 [°C]	$T_{air, ave}$ [°C]	System Pressure [kPa]	$\rho_{Air, ave\ T}$ [kg/m^3]	Gas Flow [kg/h]	Area of Column [m^2]	Vapour Flow Factor [$(m/s)\cdot(kg/m^3)^{0.5}$]	Liquid Rate [m^3/h]	Liquid Rate [$m^3/m^2\cdot h$]
-	-	-	-	-	-	-	-	-	-	-
953	25.17	25.51	25.34	100.04	1.168	254	0.1213	0.54	11.95	99
1429	25.25	25.48	25.36	100.20	1.170	313	0.1213	0.66	11.89	98
1859	25.29	25.50	25.40	100.39	1.172	357	0.1213	0.76	11.88	98
2632	25.17	25.57	25.37	100.71	1.176	420	0.1213	0.89	11.91	98
3538	25.03	25.58	25.31	101.04	1.180	483	0.1213	1.02	11.88	98
4624	25.10	25.53	25.32	101.37	1.183	545	0.1213	1.15	11.93	98
6396	25.08	25.55	25.31	101.96	1.190	625	0.1213	1.31	11.97	99
7886	25.16	25.59	25.38	102.43	1.196	672	0.1213	1.41	11.92	98
9964	24.82	25.40	25.11	103.12	1.205	725	0.1213	1.51	11.91	98
12122	24.84	25.40	25.12	103.76	1.212	762	0.1213	1.59	11.95	98
15825	24.85	25.52	25.18	104.89	1.225	795	0.1213	1.65	12.01	99

Table 8.37 continued

Liquid Density [kg/m^3]	Liquid Viscosity [mPa·s]	Surface Tension [mN/m]	Liquid Venturi dP [Pa]	K-factor	Venturi Liquid Rate [m^3/h]	T401 [^{o}C]	T405 [^{o}C]	T404 [^{o}C]	Column Pressure Drop [Pa/m]	Static Hold-up [m^3/m^3]	Dynamic Hold-up [m^3/m^3]	Total Hold-up [m^3/m^3]
-	-	-	-	-	-	-	-	-	0	0	0	0
1033	0.756	64.7	27518	0.9905	11.99	25.34	24.33	25.83	95	0.0110	0.09143	0.10242
1033	0.756	64.7	27411	0.9905	11.92	25.34	24.34	25.83	143	0.0110	0.09139	0.10239
1033	0.757	64.7	27325	0.9905	11.93	25.25	24.38	25.81	186	0.0110	0.09198	0.10298
1033	0.756	64.7	27477	0.9905	11.91	25.35	24.30	25.88	263	0.0110	0.09244	0.10343
1033	0.756	64.7	27470	0.9905	11.94	25.37	24.30	25.91	354	0.0110	0.09578	0.10677
1033	0.756	64.7	27500	0.9905	11.94	25.39	24.28	25.90	463	0.0110	0.10193	0.11292
1033	0.756	64.7	27589	0.9905	12.00	25.41	24.28	25.90	640	0.0110	0.11005	0.12105
1033	0.755	64.7	27544	0.9905	11.95	25.47	24.28	25.93	789	0.0110	0.11558	0.12658
1033	0.757	64.7	27593	0.9905	11.98	25.30	24.03	25.72	997	0.0110	0.12542	0.13641
1033	0.757	64.7	27703	0.9905	12.03	25.25	24.05	25.77	1212	0.0110	0.14001	0.15100
1033	0.757	64.7	27970	0.9905	12.03	25.34	24.08	25.81	1582	0.0110	0.17007	0.18107

Table 8.38: 1.5" Pall® Ring experimental data at a liquid rate of 14.80 m^3/h

Gas Venturi dP [Pa]	T101 [^oC]	T403 [^oC]	$T_{air, ave}$ [^oC]	System Pressure [kPa]	$\rho_{Air, ave\ T}$ [kg/m^3]	Gas Flow [kg/h]	Area of Column [m^2]	Vapour Flow Factor [$(m/s)\cdot(kg/m^3)^{0.5}$]	Liquid Rate [m^3/h]	Liquid Rate [$m^3/m^2\cdot h$]
-	-	-	-	-	-	-	-	-	-	-
1446	24.23	25.48	24.85	100.16	1.171	247	0.1213	0.52	14.91	123
2417	24.84	25.69	25.26	100.46	1.173	324	0.1213	0.69	14.85	122
3038	24.94	25.66	25.30	100.66	1.175	365	0.1213	0.77	14.82	122
3777	24.95	25.66	25.31	100.88	1.178	410	0.1213	0.86	14.84	122
4641	25.08	25.71	25.40	101.15	1.180	457	0.1213	0.96	14.82	122
5655	25.07	25.64	25.35	101.44	1.184	502	0.1213	1.06	14.82	122
7049	25.09	25.67	25.38	101.88	1.189	548	0.1213	1.15	14.85	122
8882	25.12	25.64	25.38	102.40	1.195	602	0.1213	1.26	14.83	122
11483	25.23	25.67	25.45	103.17	1.204	646	0.1213	1.35	14.82	122
14488	25.22	25.72	25.47	104.04	1.214	669	0.1213	1.39	14.81	122
15811	25.19	25.68	25.43	104.40	1.218	677	0.1213	1.40	14.83	122

Table 8.38 continued

Liquid Density [kg/m^3]	Liquid Viscosity [mPa·s]	Surface Tension [mN/m]	Liquid Venturi dP [Pa]	K-factor	Venturi Liquid Rate [m^3/h]	T401 [^{o}C]	T405 [^{o}C]	T404 [^{o}C]	Column Pressure Drop [Pa/m]	Static Hold-up [m^3/m^3]	Dynamic Hold-up [m^3/m^3]	Total Hold-up [m^3/m^3]
-	-	-	-	-	-	-	-	-	0	0	0	0
1033	0.756	64.7	22498	0.9905	14.95	25.42	23.83	25.81	137	0.0110	0.11120	0.12219
1033	0.754	64.7	23093	0.9905	14.80	25.55	24.19	26.01	234	0.0110	0.11124	0.12223
1033	0.754	64.7	23077	0.9905	14.83	25.53	24.24	26.00	296	0.0110	0.11128	0.12228
1033	0.754	64.7	23016	0.9905	14.86	25.51	24.33	26.00	373	0.0110	0.11383	0.12482
1033	0.754	64.7	23174	0.9905	14.90	25.53	24.36	26.03	460	0.0110	0.11943	0.13042
1033	0.755	64.7	23375	0.9905	14.88	25.44	24.36	25.97	566	0.0110	0.12723	0.13823
1033	0.755	64.7	22982	0.9905	14.90	25.47	24.37	26.01	705	0.0110	0.13639	0.14739
1033	0.755	64.7	22992	0.9905	14.88	25.41	24.35	25.96	888	0.0110	0.14928	0.16028
1033	0.755	64.7	23116	0.9905	14.90	25.42	24.36	25.96	1147	0.0110	0.16294	0.17394
1033	0.755	64.7	22885	0.9905	14.93	25.36	24.42	26.00	1448	0.0110	0.17356	0.18456
1033	0.756	64.7	23011	0.9905	14.87	25.30	24.40	25.96	1581	0.0110	0.18330	0.19430

The numbers in red indicates a limiting value on the data-logger that has been exceeded, and thus a negative value is shown. The conversion from pressure drop to liquid flow rate is still correct and was verified with the spot checks.

8.7.2 IMTP® Experimental Data

Table 8.39: 1.5" IMTP® experimental data at a liquid rate of 0.73 m^3/h

Gas Venturi dP [Pa]	T101 [^oC]	T403 [^oC]	$T_{air, ave}$ [^oC]	System Pressure [kPa]	$\rho_{Air, ave\ T}$ [kg/m^3]	Gas Flow [kg/h]	Area of Column [m^2]	Vapour Flow Factor [$(m/s)\cdot(kg/m^3)^{0.5}$]	Liquid Rate [m^3/h]	Liquid Rate [$m^3/m^2\cdot h$]
-	-	-	-	-	-	-	-	-	-	-
315	24.23	24.65	24.44	99.83	1.169	283	0.1213	0.60	0.731	6
803	24.28	25.19	24.74	100.03	1.170	498	0.1213	1.05	0.733	6
1821	24.80	25.25	25.02	100.36	1.173	756	0.1213	1.60	0.734	6
3225	25.04	25.91	25.48	100.90	1.177	1004	0.1213	2.12	0.734	6
4459	24.51	25.56	25.04	101.35	1.184	1170	0.1213	2.46	0.736	6
5220	24.63	25.85	25.24	101.66	1.187	1253	0.1213	2.63	0.736	6
6189	24.25	25.64	24.95	102.01	1.192	1350	0.1213	2.83	0.737	6
7216	24.69	25.91	25.30	102.42	1.196	1435	0.1213	3.01	0.737	6
8675	24.37	26.00	25.19	102.99	1.203	1546	0.1213	3.23	0.740	6
10151	24.20	26.05	25.13	103.54	1.209	1639	0.1213	3.41	0.742	6
11928	24.72	26.79	25.76	104.19	1.214	1732	0.1213	3.60	0.745	6
14243	24.58	27.01	25.79	104.99	1.224	1817	0.1213	3.76	0.747	6
15955	24.64	27.24	25.94	105.60	1.230	1863	0.1213	3.85	0.748	6

Table 8.39 continued

Liquid Density [kg/m^3]	Liquid Viscosity [mPa·s]	Surface Tension [mN/m]	Liquid Venturi dP [Pa]	K-factor	Venturi Liquid Rate [m^3/h]	T401 [^{o}C]	T405 [^{o}C]	T404 [^{o}C]	Column Pressure Drop [Pa/m]	Static Hold-up [m^3/m^3]	Dynamic Hold-up [m^3/m^3]	Total Hold-up [m^3/m^3]
-	-	-	-	-	-	-	-	-	0	0	0	0
1032	0.766	64.2	135	0.9905	0.73	24.79	23.01	24.97	28	0.0086	0.0122	0.0208
1032	0.763	64.2	133	0.9905	0.73	24.79	23.18	25.36	80	0.0086	0.0121	0.0207
1032	0.760	64.2	133	0.9905	0.74	25.15	23.57	25.55	180	0.0086	0.0125	0.0211
1032	0.755	64.2	144	0.9905	0.74	25.29	24.15	26.17	322	0.0086	0.0130	0.0215
1032	0.764	64.2	179	0.9905	0.75	24.19	24.16	25.81	446	0.0086	0.0138	0.0224
1032	0.760	64.2	140	0.9905	0.72	24.50	24.22	26.11	522	0.0086	0.0146	0.0231
1032	0.764	64.2	120	0.9905	0.73	24.15	24.28	25.90	618	0.0086	0.0156	0.0242
1032	0.759	64.2	119	0.9905	0.74	24.65	24.33	26.21	721	0.0086	0.0168	0.0254
1032	0.761	64.2	190	0.9905	0.74	24.12	24.43	26.32	867	0.0086	0.0189	0.0275
1032	0.762	64.2	148	0.9905	0.75	23.94	24.41	26.35	1016	0.0086	0.0216	0.0302
1032	0.755	64.2	151	0.9905	0.74	24.28	24.80	27.16	1192	0.0086	0.0255	0.0341
1032	0.758	64.2	173	0.9905	0.73	23.50	25.15	27.42	1423	0.0086	0.0325	0.0410
1032	0.754	64.2	158	0.9905	0.74	23.88	25.36	27.68	1596	0.0086	0.0409	0.0495

Table 8.40: 1.5" IMTP® experimental data at a liquid rate of 1.46 m^3/h

Gas Venturi dP [Pa]	T101 [^oC]	T403 [^oC]	$T_{air, ave}$ [^oC]	System Pressure [kPa]	$\rho_{Air, ave\ T}$ [kg/m^3]	Gas Flow [kg/h]	Area of Column [m^2]	Vapour Flow Factor [$(m/s)\cdot(kg/m^3)^{0.5}$]	Liquid Rate [m^3/h]	Liquid Rate [$m^3/m^2\cdot h$]
-	-	-	-	-	-	-	-	-	-	-
296	23.54	24.11	23.83	99.69	1.170	279	0.1213	0.59	1.447	12
779	23.58	24.34	23.96	99.93	1.172	472	0.1213	1.00	1.453	12
1844	24.08	24.82	24.45	100.33	1.175	737	0.1213	1.56	1.450	12
3150	24.44	25.45	24.95	100.83	1.179	959	0.1213	2.02	1.456	12
4074	25.02	26.06	25.54	101.19	1.180	1086	0.1213	2.29	1.446	12
5099	24.65	26.21	25.43	101.56	1.185	1200	0.1213	2.52	1.461	12
6242	24.52	26.20	25.36	102.00	1.191	1303	0.1213	2.73	1.450	12
7443	24.70	26.39	25.54	102.43	1.195	1404	0.1213	2.94	1.441	12
8685	24.66	26.57	25.62	102.95	1.201	1492	0.1213	3.12	1.443	12
10389	24.48	26.63	25.56	103.51	1.207	1586	0.1213	3.30	1.444	12
12625	26.28	28.08	27.18	104.27	1.210	1686	0.1213	3.51	1.441	12
14412	27.80	29.67	28.73	104.84	1.210	1744	0.1213	3.63	1.429	12
16227	28.25	30.36	29.31	105.42	1.214	1794	0.1213	3.73	1.431	12

Table 8.40 continued

Liquid Density [kg/m^3]	Liquid Viscosity [mPa·s]	Surface Tension [mN/m]	Liquid Venturi dP [Pa]	K-factor	Venturi Liquid Rate [m^3/h]	T401 [°C]	T405 [°C]	T404 [°C]	Column Pressure Drop [Pa/m]	Static Hold-up [m^3/m^3]	Dynamic Hold-up [m^3/m^3]	Total Hold-up [m^3/m^3]
-	-	-	-	-	-	-	-	-	0	0	0	0
1032	0.774	64.2	436	0.9905	1.44	24.22	22.40	24.34	30	0.0086	0.0181	0.0267
1032	0.772	64.2	482	0.9905	1.44	24.17	22.52	24.64	78	0.0086	0.0180	0.0266
1032	0.765	64.2	443	0.9905	1.44	24.69	23.04	25.14	184	0.0086	0.0183	0.0269
1032	0.759	64.2	433	0.9905	1.46	25.07	23.47	25.73	315	0.0086	0.0191	0.0277
1032	0.752	64.2	452	0.9905	1.45	25.56	24.15	26.32	408	0.0086	0.0200	0.0285
1032	0.756	64.2	451	0.9905	1.46	24.77	24.60	26.42	510	0.0086	0.0213	0.0298
1032	0.756	64.2	400	0.9905	1.45	24.80	24.62	26.42	619	0.0086	0.0231	0.0317
1032	0.754	64.2	400	0.9905	1.45	24.91	24.81	26.62	741	0.0086	0.0258	0.0344
1032	0.753	64.2	451	0.9905	1.44	24.85	24.97	26.80	869	0.0086	0.0295	0.0381
1032	0.755	64.2	455	0.9905	1.45	24.54	25.12	26.91	1039	0.0086	0.0353	0.0439
1032	0.729	64.2	467	0.9905	1.44	27.18	26.00	28.34	1264	0.0086	0.0440	0.0526
1032	0.710	64.2	466	0.9905	1.45	28.77	27.60	29.93	1442	0.0086	0.0528	0.0614
1032	0.719	64.2	437	0.9905	1.45	26.52	28.40	30.65	1623	0.0086	0.0624	0.0710

Table 8.41: 1.5" IMTP® experimental data at a liquid rate of 2.91 m^3/h

Gas Venturi dP [Pa]	T101 [^oC]	T403 [^oC]	$T_{air, ave}$ [^oC]	System Pressure [kPa]	$\rho_{Air, ave\ T}$ [kg/m^3]	Gas Flow [kg/h]	Area of Column [m^2]	Vapour Flow Factor [$(m/s)\cdot(kg/m^3)^{0.5}$]	Liquid Density [kg/m^3]	Liquid Viscosity [mPa·s]	Surface Tension [mN/m]
-	-	-	-	-	-	-	-	-	-	-	-
331	24.73	25.18	24.95	100.27	1.172	281	0.1213	0.59	1035	0.759	64.4
789	24.59	25.14	24.86	100.28	1.172	454	0.1213	0.96	1035	0.761	64.4
1252	24.79	25.76	25.27	100.42	1.172	577	0.1213	1.22	1035	0.756	64.4
1940	24.90	25.56	25.23	100.74	1.176	727	0.1213	1.54	1035	0.757	64.4
2522	25.09	25.65	25.37	100.88	1.177	827	0.1213	1.75	1035	0.754	64.4
3433	24.92	25.47	25.20	101.07	1.180	967	0.1213	2.04	1035	0.757	64.4
4630	25.41	25.62	25.51	101.40	1.183	1104	0.1213	2.32	1035	0.756	64.4
6132	25.10	25.82	25.46	101.85	1.188	1240	0.1213	2.61	1035	0.754	64.4
7673	24.87	25.87	25.37	102.20	1.193	1345	0.1213	2.82	1035	0.757	64.4
9484	24.85	26.12	25.49	102.71	1.198	1446	0.1213	3.02	1035	0.756	64.4
10941	24.60	26.05	25.33	103.06	1.203	1504	0.1213	3.14	1035	0.758	64.4
14355	24.27	26.09	25.18	103.90	1.213	1605	0.1213	3.34	1035	0.757	64.4
15505	24.41	26.33	25.37	104.24	1.217	1627	0.1213	3.38	1035	0.758	64.4

Table 8.41 continued

Liquid Venturi dP [Pa]	K-factor	Venturi Liquid Rate [m^3/h]	Liquid Rate [$m^3/m^2 \cdot h$]	T401 [^oC]	T405 [^oC]	T404 [^oC]	Column Pressure Drop [Pa/m]	Static Hold-up [m^3/m^3]	Dynamic Hold-up [m^3/m^3]	Total Hold-up [m^3/m^3]
-	-	-	-	-	-	-	0	0	0	0
1589	0.9905	2.88	24	25.19	23.95	25.57	33	0.0086	0.0375	0.0461
1677	0.9905	2.99	25	24.92	23.74	25.48	78	0.0086	0.0376	0.0461
1664	0.9905	2.96	24	25.30	24.20	26.01	125	0.0086	0.0377	0.0463
1454	0.9905	2.74	23	25.20	24.35	25.85	194	0.0086	0.0375	0.0460
1559	0.9905	2.85	24	25.54	24.23	25.96	255	0.0086	0.0376	0.0461
1669	0.9905	2.99	25	25.36	24.08	25.78	351	0.0086	0.0383	0.0468
1426	0.9905	2.76	23	25.41	24.10	25.85	463	0.0086	0.0401	0.0487
1502	0.9905	2.79	23	25.46	24.31	26.03	614	0.0086	0.0439	0.0525
1621	0.9905	2.86	24	25.05	24.38	26.03	767	0.0086	0.0480	0.0565
1466	0.9905	2.85	23	25.09	24.45	26.16	948	0.0086	0.0537	0.0622
1595	0.9905	2.82	23	24.79	24.47	26.09	1094	0.0086	0.0590	0.0676
1566	0.9905	2.93	24	24.86	24.63	26.17	1435	0.0086	0.0754	0.0840
1489	0.9905	2.75	23	24.58	24.70	26.40	1550	0.0086	0.0807	0.0892

Table 8.42: 1.5" IMTP® experimental data at a liquid rate of 4.49 m^3/h

Gas Venturi dP [Pa]	T101 [^oC]	T403 [^oC]	$T_{air, ave}$ [^oC]	System Pressure [kPa]	$\rho_{Air, ave\ T}$ [kg/m^3]	Gas Flow [kg/h]	Area of Column [m^2]	Vapour Flow Factor [$(m/s)\cdot(kg/m^3)^{0.5}$]	Liquid Density [kg/m^3]	Liquid Viscosity [mPa·s]	Surface Tension [mN/m]
-	-	-	-	-	-	-	-	-	-	-	-
333	22.64	23.45	23.05	100.36	1.181	269	0.1213	0.57	1035	0.783	64.4
842	22.81	23.52	23.17	100.54	1.182	453	0.1213	0.95	1035	0.782	64.4
1158	23.07	23.68	23.38	100.66	1.183	534	0.1213	1.12	1035	0.780	64.4
1715	23.42	24.03	23.72	100.94	1.185	655	0.1213	1.38	1035	0.776	64.4
2320	23.83	24.45	24.14	101.05	1.184	757	0.1213	1.59	1035	0.770	64.4
2912	24.54	25.43	24.98	101.27	1.184	841	0.1213	1.77	1035	0.762	64.4
3730	24.78	25.34	25.06	101.55	1.187	938	0.1213	1.97	1035	0.759	64.4
4628	24.96	25.57	25.26	101.85	1.189	1026	0.1213	2.15	1035	0.756	64.4
5785	25.08	25.69	25.39	102.24	1.193	1123	0.1213	2.35	1035	0.755	64.4
7063	25.07	25.81	25.44	102.67	1.198	1203	0.1213	2.52	1035	0.755	64.4
8744	24.94	25.77	25.36	103.22	1.205	1287	0.1213	2.69	1035	0.758	64.4
11633	24.83	25.99	25.41	104.13	1.215	1379	0.1213	2.86	1035	0.756	64.4
16727	24.63	26.02	25.32	105.69	1.234	1422	0.1213	2.93	1035	0.758	64.4

Table 8.42 continued

Liquid Venturi dP [Pa]	K-factor	Venturi Liquid Rate [m^3/h]	Liquid Rate [$m^3/m^2 \cdot h$]	T401 [^oC]	T405 [^oC]	T404 [^oC]	Column Pressure Drop [Pa/m]	Static Hold-up [m^3/m^3]	Dynamic Hold-up [m^3/m^3]	Total Hold-up [m^3/m^3]
-	-	-	-	-	-	-	0	0	0	0
3910	0.9905	4.50	37	23.43	21.88	23.78	33	0.0086	0.04890	0.05746
3908	0.9905	4.52	37	23.41	21.96	23.88	84	0.0086	0.04904	0.05759
3980	0.9905	4.50	37	23.54	22.13	24.02	116	0.0086	0.04903	0.05758
3898	0.9905	4.52	37	23.90	22.51	24.32	171	0.0086	0.04914	0.05769
3892	0.9905	4.52	37	24.30	22.92	24.78	232	0.0086	0.05008	0.05864
3943	0.9905	4.48	37	24.95	23.60	25.43	292	0.0086	0.05175	0.06030
3977	0.9905	4.52	37	25.15	23.86	25.64	373	0.0086	0.05349	0.06205
3902	0.9905	4.50	37	25.40	24.07	25.85	463	0.0086	0.05593	0.06448
3884	0.9905	4.54	37	25.49	24.20	25.98	578	0.0086	0.05820	0.06676
3916	0.9905	4.55	37	25.46	24.28	26.02	706	0.0086	0.06177	0.07032
3966	0.9905	4.57	38	25.03	24.35	25.90	875	0.0086	0.06917	0.07773
3907	0.9905	4.53	37	25.22	24.31	26.00	1163	0.0086	0.08363	0.09218
3913	0.9905	4.58	38	24.97	24.27	25.93	1673	0.0086	0.10604	0.11459

Table 8.43: 1.5" IMTP® experimental data at a liquid rate of 5.94 m^3/h

Gas Venturi dP [Pa]	T101 [^oC]	T403 [^oC]	$T_{air, ave}$ [^oC]	System Pressure [kPa]	$\rho_{Air, ave\ T}$ [kg/m^3]	Gas Flow [kg/h]	Area of Column [m^2]	Vapour Flow Factor [$(m/s)\cdot(kg/m^3)^{0.5}$]	Liquid Density [kg/m^3]	Liquid Viscosity [mPa·s]	Surface Tension [mN/m]
-	-	-	-	-	-	-	-	-	-	-	-
387	22.40	23.49	22.94	99.92	1.176	275	0.1213	0.58	1035	0.782	64.4
652	22.71	23.54	23.12	100.00	1.176	374	0.1213	0.79	1035	0.782	64.4
949	23.14	24.02	23.58	100.11	1.176	461	0.1213	0.97	1035	0.776	64.4
1311	23.70	24.52	24.11	100.23	1.175	546	0.1213	1.15	1035	0.769	64.4
1812	24.07	24.74	24.40	100.39	1.176	638	0.1213	1.35	1035	0.766	64.4
2389	24.39	25.10	24.75	100.58	1.176	727	0.1213	1.53	1035	0.762	64.4
3109	24.93	25.64	25.29	100.81	1.177	816	0.1213	1.72	1035	0.755	64.4
4138	25.12	25.68	25.40	101.14	1.180	923	0.1213	1.94	1035	0.755	64.4
5232	25.06	25.69	25.37	101.49	1.185	1008	0.1213	2.12	1035	0.755	64.4
6428	25.07	25.67	25.37	101.88	1.189	1086	0.1213	2.28	1035	0.756	64.4
8159	24.97	25.74	25.35	102.43	1.196	1169	0.1213	2.45	1035	0.757	64.4
11757	24.93	25.82	25.38	103.56	1.209	1264	0.1213	2.63	1035	0.755	64.4
15164	24.99	25.84	25.42	104.59	1.221	1294	0.1213	2.68	1035	0.755	64.4

Table 8.43 continued

Liquid Venturi dP [Pa]	K-factor	Venturi Liquid Rate [m^3/h]	Liquid Rate [$m^3/m^2 \cdot h$]	T401 [^oC]	T405 [^oC]	T404 [^oC]	Column Pressure Drop [Pa/m]	Static Hold-up [m^3/m^3]	Dynamic Hold-up [m^3/m^3]	Total Hold-up [m^3/m^3]
-	-	-	-	-	-	-	0	0	0	0
6718	0.9905	5.94	49	23.41	21.82	23.83	38	0.0086	0.06085	0.06940
6795	0.9905	5.96	49	23.43	21.92	23.88	65	0.0086	0.06061	0.06917
6784	0.9905	5.96	49	23.86	22.45	24.32	95	0.0086	0.06092	0.06947
6798	0.9905	5.96	49	24.39	23.02	24.84	131	0.0086	0.06091	0.06946
6846	0.9905	5.94	49	24.66	23.30	25.11	181	0.0086	0.06154	0.07009
6764	0.9905	5.95	49	24.97	23.62	25.42	236	0.0086	0.06238	0.07093
6779	0.9905	5.89	49	25.48	24.20	25.96	307	0.0086	0.06523	0.07378
6815	0.9905	5.97	49	25.44	24.28	25.99	414	0.0086	0.06919	0.07775
6798	0.9905	5.97	49	25.48	24.28	25.95	523	0.0086	0.07307	0.08162
6798	0.9905	5.97	49	25.32	24.29	25.94	643	0.0086	0.07720	0.08575
6810	0.9905	5.94	49	25.16	24.28	25.92	816	0.0086	0.08326	0.09181
6843	0.9905	5.94	49	25.45	24.30	26.03	1176	0.0086	0.09969	0.10824
6644	0.9905	5.87	48	25.32	24.43	26.03	1517	0.0086	0.11641	0.12497

Table 8.44: 1.5" IMTP® experimental data at a liquid rate of 8.86 m^3/h

Gas Venturi dP [Pa]	T101 [°C]	T403 [°C]	$T_{air, ave}$ [°C]	System Pressure [kPa]	$\rho_{Air, ave\ T}$ [kg/m^3]	Gas Flow [kg/h]	Area of Column [m^2]	Vapour Flow Factor [$(m/s)\cdot(kg/m^3)^{0.5}$]	Liquid Density [kg/m^3]	Liquid Viscosity [mPa·s]	Surface Tension [mN/m]
-	-	-	-	-	-	-	-	-	-	-	-
481	24.51	25.44	24.98	99.68	1.165	282	0.1213	0.60	1035	0.757	64.4
814	24.76	25.44	25.10	99.79	1.166	380	0.1213	0.81	1035	0.757	64.4
1067	24.90	25.56	25.23	99.87	1.166	443	0.1213	0.94	1035	0.756	64.4
1461	25.01	25.50	25.26	99.99	1.168	524	0.1213	1.11	1035	0.756	64.4
2069	25.08	25.55	25.31	100.21	1.170	611	0.1213	1.29	1035	0.756	64.4
2746	25.05	25.45	25.25	100.45	1.173	691	0.1213	1.46	1035	0.757	64.4
3648	24.50	25.09	24.79	100.81	1.179	772	0.1213	1.63	1035	0.761	64.4
4902	24.56	25.17	24.86	101.23	1.184	861	0.1213	1.81	1035	0.761	64.4
6056	24.61	25.29	24.95	101.63	1.188	922	0.1213	1.94	1035	0.759	64.4
8282	24.72	25.38	25.05	102.33	1.196	1005	0.1213	2.11	1035	0.758	64.4
11277	24.86	25.62	25.24	103.23	1.205	1052	0.1213	2.19	1035	0.755	64.4
14572	24.97	25.71	25.34	104.21	1.216	1067	0.1213	2.22	1035	0.754	64.4
17020	24.98	25.73	25.35	104.95	1.225	1077	0.1213	2.23	1035	0.754	64.4

Table 8.44 continued

Liquid Venturi dP [Pa]	K-factor	Venturi Liquid Rate [m^3/h]	Liquid Rate [$m^3/m^2 \cdot h$]	T401 [^oC]	T405 [^oC]	T404 [^oC]	Column Pressure Drop [Pa/m]	Static Hold-up [m^3/m^3]	Dynamic Hold-up [m^3/m^3]	Total Hold-up [m^3/m^3]
-	-	-	-	-	-	-	0	0	0	0
14925	0.9905	8.83	73	25.30	24.12	25.78	48	0.0086	0.07911	0.08767
14864	0.9905	8.79	72	25.27	24.06	25.77	81	0.0086	0.07844	0.08699
14634	0.9905	8.74	72	25.41	24.17	25.88	107	0.0086	0.07918	0.08773
14488	0.9905	8.73	72	25.44	24.16	25.83	151	0.0086	0.07916	0.08771
14756	0.9905	8.75	72	25.42	24.24	25.86	205	0.0086	0.08088	0.08943
14793	0.9905	8.78	72	25.30	24.26	25.79	275	0.0086	0.08288	0.09143
15037	0.9905	8.84	73	25.00	23.73	25.41	365	0.0086	0.08567	0.09423
14719	0.9905	8.75	72	25.03	23.84	25.51	490	0.0086	0.08903	0.09758
14712	0.9905	8.75	72	25.18	23.91	25.64	606	0.0086	0.09240	0.10095
14602	0.9905	8.78	72	25.23	23.99	25.72	828	0.0086	0.10255	0.11111
14977	0.9905	8.77	72	25.49	24.18	25.93	1128	0.0086	0.11910	0.12765
14848	0.9905	8.83	73	25.58	24.26	26.02	1458	0.0086	0.13298	0.14153
14843	0.9905	8.77	72	25.52	24.36	26.09	1702	0.0086	0.14977	0.15833

Table 8.45: 1.5" IMTP® experimental data at a liquid rate of 11.89 m^3/h

Gas Venturi dP [Pa]	T101 [^oC]	T403 [^oC]	$T_{air, ave}$ [^oC]	System Pressure [kPa]	$\rho_{Air, ave\ T}$ [kg/m^3]	Gas Flow [kg/h]	Area of Column [m^2]	Vapour Flow Factor [$(m/s)\cdot(kg/m^3)^{0.5}$]	Liquid Density [kg/m^3]	Liquid Viscosity [mPa·s]	Surface Tension [mN/m]
-	-	-	-	-	-	-	-	-	-	-	-
553	24.52	25.72	25.12	100.28	1.171	264	0.1213	0.56	1035	0.754	64.4
963	24.86	25.72	25.29	100.41	1.172	366	0.1213	0.77	1035	0.753	64.4
1324	24.92	25.72	25.32	100.52	1.173	436	0.1213	0.92	1035	0.753	64.4
1878	25.07	25.71	25.39	100.67	1.175	510	0.1213	1.08	1035	0.754	64.4
2869	25.12	25.68	25.40	100.97	1.178	605	0.1213	1.28	1035	0.754	64.4
4030	25.18	25.60	25.39	101.21	1.181	670	0.1213	1.41	1035	0.756	64.4
5980	25.18	25.61	25.40	101.81	1.188	757	0.1213	1.59	1035	0.755	64.4
8124	25.18	25.58	25.38	102.48	1.196	826	0.1213	1.73	1035	0.756	64.4
8973	25.08	25.50	25.29	102.75	1.200	846	0.1213	1.77	1035	0.756	64.4
11712	25.13	25.56	25.35	103.57	1.209	871	0.1213	1.81	1035	0.756	64.4
15253	25.09	25.54	25.32	104.64	1.222	886	0.1213	1.84	1035	0.757	64.4

Table 8.45 continued

Liquid Venturi dP [Pa]	K-factor	Venturi Liquid Rate [m^3/h]	Liquid Rate [$m^3/m^2 \cdot h$]	T401 [^oC]	T405 [^oC]	T404 [^oC]	Column Pressure Drop [Pa/m]	Static Hold-up [m^3/m^3]	Dynamic Hold-up [m^3/m^3]	Total Hold-up [m^3/m^3]
-	-	-	-	-	-	-	0	0	0	0
26831	0.9905	11.82	97	25.61	24.06	26.00	55	0.0086	0.09470	0.1033
26843	0.9905	11.86	98	25.61	24.18	26.04	96	0.0086	0.09449	0.1030
26934	0.9905	11.90	98	25.62	24.25	26.06	133	0.0086	0.09584	0.1044
27141	0.9905	11.94	98	25.54	24.30	26.06	188	0.0086	0.09786	0.1064
27049	0.9905	11.85	98	25.49	24.32	26.01	286	0.0086	0.10500	0.1136
27153	0.9905	11.86	98	25.35	24.41	25.93	402	0.0086	0.11255	0.1211
26783	0.9905	11.84	98	25.41	24.36	25.93	598	0.0086	0.12308	0.1316
26603	0.9905	11.80	97	25.36	24.35	25.92	813	0.0086	0.13399	0.1425
26684	0.9905	11.80	97	25.39	24.33	25.85	898	0.0086	0.13973	0.1483
26831	0.9905	11.85	98	25.34	24.38	25.93	1171	0.0086	0.15729	0.1658
26354	0.9905	11.71	97	25.27	24.35	25.88	1525	0.0086	0.16925	0.1778

Table 8.46: 1.5" IMTP® experimental data at a liquid rate of 14.80 m^3/h

Gas Venturi dP [Pa]	T101 [°C]	T403 [°C]	$T_{air, ave}$ [°C]	System Pressure [kPa]	$\rho_{Air, ave\ T}$ [kg/m^3]	Gas Flow [kg/h]	Area of Column [m^2]	Vapour Flow Factor [$(m/s)\cdot(kg/m^3)^{0.5}$]	Liquid Density [kg/m^3]	Liquid Viscosity [mPa·s]	Surface Tension [mN/m]
-	-	-	-	-	-	-	-	-	-	-	-
635	24.98	25.58	25.28	100.07	1.168	251	0.1213	0.53	1035	0.755	64.4
972	25.03	25.62	25.33	100.19	1.170	321	0.1213	0.68	1035	0.755	64.4
1448	25.03	25.62	25.32	100.33	1.171	386	0.1213	0.82	1035	0.755	64.4
2134	25.08	25.66	25.37	100.56	1.174	459	0.1213	0.97	1035	0.754	64.4
3348	25.07	25.67	25.37	100.96	1.178	534	0.1213	1.13	1035	0.754	64.4
5132	25.10	25.70	25.40	101.52	1.185	607	0.1213	1.28	1035	0.754	64.4
7323	25.07	25.68	25.38	102.19	1.193	669	0.1213	1.40	1035	0.755	64.4
8663	25.09	25.71	25.40	102.57	1.197	691	0.1213	1.45	1035	0.754	64.4
12921	25.02	25.58	25.30	103.81	1.212	721	0.1213	1.50	1035	0.755	64.4
15607	24.99	25.71	25.35	104.60	1.221	727	0.1213	1.51	1035	0.754	64.4

Table 8.46 continued

Liquid Venturi dP [Pa]	K-factor	Venturi Liquid Rate [m^3/h]	Liquid Rate [$m^3/m^2 \cdot h$]	T401 [°C]	T405 [°C]	T404 [°C]	Column Pressure Drop [Pa/m]	Static Hold-up [m^3/m^3]	Dynamic Hold-up [m^3/m^3]	Total Hold-up [m^3/m^3]
-	-	-	-	-	-	-	0	0	0	0
23975	0.9905	14.74	122	25.44	24.38	25.92	63	0.0086	0.11269	0.1212
25343	0.9905	14.51	120	25.45	24.34	25.93	97	0.0086	0.11275	0.1213
23803	0.9905	14.75	122	25.43	24.32	25.97	145	0.0086	0.11474	0.1233
23972	0.9905	14.68	121	25.55	24.37	25.98	213	0.0086	0.12059	0.1291
23759	0.9905	14.71	121	25.51	24.39	26.00	336	0.0086	0.12853	0.1371
23909	0.9905	14.75	122	25.49	24.39	26.01	514	0.0086	0.13767	0.1462
24209	0.9905	14.73	121	25.46	24.34	25.98	732	0.0086	0.14862	0.1572
24201	0.9905	14.67	121	25.51	24.35	26.01	866	0.0086	0.15455	0.1631
24006	0.9905	14.73	121	25.40	24.27	25.93	1292	0.0086	0.17240	0.1810
23481	0.9905	14.83	122	25.53	24.32	26.02	1560	0.0086	0.17969	0.1882

The numbers in red indicates a limiting value on the data-logger that has been exceeded, and thus a negative value is shown. The conversion from pressure drop to liquid flow rate is still correct and was verified with the spot checks.

8.7.3 Intalox® Ultra™ Experimental Data

Table 8.47: 1.5" Intalox® Ultra™ experimental data at a liquid rate of 0.73 m^3/h

Gas Venturi dP [Pa]	T403 [^oC]	T101 [^oC]	$T_{air, ave}$ [^oC]	System Pressure [kPa]	$\rho_{Air, ave\ T}$ [kg/m^3]	Gas Flow [kg/h]	Area of Column [m^2]	Vapour Flow Factor [$(m/s)\cdot(kg/m^3)^{0.5}$]	Liquid Rate [m^3/h]	Liquid Rate [$m^3/m^2\cdot h$]
174	24.36	23.67	24.02	100.47	1.178	288	0.1213	0.61	0.737	6
564	24.86	24.21	24.53	99.96	1.170	554	0.1213	1.17	0.726	6
1332	25.07	24.54	24.81	100.41	1.174	881	0.1213	1.86	0.720	6
2341	25.47	24.90	25.18	100.75	1.177	1180	0.1213	2.49	0.721	6
3112	25.99	25.33	25.66	99.90	1.165	1345	0.1213	2.85	0.727	6
3360	25.14	24.43	24.78	101.21	1.184	1403	0.1213	2.95	0.730	6
3487	25.64	24.80	25.22	101.27	1.183	1425	0.1213	3.00	0.731	6
4221	26.50	25.60	26.05	101.62	1.183	1552	0.1213	3.27	0.729	6
4482	27.02	26.06	26.54	101.72	1.183	1591	0.1213	3.35	0.729	6
4954	27.24	26.36	26.80	101.94	1.184	1683	0.1213	3.54	0.728	6
5284	27.38	26.34	26.86	102.08	1.186	1712	0.1213	3.60	0.731	6
5648	27.55	26.46	27.01	102.24	1.187	1760	0.1213	3.70	0.731	6
5923	27.97	26.61	27.29	102.36	1.187	1794	0.1213	3.77	0.729	6
6556	28.07	26.74	27.41	102.61	1.190	1863	0.1213	3.91	0.728	6
7012	28.05	26.74	27.39	102.81	1.192	1912	0.1213	4.01	0.729	6
7636	28.35	26.98	27.67	103.05	1.194	1975	0.1213	4.14	0.726	6
8089	25.73	24.27	25.00	103.42	1.209	2031	0.1213	4.23	0.729	6
8594	28.01	26.42	27.21	103.63	1.202	2069	0.1213	4.32	0.726	6
9877	27.54	26.16	26.85	104.12	1.209	2164	0.1213	4.49	0.722	6
11122	28.17	26.46	27.31	104.58	1.213	2226	0.1213	4.63	0.743	6
13902	30.39	28.38	29.38	105.13	1.211	2330	0.1213	4.85	0.739	6
16245	30.73	28.51	29.62	106.12	1.221	2401	0.1213	4.98	0.739	6

Table 8.47 continued

Liquid Density [kg/m^3]	Liquid Viscosity [mPa·s]	Surface Tension [mN/m]	Liquid Venturi dP [Pa]	K-factor	T401 [^{o}C]	T405 [^{o}C]	T404 [^{o}C]	Column Pressure Drop [Pa/m]	Static Hold-up [m^3/m^3]	Dynamic Hold-up [m^3/m^3]	Total Hold-up [m^3/m^3]
1034	0.771	58	134	0.9905	24.26	22.56	24.61	17	0.0096	0.01795	0.02754
1034	0.766	58	-	-	24.65	23.06	25.10	55	0.0096	0.01801	0.02759
1034	0.763	58	-	-	24.85	23.51	25.31	133	0.0096	0.01803	0.02761
1034	0.758	58	-	-	25.23	23.92	25.75	234	0.0096	0.01825	0.02784
1034	0.751	58	-	-	25.78	24.43	26.29	311	0.0096	0.01923	0.02881
1034	0.762	58	-	-	24.90	23.43	25.38	336	0.0096	0.01958	0.02917
1034	0.757	58	-	-	25.25	23.79	25.86	348	0.0096	0.01975	0.02934
1034	0.747	58	-	-	25.93	24.52	26.77	422	0.0096	0.02145	0.03103
1034	0.740	58	-	-	26.44	25.17	27.29	448	0.0096	0.02216	0.03175
1034	0.737	58	-	-	26.78	25.40	27.50	510	0.0096	0.02360	0.03319
1034	0.739	58	-	-	26.33	25.14	27.68	529	0.0096	0.02404	0.03362
1034	0.738	58	-	-	26.25	25.18	27.90	565	0.0096	0.02478	0.03436
1034	0.735	58	-	-	26.22	25.31	28.31	593	0.0096	0.02558	0.03517
1034	0.735	58	-	-	26.15	25.34	28.45	656	0.0096	0.02701	0.03660
1034	0.736	58	-	-	26.04	25.27	28.46	701	0.0096	0.02806	0.03765
1034	0.733	58	-	-	26.10	25.37	28.76	764	0.0096	0.03000	0.03958
1034	0.760	58	-	-	24.70	23.14	25.93	824	0.0096	0.03186	0.04145
1034	0.734	58	-	-	26.35	25.17	28.36	860	0.0096	0.03321	0.04279
1034	0.737	58	-	-	26.38	25.28	27.80	988	0.0096	0.03862	0.04821
1034	0.734	58	-	-	26.38	25.40	28.39	1112	0.0096	0.04534	0.05492
1034	0.729	58	-	-	24.60	27.35	30.95	1391	0.0096	0.06082	0.07040
1034	0.755	58	-	-	22.95	28.52	28.52	1625	0.0096	0.08087	0.09045

Table 8.48: 1.5" Intalox® Ultra™ experimental data at a liquid rate of 1.43 m^3/h

Gas Venturi dP [Pa]	T403 [^oC]	T101 [^oC]	$T_{air, ave}$ [^oC]	System Pressure [kPa]	$\rho_{Air, ave\ T}$ [kg/m^3]	Gas Flow [kg/h]	Area of Column [m^2]	Vapour Flow Factor [$(m/s)\cdot(kg/m^3)^{0.5}$]	Liquid Rate [m^3/h]	Liquid Rate [$m^3/m^2\cdot h$]
176	24.12	23.46	23.79	100.48	1.179	281	0.1213	0.59	1.445	12
458	25.81	25.80	25.81	100.03	1.166	486	0.1213	1.03	1.458	12
1749	26.32	26.03	26.17	100.65	1.172	994	0.1213	2.10	1.453	12
2244	26.21	25.68	25.94	100.91	1.176	1108	0.1213	2.34	1.454	12
2889	26.24	25.57	25.91	101.19	1.179	1254	0.1213	2.64	1.458	12
3445	26.21	25.31	25.76	101.46	1.183	1373	0.1213	2.89	1.456	12
4048	26.66	25.53	26.09	101.73	1.184	1470	0.1213	3.09	1.456	12
4862	26.68	25.31	26.00	102.06	1.189	1589	0.1213	3.34	1.457	12
5699	26.58	25.37	25.97	102.40	1.193	1695	0.1213	3.55	1.458	12
6623	27.15	25.34	26.24	102.77	1.196	1789	0.1213	3.75	1.458	12
7994	27.15	25.55	26.35	103.28	1.202	1909	0.1213	3.99	1.466	12
9642	27.28	25.40	26.34	103.90	1.209	1994	0.1213	4.15	1.464	12
12417	27.27	25.39	26.33	104.92	1.221	2088	0.1213	4.33	1.466	12
16479	27.36	25.66	26.51	106.49	1.238	2219	0.1213	4.49	1.466	12

Table 8.48 continued

Liquid Density [kg/m^3]	Liquid Viscosity [mPa·s]	Surface Tension [mN/m]	Venturi dP [Pa]	K-factor	Venturi Liquid Rate [m^3/h]	T401 [^{o}C]	T405 [^{o}C]	T404 [^{o}C]	Column Pressure Drop [Pa/m]	Static Hold-up [m^3/m^3]	Dynamic Hold-up [m^3/m^3]	Total Hold-up [m^3/m^3]
1034	0.774	58	421	0.9905	1.45	24.05	22.52	24.42	18	0.0096	0.02466	0.03425
1034	0.751	58	-	-	-	25.90	24.55	26.16	46	0.0096	0.02416	0.03375
1034	0.748	58	-	-	-	25.80	25.09	26.65	180	0.0096	0.02445	0.03404
1034	0.751	58	-	-	-	25.50	25.16	26.49	224	0.0096	0.02450	0.03408
1034	0.753	58	-	-	-	25.15	25.25	26.52	292	0.0096	0.02576	0.03535
1034	0.751	58	-	-	-	25.48	25.31	26.51	350	0.0096	0.02703	0.03661
1034	0.750	58	-	-	-	25.17	25.64	26.95	405	0.0096	0.02808	0.03767
1034	0.751	58	-	-	-	25.05	25.74	27.00	486	0.0096	0.02995	0.03953
1034	0.751	58	-	-	-	25.10	25.68	26.93	570	0.0096	0.03252	0.04210
1034	0.750	58	-	-	-	24.60	26.39	27.55	662	0.0096	0.03575	0.04534
1034	0.748	58	-	-	-	24.73	26.41	27.77	800	0.0096	0.04111	0.05070
1034	0.751	58	-	-	-	24.28	26.50	27.78	964	0.0096	0.04919	0.05877
1034	0.750	58	-	-	-	24.37	26.55	27.83	1241	0.0096	0.06100	0.07059
1034	0.745	58	-	-	-	24.53	26.33	28.52	1647	0.0096	0.08100	0.09058

Table 8.49: 1.5" Intalox® Ultra™ experimental data at a liquid rate of 2.91 m^3/h

Gas Venturi dP [Pa]	T403 [^oC]	T101 [^oC]	$T_{air, ave}$ [^oC]	System Pressure [kPa]	$\rho_{Air, ave\ T}$ [kg/m^3]	Gas Flow [kg/h]	Area of Column [m^2]	Vapour Flow Factor [$(m/s)\cdot(kg/m^3)^{0.5}$]	Liquid Density [kg/m^3]	Liquid Viscosity [mPa·s]	Surface Tension [mN/m]
196	23.62	22.86	23.24	100.51	1.182	283	0.1213	0.60	1034	0.781	58
576	26.00	25.87	25.93	99.66	1.161	527	0.1213	1.12	1034	0.751	58
1709	27.06	26.78	26.92	100.18	1.163	923	0.1213	1.96	1034	0.747	58
2218	28.05	27.79	27.92	100.38	1.162	1055	0.1213	2.24	1034	0.725	58
2895	29.22	29.00	29.11	100.64	1.160	1175	0.1213	2.50	1034	0.712	58
3589	31.32	31.11	31.22	100.88	1.155	1289	0.1213	2.75	1034	0.688	58
4499	31.95	31.66	31.81	101.21	1.156	1412	0.1213	3.01	1034	0.681	58
5384	32.68	32.24	32.46	101.51	1.157	1520	0.1213	3.24	1034	0.679	58
6560	27.00	26.58	26.79	101.93	1.184	1632	0.1213	3.43	1034	0.745	58
8210	26.72	26.20	26.46	102.48	1.192	1728	0.1213	3.62	1034	0.750	58
11745	26.96	26.05	26.51	103.61	1.205	1822	0.1213	3.80	1034	0.748	58
13452	27.11	26.00	26.55	104.13	1.211	1850	0.1213	3.85	1034	0.747	58
15502	27.18	25.70	26.44	104.92	1.220	1882	0.1213	3.90	1034	0.748	58
16385	27.66	25.68	26.67	105.35	1.224	1906	0.1213	3.93	1034	0.745	58

Table 8.49 continued

Liquid Venturi dP [Pa]	K-factor	Venturi Liquid Rate [m^3/h]	Liquid Rate [$m^3/m^2 \cdot h$]	T401 [^oC]	T405 [^oC]	T404 [^oC]	Column Pressure Drop [Pa/m]	Static Hold-up [m^3/m^3]	Dynamic Hold-up [m^3/m^3]	Total Hold-up [m^3/m^3]
1638	0.9905	2.95	24	23.49	22.05	23.94	20	0.0096	0.03541	0.04499
1579	0.9905	2.86	24	25.75	24.89	26.34	58	0.0096	0.03577	0.04536
1616	0.9905	2.93	24	26.75	25.96	25.96	171	0.0096	0.03581	0.04540
1684	0.9905	2.88	24	27.76	27.04	28.40	225	0.0096	0.03598	0.04556
1664	0.9905	2.96	24	28.87	28.26	29.52	287	0.0096	0.03731	0.04690
1695	0.9905	2.87	24	30.96	30.46	31.62	356	0.0096	0.03907	0.04866
1682	0.9905	2.97	24	31.58	31.10	32.25	450	0.0096	0.04196	0.05155
1682	0.9905	2.94	24	31.09	31.98	33.00	535	0.0096	0.04511	0.05469
1679	0.9905	2.97	24	25.66	26.62	27.37	656	0.0096	0.04936	0.05895
1633	0.9905	2.94	24	25.18	26.33	27.08	829	0.0096	0.05770	0.06729
1680	0.9905	2.91	24	25.14	26.52	27.35	1174	0.0096	0.07606	0.08565
1634	0.9905	2.96	24	25.18	26.65	27.50	1344	0.0096	0.08594	0.09553
1677	0.9905	2.95	24	24.93	26.51	27.54	1550	0.0096	0.09760	0.10718
1636	0.9905	2.93	24	24.93	26.72	28.08	1669	0.0096	0.10415	0.11374

Table 8.50: 1.5" Intalox® Ultra™ experimental data at a liquid rate of 4.49 m^3/h

Gas Venturi dP [Pa]	T403 [^oC]	T101 [^oC]	$T_{air, ave}$ [^oC]	System Pressure [kPa]	$\rho_{Air, ave\ T}$ [kg/m^3]	Gas Flow [kg/h]	Area of Column [m^2]	Vapour Flow Factor [$(m/s)\cdot(kg/m^3)^{0.5}$]	Liquid Density [kg/m^3]	Liquid Viscosity [mPa·s]	Surface Tension [mN/m]
227	23.58	22.85	23.22	100.50	1.182	281	0.1213	0.59	1034	0.781	58
558	25.25	25.16	25.20	100.05	1.168	487	0.1213	1.03	1034	0.759	58
1460	25.20	25.08	25.14	100.46	1.173	805	0.1213	1.70	1034	0.760	58
1815	25.30	25.08	25.19	100.63	1.175	895	0.1213	1.89	1034	0.759	58
2346	25.17	24.88	25.03	100.82	1.178	1011	0.1213	2.13	1034	0.760	58
2917	25.00	24.70	24.85	101.09	1.182	1112	0.1213	2.34	1034	0.764	58
3734	25.23	24.87	25.05	101.40	1.185	1231	0.1213	2.59	1034	0.760	58
4607	25.28	24.89	25.09	101.73	1.189	1333	0.1213	2.80	1034	0.761	58
5738	25.48	24.98	25.23	102.12	1.192	1434	0.1213	3.01	1034	0.762	58
7788	25.25	24.72	24.99	102.86	1.202	1550	0.1213	3.24	1034	0.763	58
9765	25.13	24.61	24.87	103.50	1.210	1610	0.1213	3.35	1034	0.763	58
13069	25.20	24.59	24.89	104.61	1.223	1653	0.1213	3.42	1034	0.764	58
14684	25.31	24.71	25.01	105.24	1.230	1668	0.1213	3.44	1034	0.762	58
15858	26.25	24.66	25.45	106.06	1.238	1676	0.1213	3.45	1034	0.757	58

Table 8.50 continued

Liquid Venturi dP [Pa]	K-factor	Venturi Liquid Rate [m^3/h]	Liquid Rate [$m^3/m^2 \cdot h$]	T401 [^oC]	T405 [^oC]	T404 [^oC]	Column Pressure Drop [Pa/m]	Static Hold-up [m^3/m^3]	Dynamic Hold-up [m^3/m^3]	Total Hold-up [m^3/m^3]
3880	0.9905	4.48	37	23.49	22.04	23.91	22	0.0096	0.04362	0.05321
3746	0.9905	4.43	37	25.13	24.17	25.60	61	0.0096	0.04350	0.05309
3823	0.9905	4.52	37	25.03	24.13	25.56	151	0.0096	0.04370	0.05329
3849	0.9905	4.49	37	25.16	24.12	25.64	188	0.0096	0.04362	0.05320
3843	0.9905	4.50	37	25.13	24.02	25.52	242	0.0096	0.04480	0.05439
3848	0.9905	4.49	37	24.60	24.07	25.36	295	0.0096	0.04634	0.05592
3889	0.9905	4.50	37	25.09	24.07	25.60	374	0.0096	0.04941	0.05900
3830	0.9905	4.48	37	24.88	24.24	25.66	461	0.0096	0.05253	0.06212
3880	0.9905	4.49	37	24.54	24.46	25.80	574	0.0096	0.05691	0.06650
3918	0.9905	4.51	37	24.52	24.25	25.63	779	0.0096	0.06642	0.07601
3866	0.9905	4.48	37	24.51	24.26	25.59	977	0.0096	0.07702	0.08660
3900	0.9905	4.49	37	24.37	24.38	25.68	1306	0.0096	0.09438	0.10397
3884	0.9905	4.51	37	24.51	24.45	25.77	1468	0.0096	0.10712	0.11670
3895	0.9905	4.51	37	24.56	24.72	26.49	1586	0.0096	0.10870	0.11829

Table 8.51: 1.5" Intalox® Ultra™ experimental data at a liquid rate of 5.94 m^3/h

Gas Venturi dP [Pa]	T403 [^oC]	T101 [^oC]	$T_{air, ave}$ [^oC]	System Pressure [kPa]	$\rho_{Air, ave\ T}$ [kg/m^3]	Gas Flow [kg/h]	Area of Column [m^2]	Vapour Flow Factor [$(m/s)\cdot(kg/m^3)^{0.5}$]	Liquid Density [kg/m^3]	Liquid Viscosity [mPa·s]	Surface Tension [mN/m]
248	23.46	22.64	23.05	100.49	1.182	284	0.1213	0.60	1034	0.783	58
557	25.31	25.50	25.41	100.10	1.168	459	0.1213	0.97	1034	0.758	58
685	25.04	25.43	25.23	100.10	1.169	519	0.1213	1.10	1034	0.763	58
1250	25.32	25.47	25.40	100.36	1.171	706	0.1213	1.49	1034	0.759	58
1643	25.30	25.30	25.30	100.54	1.174	810	0.1213	1.71	1034	0.760	58
2138	25.24	25.13	25.19	100.74	1.177	912	0.1213	1.93	1034	0.760	58
2774	25.23	25.20	25.22	101.03	1.180	1019	0.1213	2.15	1034	0.761	58
3370	25.29	25.12	25.20	101.33	1.183	1102	0.1213	2.32	1034	0.759	58
4308	25.30	25.10	25.20	101.79	1.189	1210	0.1213	2.54	1034	0.760	58
5496	25.27	24.92	25.10	102.27	1.195	1308	0.1213	2.74	1034	0.759	58
7864	25.50	25.07	25.28	103.13	1.204	1427	0.1213	2.98	1034	0.757	58
11117	25.37	24.92	25.14	104.15	1.217	1487	0.1213	3.09	1034	0.759	58
13892	25.38	24.82	25.10	105.07	1.227	1504	0.1213	3.11	1034	0.758	58
14854	25.37	24.72	25.04	105.56	1.233	1512	0.1213	3.12	1034	0.759	58

Table 8.51 continued

Liquid Venturi dP [Pa]	K-factor	Venturi Liquid Rate [m^3/h]	Liquid Rate [$m^3/m^2 \cdot h$]	T401 [^oC]	T405 [^oC]	T404 [^oC]	Column Pressure Drop [Pa/m]	Static Hold-up [m^3/m^3]	Dynamic Hold-up [m^3/m^3]	Total Hold-up [m^3/m^3]
6538	0.9905	5.82	48	23.39	21.80	23.79	25	0.0096	0.04999	0.05957
6543	0.9905	5.83	48	25.18	24.26	25.70	56	0.0096	0.05005	0.05964
6469	0.9905	5.80	48	24.67	24.20	25.46	70	0.0096	0.05003	0.05962
6631	0.9905	5.91	49	25.04	24.31	25.69	125	0.0096	0.05004	0.05963
6608	0.9905	5.87	48	25.02	24.34	25.67	165	0.0096	0.04997	0.05956
6603	0.9905	5.93	49	25.00	24.23	25.61	212	0.0096	0.05120	0.06079
6703	0.9905	5.91	49	24.93	24.33	25.62	272	0.0096	0.05328	0.06287
6688	0.9905	5.92	49	25.09	24.14	25.63	334	0.0096	0.05504	0.06462
6670	0.9905	5.89	49	25.01	24.25	25.67	431	0.0096	0.05854	0.06812
6779	0.9905	5.96	49	25.18	24.04	25.61	550	0.0096	0.06224	0.07182
6679	0.9905	5.89	49	25.22	24.27	25.87	787	0.0096	0.07081	0.08040
6651	0.9905	5.90	49	24.96	24.30	25.77	1111	0.0096	0.08813	0.09771
6620	0.9905	5.91	49	25.18	24.18	25.78	1379	0.0096	0.10560	0.11518
6582	0.9905	5.84	48	24.96	24.23	25.80	1485	0.0096	0.11992	0.12950

Table 8.52: 1.5" Intalox® Ultra™ experimental data at a liquid rate of 8.86 m^3/h

Gas Venturi dP [Pa]	T403 [°C]	T101 [°C]	$T_{air, ave}$ [°C]	System Pressure [kPa]	$\rho_{Air, ave\ T}$ [kg/m^3]	Gas Flow [kg/h]	Area of Column [m^2]	Vapour Flow Factor [$(m/s)\cdot(kg/m^3)^{0.5}$]	Liquid Density [kg/m^3]	Liquid Viscosity [mPa·s]	Surface Tension [mN/m]
318	25.48	25.03	25.25	100.41	1.172	295	0.1213	0.62	1034	0.757	58
596	25.45	24.79	25.12	100.60	1.175	431	0.1213	0.91	1034	0.756	58
863	25.30	24.81	25.06	100.70	1.177	532	0.1213	1.12	1034	0.758	58
1252	25.53	25.01	25.27	100.87	1.178	639	0.1213	1.35	1034	0.756	58
1452	25.53	25.02	25.27	100.93	1.178	684	0.1213	1.44	1034	0.756	58
2436	25.58	25.10	25.34	101.30	1.183	844	0.1213	1.78	1034	0.756	58
3150	25.51	25.00	25.25	101.56	1.186	935	0.1213	1.97	1034	0.756	58
4604	25.50	24.98	25.24	102.07	1.192	1048	0.1213	2.20	1034	0.756	58
5761	25.41	24.89	25.15	102.43	1.196	1118	0.1213	2.34	1034	0.757	58
9089	25.56	25.00	25.28	103.49	1.208	1220	0.1213	2.54	1034	0.755	58
11083	25.44	24.98	25.21	104.09	1.216	1244	0.1213	2.58	1034	0.757	58
13268	25.54	24.99	25.27	104.74	1.223	1256	0.1213	2.60	1034	0.756	58
15145	25.21	24.74	24.98	105.44	1.232	1263	0.1213	2.60	1034	0.760	58

Table 8.52 continued

Liquid Venturi dP [Pa]	K-factor	Venturi Liquid Rate [m^3/h]	Liquid Rate [$m^3/m^2 \cdot h$]	T401 [^oC]	T405 [^oC]	T404 [^oC]	Column Pressure Drop [Pa/m]	Static Hold-up [m^3/m^3]	Dynamic Hold-up [m^3/m^3]	Total Hold-up [m^3/m^3]
15255	0.9905	8.88	73	25.26	24.19	25.82	32	0.0096	0.05989	0.06947
15072	0.9905	8.86	73	25.41	23.99	25.79	60	0.0096	0.06053	0.07011
14848	0.9905	8.82	73	25.30	23.92	25.67	86	0.0096	0.06027	0.06986
15280	0.9905	8.90	73	25.43	24.16	25.87	125	0.0096	0.06023	0.06982
15159	0.9905	8.91	73	25.43	24.14	25.87	143	0.0096	0.06140	0.07099
15382	0.9905	8.98	74	25.41	24.15	25.87	239	0.0096	0.06584	0.07542
15197	0.9905	8.89	73	25.38	24.10	25.82	315	0.0096	0.06910	0.07869
15489	0.9905	8.98	74	25.43	24.06	25.80	460	0.0096	0.07362	0.08321
15457	0.9905	8.82	73	25.38	23.99	25.76	576	0.0096	0.07963	0.08921
15203	0.9905	8.91	73	25.49	24.15	25.89	909	0.0096	0.09267	0.10226
15064	0.9905	8.87	73	25.27	24.15	25.82	1108	0.0096	0.10222	0.11180
14654	0.9905	8.83	73	25.38	24.22	25.92	1327	0.0096	0.11062	0.12021
14943	0.9905	8.83	73	25.05	24.03	25.63	1516	0.0096	0.12526	0.13484

Table 8.53: 1.5" Intalox® Ultra™ experimental data at a liquid rate of 11.89 m^3/h

Gas Venturi dP [Pa]	T403 [°C]	T101 [°C]	$T_{air, ave}$ [°C]	System Pressure [kPa]	$\rho_{Air, ave\ T}$ [kg/m³]	Gas Flow [kg/h]	Area of Column [m²]	Vapour Flow Factor [(m/s)·(kg/m³)$^{0.5}$]	Liquid Density [kg/m³]	Liquid Viscosity [mPa·s]	Surface Tension [mN/m]
348	25.57	25.00	25.28	99.95	1.167	278	0.1213	0.59	1034	0.755	58
560	25.61	25.11	25.36	99.99	1.167	371	0.1213	0.79	1034	0.755	58
724	25.57	25.14	25.35	100.05	1.168	421	0.1213	0.89	1034	0.756	58
1298	25.60	25.28	25.44	100.22	1.169	573	0.1213	1.21	1034	0.755	58
1831	25.52	25.32	25.42	100.29	1.170	670	0.1213	1.42	1034	0.756	58
2196	25.54	25.28	25.41	100.51	1.173	715	0.1213	1.51	1034	0.756	58
3172	25.48	25.28	25.38	100.84	1.177	813	0.1213	1.72	1034	0.756	58
4011	25.56	25.30	25.43	101.02	1.179	874	0.1213	1.84	1034	0.757	58
4638	25.50	25.27	25.38	101.31	1.182	909	0.1213	1.91	1034	0.757	58
6881	25.55	25.24	25.39	102.02	1.191	997	0.1213	2.09	1034	0.756	58
11131	25.58	25.20	25.39	103.31	1.206	1049	0.1213	2.19	1034	0.757	58
13968	25.51	25.22	25.36	104.16	1.216	1054	0.1213	2.21	1034	0.756	58
15861	25.44	25.20	25.32	104.87	1.224	1064	0.1213	2.22	1034	0.756	58

Table 8.53 continued

Liquid Venturi dP [Pa]	K-factor	Venturi Liquid Rate [m^3/h]	Liquid Rate [$m^3/m^2 \cdot h$]	T401 [^oC]	T405 [^oC]	T404 [^oC]	Column Pressure Drop [Pa/m]	Static Hold-up [m^3/m^3]	Dynamic Hold-up [m^3/m^3]	Total Hold-up [m^3/m^3]
25702	0.9905	11.60	96	25.44	24.18	25.91	35	0.0096	0.06940	0.07899
26803	0.9905	11.83	98	25.47	24.30	25.96	56	0.0096	0.06953	0.07911
26966	0.9905	11.90	98	25.40	24.27	25.90	72	0.0096	0.06964	0.07923
26654	0.9905	11.82	97	25.41	24.32	25.93	133	0.0096	0.07085	0.08043
26746	0.9905	11.81	97	25.31	24.38	25.88	187	0.0096	0.07361	0.08319
26984	0.9905	11.89	98	25.30	24.44	25.93	222	0.0096	0.07676	0.08634
26893	0.9905	11.82	97	25.33	24.46	25.90	317	0.0096	0.08458	0.09417
26808	0.9905	11.81	97	25.28	24.38	25.82	402	0.0096	0.09180	0.10139
26989	0.9905	11.92	98	25.28	24.48	25.88	464	0.0096	0.09748	0.10707
27295	0.9905	11.96	99	25.34	24.43	25.92	688	0.0096	0.11451	0.12409
26975	0.9905	11.85	98	25.25	24.44	25.90	1113	0.0096	0.13474	0.14432
26854	0.9905	11.85	98	25.34	24.50	25.94	1396	0.0096	0.14583	0.15542
26710	0.9905	11.84	98	25.30	24.50	26.00	1585	0.0096	0.15115	0.16074

Table 8.54: 1.5" Intalox® Ultra™ experimental data at a liquid rate of 14.80 m^3/h

Gas Venturi dP [Pa]	T403 [°C]	T101 [°C]	$T_{air, ave}$ [°C]	System Pressure [kPa]	$\rho_{Air, ave\ T}$ [kg/m^3]	Gas Flow [kg/h]	Area of Column [m^2]	Vapour Flow Factor [$(m/s)\cdot(kg/m^3)^{0.5}$]	Liquid Density [kg/m^3]	Liquid Viscosity [mPa·s]	Surface Tension [mN/m]
399	25.71	24.82	25.26	99.68	1.164	268	0.1213	0.57	1034	0.763	58
592	25.70	25.00	25.35	99.74	1.164	344	0.1213	0.73	1034	0.754	58
820	25.63	25.10	25.36	99.82	1.165	407	0.1213	0.86	1034	0.755	58
1105	25.63	25.17	25.40	99.93	1.166	474	0.1213	1.01	1034	0.755	58
1552	25.62	25.20	25.41	100.07	1.168	548	0.1213	1.16	1034	0.755	58
2445	25.59	25.20	25.39	100.39	1.172	640	0.1213	1.35	1034	0.755	58
3748	25.57	25.22	25.39	100.81	1.177	727	0.1213	1.53	1034	0.755	58
6218	25.60	25.24	25.42	101.58	1.185	831	0.1213	1.75	1034	0.755	58
9203	25.60	25.24	25.42	102.54	1.197	889	0.1213	1.86	1034	0.755	58
13033	25.60	25.20	25.40	103.69	1.210	913	0.1213	1.90	1034	0.755	58
14533	25.67	25.20	25.43	104.12	1.215	917	0.1213	1.91	1034	0.755	58

Table 8.54: 1.5” Intalox® Ultra™ experimental data at a liquid rate of 14.80 m3/h **continued**

Liquid Venturi dP [Pa]	K-factor	Venturi Liquid Rate [m^3/h]	Liquid Rate [$m^3/m^2 \cdot h$]	T401 [°C]	T405 [°C]	T404 [°C]	Column Pressure Drop [Pa/m]	Static Hold-up [m^3/m^3]	Dynamic Hold-up [m^3/m^3]	Total Hold-up [m^3/m^3]
22698	0.9905	14.95	123	24.21	25.53	26.02	40	0.0096	0.08239	0.09198
23766	0.9905	14.78	122	25.52	24.21	26.00	61	0.0096	0.08263	0.09222
23497	0.9905	14.81	122	25.45	24.28	25.95	85	0.0096	0.08256	0.09215
23292	0.9905	14.83	122	25.45	24.31	25.99	116	0.0096	0.08453	0.09412
23726	0.9905	14.80	122	25.48	24.33	25.98	161	0.0096	0.08840	0.09799
23752	0.9905	14.77	122	25.42	24.32	25.95	245	0.0096	0.09426	0.10384
23638	0.9905	14.76	122	25.42	24.37	25.95	375	0.0096	0.10135	0.11093
23723	0.9905	14.79	122	25.43	24.41	25.99	622	0.0096	0.11507	0.12465
23852	0.9905	14.78	122	25.41	24.52	25.99	921	0.0096	0.13680	0.14639
23583	0.9905	14.79	122	25.38	24.51	26.03	1303	0.0096	0.15906	0.16865
23552	0.9905	14.75	122	25.42	24.48	26.05	1453	0.0096	0.16501	0.17460

The numbers in red indicates a limiting value on the data-logger that has been exceeded, and thus a negative value is shown. The conversion from pressure drop to liquid flow rate is still correct and was verified with the spot checks.

8.8 Sample Calculations

8.8.1 Loading Point Determination

Table 8.55: Loading point experimental data standard deviation

	Loading Point		
	Flow rate [kg/h]	**$Std_{dev, flow}$ [kg/h]**	**$Std_{dev, flow}$ $[(m/s)\cdot(kg/m^3)^{0.5}]$**
1	741.7	2.9	0.006
2	741.7	-	-
3	741.7	-	-
4	741.7	-	-
5	741.7	-	-
6	741.7	-	-
7	741.7	-	-
8	741.7	-	-
9	741.7	-	-
10	741.7	-	-
11	741.7	-	-
12	735.5	-	-
13	735.5	-	-
14	735.5	-	-
15	735.5	-	-
16	735.5	-	-
17	735.5	-	-
18	735.5	-	-
19	735.5	-	-
20	735.5	-	-
21	735.5	-	-
22	735.5	-	-
23	735.5	-	-
24	735.4	-	-
25	735.4	-	-
26	735.4	-	-
27	735.4	-	-
28	735.4	-	-
29	735.4	-	-
30	735.4	-	-
31	735.4	-	-
32	735.4	-	-
33	735.4	-	-

Table 8.55 continued

34	735.4	-	-
35	734.1	-	-
36	734.1	-	-
37	734.1	-	-
38	734.1	-	-
39	734.1	-	-
40	734.1	-	-
41	734.1	-	-
42	734.1	-	-
43	734.1	-	-
44	734.1	-	-
45	734.1	-	-
46	739.2	-	-
47	739.2	-	-
48	739.2	-	-
49	739.2	-	-
50	739.2	-	-
51	739.2	-	-
52	739.2	-	-
53	739.2	-	-
54	739.2	-	-
55	739.2	-	-
56	739.2	-	-
57	740.6	-	-
58	740.6	-	-
59	740.6	-	-
60	740.6	-	-

Table 8.56: Adjusted dry bed confidence prediction interval parameters

Adjusted Dry Bed Pressure Drop Curve									
Measured Values		Predicted Values							
X_{hat}	Y_{hat}	X	Y	$(Y-Y_{hat})^2$	n_{true}	s^2_E	t_{inf}	n_{gen}	$\Sigma(X-X_{average})^2$
0.594	32.92	0.594	31.78	1.297	6	26.16	0.636	408	197.485
0.960	78.38	0.960	80.18	3.230	-	-	-	-	-
1.220	124.93	1.220	127.38	6.030	-	-	-	-	-
1.536	194.24	1.536	198.66	19.531	-	-	-	-	-
1.745	254.95	1.745	254.19	0.575	-	-	-	-	-
2.037	351.29	2.037	342.69	73.979	-	-	-	-	-

Table 8.57: Adjusted dry bed confidence prediction interval test

Adjusted Dry bed: $y = 86.27x^{1.93}$						
X	Y	$X_{average}$	$(X-X_{average})^2$	$s^2_{Y,hat}$	Lower Limit	Upper Limit
1.536	198.70	-	0.0647	26.233	195.44	201.96
1.542	200.20	-	0.0617	26.233	196.95	203.46
1.548	201.71	-	0.0588	26.232	198.45	204.97
1.554	203.22	-	0.0559	26.232	199.96	206.48
1.560	204.74	-	0.0531	26.232	201.48	208.00
1.566	206.26	-	0.0504	26.231	203.00	209.52
1.572	207.79	-	0.0477	26.231	204.53	211.05
1.578	209.32	-	0.0451	26.231	206.06	212.58
1.584	210.86	-	0.0426	26.230	207.60	214.12
1.590	212.41	-	0.0402	26.230	209.15	215.66
1.596	213.96	-	0.0378	26.230	210.70	217.21
1.602	215.51	-	0.0355	26.229	212.25	218.77
1.608	217.07	-	0.0333	26.229	213.81	220.33

Table 8.57 continued

1.614	218.64	-	0.0311	26.229	215.38	221.90
1.620	220.21	-	0.0290	26.229	216.95	223.47
1.626	221.79	-	0.0270	26.228	218.53	225.04
1.632	223.37	-	0.0251	26.228	220.11	226.63
1.638	224.95	-	0.0232	26.228	221.70	228.21
1.644	226.55	-	0.0214	26.228	223.29	229.81
1.650	228.15	-	0.0197	26.227	224.89	231.40
1.656	229.75	-	0.0181	26.227	226.49	233.01
1.662	231.36	-	0.0165	26.227	228.10	234.62
1.668	232.97	-	0.0150	26.227	229.72	236.23
1.674	234.59	-	0.0136	26.226	231.34	237.85
1.680	236.22	-	0.0122	26.226	232.96	239.48
1.686	237.85	-	0.0109	26.226	234.59	241.11
1.692	239.49	-	0.0097	26.226	236.23	242.75
1.698	241.13	-	0.0085	26.226	237.87	244.39
1.704	242.78	-	0.0075	26.226	239.52	246.03
1.710	244.43	-	0.0065	26.226	241.17	247.69
1.716	246.09	-	0.0055	26.225	242.83	249.34
1.722	247.75	-	0.0047	26.225	244.49	251.01
1.728	249.42	-	0.0039	26.225	246.16	252.68
1.734	251.09	-	0.0032	26.225	247.83	254.35
1.740	252.77	-	0.0025	26.225	249.51	256.03
1.746	254.46	-	0.0020	26.225	251.20	257.72
1.752	256.15	-	0.0015	26.225	252.89	259.41
1.758	257.84	-	0.0011	26.225	254.59	261.10
1.764	259.54	-	0.0007	26.225	256.29	262.80
1.770	261.25	-	0.0004	26.225	257.99	264.51
1.776	262.96	-	0.0002	26.225	259.70	266.22

Table 8.57 continued

1.782	264.68	-	0.0001	26.225	261.42	267.94
1.788	266.40	-	0.0000	26.225	263.14	269.66
1.794	268.13	-	0.0000	26.225	264.87	271.39
1.800	269.86	-	0.0001	26.225	266.61	273.12
1.806	271.60	-	0.0002	26.225	268.35	274.86
1.812	273.35	-	0.0005	26.225	270.09	276.61
1.818	275.10	-	0.0008	26.225	271.84	278.36
1.824	276.85	-	0.0011	26.225	273.59	280.11
1.830	278.61	-	0.0016	26.225	275.35	281.87
1.836	280.38	-	0.0021	26.225	277.12	283.64
1.842	282.15	-	0.0027	26.225	278.89	285.41
1.848	283.93	-	0.0033	26.225	280.67	287.18
1.854	285.71	-	0.0040	26.225	282.45	288.97
1.860	287.49	-	0.0048	26.225	284.24	290.75
1.866	289.29	-	0.0057	26.225	286.03	292.55
1.872	291.09	-	0.0067	26.226	287.83	294.34
1.878	292.89	-	0.0077	26.226	289.63	296.15
1.884	294.70	-	0.0088	26.226	291.44	297.96
1.890	296.51	-	0.0099	26.226	293.25	299.77
1.896	298.33	-	0.0111	26.226	295.07	301.59
1.902	300.16	-	0.0125	26.226	296.90	303.41
1.908	301.99	-	0.0138	26.226	298.73	305.24
1.914	303.82	-	0.0153	26.227	300.56	307.08
1.920	305.66	-	0.0168	26.227	302.40	308.92
1.926	307.51	-	0.0184	26.227	304.25	310.77
1.932	309.36	-	0.0200	26.227	306.10	312.62
1.938	311.22	-	0.0218	26.228	307.96	314.47
1.944	313.08	-	0.0236	26.228	309.82	316.34

Table 8.57 continued

1.950	314.95	-	0.0255	26.228	311.69	318.20
1.956	316.82	-	0.0274	26.228	313.56	320.08
1.962	318.70	-	0.0294	26.229	315.44	321.96
1.968	320.58	-	0.0315	26.229	317.32	323.84
1.974	322.47	-	0.0337	26.229	319.21	325.73
1.980	324.36	-	0.0359	26.229	321.11	327.62
1.986	326.26	-	0.0383	26.230	323.01	329.52
1.992	328.17	-	0.0406	26.230	324.91	331.43
1.998	330.08	-	0.0431	26.230	326.82	333.34
2.004	332.00	-	0.0456	26.231	328.74	335.25

Table 8.58: Polynomial near loading point confidence prediction interval parameters

Polynomial Near Loading Point									
Measured Values		Predicted Values							
X_{hat}	Y_{hat}	X	Y	$(Y-Y_{hat})^2$	n_{true}	s^2_E	t_{inf}	n_{gen}	$\Sigma(X-X_{average})^2$
1.536	194.24	1.536	194.48	0.057	4	0.31	0.637	137	7.414
1.745	254.95	1.745	254.39	0.310	-	-	-	-	-
2.037	351.29	2.037	351.76	0.221	-	-	-	-	-
2.323	462.84	2.323	462.69	0.023	-	-	-	-	-

Table 8.59: Polynomial near loading point confidence prediction interval test

Loading Polynomial: $y = 93.620x^2 - 20.8x + 5.596$							
X	Y	$X_{average}$	$(X-X_{average})^2$	$s^2_{Y,hat}$	Lower Limit	Upper Limit	Test
1.536	194.48	1.931	0.1565	0.3139	194.12	194.84	0
1.542	196.13	-	0.1516	0.3137	195.77	196.49	0
1.548	197.74	-	0.1470	0.3135	197.38	198.10	0
1.554	199.36	-	0.1424	0.3134	199.00	199.71	0

Table 8.59 continued

1.560	200.98	-	0.1379	0.3132	200.63	201.34	0
1.566	202.61	-	0.1335	0.3130	202.26	202.97	0
1.572	204.25	-	0.1291	0.3128	203.89	204.61	0
1.578	205.90	-	0.1249	0.3126	205.54	206.25	0
1.584	207.55	-	0.1207	0.3125	207.19	207.90	0
1.590	209.21	-	0.1165	0.3123	208.85	209.56	0
1.596	210.87	-	0.1125	0.3121	210.51	211.23	0
1.602	212.54	-	0.1085	0.3120	212.19	212.90	0
1.608	214.22	-	0.1046	0.3118	213.86	214.58	0
1.614	215.91	-	0.1007	0.3116	215.55	216.26	0
1.620	217.60	-	0.0969	0.3115	217.24	217.95	0
1.626	219.30	-	0.0932	0.3113	218.94	219.65	0
1.632	221.00	-	0.0896	0.3112	220.65	221.36	0
1.638	222.71	-	0.0861	0.3110	222.36	223.07	0
1.644	224.43	-	0.0826	0.3109	224.08	224.79	0
1.650	226.16	-	0.0792	0.3107	225.80	226.51	0
1.656	227.89	-	0.0758	0.3106	227.53	228.24	0
1.662	229.63	-	0.0726	0.3105	229.27	229.98	0
1.668	231.37	-	0.0694	0.3103	231.02	231.73	0
1.674	233.13	-	0.0662	0.3102	232.77	233.48	0
1.680	234.89	-	0.0632	0.3101	234.53	235.24	0
1.686	236.65	-	0.0602	0.3100	236.30	237.01	0
1.692	238.42	-	0.0573	0.3098	238.07	238.78	0
1.698	240.20	-	0.0545	0.3097	239.85	240.56	0
1.704	241.99	-	0.0517	0.3096	241.64	242.34	0
1.710	243.78	-	0.0490	0.3095	243.43	244.14	0
1.716	245.58	-	0.0464	0.3094	245.23	245.94	0
1.722	247.39	-	0.0438	0.3093	247.03	247.74	0

Table 8.59 continued

1.728	249.20	-	0.0414	0.3092	248.85	249.56	0
1.734	251.02	-	0.0390	0.3091	250.67	251.38	0
1.740	252.85	-	0.0366	0.3090	252.49	253.20	0
1.746	254.68	-	0.0344	0.3089	254.33	255.04	0
1.752	256.52	-	0.0322	0.3088	256.17	256.88	0
1.758	258.37	-	0.0301	0.3087	258.02	258.72	0
1.764	260.22	-	0.0280	0.3086	259.87	260.58	0
1.770	262.08	-	0.0260	0.3086	261.73	262.44	0
1.776	263.95	-	0.0241	0.3085	263.60	264.30	0
1.782	265.82	-	0.0223	0.3084	265.47	266.18	0
1.788	267.70	-	0.0206	0.3083	267.35	268.06	0
1.794	269.59	-	0.0189	0.3083	269.24	269.95	0
1.800	271.49	-	0.0173	0.3082	271.13	271.84	0
1.806	273.39	-	0.0157	0.3081	273.03	273.74	0
1.812	275.29	-	0.0142	0.3081	274.94	275.65	0
1.818	277.21	-	0.0129	0.3080	276.85	277.56	0
1.824	279.13	-	0.0115	0.3080	278.78	279.48	0
1.830	281.06	-	0.0103	0.3079	280.70	281.41	0
1.836	282.99	-	0.0091	0.3079	282.64	283.35	0
1.842	284.93	-	0.0080	0.3078	284.58	285.29	0
1.848	286.88	-	0.0070	0.3078	286.53	287.23	0
1.854	288.84	-	0.0060	0.3077	288.48	289.19	0
1.860	290.80	-	0.0051	0.3077	290.44	291.15	0
1.866	292.77	-	0.0043	0.3077	292.41	293.12	0
1.872	294.74	-	0.0035	0.3076	294.39	295.09	1
1.878	296.72	-	0.0028	0.3076	296.37	297.08	1
1.884	298.71	-	0.0022	0.3076	298.36	299.06	1
1.890	300.71	-	0.0017	0.3076	300.35	301.06	1

Table 8.59 continued

1.896	302.71	-	0.0013	0.3075	302.35	303.06	1
1.902	304.72	-	0.0009	0.3075	304.36	305.07	1
1.908	306.73	-	0.0005	0.3075	306.38	307.08	1
1.914	308.75	-	0.0003	0.3075	308.40	309.11	1
1.920	310.78	-	0.0001	0.3075	310.43	311.14	1
1.926	312.82	-	0.0000	0.3075	312.46	313.17	1
1.932	314.86	-	0.0000	0.3075	314.51	315.21	1
1.938	316.91	-	0.0000	0.3075	316.56	317.26	1
1.944	318.96	-	0.0002	0.3075	318.61	319.32	1
1.950	321.03	-	0.0003	0.3075	320.67	321.38	1
1.956	323.10	-	0.0006	0.3075	322.74	323.45	1
1.962	325.17	-	0.0009	0.3075	324.82	325.53	1
1.968	327.26	-	0.0013	0.3075	326.90	327.61	1
1.974	329.34	-	0.0018	0.3076	328.99	329.70	1
1.980	331.44	-	0.0024	0.3076	331.09	331.79	1
1.986	333.54	-	0.0030	0.3076	333.19	333.90	1
1.992	335.65	-	0.0037	0.3076	335.30	336.01	1
1.998	337.77	-	0.0044	0.3077	337.42	338.12	1
2.004	339.89	-	0.0053	0.3077	339.54	340.25	1

8.8.2 Onset of Flooding Determination

Table 8.60: Onset of flooding experimental data standard deviation

Flooding Point			
	Flow rate [kg/h]	**$Std_{dev, flow}$ [kg/h]**	**$Std_{dev, flow}$ [(m/s)·(kg/m^3)$^{0.5}$]**
1	1587	3.7	0.008
2	1587	-	-
3	1587	-	-
4	1587	-	-
5	1587	-	-
6	1587	-	-
7	1587	-	-
8	1587	-	-
9	1596.3	-	-
10	1596.3	-	-
11	1596.3	-	-
12	1596.3	-	-
13	1596.3	-	-
14	1596.3	-	-
15	1596.3	-	-
16	1596.3	-	-
17	1596.3	-	-
18	1596.3	-	-
19	1596.3	-	-
20	1599.1	-	-
21	1599.1	-	-
22	1599.1	-	-
23	1599.1	-	-
24	1599.1	-	-
25	1599.1	-	-
26	1599.1	-	-
27	1599.1	-	-
28	1599.1	-	-
29	1599.1	-	-
30	1599.1	-	-
31	1592.5	-	-
32	1592.5	-	-
33	1592.5	-	-
34	1592.5	-	-
35	1592.5	-	-
36	1592.5	-	-
37	1592.5	-	-

Table 8.60 continued

38	1592.5	-	-
39	1592.5	-	-
40	1592.5	-	-
41	1592.5	-	-
42	1595.2	-	-
43	1595.2	-	-
44	1595.2	-	-
45	1595.2	-	-
46	1595.2	-	-
47	1595.2	-	-
48	1595.2	-	-
49	1595.2	-	-
50	1595.2	-	-
51	1595.2	-	-
52	1595.2	-	-
53	1596.7	-	-
54	1596.7	-	-
55	1596.7	-	-
56	1596.7	-	-
57	1596.7	-	-
58	1596.7	-	-
59	1596.7	-	-
60	1596.7	-	-

Table 8.61: Loading curve confidence prediction interval parameters

Loading Curve									
Measured Values		Predicted Values							
X_{hat}	Y_{hat}	X	Y	$(Y-Y_{hat})^2$	n_{true}	s^2_E	t_{inf}	n_{gen}	$\Sigma(X-X_{average})^2$
2.037	351.29	2.037	352.78	2.224	6	527.49	0.636	291	122.517
2.323	462.84	2.323	474.19	128.781	-	-	-	-	-
2.605	613.52	2.605	634.40	435.880	-	-	-	-	-
2.821	767.15	2.821	792.40	637.561	-	-	-	-	-
3.025	948.40	3.025	978.50	905.524	-	-	-	-	-
3.139	1093.63	3.139	1101.01	54.459	-	-	-	-	-

Table 8.62: Loading curve confidence prediction interval test & model test

Loading Curve Extrapolate: $y = 43.01e^{1.024x}$							
X	Y	$X_{average}$	$(X-X_{average})^2$	$s^2_{Y,hat}$	Lower Limit	Upper Limit	Test
3.025	978.732	2.872	0.023	529.406	964.088	993.375	0
3.033	986.854	-	0.026	529.417	972.210	1001.497	0
3.041	995.043	-	0.029	529.428	980.399	1009.687	0
3.049	1003.300	-	0.031	529.440	988.656	1017.944	0
3.057	1011.625	-	0.034	529.453	996.981	1026.270	0
3.065	1020.020	-	0.037	529.466	1005.376	1034.664	0
3.073	1028.485	-	0.040	529.479	1013.840	1043.129	0
3.081	1037.019	-	0.044	529.493	1022.374	1051.664	0
3.089	1045.625	-	0.047	529.508	1030.980	1060.269	0
3.097	1054.301	-	0.051	529.523	1039.656	1068.947	0
3.105	1063.050	-	0.054	529.539	1048.405	1077.696	0
3.113	1071.872	-	0.058	529.556	1057.226	1086.517	0
3.121	1080.766	-	0.062	529.572	1066.121	1095.412	0

Table 8.62 continued

3.129	1089.735	-	0.066	529.590	1075.089	1104.381	0
3.137	1098.778	-	0.070	529.608	1084.131	1113.424	0
3.145	1107.896	-	0.075	529.626	1093.249	1122.542	0
3.153	1117.089	-	0.079	529.645	1102.442	1131.736	0
3.161	1126.359	-	0.084	529.665	1111.712	1141.006	0
3.169	1135.706	-	0.088	529.685	1121.059	1150.353	0
3.177	1145.130	-	0.093	529.706	1130.483	1159.778	0
3.185	1154.633	-	0.098	529.727	1139.985	1169.281	0
3.193	1164.214	-	0.103	529.749	1149.566	1178.862	0
3.201	1173.875	-	0.108	529.772	1159.227	1188.524	0
3.209	1183.616	-	0.114	529.794	1168.967	1198.265	0
3.217	1193.438	-	0.119	529.818	1178.789	1208.087	0
3.225	1203.342	-	0.125	529.842	1188.692	1217.991	0
3.233	1213.327	-	0.130	529.867	1198.677	1227.977	0
3.241	1223.396	-	0.136	529.892	1208.745	1238.046	0
3.249	1233.548	-	0.142	529.917	1218.897	1248.198	0
3.257	1243.784	-	0.148	529.944	1229.133	1258.435	0
3.265	1254.105	-	0.155	529.971	1239.454	1268.757	0
3.273	1264.512	-	0.161	529.998	1249.860	1279.164	0
3.281	1275.005	-	0.167	530.026	1260.353	1289.657	0
3.289	1285.586	-	0.174	530.054	1270.933	1300.238	0
3.297	1296.254	-	0.181	530.083	1281.601	1310.907	0
3.305	1307.010	-	0.188	530.113	1292.357	1321.664	0
3.313	1317.856	-	0.195	530.143	1303.203	1332.510	0
3.321	1328.792	-	0.202	530.174	1314.138	1343.446	0
3.329	1339.819	-	0.209	530.205	1325.164	1354.473	0
3.337	1350.937	-	0.216	530.237	1336.282	1365.592	0

Table 8.62 continued

3.345	1362.147	-	0.224	530.269	1347.492	1376.803	0
3.353	1373.451	-	0.231	530.302	1358.795	1388.107	0
3.361	1384.848	-	0.239	530.335	1370.192	1399.504	0
3.369	1396.340	-	0.247	530.369	1381.683	1410.997	0
3.377	1407.927	-	0.255	530.404	1393.270	1422.584	0
3.385	1419.610	-	0.263	530.439	1404.952	1434.268	0
3.393	1431.391	-	0.272	530.474	1416.732	1446.049	0
3.401	1443.269	-	0.280	530.511	1428.610	1457.927	0
3.409	1455.245	-	0.288	530.547	1440.586	1469.904	0
3.417	1467.321	-	0.297	530.585	1452.661	1481.981	0
3.425	1479.497	-	0.306	530.622	1464.837	1494.158	0
3.433	1491.775	-	0.315	530.661	1477.114	1506.435	0
3.441	1504.154	-	0.324	530.700	1489.492	1518.815	0
3.449	1516.635	-	0.333	530.739	1501.974	1531.297	0
3.457	1529.221	-	0.342	530.779	1514.558	1543.883	0
3.465	1541.911	-	0.352	530.820	1527.248	1556.574	0
3.473	1554.706	-	0.361	530.861	1540.042	1569.369	0
3.481	1567.607	-	0.371	530.903	1552.943	1582.271	0
3.489	1580.616	-	0.381	530.945	1565.951	1595.280	0
3.497	1593.732	-	0.391	530.988	1579.067	1608.397	0
3.505	1606.957	-	0.401	531.031	1592.291	1621.623	0
3.513	1620.292	-	0.411	531.075	1605.625	1634.959	0
3.521	1633.738	-	0.421	531.119	1619.070	1648.405	0
3.529	1647.295	-	0.432	531.164	1632.627	1661.963	0
3.537	1660.964	-	0.442	531.210	1646.296	1675.633	0
3.545	1674.747	-	0.453	531.256	1660.078	1689.416	0
3.553	1688.645	-	0.464	531.303	1673.975	1703.315	0
3.561	1702.658	-	0.475	531.350	1687.987	1717.328	0

Table 8.62 continued

3.569	1716.787	-	0.486	531.397	1702.116	1731.458	0
3.577	1731.033	-	0.497	531.446	1716.361	1745.705	0
3.585	1745.398	-	0.509	531.495	1730.725	1760.070	0
3.593	1759.881	-	0.520	531.544	1745.208	1774.554	0
3.601	1774.485	-	0.532	531.594	1759.811	1789.159	0
3.609	1789.210	-	0.543	531.644	1774.536	1803.885	1
3.617	1804.058	-	0.555	531.696	1789.382	1818.733	1
3.625	1819.028	-	0.567	531.747	1804.352	1833.704	1
3.633	1834.123	-	0.579	531.799	1819.446	1848.799	1
3.641	1849.343	-	0.592	531.852	1834.666	1864.020	1
3.649	1864.689	-	0.604	531.905	1850.011	1879.367	1
3.657	1880.163	-	0.616	531.959	1865.484	1894.842	1
3.665	1895.765	-	0.629	532.013	1881.085	1910.444	1
3.673	1911.496	-	0.642	532.068	1896.816	1926.177	1
3.681	1927.358	-	0.655	532.124	1912.677	1942.039	1
3.689	1943.352	-	0.668	532.180	1928.670	1958.034	1
3.697	1959.479	-	0.681	532.236	1944.796	1974.161	1
3.705	1975.739	-	0.694	532.293	1961.055	1990.422	1

Table 8.63: Flooding curve confidence prediction interval parameters

Flooding Curve									
Measured Values		Predicted Values							
X_{hat}	Y_{hat}	X	Y	$(Y-Y_{hat})^2$	n_{true}	s^2_E	t_{inf}	n_{gen}	$\Sigma(X-X_{average})^2$
3.025	948.40	3.025	950.672	5.142	4.000	108.648	0.639	61	644.223
3.139	1093.63	3.139	1088.336	28.007	-	-	-	-	-
3.336	1434.83	3.336	1445.818	120.732	-	-	-	-	-
3.378	1550.35	3.378	1542.386	63.415	-	-	-	-	-

Table 8.64: Flooding curve confidence prediction interval test

Flooding Curve: $y = 1958.22x^2 - 10864.431x + 15896.868$							
X	Y	$X_{average}$	$(X-X_{average})^2$	$s^2_{Y,hat}$	Lower Limit	Upper Limit	Test
3.025	950.901	3.247	9.151	10.855	948.794	953.008	0
3.033	958.889	-	9.199	10.859	956.781	960.996	0
3.041	967.127	-	9.248	10.862	965.020	969.234	0
3.049	975.616	-	9.296	10.865	973.508	977.724	0
3.057	984.356	-	9.345	10.868	982.248	986.464	0
3.065	993.346	-	9.394	10.871	991.238	995.454	0
3.073	1002.587	-	9.443	10.875	1000.478	1004.696	0
3.081	1012.079	-	9.493	10.878	1009.970	1014.188	0
3.089	1021.821	-	9.542	10.881	1019.712	1023.930	0
3.097	1031.814	-	9.591	10.884	1029.704	1033.924	0
3.105	1042.058	-	9.641	10.887	1039.948	1044.168	0
3.113	1052.552	-	9.691	10.891	1050.442	1054.662	0
3.121	1063.297	-	9.741	10.894	1061.186	1065.407	0
3.129	1074.292	-	9.791	10.897	1072.181	1076.403	0
3.137	1085.538	-	9.841	10.901	1083.427	1087.650	0
3.145	1097.035	-	9.891	10.904	1094.924	1099.147	0
3.153	1108.783	-	9.941	10.907	1106.671	1110.895	0
3.161	1120.781	-	9.992	10.911	1118.669	1122.893	0
3.169	1133.030	-	10.043	10.914	1130.917	1135.142	0
3.177	1145.529	-	10.093	10.917	1143.416	1147.642	0
3.185	1158.279	-	10.144	10.920	1156.166	1160.393	0
3.193	1171.280	-	10.195	10.924	1169.167	1173.394	0
3.201	1184.532	-	10.246	10.927	1182.418	1186.645	0
3.209	1198.034	-	10.298	10.931	1195.920	1200.148	0
3.217	1211.786	-	10.349	10.934	1209.672	1213.901	1

Table 8.64 continued

3.225	1225.790	-	10.401	10.937	1223.675	1227.905	1
3.233	1240.044	-	10.452	10.941	1237.929	1242.159	1
3.241	1254.549	-	10.504	10.944	1252.433	1256.664	1
3.249	1269.304	-	10.556	10.947	1267.188	1271.420	1
3.257	1284.310	-	10.608	10.951	1282.194	1286.426	1
3.265	1299.566	-	10.660	10.954	1297.450	1301.683	1
3.273	1315.074	-	10.713	10.958	1312.957	1317.191	1
3.281	1330.832	-	10.765	10.961	1328.715	1332.949	1
3.289	1346.840	-	10.818	10.965	1344.723	1348.958	1
3.297	1363.100	-	10.870	10.968	1360.982	1365.217	1
3.305	1379.609	-	10.923	10.972	1377.491	1381.728	1
3.313	1396.370	-	10.976	10.975	1394.252	1398.488	1
3.321	1413.381	-	11.029	10.979	1411.262	1415.500	1
3.329	1430.643	-	11.082	10.982	1428.524	1432.762	1
3.337	1448.156	-	11.136	10.985	1446.036	1450.275	1
3.345	1465.919	-	11.189	10.989	1463.799	1468.039	1
3.353	1483.933	-	11.243	10.993	1481.812	1486.053	1
3.361	1502.197	-	11.296	10.996	1500.077	1504.318	1
3.369	1520.712	-	11.350	11.000	1518.591	1522.833	1
3.377	1539.478	-	11.404	11.003	1537.357	1541.599	1
3.385	1558.494	-	11.458	11.007	1556.373	1560.616	1

Table 8.65: Flooding range check point summary

Flooding Range Check Point							
Measured Values		Predicted Values					
X_{hat}	Y_{hat}	X	Y	Upper Limit	Absolute Test	Predicted Limiting Value	Measured Limiting Value
2.037	351.29	2.037	352.78	367.46	0	3.61	3.34
2.323	462.84	2.323	474.19	488.85	0	-	-
2.605	613.52	2.605	634.40	649.04	0	-	-
2.821	767.15	2.821	792.40	807.04	0	-	-
3.025	948.40	3.025	978.50	993.14	0	-	-
3.139	1093.63	3.139	1101.01	1115.65	0	-	-
3.336	1434.83	3.336	1349.46	1364.11	1	-	-
3.378	1550.35	3.378	1409.72	1424.37	1	-	-